Peptide–Drug Conjugates:

An Exploration for Antimalarial and Anticancer Treatments

A thesis submitted for the degree of

Doctor of Philosophy

of The Australian National University

Isabella Palombi

Australian National University

Research School of Chemistry

October 2024

Contents

Declaration

This thesis is a report of the scientific investigations undertaken by myself during the period of April 2021 to October 2024 at the Research School of Chemistry, Australian National University, under the supervision of Professor Lara R. Malins. Except where specific acknowledgements of others are made, all of the material contained within is my own work. The material presented has not been submitted for any other degree and is less than 100,000 words in length.

Isabella Palombi

October 2024

Acknowledgements

I would like to begin by thanking Prof. Lara Malins for being an extraordinary supervisor and providing continuous support throughout my PhD. Your dedication to your research group is truly inspiring and it has been an absolute honour to work with you. Thank you for all of your help with research, writing and presentations, as well as the constant flow of snacks, laughs and memes throughout the years. It has been wonderful to watch you excel in your career, and you will continue to be a mentor for myself and your other students.

I would also like to thank all past and present members of the Malins group for the non-stop banter and for making the lab an enjoyable place to be during my PhD. A special mention to Dr Andrew White and Caitlin Gare, for the continuous help and support with our PDC studies – it has been great to work as a team with you both.

Thank you to our collaborators (Team PDC) for making this project possible. Firstly, I would like to thank Dr Nicole Lawrence and Prof. David Craik for hosting me at the Institute of Molecular Biology, University of Queensland, so I could conduct the cancer research component of my studies. Nicole, I really appreciate all the help, guidance and feedback you have provided towards my projects/writing and enjoyed my time working with you. Secondly, I would like to thank Assoc. Prof. Brendan McMorran at the John Curtin School of Medical Research, ANU, for welcoming me into your lab to complete testing against the malaria parasite. Your guidance and feedback have been truly valuable. Thirdly, thank you to Assoc. Prof. Sónia Henriques for your contributions to project conceptualisation and feedback for our cancer studies.

I would also like to extend my gratitude to the technical and administrative teams at the RSC, JCSMR and IMB for their help with various aspects of my project and their commitment to maintaining a safe laboratory environment. Thank you to Ms Anitha Jeyasingham, Mr Joseph Boileau, Dr Hideki Onagi, Mr Daniel Bartkus, Dr Chris Blake, Dr Douglas Lawes, Dr Harpreet Vohra and Mr Mick Devoy, to name a few.

Finally, a big thank you to all my family and friends who have continued to support me throughout my studies. I could not have achieved this without the constant encouragement you have all provided.

Publications and Presentations

This thesis is submitted in compilation with published work. The following list of publications and presentations are those completed during the author's research candidature.

Publications:

I. R. Palombi, A. M. White, Y. Koda, D. J. Craik, N. Lawrence, L. R. Malins. Synthesis and investigation of peptide–drug conjugates comprising camptothecin and a human protein-derived cell-penetrating peptide. *Chem. Biol. Drug Des*. **2025**, *105*, e70051.

I. R. Palombi, N. Lawrence, A. M. White, C. L. Gare, D. J. Craik, B. J. McMorran, L. R. Malins. Development of antiplasmodial peptide–drug conjugates using a human protein-derived cell-penetrating peptide with selectivity for infected cells. *Bioconjugate Chem.* **2023**, *34*, 1105–1113.

A. M. White,* I. R. Palombi* and L. R. Malins. Umpolung strategies for the functionalization of peptides and proteins. *Chem. Sci.* **2022**, *13*, 2809–2823. *[Chosen as a Chemical Science "Pick of the Week" article]*

C. L. Gare, I. R. Palombi, A. M. White, D. J. Craik, M. Chavchich, M. D. Edstein, A. Lock, V. M. Avery, B. J. McMorran, N. Lawrence and L. R. Malins. Exploring the utility of cell-penetrating peptides as vehicles for the delivery of distinct antimalarial drug cargoes. *ChemMedChem* **2025**, *20*, e202400637. *[Designated a ChemMedChem Very Important Paper]*

*Denotes co-first authorship

Presentations:

Three Minute Thesis Competition | *presentation*
July 2021, ANU, ACT.

8th Modern Solid Phase Peptide Synthesis and Its Applications Symposium | *poster presentation*
May 2022, Gold Coast, QLD.

14th Australian Peptide Conference | *poster presentation*
May 2022, Gold Coast, QLD.

Annual Centre of Excellence for Innovations in Peptide and Protein Science (CIPPS) Conference | *poster presentation*
December 2022, Sydney, NSW.

13th International Peptide Symposium | *poster presentation*
October 2023, Brisbane, QLD.

Annual CIPPS Retreat | *poster presentation*
May 2024, Kingscliff, NSW.

List of Abbreviations

ACT	Artemisinin-based combination therapy
ADC	Antibody–drug conjugate
AMP	Antimicrobial peptide
ART	Artemisinin
Boc	*Tert*-butyloxycarbonyl
cGm	Cyclic gomesin
CPP	Cell-penetrating peptide
CPT	Camptothecin
CQ	Chloroquine
CTP	Cell-targeting peptide
CuAAC	Copper-catalysed azide–alkyne cycloaddition
Da	Dalton
Dab	Dabrafenib
DBCO	Dibenzocyclooctyne
DCM	Dichloromethane
DIEA	*N,N*-diisopropylethylamine
DMF	*N,N*-dimethylformamide
DMSO	Dimethyl sulfoxide
ESI	Electrospray-ionisation
EtOAc	Ethyl acetate
FDA	U.S. Food and Drug Administration
Fmoc	Fluorenylmethyloxycarbonyl
G6PD	Glucose-6-phosphate dehydrogenase
Gm	Gomesin
GSH	Glutathione
IEDDA	Inverse electron-demand Diels–Alder
mAb	Monoclonal antibody
Me	Methyl
MeCN	Acetonitrile

AMINO ACIDS:

Ala	Alanine (A)
Arg	Arginine (R)
Asn	Asparagine (N)
Asp	Aspartic acid (D)
Cit	Citrulline
Cys	Cysteine (C)
Gln	Glutamine (Q)
Glu	Glutamic acid (E)
Gly	Glycine (G)
His	Histidine (H)
Ile	Isoleucine (I)
Leu	Leucine (L)
Lys	Lysine (K)
Met	Methionine (M)
Phe	Phenylalanine (F)
Pro	Proline (P)
Ser	Serine (S)
Thr	Threonine (T)
Trp	Tryptophan (W)
Tyr	Tyrosine (Y)
Val	Valine (V)

MeOH	Methanol
MMAE	Monomethyl auristatin E
MS	Mass spectrometry
PDB	Protein data bank
PDC	Peptide–drug conjugate
PDIP	Platelet factor 4-derived internalisation peptide
PEG	Polyethylene glycol
PF4	Platelet factor 4
PQ	Primaquine
PS	Phosphatidylserine
RBC	Red blood cell
SP	Sulfadoxine–pyrimethamine
SPAAC	Strain-promoted azide–alkyne cycloaddition
SPPS	Solid-phase peptide-synthesis
TQ	Tafenoquine
Vem	Vemurafenib
WHO	World Health Organisation

NOTICE TO READERS:

Figures, schemes, compounds and references are numbered independently in each chapter. Reference lists are included at the end of each chapter. The manuscripts embedded in Chapters 2–4 are self-contained and have their own numbering for figures, schemes, compounds and references. The corresponding Supporting Information for these chapters match the numbering system in each manuscript.

Abstract

Small molecule drugs are essential in the treatment and management of acute and chronic diseases. However, they often possess disadvantages such as nonspecific interactions with healthy cells and can suffer from loss of efficacy as pathogens or diseased cells gain drug resistance. The approval of antibody–drug conjugates (ADCs) for cancer treatment has highlighted targeted drug delivery as a novel therapeutic approach to overcome some of the limitations of small molecules. Inspired by the success of ADCs, peptide–drug conjugates (PDCs) provide an attractive and cheaper alternative for the exploration of targeted drug delivery. In this thesis, three small molecule drugs—primaquine (PQ), camptothecin (CPT) and vemurafenib (Vem)—are conjugated onto bioactive cell-penetrating peptides to understand if certain drug liabilities, such as off-target toxicity or drug resistance, can be mitigated through peptide conjugation. The exploration of PDCs in both an infectious disease context (malaria) and a noncommunicable disease context (cancer) will highlight these emerging therapeutic modalities as a versatile tool for targeted treatments.

Chapter One introduces PDCs as a promising tool for targeted therapy and highlights the need for such an approach in the treatment of both infectious and noncommunicable diseases. The different design aspects of PDCs are discussed, including the types of targeting peptides, different linker technologies and alternative conjugation strategies. The design, synthesis and biological evaluation of a suite of PDCs in different disease contexts will be underlined as the key theme explored in this thesis, which is subdivided into chapters based on the identity of the PDC drug cargo.

Chapter Two discusses the synthesis of six PQ-containing antimalarial PDCs, each with varied design characteristics, and the subsequent biological evaluation of their killing ability against *Plasmodium* parasites. The insights provided by changes in the low micromolar activity for different PDC analogues revealed that conjugation site and linker type play an important role in PDC potency. These first-generation conjugates highlighted PDCs as a feasible approach to antimalarial therapy, an area that remains underexplored for this treatment type.

Chapter Three investigates the synthesis of four anticancer PDCs containing CPT, a small molecule drug with off-target toxicity. The knowledge of the relationship between design characteristics and potency from the previous chapter was used to inform PDC construction. Biological evaluation of the PDCs against a melanoma cancer cell line revealed nanomolar to low micromolar potency, albeit with toxicity against a noncancerous cell line. The non-selective nature of the PDCs reinforced the importance of design in PDC development, including matching drug cargo with the correct carrier molecule.

Chapter Four explores the synthesis of five Vem-containing anticancer PDCs and details their killing ability against melanoma cell lines that are sensitive and resistant to the drug cargo. The resulting PDCs had selective low micromolar activity against the drug-sensitive cell line. Evaluation of peptide-linker controls containing no drug highlighted the contribution of each PDC component to PDC activity and indicated the importance of the peptide carrier to overall potency. One of the PDCs was also active against the drug-resistant cell line, emphasising this approach as a feasible means to reinvigorate interest in small molecule drugs with resistance issues.

Chapter Five summarises the above projects on antimalarial and anticancer PDCs utilising bioactive cell-penetrating peptides. A perspective is provided on the prospects of future generations of PDCs and how the lessons learned throughout this thesis will inform design considerations.

Chapter 1:

The design features of peptide–drug conjugates and their use as targeted therapeutics

Introduction

Three common drug classes—small molecule, peptide and biologic—provide an array of treatment options for many diseases. Each drug class displays distinct strengths and limitations that dictate treatment applications (Figure 1.1). Small molecule drugs are versatile as they are often orally bioavailable and are cost effective to produce.[1] In comparison, biologics—such as a protein or antibody—have high production costs but superior target specificity, making them useful in disease contexts such as cancer, where small molecule chemotherapeutics may display systemic toxicity.[2,3] The remaining drug class, peptides, is an important intermediary, often filling the niche between small molecule drugs and larger biologics. The ability of peptides to interact with an intracellular target with high affinity and specificity limits promiscuous binding, a drawback sometimes associated with small molecule drugs.[1,4] This specificity is reminiscent of a biologic, however, in comparison, peptides generally display less immunogenicity and have lower production costs.[1] Careful consideration of peptide design is required for their use as medicines because linear peptides often have limited membrane permeability and poor stability.[5] However, strategies such as peptide stapling,[6] cyclisation,[7] *N*-methylation[8] and stabilisation of secondary structure have resulted in peptides with improved drug-like properties.

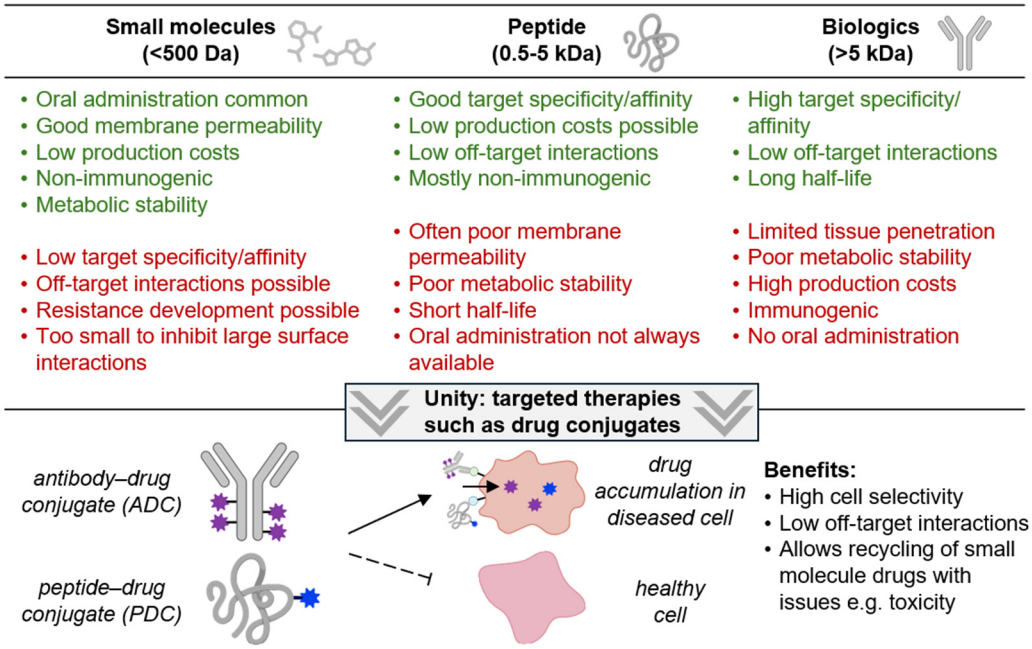

Figure 1.1. Strengths and limitations of three common drug classes—small molecules, peptides and biologics—and how targeted therapies, such as drug conjugates, can unite the strengths of the different drug types. Some images used in the figure were adapted from BioRender.

The benefits and drawbacks of small molecule, peptide and biologic treatments have prompted consideration into alternative therapeutic avenues that unite the advantages of each drug type (Figure 1.1). Targeted therapeutics, such as antibody–drug conjugates (ADCs) and peptide–drug conjugates (PDCs), that aim to integrate the strengths of two drug classes have emerged

as a promising alternative to traditional treatments. Drug conjugates—where a small molecule drug is covalently attached to a targeting moiety, such as an antibody or peptide—utilise the specificity of the targeting moiety to direct a small molecule drug to disease-causing cells within the body (Figure 1.1).[9] This thesis will investigate the utility of PDCs that employ cell-penetrating peptides as a tool to target small molecule drugs to parasites and diseased cells, in the context of malaria and cancer treatment. In this chapter, an overview of targeted therapies will be provided to highlight the requirement for alternate treatment strategies. With PDC design a key theme in this thesis, the components of a PDC will be outlined, followed by discussion of the objectives of this study.

1.1 Drug conjugates as targeted therapeutics

1.1.1 The requirement for targeted therapies

Despite the steady increase in new biologic and peptide treatments introduced into the market over the past decade, small molecules prevail as the most common therapeutic class, likely due to the low production costs, membrane permeability and oral administration route of many small molecule drugs.[10] In 2023, 29 of the 55 treatments approved by the U.S. Food and Drug Administration (FDA) were small molecule drugs. The remaining FDA approved treatments were divided between 17 biologics, 5 peptides and 4 oligonucleotides,[a] highlighting the dominance of small molecules in pharmaceutical treatments.[10]

While small molecule drugs have been imperative in treating many diseases, they can possess disadvantages such as nonspecific interactions with healthy cells, which may manifest as patient side effects.[4] Furthermore, since many small molecule drugs have one defined target, such as an enzyme or receptor, they can suffer from loss of efficacy as parasites, bacteria or disease-causing cells acquire mechanisms for drug resistance.[11–13] Thus, pairing such small molecule drugs with a targeting moiety to direct the drug to disease-causing cells within the body may help to overcome these challenges, potentially reducing off-target toxicity and resistance development associated with the drug cargo. An additional benefit of targeted therapeutics is that they allow for recycling and repurposing of small molecule drugs that have already undergone considerable research and development but have issues with toxicity, acquired resistance or are membrane impermeable. It should be noted that the strategy can also be applied in the reverse, where a small molecule could improve the activity or overcome the limitations of the targeting molecule.[14]

Several types of targeted therapies have emerged, often in the form of a prodrug that remains inactive until it reaches the disease-causing cells, where it can then be activated to effect a desired outcome.[15] This includes drug conjugates, where a drug is attached to an antibody,[16]

[a] In 2023, no drug conjugates were released onto the market. In 2022, one ADC (Mirvetuximab soravtansine) was approved.[10,112]

peptide[14] or self-assembling nanostructure,[17] or drugs encapsulated in liposomes or micelles.[15,17] Other modalities, such as monoclonal antibodies and some small molecule drugs that have a target that is not found in healthy cells, are also inherently targeted therapeutics.

As this thesis will focus on drug conjugates, specifically ADCs and PDCs, these therapeutic modalities will be discussed in detail in the following sections. Drug conjugates are composed of three main components that are covalently attached—a small molecule drug, the targeting device and a linking region (Figure 1.2). The targeting moiety is designed to recognise a molecular target specific to the disease being treated. This allows the conjugate to be delivered to the disease-causing cells, where the drug cargo can exert its killing mechanism of action. The linker, the region that bridges the targeting moiety and drug payload, can be constructed to allow for liberation of the drug under specific conditions, once inside the disease-causing cells.[18] A non-cleavable linker, that does not allow for drug release, is also possible.

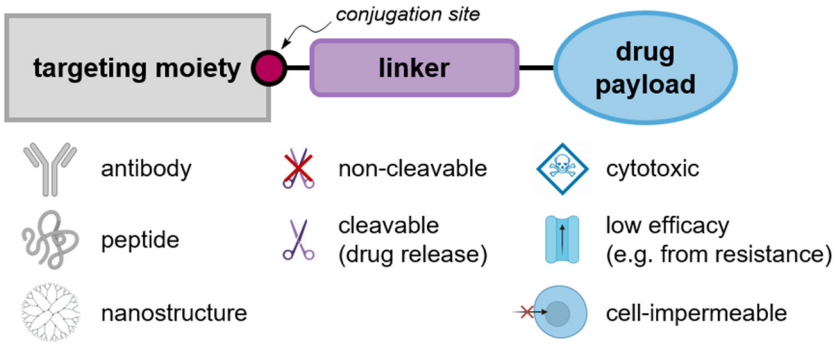

Figure 1.2. The general structure of a drug conjugate, which is composed of three main components: a targeting molecule, linker and drug payload. The targeting molecule delivers the construct to the disease-causing cells, where the drug payload can then kill the cells. The linking region connects the targeting moiety and drug payload and can be strategically designed to allow for drug release under specific conditions. Some images used in the figure were adapted from BioRender.

1.1.2 Antibody–drug conjugates (ADCs)

ADCs have paved the way for targeted therapeutics, bridging the gap between monoclonal antibodies and cytotoxic drugs.[16] However, the concept of conjugating a toxic compound to a targeting agent is not new, but rather was originally proposed in 1913 by German scientist Paul Ehrlich, who described such a construct as a 'magic bullet'.[19,20] Four decades later, Ehrlich's concept was first demonstrated with the successful construction of an ADC for leukaemia treatment by Bernard and co-workers.[21] Further advances in antibody engineering, such as the ability to produce antibodies in animals and the development of humanised monoclonal antibodies, were required for drug conjugates to be practical as therapeutics.[22] These advances led to the FDA approval of the first ADCs: gemtuzumab ozogamicin[b] (Mylotarg®) in

[b] Gemtuzumab ozogamicin was withdrawn from the market in 2010 due to a lack of clinical benefit, however, gained reapproval in 2017 for lower doses of the ADC.[23]

2000 for acute myelogenous leukaemia and brentuximab vedotin (Adcetris®) in 2011 for Hodgkin's lymphoma.[23]

ADCs are uniquely suited to cancer treatment because cytotoxic chemotherapeutic drugs can be selectively targeted to cancer cells, thereby preventing their interaction with healthy tissues. For example, brentuximab vedotin (**1.1**, Figure 1.3A) contains the potent chemotherapy drug monomethyl auristatin E (MMAE), which inhibits cell division by disrupting microtubule formation.[24,25] When administered alone, MMAE is highly cytotoxic against healthy proliferative cells, due to its antimitotic mechanism of action. In the ADC approach, brentuximab vedotin contains MMAE conjugated to an anti-CD30 monoclonal antibody (mAb) that recognises and binds to a receptor that is highly expressed on the surface of lymphoma cells (Figure 1.3B).[24] Following ADC internalisation through endocytosis, MMAE can be released from the antibody *via* cleavage of the dipeptide linker by cathepsin B, a protease found in the lysosome.[22] The released MMAE can then disrupt microtubule formation, resulting in cell apoptosis (Figure 1.3B). A detailed discussion of linkers utilised in drug conjugates and their associated cleavage mechanisms can be found in Section 1.2.3.

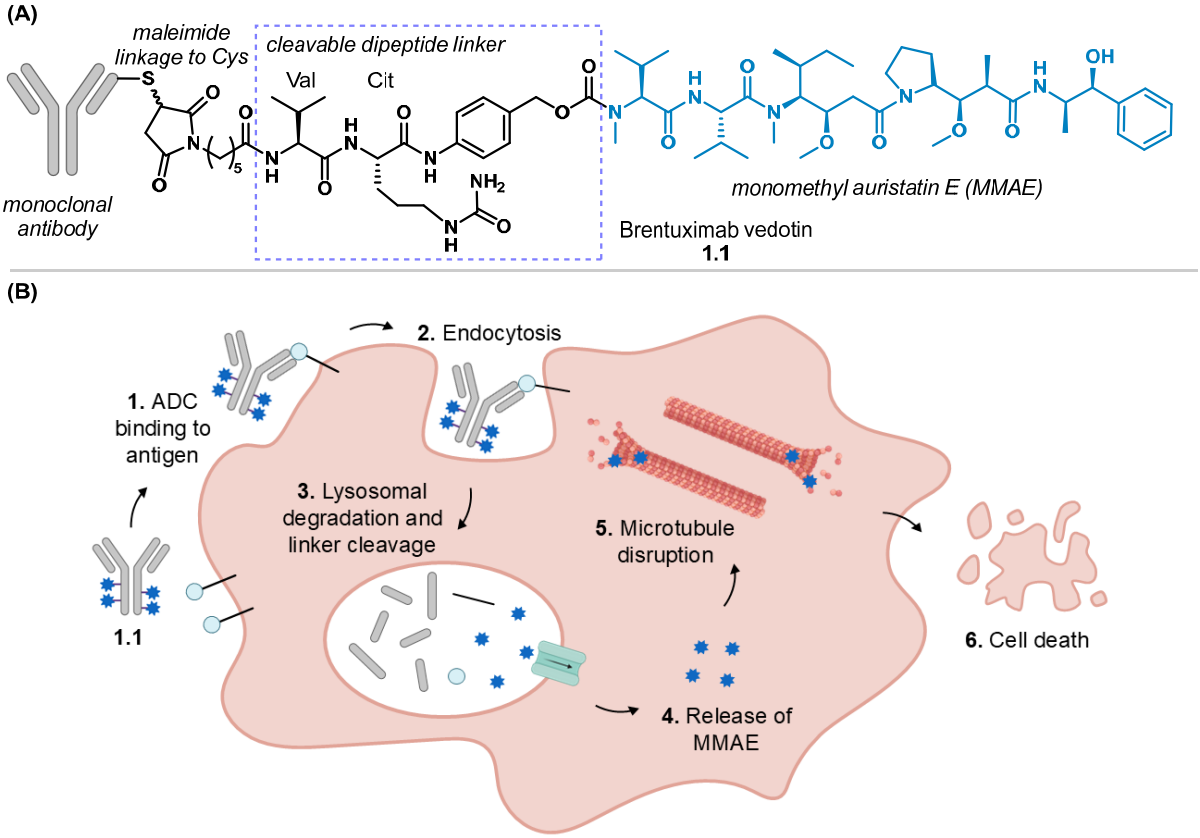

Figure 1.3. (A) The structure of brentuximab vedotin (**1.1**), with its cleavable dipeptide linker outlined in a light purple box. (B) General mechanism of MMAE-containing ADCs such as brentuximab vedotin. The ADC binds to an antigen on the cell surface (for **1.1** this is the CD30 antigen), leading to endocytosis of the complex into the cell. The lysosome degrades the ADC, and the linker is cleaved to release the cytotoxic drug. MMAE subsequently disrupts microtubule formation, resulting in cell death. Some images used in the figure were adapted from BioRender and Tsuchikama and An.[22]

The FDA has now approved eleven ADCs[c] for clinical use, all on the market for the treatment of human cancers.[23,26,27] More than half of these ADCs were approved in the last five years, highlighting targeted therapeutics as promising treatments in noncommunicable diseases such as cancer. However, despite their success, ADC therapies come with a range of limitations which has prompted the development of alternative drug conjugate treatments.[14] The large size and molecular weight of ADCs often results in poor tumour penetration, relying on endocytosis for the small molecule to be delivered into the cell. Furthermore, the antibody portion of an ADC can limit the conjugation strategies possible to install a drug and may increase the risk for immunogenicity during treatment.[14,28] Finally, antibodies are costly to produce, which restricts the use of ADCs in the treatment of infectious diseases, such as those that occur in low-income countries. To overcome these limitations, peptides have been investigated as a substitute for antibodies as targeting devices. The smaller size of peptides leads to lower production costs—as they can be produced *via* cheaper synthetic or recombinant expression methods—whilst maintaining the benefit of high target selectivity observed with antibodies.[29]

1.1.3 Peptide–drug conjugates (PDCs)

PDCs represent the next generation of targeted therapeutics, with the aim of extending such therapies beyond cancer treatment. Consistent with ADCs, PDCs consist of three components: a peptide as the targeting moiety, a linker region and a small molecule drug. The peptide component can include a cell-targeting peptide (CTP), which recognises a specific target and directs the drug to disease-causing cells, a cell-penetrating peptide (CPP) that can assist with internalisation of the conjugate into cells, or comprise a combination of both characteristics.[30] CTPs often enter the cell in a similar manner to antibodies, however, the uptake of CPPs can occur *via* energy-dependent processes such as endocytosis or energy-independent translocation routes.[31] This means that the peptide scaffold can be tailored to the disease application and does not rely on the overexpression of receptors as the only targeting mechanism. Further information about types of peptides that can target disease-causing cells can be found in Section 1.3.1.

Currently, only one PDC has received FDA approval and is used for treatment of gastrointestinal, pancreatic and neuroendocrine tumours.[d] Approved in 2018, ^{177}Lu-dotatate (**1.2**) contains a chelated radionucleotide conjugated to a peptide that binds to the somatostatin receptor (Figure 1.4). This receptor is overexpressed on the surface of tumour cells, allowing for targeted delivery of cytotoxic radiation to cancer cells.[32] Additionally, multiple

[c] The number of approved ADCs provided here excludes any ADCs that have been withdrawn from the market or do not have current FDA approval (but may be approved for clinical use elsewhere).
[d] Another PDC, melflufen (Pepaxto) was approved by the FDA in 2021, however, was withdrawn from the market in the same year due to Phase 3 clinical failure.[113]

radionucleotide–peptide conjugates have been approved for imaging purposes and over 90 PDCs are in clinical trials, all for the diagnosis or treatment of various cancers.[28,33] While cancer therapeutics have been a prominent area of PDC development, researchers have begun to extend their application into the treatment of pathogens, such as viruses and bacteria, inflammation and neurodegenerative diseases.[14]

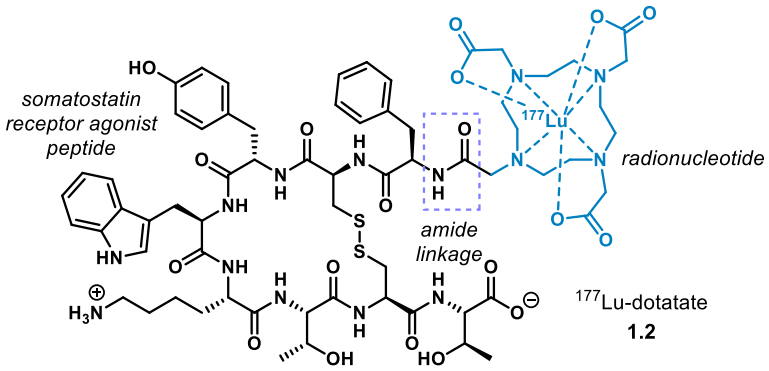

Figure 1.4. The structure of FDA approved PDC ^{177}Lu-dotatate (**1.2**), consisting of a peptide (octreotate) that binds to the somatostatin receptor, which is expressed on the cancer cell surface. This allows for targeted delivery of a radionucleotide to the cancer cells. Octreotate sequence: D-Phe-c(Cys-Tyr-D-Trp-Lys-Thr-Cys)-Thr.

1.2 Design features of PDCs

Design is an important aspect of PDC construction and is not as straightforward as joining all components together. The activities and limitations of the small molecule drug, linker and peptide must be considered to ensure that the resulting PDC provides synergy between each component.[14] It is also important to examine the structure of the peptide and drug to determine optimal sites to connect the independent molecules, as the conjugation site and strategy must not impede the peptide or drug from carrying out their intended mechanism of action. Incorporation of a cleavable linker, that allows for targeted drug release from the peptide, can be beneficial to maintain the activity of each component, however, must not result in premature drug liberation. Other linker properties, such as length and hydrophilicity, can be varied to enhance water solubility, improve flexibility and reduce steric hindrance between the peptide and drug.[14] The following subsections will detail aspects of PDC design to showcase why it is important to select components and conjugation strategies that complement each other for a successful PDC approach.

1.2.1 Click chemistry as a conjugation strategy

An important aspect of a PDC approach involves how the peptide and drug components will be covalently joined together. Click reactions, a class of modular “spring-loaded” transformations, are rapidly becoming exemplar tools for conjugation. A transformation is considered a click reaction if it is high yielding, wide in scope, stereospecific, generates only inoffensive by-products and employs simple reaction conditions.[34] Due to their favourable properties, click reactions are routinely utilised to conjugate a variety of compounds together,

including drugs, fluorescent probes and biomolecules. For PDC construction, a drug cargo can be attached to a peptide *via* reaction with either proteinogenic amino acids or a bioorthogonal functional group that has been incorporated during peptide synthesis.

Functionalisation of proteinogenic amino acids. An operationally simple method of bioconjugation involves the late-stage modification of proteinogenic amino acids within the peptide sequence. This is beneficial as the peptide can be synthesised using routine synthetic or recombinant expression methods, without the requirement for additional expensive reagents to install alternate functional groups. The most widely used amino acid for bioconjugation is cysteine (Cys), due to the nucleophilic character of its side chain at physiological pH.[35] Thiols readily react *via* a selective click reaction involving a Michael-type addition, where the thiol of a Cys side chain (**1.3**) can undergo conjugate addition with an *N*-alkyl maleimide **1.4**, to form a maleimide-thiol linkage **1.5** (Scheme 1.1A). Seven of the eleven approved anticancer ADCs contain a maleimide-thiol linkage (*e.g.* see **1.1** in Figure 1.3A), showcasing the suitability of this click reaction as a bioconjugation strategy.[35] However, the reversibility of the Michael addition may result in premature liberation of the drug from the antibody *via* a retro-Michael reaction (Scheme 1.1A). The eliminated maleimide can then react with endogenous thiols, increasing the opportunity for off-target interactions.[36]

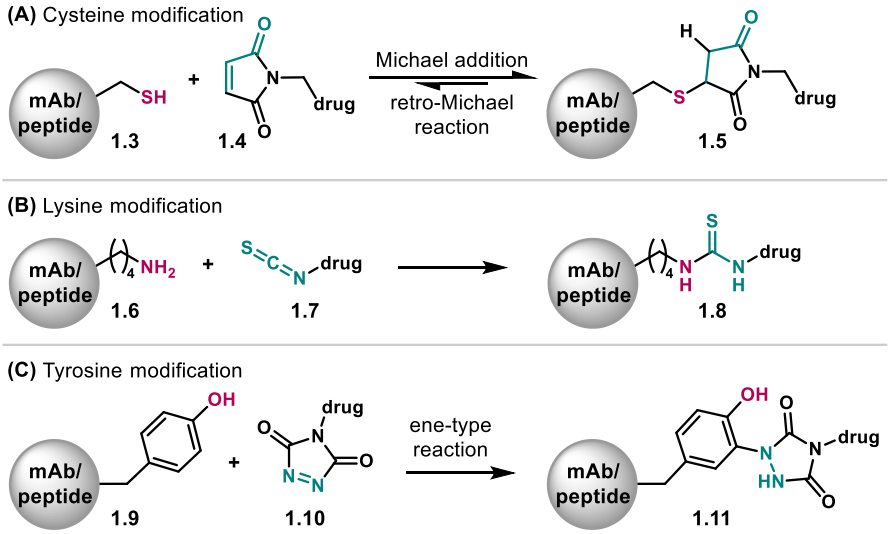

Scheme 1.1. Examples of bioconjugation strategies that utilise proteinogenic amino acids, including (A) cysteine, (B) lysine and (C) tyrosine.

Lysine (Lys) is an abundant amino acid within proteins that contains a nucleophilic ε-amino side chain that can be modified under mild conditions for bioconjugation.[35] Reactions have to be amine-selective due to competition from the nucleophilic Cys side chain. One example of such a reaction is the conversion of the Lys side chain (**1.6**) into a thiourea moiety (**1.8**) using an isothiocyanate derivative (**1.7**) modified to contain a cargo (Scheme 1.1B). This method has been extensively used in the labelling of biomolecules with fluorescein isothiocyanate.[35,37] The selectivity for amine functional groups arises from the irreversible formation of a stable thiourea

linkage, which does not occur with other nucleophiles, such as thiols. However, the routine use of isothiocyanates as a bioconjugation tool is limited by their poor water solubility and the harsh and toxic conditions required for their synthesis.[38] The development of other reagents for Lys modification, including iminoboronates[39,40] and diazonium salts,[41] has improved on these drawbacks.

It should be noted that conjugation strategies involving Cys and Lys can also entail non-click chemistry reactions. As Cys is readily oxidised into its disulfide form, components in a drug conjugate can be linked *via* a disulfide bond. Additionally, nucleophilic thiols are amenable to a rebridged disulfide strategy. Following disulfide reduction, two thiols can be linked together with a reactive bis-electrophile (*e.g.* a dibromomaleimide reagent) that contains an attached cargo.[42] For Lys, conjugation can be achieved with conventional amide bond formation, *via* reaction of the amine side chain with a cargo coupling partner that contains an activated acyl group (*e.g. N*-hydroxysuccinimide ester).[43] Four of the approved ADCs and the only approved PDC contain the drug attached *via* an amide bond—to Lys residues for the former and at the peptide N-terminus for the latter (see Figure 1.4).[22,23,32] While amide bond formation is a reliable conjugation method, it is not always chemoselective and may require careful protecting group strategies to obtain drug attachment at the correct position.[43]

Although the majority of bioconjugation strategies involving proteinogenic amino acids target Cys and Lys, there are a few examples of click reactions that are selective for other amino acid side chains. For example, the phenol side chain of tyrosine (**1.9**) can selectively react *via* an ene-type cycloaddition with phenyltriazolinediones bearing a drug cargo (**1.10**), to form a stable C–N linkage (**1.11**) on the aromatic ring (Scheme 1.1C).[44,45] While providing a promising alternative to Cys and Lys approaches, the tyrosine-click reaction is yet to gain traction as a mainstay conjugation strategy. There is considerable value in the continued discovery of alternative proteinogenic bioconjugation strategies to complement traditional methods, including strategies that utilise unconventional reactivity modes of amino acids,[46] or those that allow for modification of previously untargetable residues.[47,48]

Conjugation via a bioorthogonal functional group. It may not always be possible to selectively install a cargo onto proteinogenic amino acids. In the case of a peptide, especially in a short peptide with few residues, an amino acid suitable for conjugation may not be present in the sequence or may be essential for peptide activity or structure. For example, the available Cys residues may be involved in disulfide bonds that are imperative for structure and rigidity or may be important for target binding or peptide function. In these situations, a bioorthogonal conjugation strategy, that utilises functional groups that are not present in endogenous biomolecules, can be beneficial. Copper-catalysed azide–alkyne cycloaddition (CuAAC), independently reported in 2002 by the groups of Sharpless[49] and Meldal,[50] is often referred to

as the quintessential bioorthogonal click reaction. The CuAAC reaction utilises copper(I) to catalyse the formation of a 1,4-disubstituted 1,2,3-triazole **1.14a** from a terminal alkyne **1.12** and an azide **1.13** (Scheme 1.2A). The addition of Cu(I) in the CuAAC reaction results in an acceleration of the rate and enhancement of regioselectivity in comparison to the uncatalysed azide–alkyne cycloaddition, originally proposed by Huisgen (Scheme 1.2B).[51,52]

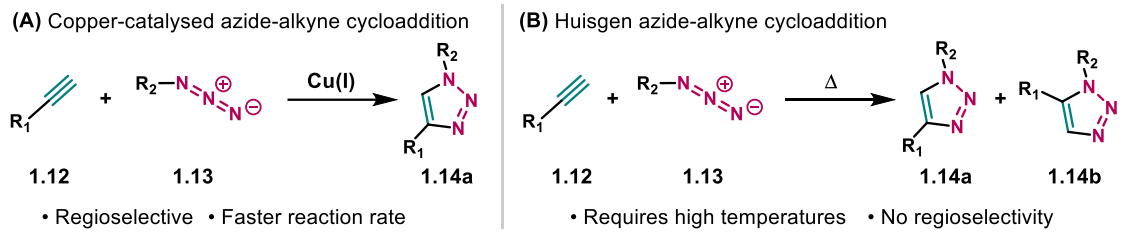

Scheme 1.2. (A) Azide–alkyne cycloaddition using a copper(I) catalyst, reported by Sharpless[49] and Meldal.[50] One regioisomer (**1.14a**) is produced from this reaction. (B) Azide–alkyne cycloaddition, originally reported by Huisgen, which gives two regioisomers (**1.14a** and **1.14b**) as the products.[52]

CuAAC reactions are a valuable tool for bioorthogonal conjugation because the reagent functionalities (**1.12** and **1.13**) are essentially absent in a biological setting and the triazole product (**1.14a**) is not prone to oxidation, reduction or hydrolysis.[53,54] However, Cu(I)-species are generally toxic to organisms, hindering the *in vivo* use of the CuAAC reaction. Cytotoxicity can be reduced through the addition of water-soluble Cu(I) ligands, allowing for CuAAC reactions to be conducted in the presence of cells.[54] The cytotoxicity of the Cu(I)-species is less of an issue for PDC synthesis, as this is not conducted inside an organism, however, requires complete removal of the catalyst prior to biological treatment. The development of strain-promoted azide–alkyne cycloaddition (SPAAC) by Bertozzi and co-workers (Scheme 1.3A),[55] which does not require the Cu(I) catalyst, has further improved the biocompatibility of azide–alkyne cycloadditions.

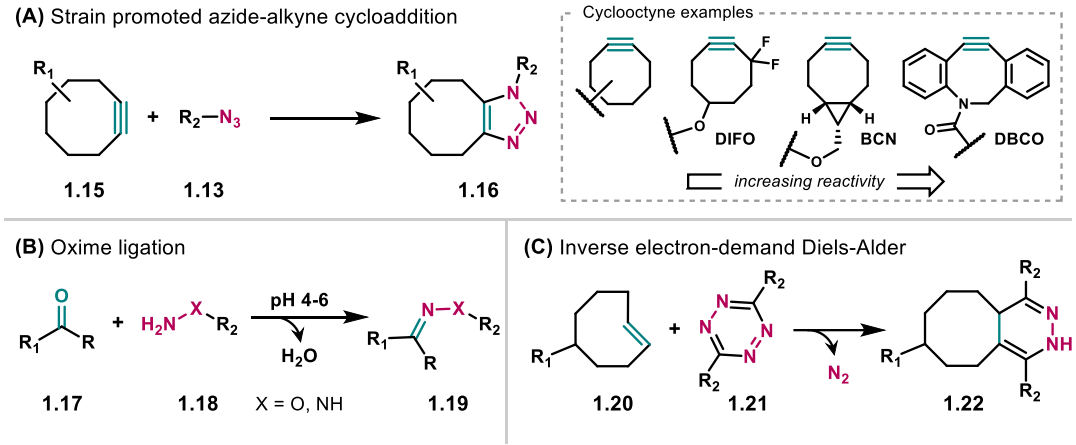

Scheme 1.3. Additional examples of bioorthogonal click reactions. (A) Strain promoted azide–alkyne cycloaddition, including examples of cyclooctyne derivatives. DIFO: difluorocyclooctyne, BCN: bicyclononyne, DBCO: dibenzocyclooctyne. (B) Oxime ligation. (C) Inverse electron-demand Diels–Alder.

The SPAAC reaction is driven by the release of ring strain from a cyclooctyne species (**1.15**), eliminating the requirement for an exogenous catalyst (Scheme 1.3A). While the resulting triazole (**1.16**) usually consists of two regioisomers—unless a symmetric cyclooctyne is used—the mild, physiological conditions required for product formation have cemented this click-like reaction as a useful strategy for bioconjugation.[35,56] Unfortunately, the reaction kinetics of SPAAC are relatively slow compared to CuAAC, however, the reaction rate can be improved by functionalising the cyclooctyne. Generally, the rate can be enhanced by adding electron withdrawing groups onto the cyclooctyne (*e.g.* difluorocyclooctyne, DIFO) or by increasing cyclooctyne ring strain with fused ring systems (*e.g.* bicyclononyne, BCN and dibenzocyclooctyne, DBCO, Scheme 1.3A).[56] While such cyclooctynes can be beneficial for the rate, the extra bulk can result in concomitant drawbacks. For example, the dibenzoannulated DBCO alkyne can produce undesirable steric interactions and lipophilicity.[56]

The ketone functional group, which is not present in proteinogenic amino acids, can be utilised as a another bioconjugation handle *via* a condensation reaction.[35] A ketone (**1.17**) can react with a nucleophile (**1.18**) such as an alkoxyamine (if X = O) or hydrazine (if X = NH) under acidic conditions (pH 4-6) to form an oxime or hydrazone linkage (**1.19**), respectively (Scheme 1.3B). These condensation reactions have been a powerful tool for fluorescent labelling of biomolecules, although often have slow reaction kinetics.[54] In comparison, the inverse electron-demand Diels–Alder (IEDDA) reaction is one of the fastest bioorthogonal conjugation strategies. As first used by the Fox group,[57] a tetrazine (**1.21**) can undergo an IEDDA cycloaddition with either a strained alkene or alkyne (*e.g. trans*-cyclooctene **1.20**) followed by a retro-Diels–Alder reaction to yield a dihydropyridazine linked compound (**1.22**), with nitrogen gas as the only byproduct (Scheme 1.3C). Additional bioorthogonal conjugation reactions include the Staudinger ligation,[58–60] photoclick 1,3-dipolar cycloaddition,[61] cross-coupling[62,63] and strain-promoted alkyne–nitrone cycloaddition.[64,65]

1.2.2 Incorporation of bioorthogonal handles for conjugation

For a bioorthogonal click reaction to be a feasible conjugation strategy, the required functional groups need to be incorporated into the drug and peptide components of the PDC. Many small molecule drugs contain conventional functional groups that are amenable to further modification, including amines, carboxylic acids and alcohols, to install bioorthogonal moieties (Figure 1.5A). Functional groups such as aryl halides and heteroaromatic C–H bonds represent nonconventional handles that can be exploited if conventional functional groups are essential for activity of the drug or are not present in the structure. In comparison, unnatural amino acids bearing bioorthogonal functional groups can be incorporated into peptides during solid-phase peptide-synthesis (SPPS). Using CuAAC as an example, one approach is to incorporate an alkyne into the drug cargo and an azide into the peptide. To this end, an alkyne-

functionalised linker can be installed onto either a conventional or nonconventional handle of the small molecule drug (Figure 1.5A). The azide functionality can be readily incorporated into an amino acid side chain using methods described by Jiráček and co-workers,[66] allowing for incorporation of an azide handle during SPPS (Figure 1.5B).

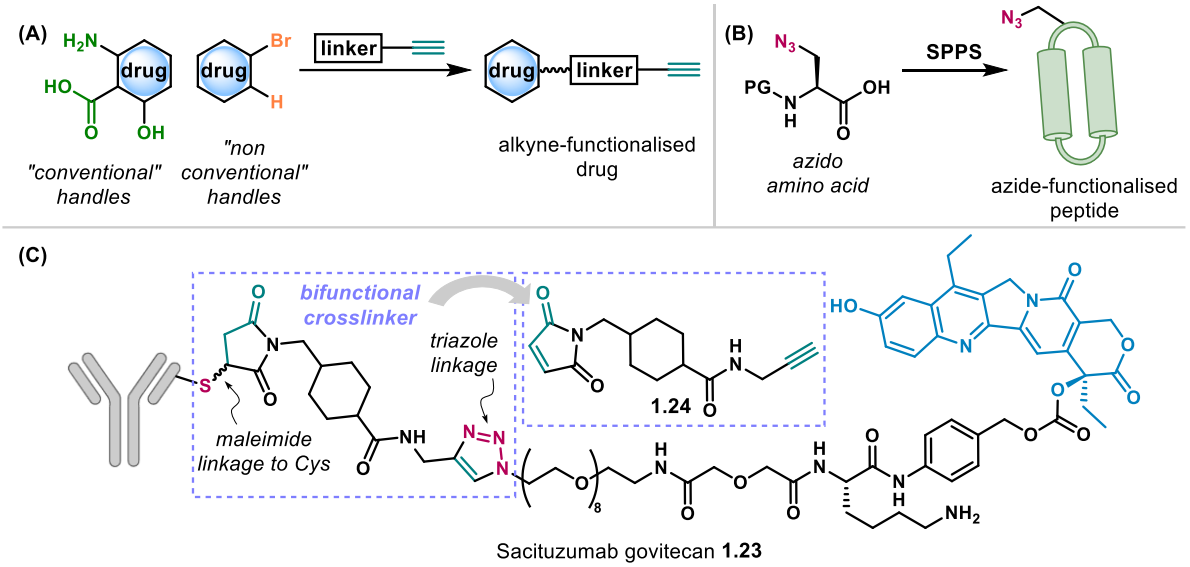

Figure 1.5. (A) Conventional (green) and nonconventional (orange) functional groups on a small molecule drug that can be used for alkyne attachment. (B) Incorporation of an azide-containing unnatural amino acid into a peptide *via* SPPS. (C) The structure of sacituzumab govitecan (**1.23**), an ADC that contains a bifunctional crosslinker (**1.24**).

It is also possible to install bioorthogonal functional groups through incorporation of a bifunctional crosslinker (*e.g.* **1.24**), that utilises a mixture of conjugation strategies to link the drug and biomolecule together. Sacituzumab govitecan (**1.23**) is an ADC approved by the FDA that contains an example of a bifunctional crosslinker (purple boxes, Figure 1.5C).[23] One end of **1.24** consists of an alkyne that can join the spacer region to the pH sensitive cleavable linker *via* a CuAAC reaction. The other end, that reacts with the antibody, contains a maleimide for attachment to Cys residues. Implementing the crosslinker negates the requirement for alkyne incorporation into the antibody, while promoting increased spacing and hydrophilicity between the drug and antibody components.[67] With a wealth of bioconjugation strategies available to link a drug and biomolecule together, one can be carefully chosen depending on the application, the conjugation handles present within the molecules and the desired type of linker technology.

1.2.3 Linker technologies

The linker region between the drug and biomolecule plays an important role in the function and selectivity of a drug conjugate. To be effective, the linker needs to be stable during circulation, have hydrophilic character to prevent aggregation and allow for efficient release of the drug under specific conditions.[18] Certain properties of the linker, such as linker length, water solubility and cleavability can be varied to meet these requirements.

PDC linkers are generally categorised as cleavable or non-cleavable, depending on how the drug is released from the peptide. Cleavable linkers, that allow for targeted drug release, exploit specific conditions at the disease-causing cells to trigger linker degradation. Such linkers can be further characterised as enzyme-cleavable or chemically cleavable linkers, depending on the cleavage mechanism.[18]

Non-cleavable linkers. A non-cleavable linker does not contain an inbuilt chemical moiety that can trigger targeted drug release.[18] For a PDC, the drug can eventually be released from the conjugate following proteolysis of the peptide, however, this usually leaves behind the linker and an amino acid appended to the drug. Non-cleavable linkers offer the benefit of plasma stability and limited premature drug liberation, often resulting in low off-target toxicity.[68] Trastuzumab emtansine (**1.25**) is an ADC with FDA approval that contains a non-cleavable linker between a HER2-targeting antibody and the microtubule inhibitor mertansine (Figure 1.6). Following proteolytic degradation of the antibody portion of the ADC in the lysosome, the mertansine-containing compounds are still able to inhibit microtubule formation, despite the linker and attached Lys residue being connected to the drug.[69] For a PDC approach, non-cleavable linkers are simple to install so are beneficial if drug activity is maintained following modification and peptide attachment. However, if the drug pharmacophore is irreversibly modified by peptide attachment or the drug cannot reach its intracellular target, then a linker that allows for traceless release of the drug from the peptide may be required.

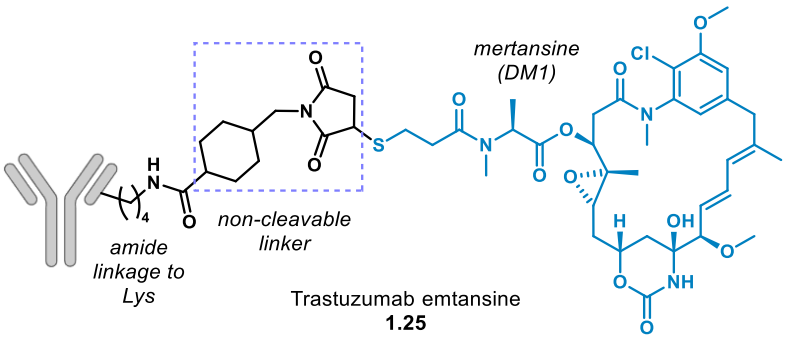

Figure 1.6. The structure of trastuzumab emtansine (**1.25**), consisting of an anti-HER2 antibody joined to mertansine (also known as DM1), a microtubule inhibitor. The drug and antibody are attached *via* a non-cleavable linkage (purple box).

Enzyme-cleavable linkers. Abundant enzymes found in the lysosomes and endosomes of disease-causing cells, such as cancer cells, can be exploited for intracellular drug release.[70] For instance, esterases and amidases are often overexpressed in these cells, leading to a collection of PDCs that have emerged containing a strategic amide or ester linkage, with the aim that these enzymes will liberate the drug once at the target cell.[71–74] Lysosomal proteases, such as cathepsin B, are also often overexpressed in tumour cells and provide a logical target for linker cleavage.[70]

Protease-sensitive linkers, such as the valine-citrulline (Val-Cit) dipeptide **1.26** (Figure 1.7A),[75] are perhaps the most utilised cleavable linker in ADC and PDC research.[18] Indeed, five of the eleven FDA approved ADCs contain a protease-sensitive dipeptide linker, as seen in brentuximab vedotin **1.1** (see Figure 1.3A).[23] These linkers are cleaved in the lysosome by carboxypeptidases, such as cathepsin B, upon cell internalisation of a conjugate *via* endocytosis.

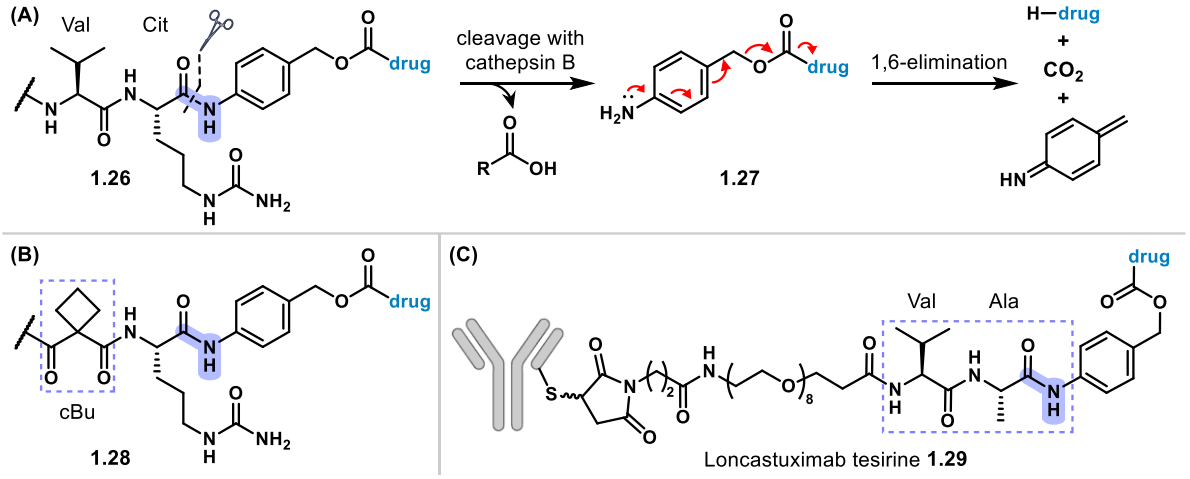

Figure 1.7. (A) The structure and mechanism of the valine-citrulline (Val-Cit) linker **1.26**, a protease-sensitive linker that is cleaved by cathepsin B in the lysosome. (B) The structure of the peptidomimetic dipeptide linker **1.28**,[76] containing a cyclobutane-1,1-dicarboxamide moiety. (C) The structure of loncastuximab tesirine **1.29**, that contains a valine-alanine (Val-Ala) linker. Drug = pyrrolobenzodiazepine dimer.

The Val-Cit sequence is usually coupled with a *p*-aminobenzyloxycarbonyl (PABC) moiety (Figure 1.7A), which functions as a spacer between the dipeptide and payload, to prevent steric hindrance from the drug interfering with the activity of cathepsin B.[22] Following sequence recognition and proteolysis on the C-terminal side of the dipeptide within **1.26** (purple highlight, Figure 1.7A), the PABC spacer moiety **1.27** undergoes a spontaneous 1,6-elimination to release the unmodified drug. However, despite success in the clinical setting, the plethora of research surrounding this linker has revealed some downfalls, especially in the ADC space. The discovery that the Val-Cit linker could be processed by a variety of cathepsins—not only cathepsin B—which could result in off-target cleavage in normal cells, has prompted the design of alternative peptide-based linker structures.[77] The development of a peptidomimetic linker (**1.28**) by Wei *et al.*, containing a cyclobutane-1,1-dicarboxamide (cBu) moiety (purple box, Figure 1.7B), led to improved selectivity for cathepsin B cleavage compared to the Val-Cit linker.[76] Additionally, issues with aggregation and precipitation of the Val-Cit linker have driven research towards less hydrophobic linkers, such as the valine-alanine (Val-Ala) dipeptide,[78] which features in the recently approved ADC loncastuximab tesirine **1.29** (Figure 1.7C).[79]

Chemically cleavable linkers. The intracellular chemical environment of diseased cells can also be exploited for linker cleavage. The acidity of the lysosomal (pH 4.5–5.0) and endosomal

compartments (pH 5.5–6.2) is a property that can be utilised for selective cleavage inside cells, because it differs from the near neutral pH experienced by a PDC during circulation (pH 7.4).[18] Acid-labile functional groups, such as a hydrazone or carbonate, provide opportune linkers for this strategy. For instance, hydrazone linker **1.30** hydrolyses into acyl hydrazide **1.31** and ketone **1.32** when exposed to an acid catalyst (Scheme 1.4A). In this approach, a hydrazide or ketone appendage remains on the drug after cleavage, so works best for payloads that contain these functional groups within their structure. For example, PDCs containing the anticancer drug doxorubicin (**1.33**), a cytotoxic agent that contains a ketone moiety, successfully provide the unmodified drug after linker hydrolysis when a hydrazone linker strategy is used (Scheme 1.4A).[80–82] For drugs where this is not feasible, strategies that allow for traceless release have been developed, including incorporation of a self-immolative 2-amino-2-methylpropanoic carbamate spacer between the hydrazone and payload.[83]

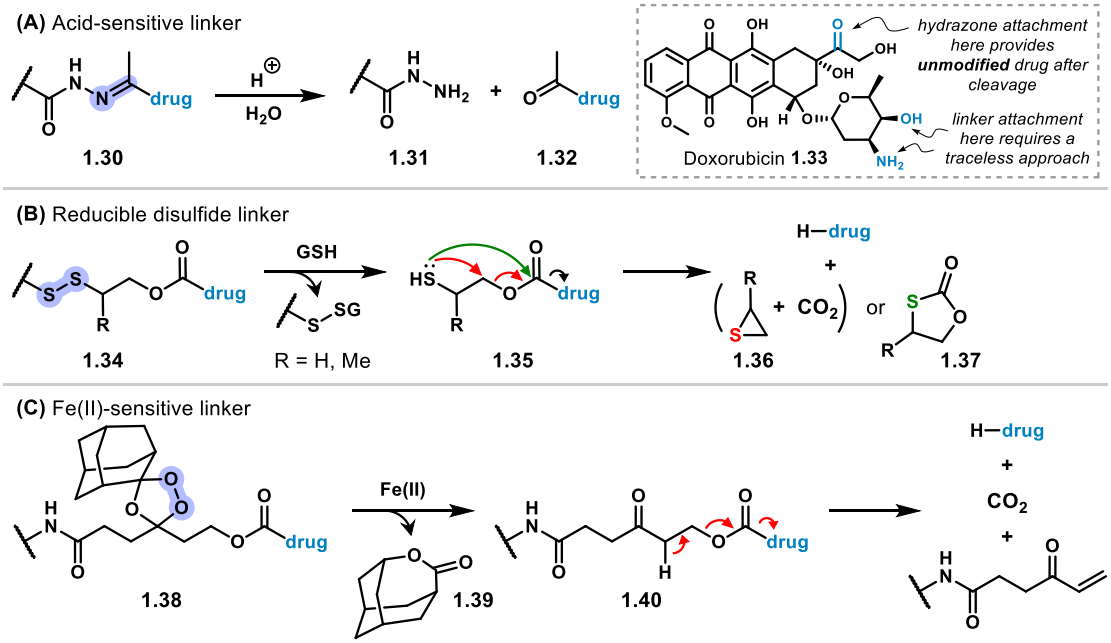

Scheme 1.4. (A) Cleavage of an acid-sensitive hydrazone linker (**1.30**) and the structure of doxorubicin (**1.33**), with conjugation handles highlighted. (B) Cleavage mechanism of a reducible disulfide linker (**1.34**), involving traceless release of the drug. GSH = glutathione (γ-glutamyl-cysteinyl-glycine). (C) A Fe(II)-sensitive cleavable linker (**1.38**) developed by Renslo and co-workers[84,85] containing a 1,2,4-trioxolane moiety, featuring traceless drug release.

Variations in the plasma stability of hydrazone linkers have prevented their widespread use in ADC and PDC research, due to concerns of increased off-target effects if premature hydrolysis occurs.[86] Nevertheless, two approved ADCs feature a hydrazone linker, both for the treatment of haematological cancers. More recently, other acid-sensitive groups, such as acetals and carbonates, have garnered attention as alternatives to the hydrazone linker. Sacituzumab govitecan (**1.23**), displayed in Figure 1.5C, contains an acid-labile carbonate as the cleavable functionality.[67]

The reductive environment inside cells, which arises from high levels of glutathione (GSH), is a second property that can be exploited for linker cleavage. The intracellular concentration of GSH (1–10 mM) is several-fold higher than the extracellular concentration (<20 μM),[87] providing an opportunity for selective drug release inside diseased cells. Disulfide containing linkers have thus been developed, as they are susceptible to nucleophilic attack from thiols such as GSH.[18] The simplest approach to a redox-sensitive linker involves incorporation of a disulfide bond between the payload and biomolecule, resulting in release of a thiolated drug following disulfide reduction. A self-immolative strategy that enables traceless payload release is also possible if the drug contains an alcohol, amine or hydrazine functional group.[88–90] In this approach, the free thiol (**1.35**) that is produced after disulfide reduction of **1.34** with GSH can release the unmodified drug *via* elimination of thiirane **1.36** and carbon dioxide (red arrows) or oxathiolanone **1.37** (green arrow) (Scheme 1.4B).

The stability of the disulfide linkage during circulation can be improved through α-methyl substitutions. Generally, an intermediary level of substitution (*e.g.* one α-methyl group) is beneficial as heavily substituted disulfides are sterically hindered and thus resistant to reduction.[91,92] Disulfide linkers are present in three of the FDA approved ADCs, however, the traceless variation of this linker class is yet to be seen in a clinical setting.[23] It should be noted that the conditions required for the cleavage of acid-sensitive and reduction-sensitive linkers are not specific to diseased cells, so such linkers may be cleaved if the conjugate is able to enter healthy cells.

Abnormal iron metabolism is another hallmark of disease-causing cells, that results in high levels of unbound ferrous iron inside these cells compared to human plasma.[93] Renslo and co-workers utilised this property to develop a novel cleavable linker featuring an iron-labile 1,2,4-trioxolane moiety (**1.38**).[84,85] In the presence of ferrous iron, the O–O peroxide bond of **1.38** is cleaved by a Fenton-type reaction, affording an oxygen-centred radical that ultimately leads to the elimination of adamantane lactone (**1.39**) from the linker scaffold (Scheme 1.4C). Subsequently, the resulting retro-Michael substrate **1.40** undergoes *β*-elimination and decarboxylation to release the unmodified drug. The trioxolane linker has been utilised in an ADC context but is yet to feature in a PDC.[85]

Ultimately, the comprehensive ensemble of conjugation strategies and linker technologies discussed throughout this section provides evidence that design is a crucial aspect of the PDC approach. Through the exploration of the benefits and limitations of each technique it is apparent that no superior strategy exists. Rather, PDC design is application specific and likely requires a systematic structure-activity relationship-style approach to determine the key characteristics for potent and efficacious PDCs.

1.3 Peptides as a targeting moiety

1.3.1 Types of peptides that target disease-causing cells

The final component in PDC design is the peptide scaffold itself, which is of critical importance to ensure an effective PDC strategy. Ideally, the peptide should have sufficient target recognition, high stability during circulation, low toxicity to healthy cells and efficient cell internalisation.[30] Peptides utilised in PDCs are generally categorised as either cell-targeting peptides (CTPs) or cell-penetrating peptides (CPPs).

Cell-targeting peptides. CTPs are peptides that have high recognition and affinity for a specific cellular target associated with a disease, typically a cell-surface receptor.[94] They have attracted considerable attention as peptide scaffolds for PDCs, due to their small size and similar functionality to antibodies. Like an antibody, the mechanism of a CTP involves binding to its target on the cell surface, followed by internalisation *via* endocytosis (*i.e.* similar to Figure 1.3B), making them ideal candidates for drug delivery.[28] CTPs have proved to be successful for a PDC strategy, with the FDA approved ^{177}Lu-dotatate **1.2** (see Figure 1.4) containing a peptide that recognises and binds to the somatostatin hormone receptor. Furthermore, many PDCs in clinical trials contain a CTP as the peptide scaffold.[30] One limitation of CTPs is that they rely on the expression of a specific target to exert their mechanism of action, however, techniques such as phage display can be used to discover peptides that bind to novel targets on disease-causing cells.[28]

Cell-penetrating peptides. Peptides that can traverse biological membranes, known as CPPs, also provide an opportunity to deliver drugs into diseased cells. Most CPPs are either cationic or amphipathic in nature, however, anionic and hydrophobic examples also exist.[95] These peptides can cross through cell membranes *via* either energy-independent pathways, such as direct translocation, or energy-dependent pathways, such as endocytosis.[96] While CPPs provide a useful tool for intracellular delivery, especially for cell impermeable cargoes, their widespread use in PDC research has been hindered by the non-specific cell entry sometimes associated with these peptides. This limitation is mostly observed for cationic CPPs, so PDC strategies have turned to amphipathic and anionic CPPs to improve selectivity for disease-causing cells over healthy cells.[30]

1.3.2 PDIP and cGm6 are CPPs derived from host defence molecules

Platelet factor 4-derived internalisation peptide (PDIP)[97] and cyclic gomesin analogue 6 (cGm6; also known as [G1K,K8R]cGm)[98] are two CPPs utilised throughout this thesis in the design and construction of antimalarial and anticancer PDCs. cGm6 is derived from an antimicrobial peptide (AMP) and PDIP is designed from an AMP-like protein domain. AMPs are a class of peptides with antimicrobial activity that are produced by many organisms as part of their host defence mechanisms. The majority of AMPs are amphipathic, consisting of both cationic and

hydrophobic residues, which confers their selectivity for negatively charged microbial membranes over the neutral membranes of healthy cells.[95] In healthy cells, anionic lipids such as phosphatidylserine (PS) are maintained in the inner leaflet of the membrane by flippase enzymes,[99] providing a distinct feature that an AMP can exploit for selective killing of pathogens. The mechanism of many AMPs is to lyse the cell membrane, however, some can instead cross it to gain access and inhibit specific intracellular processes.[100] AMPs have been utilised as the peptide scaffold and paired with antibiotics for antibacterial treatment,[101] however, are underexplored as the delivery tool in other disease contexts. The remainder of this section will showcase why PDIP and cGm6 are attractive peptide scaffolds for PDCs, due to the combination of CPP and AMP characteristics they possess.

Platelet factor 4-derived internalisation peptide (PDIP). PDIP is a peptide designed by McMorran and co-workers from platelet factor 4 (PF4), a human defence protein.[97] PF4 is a tetrameric chemokine that is released from activated platelets in response to infection with the malaria parasite *Plasmodium falciparum* and can kill the parasite by lysing its digestive vacuole.[102,103] This activity is attributed to the AMP-like domain of PF4, an amphipathic α-helical domain, that is located on the C-terminus of each monomer (black box, Figure 1.8A). The original PDIP analogue, known as cPF4PD (**1.41**), is a synthetic analogue derived from PF4, comprising a head-to-tail dimer of the α-helical domain that is cyclised *via* a disulfide bond for stability, to mimic the paired AMP domains in the PF4 tetramer (Figure 1.8B and C). The minimised peptide can selectively internalise into red blood cells (RBCs) infected with *P. falciparum* and can enter without receptor binding, a requisite for entry of the parent protein. Furthermore, it recapitulates the mechanism of killing displayed by PF4, is stable to protease degradation and has low haemolytic activity (Figure 1.8D).[97]

The α-helical domain of cPF4PD contains both hydrophobic and positively charged Lys (K) residues (see Figure 1.8C for sequence). Since infected RBCs have increased proportions of negatively charged PS lipids on the outer membrane leaflet compared to uninfected RBCs,[104] electrostatic interactions between the anionic membrane environment and the outward facing Lys residues on the α-helices confers the preferential entry of cPF4PD into these cells. Furthermore, these amphipathic helices drive the disruption of the parasite digestive vacuole membrane, which contains negatively charged phosphatidylinositol 3-phosphate lipids.[105]

The surface exposure of PS lipids is also a hallmark of cancer cells.[106] Concurrent exploration of the anticancer activity of cPF4PD revealed potency against melanoma (MM96L) and leukaemia (K562) cell lines (Figure 1.8D), attributed to the disruption of mitochondrial membrane function.[107] Additionally, cPF4PD has been shown to be capable of delivering cargo into both *Plasmodium*-infected and cancer cells *via* direct translocation across the plasma membrane, without entering or damaging healthy cells.[97,107,108] Therefore, we postulated that

cPF4PD could serve as the peptide partner for antimalarial and anticancer drugs, to enable selective drug delivery. This study utilises an analogue of cPF4PD, known as PDIP (**1.42**), which contains an additional glycine (Gly) residue at the N-terminus (Figure 1.8C), but retains the same features as the original analogue.

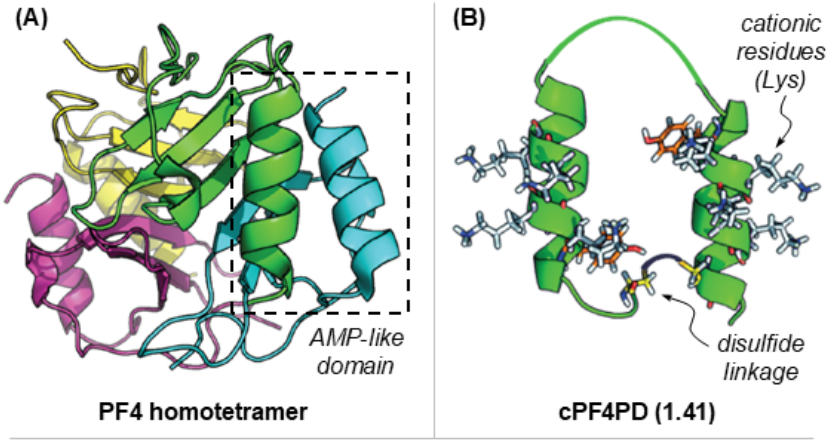

(C) cPF4PD (**1.41**): CGGPLYKKIIKKLLESGGSGGAPLYKKIIKKLCES*

PDIP (**1.42**): GCGGPLYKKIIKKLLESGGSGGAPLYKKIIKKLCES*

(D)

	Pf IC_{50} (μM)	MM96L CC_{50} (μM)	K562 CC_{50} (μM)	RBC HC_{10} (μM)
PF4	0.6			
cPF4PD	4.3	4.1	5.7	>100

Figure 1.8. (A) Structure of the PF4 tetramer (PDB: 1F9Q), with the C-terminal AMP-like domain highlighted (black box). (B) Predicted structure of cPF4PD (**1.41**), showing the outward facing lysine residues (white sticks). (C) Primary amino acid sequence for the cPF4PD and PDIP analogues. Residues contributing to the α-helices are coloured green. Disulfide bonds are displayed with grey lines. * = amidated C-terminus. (D) Summary of the activity of the cPF4PD analogue against *P. falciparum* (*Pf*), melanoma (MM96L) and leukaemia (K562) cell lines, and haemolytic activity against RBCs.[97,107] IC_{50} = half maximal inhibitory concentration. CC_{50} = half maximal cytotoxicity concentration. HC_{10} = concentration required for 10% lysis of RBCs.

Cyclic gomesin analogue 6 (cGm6). cGm6 is a synthetic derivative of gomesin (Gm, **1.43**), a host defence peptide originally isolated from the haemocytes of the tarantula spider *Acanthoscurria gomesiana*.[109] Gm is an amphipathic AMP that can kill pathogens such as bacteria, yeast and fungus. It consists of a β-hairpin structure that is stabilised by two disulfide bonds and contains multiple positively charged arginine (R) residues (Figure 1.9A and B). Along with antimicrobial activity, Gm has been shown to be potent against melanoma and leukaemia cell lines (Figure 1.9C), attributed to its ability to selectively disrupt negatively charged microbial and cancer cell membranes.[98,110]

Daly and co-workers produced a backbone cyclised variant of Gm (cGm, **1.44**), which improved serum stability relative to the parent peptide, whilst maintaining its anticancer activity and low haemolytic properties (Figure 1.9A and C).[110] Henriques and co-workers further enhanced its potency by generating an analogue (cGm6, **1.45**) with an Arg replacing the

naturally occurring Lys (residue 8) and an additional positive charge, through replacement of a Gly residue with a Lys (residue 1) (Figure 1.9B).[98] Since cGm6 has been shown to enter cancer cells *via* endocytosis and direct membrane translocation mechanisms,[111] we proposed that it would also make an ideal candidate for drug delivery.

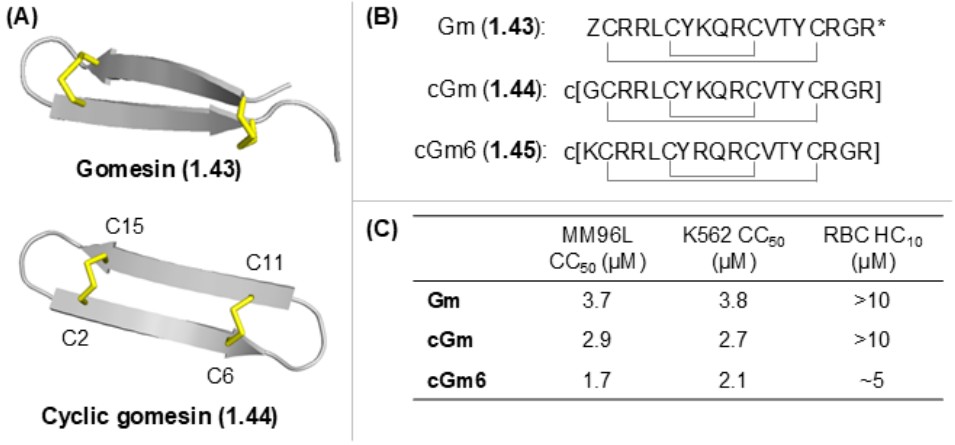

	MM96L CC_{50} (μM)	K562 CC_{50} (μM)	RBC HC_{10} (μM)
Gm	3.7	3.8	>10
cGm	2.9	2.7	>10
cGm6	1.7	2.1	~5

Figure 1.9. (A) Structure of Gm (**1.43**, PDB: 1KFP) and the structure of cGm (**1.44**, BMRB: 17986),[110] with the disulfide bonds highlighted in yellow. (B) Primary amino acid sequence for Gm, cGm and cGm6 analogues. Disulfide bonds are displayed with grey lines. Z = pyroglutamic acid, * = amidated C-terminus. (C) Summary of the activity of the gomesin analogues against melanoma (MM96L) and leukaemia (K562) cell lines, and haemolytic activity against RBCs.[98] CC_{50} = half maximal cytotoxicity concentration. HC_{10} = concentration required for 10% lysis of RBCs.

1.4 Aims and objectives

The overarching objective of this thesis is to design, synthesise and biologically evaluate a suite of PDCs in different disease contexts—for the treatment of an infectious disease, malaria, and a noncommunicable disease, cancer. Two CPP scaffolds with AMP-like characteristics and selectivity for diseased cells—PDIP (**1.42**) and cGm6 (**1.45**)—are utilised as drug delivery tools. As a PDC strategy, the use of AMPs as the targeting peptide remains underexplored for both malaria and cancer treatment. In the following chapters, small libraries of PDCs are produced with varying drugs, linkers, conjugation strategies and peptide scaffolds, to understand how these design features influence PDC potency. Structure–activity insights are used to optimise PDC design, which is found to be unique for each drug and peptide combination.

The chapters are subdivided based on the identity of the PDC drug cargo, as highlighted in Figure 1.10. Chapter 2 discusses our published proof-of-principle study for PDCs containing primaquine (**1.46**), as an alternative approach for malaria treatment. Chapter 3 explores anticancer PDIP conjugates containing the cytotoxic drug camptothecin (**1.47**) as the cargo. Chapter 4 focuses on PDIP and cGm6 PDCs containing vemurafenib (**1.48**), an anticancer drug with resistance issues. The relevant diseases and drugs will be further introduced at the beginning of each chapter. Finally, chapter 5 will outline the conclusions and future outlook for

the study, to highlight the versatility of PDCs as a targeted treatment approach and the insights gained for the design of future conjugates.

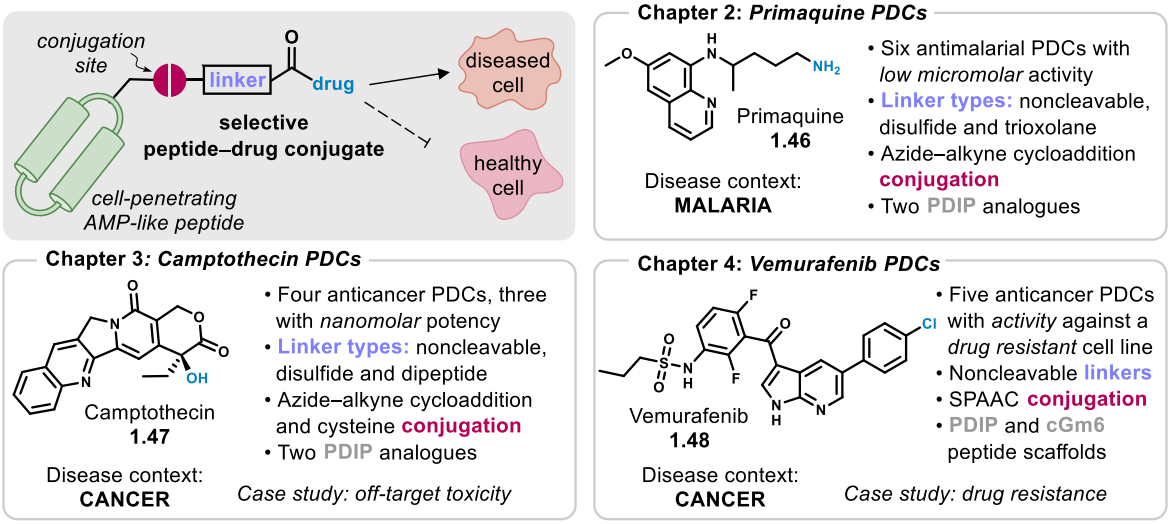

Figure 1.10. A summary of the work presented in this thesis. The overarching goal of this work is to design and synthesise PDCs, containing cell-penetrating AMP-like peptide scaffolds, with proposed selectivity for diseased cells (top left panel). The remaining panels highlight key aspects of studies that explore PDCs containing primaquine **1.46** (top right panel), camptothecin **1.47** (bottom left panel) and vemurafenib **1.48** (bottom right panel).

References

(1) Wang, L.; Wang, N.; Zhang, W.; Cheng, X.; Yan, Z.; Shao, G.; Wang, X.; Wang, R.; Fu, C. *Signal Transduct. Target. Ther.* **2022**, *7*, 48.

(2) Makurvet, F. D. *Med. Drug Discov.* **2021**, *9*, 100075.

(3) Zhong, L.; Li, Y.; Xiong, L.; Wang, W.; Wu, M.; Yuan, T.; Yang, W.; Tian, C.; Miao, Z.; Wang, T.; Yang, S. *Signal Transduct. Target. Ther.* **2021**, *6*, 201.

(4) Rao, M. S.; Gupta, R.; Liguori, M. J.; Hu, M.; Huang, X.; Mantena, S. R.; Mittelstadt, S. W.; Blomme, E. A.; Van Vleet, T. R. *Front. Big Data* **2019**, *2*, 25.

(5) Fosgerau, K.; Hoffmann, T. *Drug Discov. Today* **2015**, *20*, 122–128.

(6) Lau, Y. H.; de Andrade, P.; Wu, Y.; Spring, D. R. *Chem. Soc. Rev.* **2015**, *44*, 91–102.

(7) He, J.; Ghosh, P.; Nitsche, C. *Chem. Sci.* **2024**, *15*, 2300–2322.

(8) Li, X.; Wang, N.; Liu, Y.; Li, W.; Bai, X.; Liu, P.; He, C. Y. *Bioorg. Chem.* **2023**, *141*, 106892.

(9) Lu, J.; Jiang, F.; Lu, A.; Zhang, G. *Int. J. Mol. Sci.* **2016**, *17*, 561.

(10) de la Torre, B. G.; Albericio, F. *Molecules* **2024**, *29*, 585.

(11) Bergkessel, M.; Forte, B.; Gilbert, I. H. *ACS Infect. Dis.* **2023**, *9*, 2062–2071.

(12) Blasco, B.; Leroy, D.; Fidock, D. A. *Nat. Med.* **2017**, *23*, 917–928.

(13) Vasan, N.; Baselga, J.; Hyman, D. M. *Nature* **2019**, *575*, 299–309.

(14) Dean, T. T.; Jelú-Reyes, J.; Allen, A. C.; Moore, T. W. *J. Med. Chem.* **2024**, *67*, 1641–1661.

(15) Victoir, B.; Croix, C.; Gouilleux, F.; Prié, G. *Cancers.* **2024**, *16*, 461.

(16) Aggarwal, D.; Yang, J.; Salam, M. A.; Sengupta, S.; Al-Amin, M. Y.; Mustafa, S.; Khan, M. A.; Huang, X.; Pawar, J. S. *Front. Immunol.* **2023**, *14*, 1203073.

(17) Yadav, S.; Sharma, A. K.; Kumar, P. *Front. Bioeng. Biotechnol.* **2020**, *8*, 127.

(18) Bargh, J. D.; Isidro-Llobet, A.; Parker, J. S.; Spring, D. R. *Chem. Soc. Rev.* **2019**, *48*, 4361–4374.

(19) Ehrlich, P. *Br. Med. J.* **1913**, *2*, 353–359.

(20) Perez, H. L.; Cardarelli, P. M.; Deshpande, S.; Gangwar, S.; Schroeder, G. M.; Vite, G. D.; Borzilleri, R. M. *Drug Discov. Today* **2014**, *19*, 869–881.

(21) Mathé, G.; Tran Ba, L. O.; Bernard, J. *C. R. Hebd. Seances Acad. Sci.* **1958**, *246*, 1626–1628.

(22) Tsuchikama, K.; An, Z. *Protein Cell* **2018**, *9*, 33–46.

(23) Liu, K.; Li, M.; Li, Y.; Li, Y.; Chen, Z.; Tang, Y.; Yang, M.; Deng, G.; Liu, H. *Mol. Cancer* **2024**, *23*, 62.

(24) Francisco, J. A.; Cerveny, C. G.; Meyer, D. L.; Mixan, B. J.; Klussman, K.; Chace, D. F.; Rejniak, S. X.; Gordon, K. A.; DeBlanc, R.; Toki, B. E.; Law, C. L.; Doronina, S. O.; Siegall, C. B.; Senter, P. D.; Wahl, A. F. *Blood* **2003**, *102*, 1458–1465.

(25) Chang, H. P.; Cheung, Y. K.; Shah, D. K. *J. Clin. Med.* **2021**, *10*, 1332.

(26) Gogia, P.; Ashraf, H.; Bhasin, S.; Xu, Y. *Cancers.* **2023**, *15*, 3886.

(27) Dumontet, C.; Reichert, J. M.; Senter, P. D.; Lambert, J. M.; Beck, A. *Nat. Rev. Drug Discov.* **2023**, *22*, 641–661.

(28) Heh, E.; Allen, J.; Ramirez, F.; Lovasz, D.; Fernandez, L.; Hogg, T.; Riva, H.; Holland, N.; Chacon, J. *Int. J. Mol. Sci.* **2023**, *24*, 829.

(29) Chavda, V. P.; Solanki, H. K.; Davidson, M.; Apostolopoulos, V.; Bojarska, J. *Molecules* **2022**, *27*, 7232.

(30) Fu, C.; Yu, L.; Miao, Y.; Liu, X.; Yu, Z.; Wei, M. *Acta Pharm. Sin. B* **2023**, *13*, 498–516.

(31) Hoppenz, P.; Els-Heindl, S.; Beck-Sickinger, A. G. *Front. Chem.* **2020**, *8*, 571.

(32) Das, S.; Al-Toubah, T.; El-Haddad, G.; Strosberg, J. *Expert Rev. Gastroenterol. Hepatol.* **2019**, *13*, 1023–1031.

(33) Zhou, L.; Lu, Y.; Liu, W.; Wang, S.; Wang, L.; Zheng, P.; Zi, G.; Liu, H.; Liu, W.; Wei, S. *Exp. Hematol. Oncol.* **2024**, *13*, 26.

(34) Kolb, H. C.; Finn, M. G.; Sharpless, K. B. *Angew. Chem. Int. Ed.* **2001**, *40*, 2004–2021.

(35) Stump, B. *ChemBioChem* **2022**, *23*, e202200016.

(36) Beck, A.; Goetsch, L.; Dumontet, C.; Corvaïa, N. *Nat. Rev. Drug Discov.* **2017**, *16*, 315–337.

(37) The, T. H.; Feltkamp, T. E. W. *Immunology* **1970**, *18*, 865–873.

(38) Fredy, J. W.; Cutolo, G.; Poret, B.; Nehmé, R.; Hubert-Roux, M.; Gandolfo, P.; Castel, H.; Schuler, M.; Tatibouët, A.; Sabot, C.; Renard, P. Y. *Bioconjug. Chem.* **2019**, *30*, 1385–1394.

(39) Cal, P. M. S. D.; Vicente, J. B.; Pires, E.; Coelho, A. V.; Veiros, L. F.; Cordeiro, C.; Gois, P. M. P. *J. Am. Chem. Soc.* **2012**, *134*, 10299–10305.

(40) Hao, L.; Zhou, Q.; Piao, Y.; Zhou, Z.; Tang, J.; Shen, Y. *J. Control. Release* **2021**, *330*, 362–371.

(41) Diethelm, S.; Schafroth, M. A.; Carreira, E. M. *Org. Lett.* **2014**, *16*, 3908–3911.

(42) Kuan, S. L.; Wang, T.; Weil, T. *Chem. Eur. J.* **2016**, *22*, 17112–17129.

(43) Haque, M.; Forte, N.; Baker, J. R. *Chem. Commun.* **2021**, *57*, 10689–10702.

(44) Ban, H.; Gavrilyuk, J.; Barbas, C. F. *J. Am. Chem. Soc.* **2010**, *132*, 1523–1525.

(45) Ban, H.; Nagano, M.; Gavrilyuk, J.; Hakamata, W.; Inokuma, T.; Barbas, C. F. *Bioconjug. Chem.* **2013**, *24*, 520–532.

(46) White, A. M.; Palombi, I. R.; Malins, L. R. *Chem. Sci.* **2022**, *13*, 2809–2823.

(47) Karipal Padinjare Veedu, D.; Connal, L. A.; Malins, L. R. *Angew. Chem. Int. Ed.* **2023**, *62*, e202215470.

(48) DeGruyter, J. N.; Malins, L. R.; Baran, P. S. *Biochemistry* **2017**, *56*, 3863–3873.

(49) Rostovtsev, V. V.; Green, L. G.; Fokin, V. V.; Sharpless, K. B. *Angew. Chem. Int. Ed.* **2002**, *41*, 2596–2599.

(50) Tornøe, C. W.; Christensen, C.; Meldal, M. *J. Org. Chem.* **2002**, *67*, 3057–3064.

(51) Haldón, E.; Nicasio, M. C.; Pérez, P. J. *Org. Biomol. Chem.* **2015**, *13*, 9528–9550.

(52) Huisgen, R. *Angew. Chem. Int. Ed.* **1963**, *2*, 565–598.

(53) Meldal, M.; Tornøe, C. W. *Chem. Rev.* **2008**, *108*, 2952–3015.

(54) Lang, K.; Chin, J. W. *ACS Chem. Biol.* **2014**, *9*, 16–20.

(55) Agard, N. J.; Prescher, J. A.; Bertozzi, C. R. *J. Am. Chem. Soc.* **2004**, *126*, 15046–15047.

(56) Dommerholt, J.; Rutjes, F. P. J. T.; van Delft, F. L. *Top. Curr. Chem.* **2016**, *374*, 16.

(57) Blackman, M. L.; Royzen, M.; Fox, J. M. *J. Am. Chem. Soc.* **2008**, *130*, 13518–13519.

(58) Saxon, E.; Bertozzi, C. R. *Science* **2000**, *287*, 2007–2010.

(59) Saxon, E.; Armstrong, J. I.; Bertozzi, C. R. *Org. Lett.* **2000**, *2*, 2141–2143.

(60) Nilsson, B. L.; Kiessling, L. L.; Raines, R. T. *Org. Lett.* **2000**, *2*, 1939–1941.

(61) Song, W.; Wang, Y.; Qu, J.; Madden, M. M.; Lin, Q. *Angew. Chem. Int. Ed.* **2008**, *47*, 2832–2835.

(62) Li, N.; Lim, R. K. V.; Edwardraja, S.; Lin, Q. *J. Am. Chem. Soc.* **2011**, *133*, 15316–15319.

(63) Chalker, J. M.; Wood, C. S. C.; Davis, B. G. *J. Am. Chem. Soc.* **2009**, *131*, 16346–16347.

(64) Ning, X.; Temming, R. P.; Dommerholt, J.; Guo, J.; Ania, D. B.; Debets, M. F.; Wolfert, M. A.; Boons, G. J.; van Delft, F. L. *Angew. Chem. Int. Ed.* **2010**, *49*, 3065–3068.

(65) McKay, C. S.; Moran, J.; Pezacki, J. P. *Chem. Commun.* **2010**, *46*, 931–933.

(66) Pícha, J.; Buděšínský, M.; Macháčková, K.; Collinsová, M.; Jiráček, J. *J. Pept. Sci.* **2017**, *23*, 202–214.

(67) Goldenberg, D. M.; Cardillo, T. M.; Govindan, S. V.; Rossi, E. A.; Sharkey, R. M. *Oncotarget* **2015**, *6*, 22496–22512.

(68) Gong, L.; Zhao, H.; Liu, Y.; Wu, H.; Liu, C.; Chang, S.; Chen, L.; Jin, M.; Wang, Q.; Gao, Z.; Huang, W. *Acta Pharm. Sin. B* **2023**, *13*, 3659–3677.

(69) Barok, M.; Joensuu, H.; Isola, J. *Breast Cancer Res.* **2014**, *16*, 209.

(70) Alas, M.; Saghaeidehkordi, A.; Kaur, K. *J. Med. Chem.* **2021**, *64*, 216–232.

(71) Régina, A.; Demeule, M.; Ché, C.; Lavallée, I.; Poirier, J.; Gabathuler, R.; Béliveau, R.; Castaigne, J. P. *Br. J. Pharmacol.* **2008**, *155*, 185–197.

(72) Hou, L.; Hou, Y.; Liang, Y.; Chen, B.; Zhang, X.; Wang, Y.; Zhou, K.; Zhong, T.; Long, B.; Pang, W.; Wang, L.; Han, X.; Li, L.; Xu, C.; Gross, I.; Gaiddon, C.; Fu, W.; Yao, H.; Meng, X. *Commun. Biol.* **2022**, *5*, 1248.

(73) Karampelas, T.; Argyros, O.; Sayyad, N.; Spyridaki, K.; Pappas, C.; Morgan, K.; Kolios, G.; Millar, R. P.; Liapakis, G.; Tzakos, A. G.; Fokas, D.; Tamvakopoulos, C. *Bioconjug. Chem.* **2014**, *25*, 813–823.

(74) Soudy, R.; Chen, C.; Kaur, K. *J. Med. Chem.* **2013**, *56*, 7564–7573.

(75) Dubowchik, G. M.; Firestone, R. A.; Padilla, L.; Willner, D.; Hofstead, S. J.; Mosure, K.; Knipe, J. O.; Lasch, S. J.; Trail, P. A. *Bioconjug. Chem.* **2002**, *13*, 855–869.

(76) Wei, B.; Gunzner-Toste, J.; Yao, H.; Wang, T.; Wang, J.; Xu, Z.; Chen, J.; Wai, J.; Nonomiya, J.; Tsai, S. P.; Chuh, J.; Kozak, K. R.; Liu, Y.; Yu, S. F.; Lau, J.; Li, G.; Phillips, G. D.; Leipold, D.; Kamath, A.; Su, D.; Xu, K.; Eigenbrot, C.; Steinbacher, S.; Ohri, R.; Raab, H.; Staben, L. R.; Zhao, G.; Flygare, J. A.; Pillow, T. H.; Verma, V.; Masterson, L. A.; Howard, P. W.; Safina, B. *J. Med. Chem.* **2018**, *61*, 989–1000.

(77) Caculitan, N. G.; Chuh, J. dela C.; Ma, Y.; Zhang, D.; Kozak, K. R.; Liu, Y.; Pillow, T. H.; Sadowsky, J.; Cheung, T. K.; Phung, Q.; Haley, B.; Lee, B. C.; Akita, R. W.; Sliwkowski, M. X.; Polson, A. G. *Cancer Res.* **2017**, *77*, 7027–7037.

(78) Jeffrey, S. C.; Nguyen, M. T.; Andreyka, J. B.; Meyer, D. L.; Doronina, S. O.; Senter, P. D. *Bioorg. Med. Chem. Lett.* **2006**, *16*, 358–362.

(79) Zammarchi, F.; Corbett, S.; Adams, L.; Tyrer, P. C.; Kiakos, K.; Janghra, N.; Marafioti, T.; Britten, C. E.; Havenith, C. E. G.; Chivers, S.; D'Hooge, F.; Williams, D. G.; Tiberghien, A.; Howard, P. W.; Hartley, J. A.; van Berkel, P. H. *Blood* **2018**, *131*, 1094–1105.

(80) Ziaei, E.; Saghaeidehkordi, A.; Dill, C.; Maslennikov, I.; Chen, S.; Kaur, K. *Bioconjug.*

Chem. **2019**, *30*, 3098–3106.

(81) Sheng, Y.; You, Y.; Chen, Y. *Int. J. Pharm.* **2016**, *512*, 1–13.

(82) Yousefpour, P.; Ahn, L.; Tewksbury, J.; Saha, S.; Costa, S. A.; Bellucci, J. J.; Li, X.; Chilkoti, A. *Small* **2019**, *15*, 1804452.

(83) Paulus, J.; Sewald, N. *J. Pept. Sci.* **2024**, *30*, e3561.

(84) Mahajan, S. S.; Deu, E.; Lauterwasser, E. M.; Leyva, M. J.; Ellman, J. A.; Bogyo, M.; Renslo, A. R. *ChemMedChem* **2011**, *6*, 415–419.

(85) Spangler, B.; Kline, T.; Hanson, J.; Li, X.; Zhou, S.; Wells, J. A.; Sato, A. K.; Renslo, A. R. *Mol. Pharm.* **2018**, *15*, 2054–2059.

(86) Fu, Z.; Li, S.; Han, S.; Shi, C.; Zhang, Y. *Signal Transduct. Target. Ther.* **2022**, *7*, 93.

(87) Wu, G.; Fang, Y. Z.; Yang, S.; Lupton, J. R.; Turner, N. D. *J. Nutr.* **2004**, *134*, 489–492.

(88) Jones, L. R.; Goun, E. A.; Shinde, R.; Rothbard, J. B.; Contag, C. H.; Wender, P. A. *J. Am. Chem. Soc.* **2006**, *128*, 6526–6527.

(89) Henne, W. A.; Doorneweerd, D. D.; Hilgenbrink, A. R.; Kularatne, S. A.; Low, P. S. *Bioorg. Med. Chem. Lett.* **2006**, *16*, 5350–5355.

(90) Vlahov, I. R.; Santhapuram, H. K. R.; Kleindl, P. J.; Howard, S. J.; Stanford, K. M.; Leamon, C. P. *Bioorg. Med. Chem. Lett.* **2006**, *16*, 5093–5096.

(91) Pillow, T. H.; Sadowsky, J. D.; Zhang, D.; Yu, S. F.; Del Rosario, G.; Xu, K.; He, J.; Bhakta, S.; Ohri, R.; Kozak, K. R.; Ha, E.; Junutula, J. R.; Flygare, J. A. *Chem. Sci.* **2017**, *8*, 366–370.

(92) Saito, G.; Swanson, J. A.; Lee, K.-D. *Adv. Drug Deliv. Rev.* **2003**, *55*, 199–215.

(93) Torti, S. V.; Torti, F. M. *Nat. Rev. Cancer* **2013**, *13*, 342–355.

(94) Mousavizadeh, A.; Jabbari, A.; Akrami, M.; Bardania, H. *Colloids Surf. B Biointerfaces* **2017**, *158*, 507–517.

(95) Milletti, F. *Drug Discov. Today* **2012**, *17*, 850–860.

(96) Derakhshankhah, H.; Jafari, S. *Biomed. Pharmacother.* **2018**, *108*, 1090–1096.

(97) Lawrence, N.; Dennis, A. S. M.; Lehane, A. M.; Ehmann, A.; Harvey, P. J.; Benfield, A. H.; Cheneval, O.; Henriques, S. T.; Craik, D. J.; McMorran, B. J. *Cell Chem. Biol.* **2018**, *25*, 1140–1150.

(98) Henriques, S. T.; Lawrence, N.; Chaousis, S.; Ravipati, A. S.; Cheneval, O.; Benfield, A. H.; Elliott, A. G.; Kavanagh, A. M.; Cooper, M. A.; Chan, L. Y.; Huang, Y. H.; Craik, D. J. *ACS Chem. Biol.* **2017**, *12*, 2324–2334.

(99) Nagata, S.; Suzuki, J.; Segawa, K.; Fujii, T. *Cell Death Differ.* **2016**, *23*, 952–961.

(100) Yeaman, M. R.; Yount, N. Y. *Pharmacol. Rev.* **2003**, *55*, 27–55.

(101) Silva, A. R. P.; Guimaraes, M. S.; Rabelo, J.; Belen, L. H.; Perecin, C. J.; Farias, J. G.; Santos, J. H. P. M.; Rangel-Yagui, C. O. *J. Mater. Chem. B* **2022**, *10*, 3587–3600.

(102) McMorran, B. J.; Wieczorski, L.; Drysdale, K. E.; Chan, J. A.; Huang, H. M.; Smith, C.; Mitiku, C.; Beeson, J. G.; Burgio, G.; Foote, S. J. *Science* **2012**, *338*, 1348–1351.

(103) Love, M. S.; Millholland, M. G.; Mishra, S.; Kulkarni, S.; Freeman, K. B.; Pan, W.; Kavash, R. W.; Costanzo, M. J.; Jo, H.; Daly, T. M.; Williams, D. R.; Kowalska, M. A.; Bergman, L. W.; Poncz, M.; Degrado, W. F.; Sinnis, P.; Scott, R. W.; Greenbaum, D. C. *Cell Host Microbe* **2012**, *12*, 815–823.

(104) Engelbrecht, D.; Coetzer, T. L. *Parasitol. Int.* **2016**, *65*, 715–727.

(105) Tawk, L.; Chicanne, G.; Dubremetz, J. F.; Richard, V.; Payrastre, B.; Vial, H. J.; Roy, C.; Wengelnik, K. *Eukaryot. Cell* **2010**, *9*, 1519–1530.

(106) Vallabhapurapu, S. D.; Blanco, V. M.; Sulaiman, M. K.; Vallabhapurapu, S. L.; Chu, Z.; Franco, R. S.; Qi, X. *Oncotarget* **2015**, *6*, 34375–34388.

(107) Lawrence, N.; Philippe, G.; Harvey, P. J.; Condon, N. D.; Benfield, A. H.; Cheneval, O.; Craik, D. J.; Henriques, S. T. *RSC Chem. Biol.* **2020**, *1*, 405–420.

(108) Philippe, G. J. B.; Mittermeier, A.; Lawrence, N.; Huang, Y. H.; Condon, N. D.; Loewer, A.; Craik, D. J.; Henriques, S. T. *ACS Chem. Biol.* **2021**, *16*, 414–428.

(109) Silva, P. I.; Daffre, S.; Bulet, P. *J. Biol. Chem.* **2000**, *275*, 33464–33470.

(110) Chan, L. Y.; Zhang, V. M.; Huang, Y. H.; Waters, N. C.; Bansal, P. S.; Craik, D. J.; Daly, N. L. *ChemBioChem* **2013**, *14*, 617–624.

(111) Benfield, A. H.; Defaus, S.; Lawrence, N.; Chaousis, S.; Condon, N.; Cheneval, O.; Huang, Y. H.; Chan, L. Y.; Andreu, D.; Craik, D. J.; Henriques, S. T. *Biochim. Biophys. Acta Biomembr.* **2021**, *1863*, 183480.

(112) de la Torre, B. G.; Albericio, F. *Molecules* **2023**, *28*, 1038.

(113) Wang, M.; Liu, J.; Xia, M.; Yin, L.; Zhang, L.; Liu, X.; Cheng, Y. *Eur. J. Med. Chem.* **2024**, *265*, 116119.

Chapter 2:

Primaquine PDCs as an alternative modality for antimalarial treatment

Introduction

Malaria is an infectious disease that is prevalent throughout the tropical and sub-tropical areas of Africa, Southeast Asia and South America. In 2022, there were an estimated 249 million cases and 608 thousand deaths attributed to malaria.[1] The causative parasite is a unicellular protozoan organism from the genus *Plasmodium* (including *P. falciparum*, *P. vivax*, *P. ovale, P. knowlesi* and *P. malariae* species), which is transmitted between humans by an infected female *Anopheles* mosquito vector. The parasite causes symptoms representative of an acute fever, however, this can progress to a life-threatening illness if infected red blood cells (RBCs) become sequestered into tissues, leading to organ damage.[2] Infection with *P. falciparum*, the deadliest *Plasmodium* species, is the cause of almost 90% of cases and resulting fatalities, many of which occur in African children.[3] The global burden of malaria is disproportionate, with most incidences of *P. falciparum* occurring in sub-Saharan Africa (Figure 2.1A) and *P. vivax* occurring in Southeast Asia and South America (Figure 2.1B).

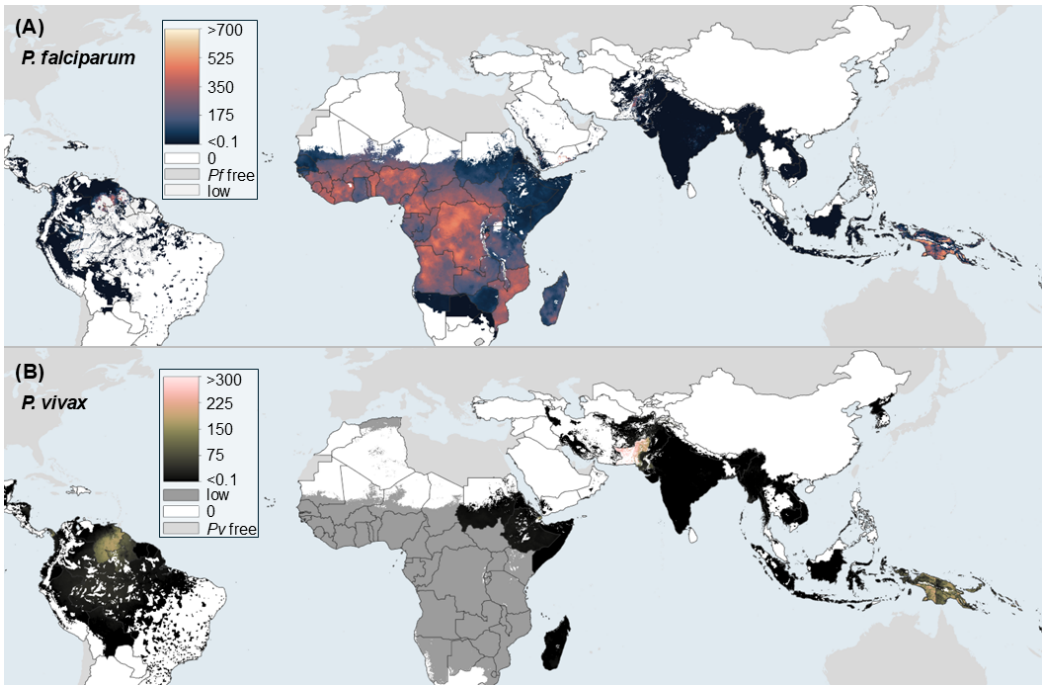

Figure 2.1. The predicted incidence rate (cases per 1,000 people) in 2022 for (A) *P. falciparum* and (B) *P. vivax*, the two most prevalent *Plasmodium* strains. Figure adapted from the Malaria Atlas Project.[4]

The current strategies to combat malaria involve vector control with insecticide-treated bed nets and treatment with combination therapies.[3] While these measures have led to a reduction in the number of malaria-endemic countries over the last few decades,[1] the emergence of drug-resistant parasites to antimalarial therapies continues to threaten the future eradication of malaria. Additionally, continuous temperature increases could result in the return or introduction of malaria to other tropical or sub-tropical areas—such as northern Australia—where the *Anopheles* mosquito vector is present.[5,6] The fear of resistance to current treatments, with no alternative therapies available, fuels the continuous development of

antimalarial drugs and prompts the design of therapies with novel mechanisms to target the parasite.

2.1 The complex life cycle of *Plasmodium* complicates treatment

Antimalarial drug discovery is complicated by the intricate biology of the *Plasmodium* parasite.[7] Its life cycle consists of a combination of asexual and sexual parasite stages, with the dual involvement of a mosquito vector and human host (Figure 2.2). Briefly, infection begins when a parasitised female *Anopheles* mosquito bites a human, delivering the parasite into the bloodstream as sporozoites (labelled **A** in Figure 2.2). The sporozoites invade liver cells where they replicate asexually resulting in the release of thousands of merozoites (**B**).[8,9] In *P. vivax* and *P. ovale* infections, some parasites in the liver stage remain dormant as hypnozoites, leading to infection relapse when the hypnozoite re-enters the life cycle (**B***).[3] Invasion of merozoites into RBCs enables further asexual replication, where parasites cycle through ring, trophozoite and schizont stages, until a mature schizont ruptures and releases more merozoites into the bloodstream (**C**). Some blood stage parasites instead differentiate into male and female gametocytes (**D**), which form gametes when ingested by a mosquito during a blood meal.[10] Sexual reproduction occurs in the midgut of the mosquito, forming a zygote that develops into an ookinete and further into an oocyst (**E**). Sporozoites rupture from the oocyst and migrate to the salivary glands of the insect (**F**), completing the life cycle and enabling transmission to a new human host during the next blood meal.[7]

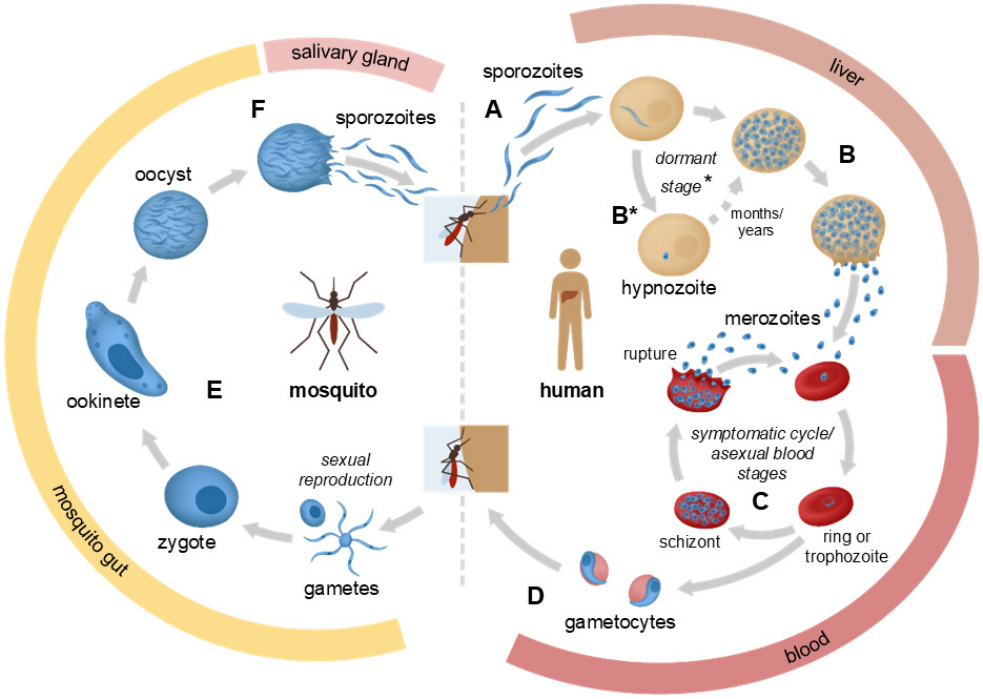

Figure 2.2. The life cycle of *Plasmodium*, consisting of stages in both a mosquito vector and a human host. *The dormant liver stage only occurs in *P. vivax* and *P. ovale* infections. Figure adapted from Wellcome Connecting Science.[11]

Since the pathogenesis of malaria is caused by the asexual blood stage parasites (**C**), many existing antimalarial treatments target these parasites. Whilst this improves patient symptoms, it does not prevent transmission between individuals or reinfection in relapsing malaria cases.[8] A drug that can eliminate all parasite stages from the body would revolutionise malaria treatment, however, this remains a current challenge for antimalarial drug discovery.

2.2 The requirement for new antimalarials

2.2.1 Drug discovery is complicated by extensive criteria for ideal treatments

The criteria for compounds that can be used as antimalarials are constrained by the occurrence of the disease primarily in low-income countries (Figure 2.1). Aside from exhibiting antiplasmodial activity, an antimalarial additionally needs to be (1) affordable, (2) easy to administer (*e.g.* orally available), (3) distributable without refrigeration, (4) useful as a curative and preventative treatment, (5) effective against all stages of the parasite, (6) safe for use to treat pregnant women and young children, (7) contain a mechanism of action that *Plasmodium* cannot easily acquire resistance against and (8) be able to cross both the host and parasite cell membranes, whilst avoiding off-target interactions within the body.[3,12] These extensive requirements have made discovering the ideal antimalarial treatment difficult, accounting for the limited number of novel drugs ready to be deployed in areas where existing treatments are declining in effectiveness.[12]

2.2.2 *Plasmodium* has developed resistance to most antimalarial treatments

The continual emergence of parasites resistant to antimalarial drugs has increased the urgency for the development of new treatments. Figure 2.3A depicts the widespread resistance throughout malaria endemic areas (South America not shown) for *P. falciparum* against three existing small molecule drugs. One such therapy is chloroquine (CQ, **2.1**), the first synthetic drug to be utilised for antimalarial treatment. Initially deployed in the mid-1940s,[9] CQ is a 4-aminoquinoline derivative that acts by preventing the detoxification of haem—which is released as the parasite degrades haemoglobin in its digestive vacuole—leading to a buildup of haem and subsequent parasite death.[13] However, within a decade of its release CQ-resistant *Plasmodium* strains were detected, necessitating new treatments.[10] Resistance is attributed to mutations in *P. falciparum* CQ resistance transporter (*PfCRT*), which encode a mutant efflux pump that can prevent the accumulation of drugs in the parasite digestive vacuole.[14] CQ resistance is now widespread (Figure 2.3A), restricting use of the drug to the treatment of *P. vivax* in the few regions where resistance has not yet developed.[15,16]

The antifolate combination sulfadoxine–pyrimethamine (SP, **2.2** and **2.3**) was introduced to replace CQ as a first-line treatment, following a reduction in the effectiveness of CQ. However, resistance was observed within the first year of SP release, starting in Southeast Asia and now prominent throughout malaria endemic regions (Figure 2.3A).[10] Both drugs inhibit enzymes in

the parasite folate biosynthesis pathway—sulfadoxine targets dihydrofolate reductase (DHFR) and pyrimethamine targets dihydropteroate synthetase (DHPS)—and as a result, resistance to SP is often conferred by mutations in these enzymes.[15] Today, SP is primarily used in combination with artesunate in areas with SP-sensitivity.[10]

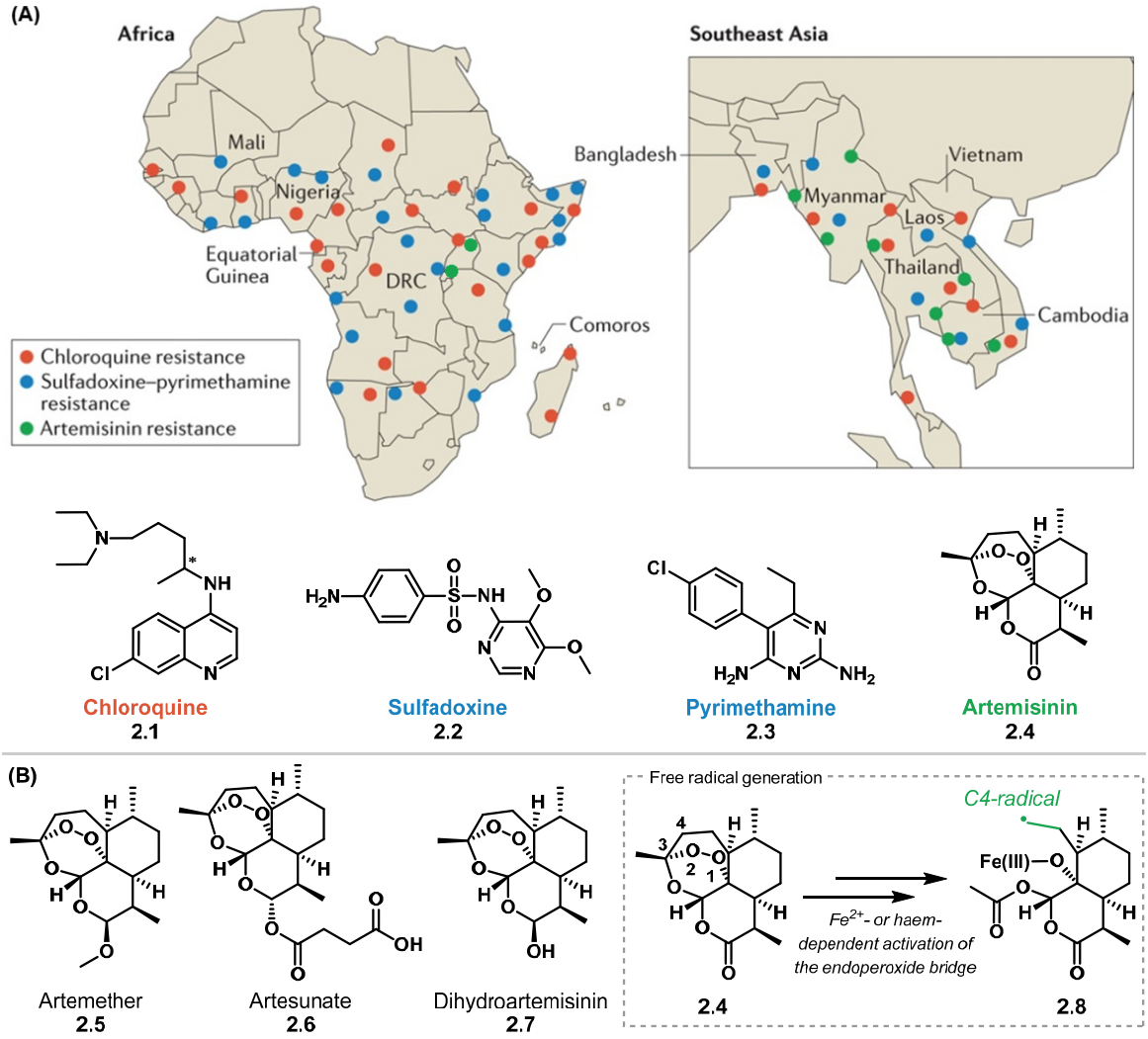

Figure 2.3. (A) Distribution of the emergence of *P. falciparum* resistance to chloroquine (**2.1**), sulfadoxine–pyrimethamine (**2.2** and **2.3**) and artemisinin (**2.4**) throughout Africa and Southeast Asia (South America not shown). The structure of each drug is shown below the map. Figure adapted from Haldar *et al*.[15] (B) The structure of two artemisinin derivatives (**2.5** and **2.6**) and the active metabolite dihydroartemisinin (**2.7**). Depicted in the grey box is a possible C4-radical that can be produced following cleavage of the endoperoxide bridge.[17]

The current gold standard for malaria treatment is artemisinin (ART, **2.4**), a sesquiterpene lactone, and its semi-synthetic derivatives such as artemether **2.5** and artesunate **2.6** (Figure 2.3B). Despite the structural complexity of the ART-based therapies, the ability to generate these compounds using expression-based technologies enables low-cost production.[18] The ART derivatives are prodrugs that are converted to the active variant dihydroartemisinin (**2.7**) in the body.[16] The endoperoxide bridge is responsible for the activity of ART, and is thought to be cleaved by haem or free ferrous iron (Fe^{2+}) inside the parasite, producing a carbon centred

radical (**2.8**) that can alkylate and disrupt the function of cellular proteins required for the parasite's survival (grey box, Figure 2.3B).[19] As the ART derivatives have short elimination half-lives (2–5 hours), they are generally paired with a longer-acting antimalarial—a strategy termed ART-based combination therapies (ACTs)—to effectively eliminate the parasite infection and prevent resistance development.[20] Despite the implementation of the ACT approach, resistance to ART was first observed in Cambodia in 2008, and is attributed to mutations in the gene for the Kelch-like protein K13.[10] Independently developed resistance was also reported in 2021 in Uganda and Rwanda, where the deadliest *Plasmodium* species is prevalent (Figure 2.3A).[21,22] This is concerning as there are limited alternative treatments available for use when ART resistance becomes widespread throughout Africa. The successive cycles of drug resistance highlight the necessity for alternative types of drugs that employ novel methods to kill the parasite.

2.2.3 8-aminoquinoline drugs are limited by poor safety profiles

Some of the few monotherapies without widespread resistance are the 8-aminoquinoline drugs, including primaquine (PQ, **2.9**) and tafenoquine (TQ, **2.10**) (Figure 2.4). The 8-aminoquinoline derivatives are the only available antimalarials that are active against the dormant hypnozoite stage, so can be used to prevent relapsing *P. vivax* infections.[23] Alongside activity against liver and blood stage parasites, these drugs are also gametocytocidal, so a single dose can be used to prevent transmission.[3,24] However, the widespread use of PQ and TQ is limited due to their poor safety profile in individuals who are deficient in glucose-6-phosphate dehydrogenase (G6PD), an enzyme involved in defence against oxidative stress in RBCs.[23,25] While the mechanism of action for these drugs is not completely understood, it has been proposed that hydrogen peroxide is produced following the administration of PQ,[26] signifying that individuals with impaired oxidative defence enzymes may suffer from RBC damage after PQ treatment. G6PD deficiency is notably prevalent in malaria endemic areas within Africa and Southeast Asia (the average prevalence of the allele is 8.0%)[27] where PQ and TQ use would be valuable, highlighting the requirement for alternative methods for relapse prevention in individuals with G6PD deficiency.

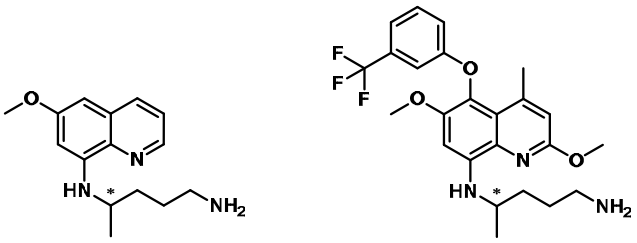

Primaquine **2.9** Tafenoquine **2.10**

Figure 2.4. The structure of the 8-aminoquinoline derivatives, primaquine (**2.9**) and tafenoquine (**2.10**).

2.3 PDCs as an alternative modality for the treatment of malaria

To date, all approved malaria treatments have been small molecule drugs. The aforementioned issues indicate that antimalarials may benefit from the advantages of other drug modalities, such as peptides which are often highly selective.[28,29] PDCs that pair an antiplasmodial peptide with a small molecule drug could be a viable dual-acting treatment alternative to the ACTs. Such PDCs could have the potential to deliver antimalarial drugs to intracellular *Plasmodium* targets, to overcome the nonselective nature of small molecules such as PQ. Analogous to ACTs, pairing two drug modalities with different mechanisms of action could reduce the possibility for the development of drug-resistant parasites and increase the number of parasite stages that can be targeted.

While PDCs have been widely employed for cancer applications,[30] infectious disease contexts can also benefit from the target selectivity provided by a PDC approach.[31] The recent investigation of PDCs for antiviral,[32] antibacterial[33,34] and antifungal[35,36] treatment, as well as for diseases caused by protozoan parasites such as malaria[37–39] and leishmaniasis,[40] have cemented this strategy as a promising alternative for infectious disease treatment. Previous antimalarial PDCs, designed by Gomes and co-workers,[37,38] were comprised of PQ and a CQ analogue (Cq) attached to peptides such as transportan 10 (TP10), a cell-penetrating peptide with antiplasmodial activity, or IDR-1018 and TAT, two inactive cell-penetrating peptides (Figure 2.5). Multiple PDCs were successfully synthesised with either non-cleavable linkers or a cleavable disulfide linker that could release a thiolated drug. While PDCs containing the TP10 peptide were potent to parasites in the liver or blood stages, they had increased haemolytic activity towards uninfected cells (compared to TP10), especially for the PQ-based PDCs (Figure 2.5).[39]

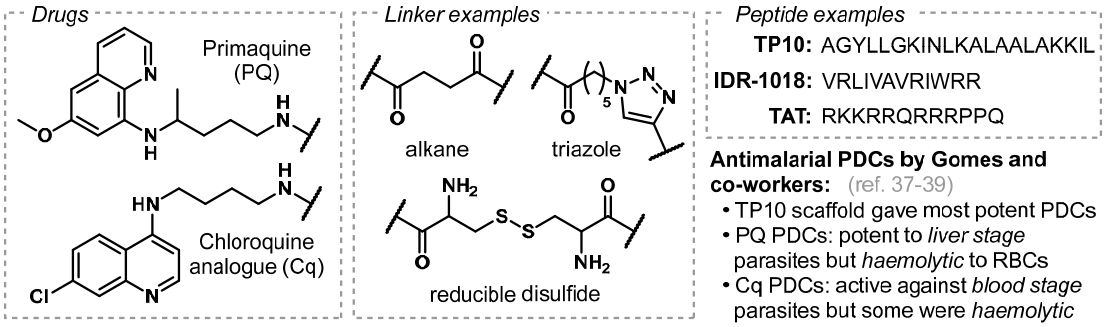

Figure 2.5. Summary of previously reported antimalarial PDCs that were designed by Gomes and co-workers.[37–39] Examples of the drugs, linkers and peptides incorporated into their PDC design are provided.

We rationalised that PDIP, a CPP with antiplasmodial activity and selective entry into infected RBCs (see Section 1.3.2),[41] could be a successful carrier peptide and drug partner for antimalarial small molecules. For the first-generation of PDIP-based antimalarial PDCs, we sought to conjugate PQ onto PDIP, envisaging that this approach could provide three potential

benefits compared to PQ monotherapy: (i) prevent the interaction of PQ with healthy tissues, which could reduce off-target toxicity in individuals with G6PD deficiency, (ii) slow the conversion of PQ into inactive byproducts (*e.g.* carboxyprimaquine)[42] in the body, and (iii) reduce the ability of the parasite to acquire drug resistance, as PQ and PDIP each have distinct antiplasmodial mechanisms of action.

Accordingly, this chapter, presented as a published manuscript,[43] details the design and synthesis of PDIP-PQ PDCs and the evaluation of their activity against blood stage *P. falciparum* parasites, using assays that were previously used to examine the activity of the PDIP scaffold. As prior antimalarial PDCs indicated the importance of careful design to avoid altering the properties of the peptide,[39] we aimed to explore how various design elements affected the biological activity of the PDCs. Changes in PDC activity based on linker type and peptide conjugation site revealed that activity is inextricably linked to PDC design and is important for maintaining the potency of the drug and peptide against *P. falciparum*.

Australian National University

Statement of Contribution

This thesis is submitted as a Thesis by Compilation in accordance with https://policies.anu.edu.au/ppl/document/ANUP_003405

I declare that the research presented in this Thesis represents original work that I carried out during my candidature at the Australian National University, except for contributions to multi-author papers incorporated in the Thesis where my contributions are specified in this Statement of Contribution.

Title: Development of Antiplasmodial Peptide–Drug Conjugates Using a Human Protein-Derived Cell-Penetrating Peptide with Selectivity for Infected Cells

Authors: Isabella R. Palombi, Nicole Lawrence, Andrew M. White, Caitlin L. Gare, David J. Craik, Brendan J. McMorran,* and Lara R. Malins*

Publication outlet: Bioconjugate Chemistry

Current status of paper: Not Yet Submitted/Submitted/Under Revision/Accepted/**Published**

Contribution to paper: Conducted the majority (95%) of the planning, experimental work (both synthetic chemistry and biology testing) and data analysis/compound characterisation. Wrote the original draft of the manuscript and the accompanying Supporting Material and incorporated edits from other authors. Chemistry components were conducted at the Research School of Chemistry, ANU, and the biology component was completed at the John Curtin School of Medical Research, ANU.

Senior author or collaborating authors endorsement: The above statement is accurate. The candidate performed the majority of the experimental work as indicated, including biological experiments at the John Curtin School of Medical Research, ANU. The candidate wrote the original manuscript and Supporting Information file.

Isabella Palombi		25/10/2024
Candidate – Print Name	Signature	Date

Endorsed

Nicole Lawrence		25/10/2024
Primary Supervisor – Print Name	Signature	Date
Mark Humphrey		25/10/2024
Delegated Authority – Print Name	Signature	Date

Bioconjugate Chemistry

pubs.acs.org/bc Article

Development of Antiplasmodial Peptide–Drug Conjugates Using a Human Protein-Derived Cell-Penetrating Peptide with Selectivity for Infected Cells

Isabella R. Palombi, Nicole Lawrence, Andrew M. White, Caitlin L. Gare, David J. Craik, Brendan J. McMorran,* and Lara R. Malins*

Cite This: *Bioconjugate Chem.* 2023, 34, 1105–1113 Read Online

ACCESS | Metrics & More | Article Recommendations | Supporting Information

ABSTRACT: Malaria continues to impose a global health burden. Drug-resistant parasites have emerged to each introduced small-molecule therapy, highlighting the need for novel treatment approaches for the future eradication of malaria. Herein, targeted drug delivery with peptide–drug conjugates (PDCs) was investigated as an alternative antimalarial therapy, inspired by the success of emerging antibody–drug conjugates utilized in cancer treatment. A synthetic peptide derived from an innate human defense molecule was conjugated to the antimalarial drug primaquine (PQ) to produce PDCs with low micromolar potency toward *Plasmodium falciparum in vitro*. A suite of PDCs with different design features was developed to identify optimal conjugation site and investigate linker length, hydrophilicity, and cleavability. Conjugation within a flexible spacer region of the peptide, with a cleavable linker to liberate the PQ cargo, was important to retain activity of the peptide and drug.

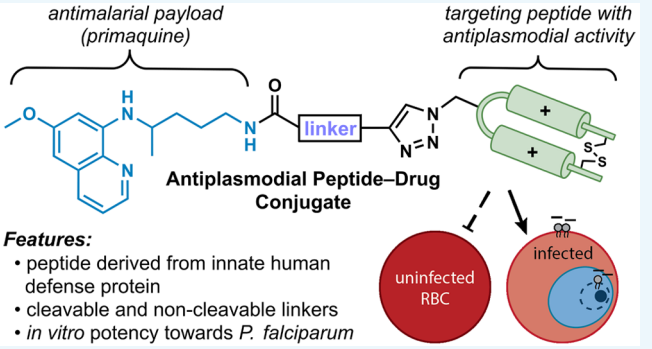

INTRODUCTION

Malaria is a mosquito-borne, infectious disease that is caused by the protozoan parasite *Plasmodium*.[1] The health burden of malaria is apparent, with an estimated 247 million cases and 619 000 deaths in 2021, mostly in African countries.[2] Although malaria is a preventable and curable disease, the continual emergence of parasites resistant to antimalarial therapies has impacted the clinical efficacy of past and existing treatments.[3,4] Alarmingly, resistance to artemisinin has been observed in southeast Asia, and more recently Africa, with limited alternative treatments currently available.[5−7] To date, all approved antimalarial treatments have been small-molecule drugs, which possess disadvantages such as off-target interactions due to nonspecific binding.[8] The successive cycles of drug resistance and the downfalls of small-molecule therapies underscore the urgent need for new and additional classes of drugs that employ novel methods to target and kill *Plasmodium* parasites.

Peptide-based drugs are a promising and unprecedented avenue for malaria treatment, due to their high selectivity for specific intracellular targets.[9] Previously, we developed a cell-penetrating alpha hairpin peptide from the active domain of human platelet factor 4 (PF4)[10] (Figure 1A), a protein released by platelets in response to *Plasmodium* infection and able to rapidly lyse the parasite digestive vacuole membrane.[11−13] This activity is attributed to the paired amphipathic alpha helices, located on the C-terminus of each monomer (black box in Figure 1A). The alpha hairpin peptide, herein referred to as platelet factor 4-derived internalization peptide (PDIP), is a minimized, synthetic analogue derived from PF4, comprising a head-to-tail dimer of two of the C-terminal helices cyclized *via* a disulfide bond (Figure 1A). The minimized peptide is selectively internalized into parasitized red blood cells (RBCs) and recapitulates the activity against *Plasmodium falciparum* parasites and the mechanism of killing displayed by the parent PF4 protein.[10] The cationic nature of PDIP confers this specificity due to increased proportions of negatively charged phosphatidylserine lipid headgroups on the outer membrane leaflet of *Plasmodium*-infected, relative to uninfected, RBCs (Figure 1A).[14]

We aspired to leverage these properties of PDIP as a targeting device to deliver small-molecule drugs directly to the parasite and thereby prevent their interaction with healthy tissues (Figure 1B). Inspired by the emerging success of drug

Received: April 3, 2023
Revised: May 5, 2023
Published: May 26, 2023

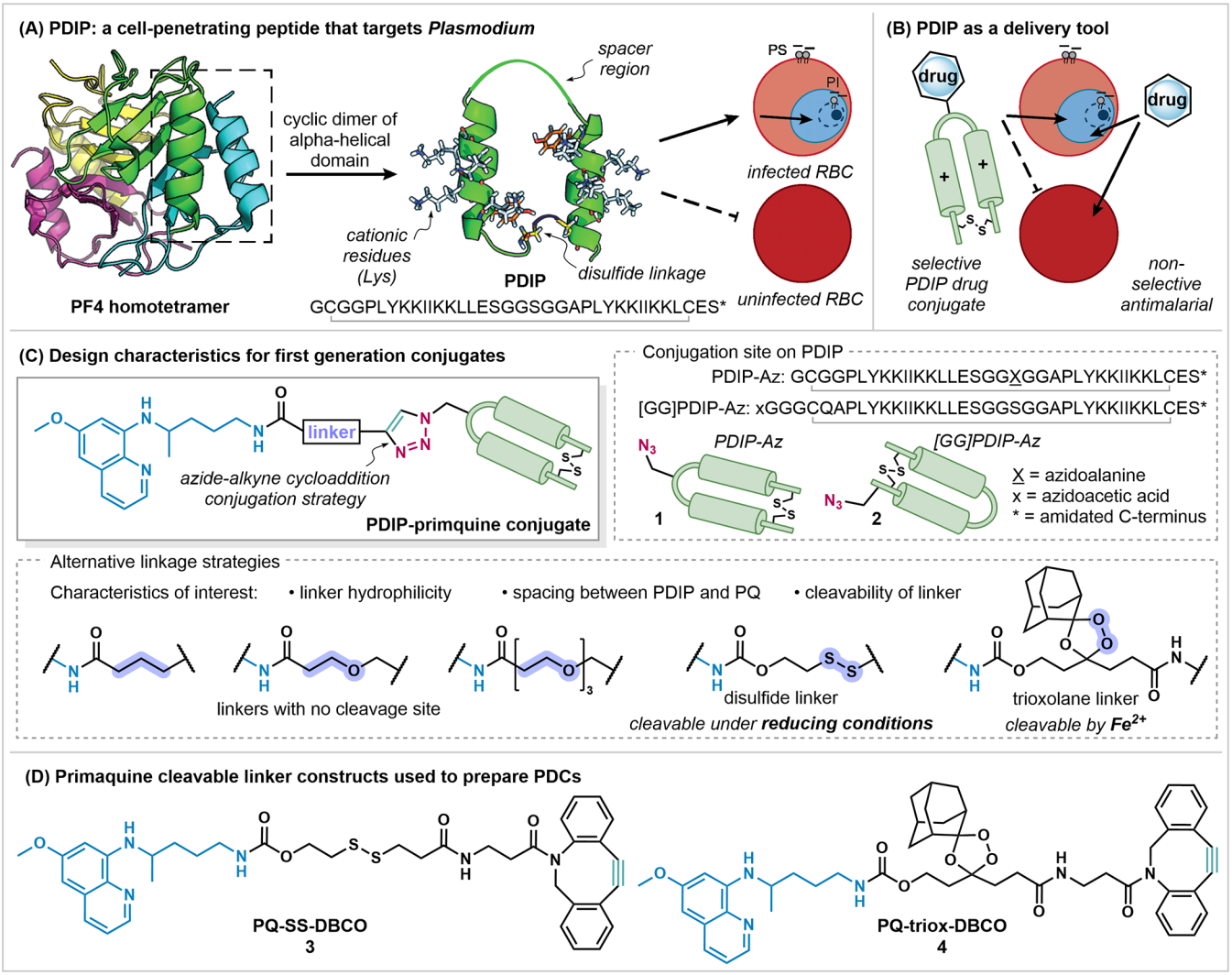

Figure 1. (A) Design of PDIP from the PF4 homotetramer, with selectivity for *Plasmodium*-infected blood cells highlighted. PS: phosphatidylserine; PI: phosphatidylinositol. PDB code: 1F9Q. (B) Proposed targeted delivery of antimalarial drugs in a PDC to infected RBCs *vs* nonselective entry of an unmodified drug. (C) Characteristics varied to generate a library of PDCs including the position of the peptide conjugation site, linker properties, and linker cleavability. (D) PQ-linker constructs used to prepare PDCs with a cleavable linkage.

conjugates in cancer therapeutics,[15] including the demonstrated ability of a PDIP analogue to deliver a cell impermeable peptide cargo inside cancer cells,[16,17] we sought to develop peptide−drug conjugates (PDCs) as novel antimalarials. While PDCs have been widely employed for cancer applications,[18] this approach is underexplored in the context of intracellular pathogens such as malaria.[19−21]

As a proof of concept, we aimed to produce first-generation PDCs by conjugating the antimalarial drug primaquine (PQ) onto PDIP. Although PQ is one of the few drugs without clinically relevant resistance, it does not have widespread use because it causes hemolysis in individuals who are deficient in glucose-6-phosphate dehydrogenase (G6PD), a genetic trait common in malaria-endemic areas.[22,23] Furthermore, PQ is metabolized into carboxyprimaquine in the body, which does not have any activity against the parasite.[24] The proposed PDC approach provides the potential to deliver PQ directly to the parasite, which could prevent its interaction with healthy tissues and slow the conversion of PQ into inactive byproducts. Further, the combination of the peptide and drug, each with distinct antiplasmodial mechanisms of action, provides the potential to avoid the formation of drug-resistant parasites.

Herein, we report the design, synthesis, and biological evaluation of a library of PDIP-PQ conjugates. Various design elements of the PDCs were probed to investigate their effect on biological activity, including: (i) the location of the PDIP conjugation site, (ii) the hydrophilicity of the linker between the peptide and drug, (iii) the spacing between the peptide and drug, and (iv) whether the linker can be cleaved to release the drug cargo under conditions which mimic the intracellular environment of infected RBCs (Figure 1C). This work demonstrates that conjugation within the flexible interhelix spacer of PDIP and incorporation of traceless cleavable linkers—bearing either a disulfide or trioxolane moiety—are important for maintaining the low micromolar potency of the PQ drug cargo against *P. falciparum*.

RESULTS AND DISCUSSION

Design and Synthesis of Modified Primaquine and PDIP Analogues for Conjugation. To generate the desired PDIP-based drug conjugates, we envisioned using azide−

https://doi.org/10.1021/acs.bioconjchem.3c00147
Bioconjugate Chem. 2023, 34, 1105−1113

Scheme 1. Synthesis of Primaquine Analogues Modified with (A) an Alkyne Handle Containing No Cleavage Site, (B) a Disulfide-Cleavable Linkage, and (C) a Trioxolane-Cleavable Linkage

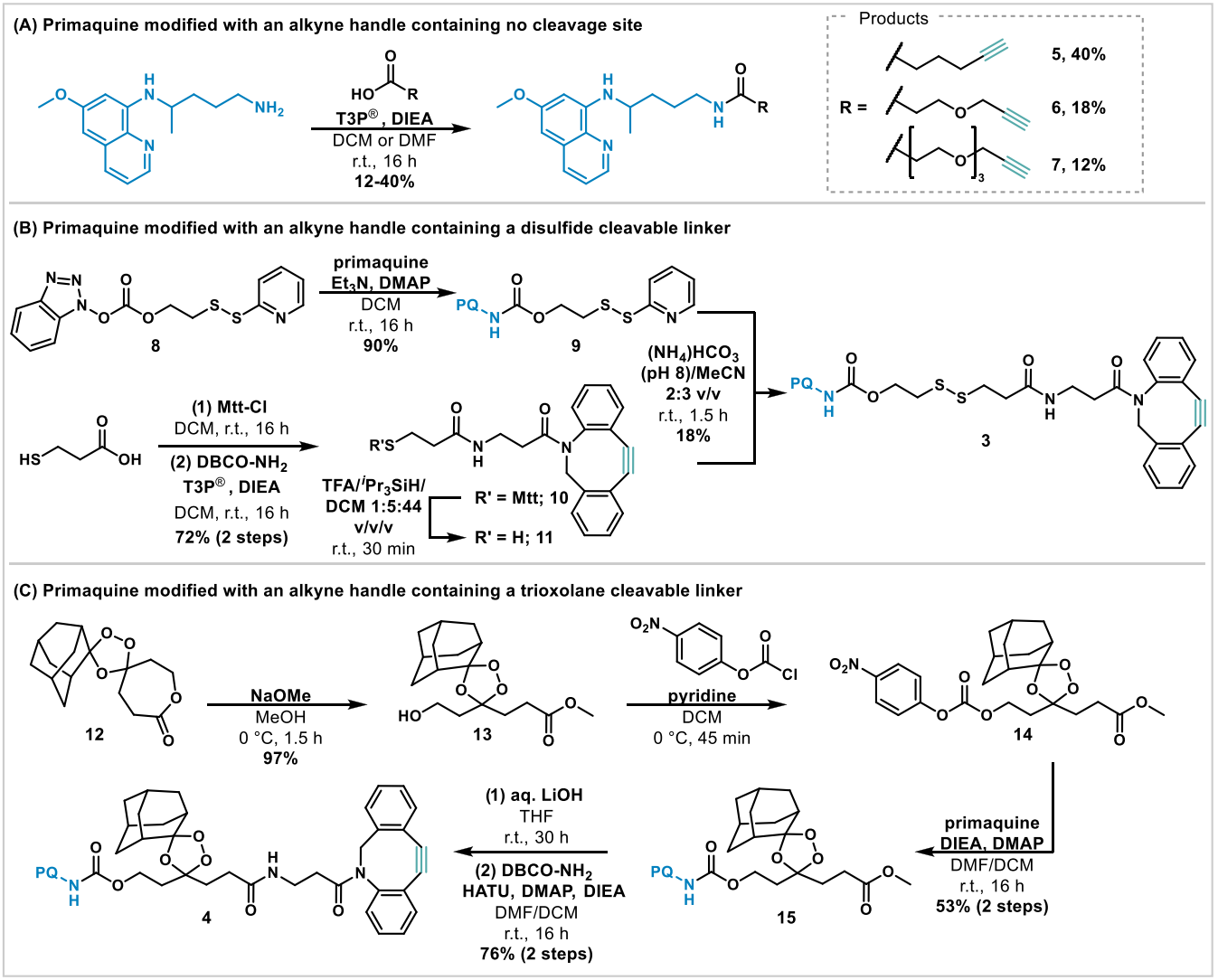

alkyne cycloaddition click chemistry[25−27] as an initial conjugation strategy since it is orthogonal to the crucial disulfide linkage within the macrocyclic PDIP scaffold. Therefore, we focused on the design of azide-modified PDIP analogues to provide a chemoselective moiety for conjugation to alkyne-modified PQ analogues. Two peptides were synthesized using automated solid-phase peptide synthesis, positioning an azide handle either within the spacer region between the two helices (labeled PDIP-Az **1** in Figure 1C) or at the N-terminus (labeled [GG]PDIP-Az **2** in Figure 1C). Preliminary studies exploring the antiplasmodial activity of fluorescently labeled PDIP analogues identified the ideal conjugation site within the spacer region of the peptide (**1**), as this retained activity was comparable to the parent peptide (see Supporting Information Figure S1 for further information).[10] In contrast, positioning of the azide handle at the peptide N-terminus resulted in reduced activity compared to the parent peptide (see the Supporting Information). However, as [GG]PDIP-Az **2** was synthetically more accessible, we were still interested in exploring PDCs derived from this peptide scaffold.

We next synthesized modified PQ analogues using the primary amine as a convenient handle to attach a terminal alkyne, in preparation for copper(I)-catalyzed azide−alkyne cycloaddition (CuAAC) with the aim of generating non-cleavable PDCs.[25,26] Modification of the primary amine of PQ with 5-hexynoic acid, propargyl-PEG1-acid, and propargyl-PEG3-acid, aided by the coupling reagent T3P®, produced PQ analogues **5**, **6**, and **7**, respectively (Scheme 1A). Notably, it was envisaged that increasing the number of poly(ethylene glycol) (PEG) units would allow us to probe the effects of greater linker hydrophilicity and increased spacing between the two components of the conjugate.

Although synthetically tractable, the incorporation of noncleavable linkers into conjugates may contribute to poor efficacy, especially if the pharmacophore of the drug is irreversibly modified. Accordingly, PDIP-PQ PDCs with cleavable linker moieties were also designed to facilitate the release of drug cargos in a traceless manner within the infected RBC. These consisted of either a trioxolane or disulfide-cleavable motif situated between PQ and an alkyne handle (Figure 1D). The first cleavable linker (**3**) comprises a disulfide linkage that can be cleaved by endogenous

https://doi.org/10.1021/acs.bioconjchem.3c00147
Bioconjugate Chem. 2023, 34, 1105−1113

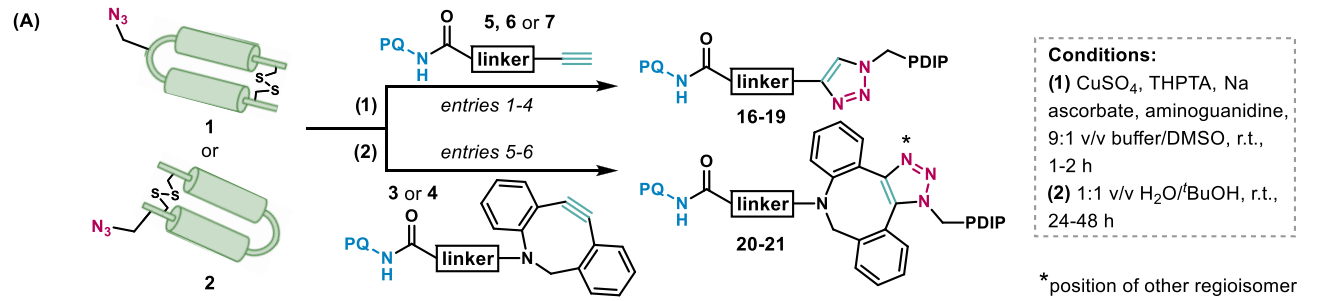

(B)

Entry	Alkyne	Azide	Conditions	Product	Yield (%)[a]
1	PQ-alkyne **5**	[GG]PDIP-Az **2**	1	**16**	45
2	PQ-alkyne **5**	PDIP-Az **1**	1	**17**	43
3	PQ-PEG1-alkyne **6**	PDIP-Az **1**	1	**18**	38
4	PQ-PEG3-alkyne **7**	PDIP-Az **1**	1	**19**	24
5	PQ-SS-DBCO **3**	PDIP-Az **1**	2	**20**	65
6	PQ-triox-DBCO **4**	PDIP-Az **1**	2	**21**	72

Figure 2. (A) General scheme for the synthesis of antimalarial PDCs, using either CuAAC or SPAAC conditions. (B) Yields and structures of the six PDCs. [a]Yield of isolated material determined by mass on a microbalance using the molecular weight of the TFA salt, assuming all basic residues and the terminal amine are protonated.

glutathione (GSH) within infected RBCs.[28,29] In comparison, the second cleavable linker (**4**) contains a 1,2,4-trioxolane moiety that is labile to ferrous iron, allowing for targeted drug release in the heme-rich cytoplasm of infected RBCs.[30−32] Dibenzocyclooctyne (DBCO)-containing linkers **3** and **4** were thus produced in preparation for strain-promoted azide−alkyne cycloaddition (SPAAC), to avoid the use of copper and excess reducing agents, which may compromise the stability of the cleavable functionalities.

The synthesis of disulfide containing linker **3** first involved treatment of HOBt-activated compound **8**[28] with PQ, forming carbamate **9** in 90% yield (Scheme 1B). Concurrently, the thiol of 3-mercaptopropionic acid was protected with 4-methyltrityl chloride, which allowed for amide formation at the carboxylic acid with DBCO-amine, giving compound **10** (72% yield over two steps). The methyltrityl group was next removed with a TFA/$^{i}Pr_3SiH$/DCM mixture to provide thiol **11**, primed for exchange with the activated disulfide **9** under mildly basic conditions (pH 8), affording linker **3** (18% yield over two steps).

The synthesis of trioxolane containing linker **4** began with the ring opening of lactone **12**[30] with NaOMe, which provided primary alcohol **13** in 97% yield (Scheme 1C). Treatment of compound **13** with *p*-nitrophenyl chloroformate produced carbonate **14**, which was subsequently reacted with PQ to install the drug *via* a carbamate linkage (53% yield over two steps). Hydrolysis of the methyl ester of **15** with LiOH produced the corresponding free acid that was then coupled to DBCO-amine, in the presence of HATU, affording linker **4** (76% yield over two steps).

Synthesis of PDIP-PQ Conjugates and Evaluation of Linker Cleavage. The synthesis of PDIP-PQ PDCs was achieved using bioorthogonal click chemistry conditions.[33,34] Six PDCs were generated in moderate yield (24−72%) from the prepared drug-linker constructs, the structures of which are displayed in Figure 2. PDCs with a noncleavable linkage were produced by reacting modified PQ compounds containing a terminal alkyne with either PDIP-Az **1** or [GG]PDIP-Az **2**. A PDC with PQ conjugated at the terminal position comprising an alkane linker (**16**), as well as PDCs conjugated in the spacer

https://doi.org/10.1021/acs.bioconjchem.3c00147
Bioconjugate Chem. 2023, 34, 1105−1113

region containing an alkane (**17**), PEG1 (**18**), or PEG3 (**19**) linker, were successfully synthesized in the presence of $CuSO_4$, sodium ascorbate and the water-soluble ligand tris(3-hydroxypropyltriazolylmethyl)amine (THPTA). Alternatively, PDCs with a cleavable linkage (**20** and **21**) were generated by reacting strained cyclooctyne constructs **3** or **4** with PDIP-Az **1** in 1:1 $^{t}BuOH/H_2O$.

With PDCs **20** and **21** in hand, the *in vitro* fragmentation of the disulfide and trioxolane linkers was investigated by mimicking the intracellular conditions required for the corresponding cleavage mechanism. Briefly, cleavage of the disulfide linker occurs in the presence of a reducing agent (*e.g.*, GSH), producing a free thiol (**23**) that triggers release of the unmodified drug after elimination of oxathiolanone **24** or thiirane **25** and carbon dioxide (Figure 3A).[28,35,36] Cleavage of

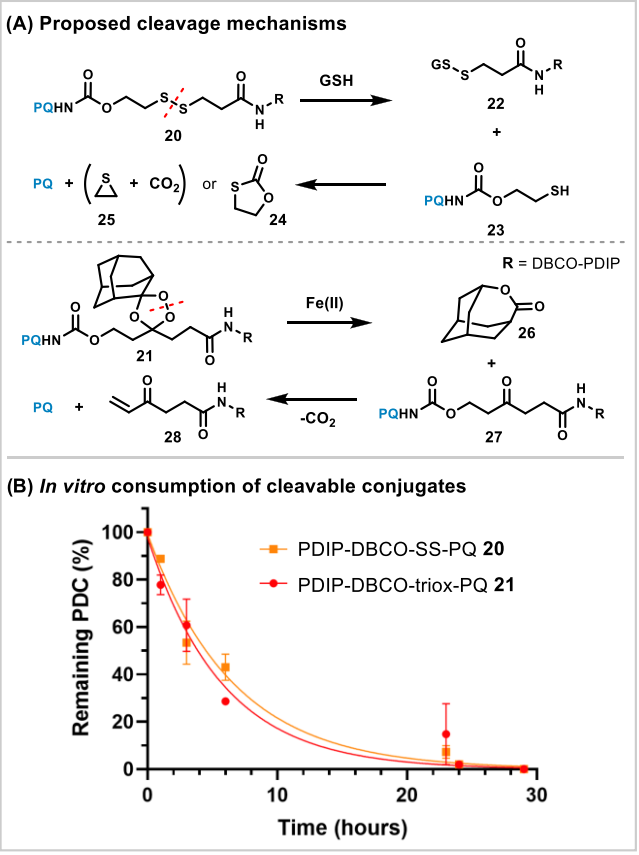

Figure 3. (A) Proposed mechanisms to release PQ from PDIP *via* self-immolative linkers. (B) Consumption of the disulfide and trioxolane cleavable PDCs, as monitored by liquid chromatography–mass spectrometry (LC–MS) analysis. Data points are expressed as mean ± standard error of the mean (SEM) for three replicates.

the trioxolane linker occurs *via* Fe(II)-mediated homolysis of the O–O peroxide bond, affording an oxygen-centered radical that ultimately facilitates the elimination of adamantane lactone **26** and concomitant production of ketone **27** in place of the trioxolane ring. The unmasked ketone **27** is a retro-Michael substrate that undergoes β-elimination and decarboxylation to release the drug in a traceless manner (Figure 3A).[30,32,37]

Cleavage of **20** and **21** was evaluated by treating each conjugate in phosphate buffer with a 100-fold excess of either GSH or $Fe(II)Cl_2$, respectively, to mimic intracellularly relevant concentrations.[30,38,39] The consumption of each conjugate was monitored by LC–MS, showing complete depletion of the PDCs after 30 h (Figure 3B). Fragmentation of both PDCs occurred within a time frame useful for antimalarial treatment, with cleavage half-lives of 4–5 h (Table 1). The formation of intermediates such as thiol **23** and

Table 1. Antiplasmodial Activity and Half-Lives of Linker Cleavage for PDIP-PQ PDCs[a]

compound	IC_{50} (μM)	$t_{1/2}$ cleavage (h)
PQ	2.07(0.16)	n/a
PDIP	9.50(0.65)	n/a
PDIP-Az **1**	8.70(0.41)	n/a
[GG]PDIP-Az **2**	>32	n/a
[GG]PDIP-alk-PQ **16**	22.5(0.89)	n/a
PDIP-alk-PQ **17**	12.9(1.2)	n/a
PDIP-PEG1-PQ **18**	11.3(1.1)	n/a
PDIP-PEG3-PQ **19**	8.81(1.3)	n/a
PDIP-DBCO-SS-PQ **20**	4.25(0.22)	4.55
PDIP-DBCO-triox-PQ **21**	4.68(0.11)	3.99

[a]IC_{50} and cleavage half-life values are given as mean (SEM). n/a: not applicable.

glutathione adduct **22** was observed during the fragmentation of the disulfide conjugate **20**, and ketone **27** was observed for the trioxolane conjugate **21**. Interestingly, in the present study, PQ was not able to be identified in the crude cleavage mixture. However, based on extensive literature precedent demonstrating complete cleavage of these linker types under comparable conditions,[28,30,31] it is likely that release of the free drug is occurring despite the lack of direct detection (see Supporting Information Figures S2 and S3 for further details).

Conjugate Design Characteristics Influence the Antiplasmodial Activity of PDIP-PQ Conjugates. The six PDIP-PQ conjugates were analyzed for their ability to inhibit the *in vitro* growth of *P. falciparum* asexual blood stage parasites (strain 3D7) in RBCs and were compared to the activity of the parent drug and peptide. We were encouraged to discover that most of the PDIP-PQ PDCs retained antiplasmodial activity similar to PDIP, with IC_{50} values in the low micromolar range (Figure 4 and Table 1). Notably, the various design elements probed provided valuable information regarding which PDC characteristics can be modified to improve activity.

Conjugation site was deemed to be an important design element, since PDC **17**, with PQ conjugated between the two helices of PDIP, was twofold more active than **16**, with PQ conjugated at the N-terminus (Figure 4, left). Interestingly, conjugate **16** had moderate antiplasmodial activity, despite containing an azide-modified PDIP analogue (**2**) that had poor potency. This restoration of activity may imply that the bioactivity of the PDC is largely driven by the drug component; hence, cell-penetrating peptide scaffolds with low activity might also be used without compromising drug potency. To further understand the contribution of each PDC component on activity, we are actively exploring the suitability of other antimalarial drugs and cell-penetrating peptides for antimalarial PDC development.

Increasing linker hydrophilicity and length had little effect on efficacy, with PDCs **17**, **18**, and **19** displaying similar potency toward the parasite (Figure 4, middle). However,

https://doi.org/10.1021/acs.bioconjchem.3c00147
Bioconjugate Chem. 2023, 34, 1105–1113

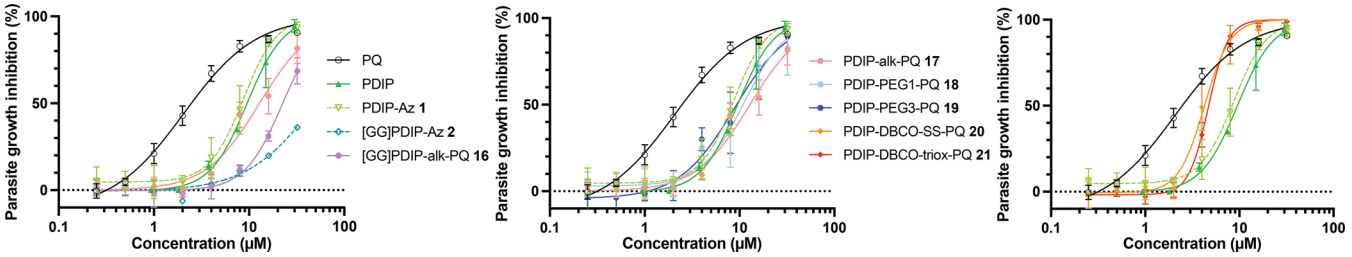

Figure 4. *In vitro* inhibition of *P. falciparum* growth in human RBCs by increasing concentrations of PDIP-PQ PDCs with different conjugation sites (left), noncleavable PDCs (middle), and cleavable PDCs (right). Activity of the PDCs was compared to PQ, PDIP, and the azide-modified peptides. Data points are expressed as mean ± standard deviation (SD) for at least two biological replicates. The legend applies to all three graphs.

increasing the number of PEG units in the linker region increased the observed hemolysis of RBCs at high PDC concentrations (*e.g.*, 32 μmol and above), an unexpected result as PEG incorporation is considered to be nontoxic.[18] Hemolysis caused by PDCs containing cell-penetrating peptides has been previously reported,[19,21] reinforcing that careful conjugate design, including discriminant use of linkers, is important to maximize the therapeutic window by improving drug efficacy without increasing harmful effects.

The incorporation of a traceless cleavable linker into the PDCs was found to have a positive effect on conjugate activity. Cleavable PDCs **20** and **21** were twofold more potent than any of the noncleavable PDCs and were the most active PDCs in this study, with IC_{50} values close to 4 μM (Figure 4, right). Thus, the efficacy of the PDCs seems to benefit from the release of PQ from PDIP, bringing the IC_{50} value for these conjugates closer to PQ and corroborating prior studies in which noncleavable conjugates showed poor efficacy, especially if the pharmacophore of the drug was irreversibly modified.[40] The tethering of PDIP and PQ within noncleavable PDCs (**16**–**19**) may affect the ability of each component to carry out its respective mechanism of action, while cleavable conjugates, in contrast, may provide more appropriate spatial and temporal release of the drug cargo. At this stage, however, we cannot rule out the possibility that reactive byproducts produced from linker cleavage (*e.g.*, **25**, **26**, **28**, Figure 3A) could form cytotoxic adducts that lead to further parasite death and thus better potency for PDCs **20** and **21**.[30,31]

Interestingly, the activity of the cleavable PDCs did not improve the activity of PQ itself—the component with the lower IC_{50} value—indicating the lack of an additive relationship between PQ and PDIP. Treatment of parasites with an equimolar mixture of unconjugated PQ and PDIP-Az **1** resulted in similar activity to PDIP-Az **1** (see Supporting Information, Figure S4), further confirming that PQ and PDIP may not have cooperative mechanisms of action, at least not in the 48 h time frame used herein to capture the expected fast-acting mechanism of PDIP.[10] With activity of the co-administered, but unconjugated PDIP-Az **1** and PQ mixture seemingly dictated by the peptide component, it is possible that the fast-acting mechanism of PDIP alters the internalization or uptake of PQ, thus slightly lowering the activity relative to PQ.[41] Even without additive activity, however, PDCs with PQ cargo might still benefit from improved selectivity for infected RBCs, with the prospect of enhanced safety profiles in G6PD deficient individuals a focus for follow-up studies.

Optimization of PDC design has proven to be imperative for maximizing antiplasmodial efficacy. Since the site of conjugation on PDIP was found to have a profound effect on activity, we have already begun to explore alternative ways to attach PQ to PDIP. To this end, we are developing disulfide-cleavable PDCs where PQ is attached to a backbone cyclized PDIP analogue with a single cysteine. Preliminary data suggests that this approach yields similar activity to the cleavable PDCs described above (see the Supporting Information for synthesis and biological evaluation, Figure S5 and Scheme S1), and supports the notion that the conjugation strategy can be simplified—removing the need for the incorporation of bioorthogonal functionalities, such as azides—without negatively impacting potency. The conjugation site on the drug could also be important for conserving bioactivity; hence, PDCs with PDIP attached to PQ at alternative sites to the primary amine should be explored. Initial studies employing an *O*-linked PDIP-PQ PDC offered slight improvements in activity (see the Supporting Information for synthesis and biological evaluation, Figure S5 and Scheme S1).

CONCLUSIONS

In summary, we have utilized a selective cell-penetrating peptide, PDIP, derived from an innate human defense molecule to successfully synthesize a suite of antiplasmodial PDCs. The different activities displayed by a library of PDIP-PQ conjugates with varied conjugation sites and linker characteristics highlight the importance of conjugate design so as not to impose on the mechanism of action of the drug and peptide components. Given the low micromolar potency of most PDIP-containing PDCs within the study, such PDCs present a feasible approach to antimalarial treatment and a promising step forward for the development of therapies with different mechanisms of killing malarial parasites compared to existing drugs. Leveraging the ability of PDIP to selectively deliver small-molecule drugs into infected RBCs may allow for therapies with contraindications, such as PQ, to be repurposed as treatment options. The PDCs may also prevent the development of resistance by coupling a fast-acting peptide (PDIP) with a slower-acting small-molecule drug, analogous to the strategy provided by current artemisinin combination therapies. This approach could also be directed toward other antimalarial drugs that suffer from off-target toxicities or drug resistance. Furthermore, investigating the mechanistic aspects of antimalarial PDCs could provide insights into the design of alternative therapies that might ultimately lessen the global burden of malaria.

EXPERIMENTAL PROCEDURES

Materials and Methods. General chemistry procedures, including materials, methods, and instrumentation, are detailed in the accompanying Supporting Information File.

https://doi.org/10.1021/acs.bioconjchem.3c00147
Bioconjugate Chem. 2023, 34, 1105−1113

Synthesis of PQ-Alkyne Analogues. Methods for the synthesis of noncleavable and cleavable PQ-alkyne analogues **3**−**7** are detailed in the Supporting Information. Associated characterization data (NMR, mass spectrometry) is provided for new compounds.

General Procedure for the Synthesis of PDCs 16−21. *CuAAC Conjugation.* Performed according to established methods.[33] Concentrations provided are the final concentration in the reaction mixture. Peptide-azide (**1** or **2**, 200 μM, 1.0 equiv) was dissolved in sodium phosphate buffer (100 mM, pH = 7). The following reagents were added sequentially to the reaction vial and magnetically stirred after each new addition: aminoguanidine hydrochloride (5 mM, 25 equiv), dimethyl sulfoxide (DMSO) (10−20%), drug-alkyne (400 μM, 2.0 equiv), copper(II) sulfate (100 μM, 0.5 equiv) premixed with THPTA (500 μM, 2.5 equiv), and sodium ascorbate (5 mM, 25 equiv). The conjugation mixture was stirred at room temperature for 1−2 h. The reaction was quenched with ethylenediamine tetraacetic acid (EDTA) (5.0 equiv) and purified by reversed-phase semipreparative HPLC (24−45% isolated yield). See the Supporting Information for detailed characterization data.

SPAAC Conjugation. Peptide-azide **1** (1.0 equiv) and drug-alkyne (**3** or **4**, 2.0 equiv) were dissolved in water/*t*-butanol (1:1 v/v, 0.7−0.8 mM with respect to the peptide). The mixture was stirred for 24−48 h to produce two regioisomers that were purified by reversed-phase semipreparative HPLC (65−72% isolated yield). See the Supporting Information for detailed characterization data.

Linker Cleavage Studies to Monitor Drug Release. A solution of **20** or **21** (20 μM, 1.0 equiv) in phosphate buffer (1 mM, pH 7) was treated with either reduced glutathione (100 equiv) or $Fe(II)Cl_2$ (100 equiv), respectively. The solutions were incubated at 37 °C, and aliquots were quenched at various time intervals with either MeCN (containing 0.1% formic acid) for tests containing **20** or EDTA (100 mM) for tests containing **21**. Samples were analyzed with reversed-phase LCMS (10−55% MeCN over 40 min, 0.01% formic acid) at λ = 214 nm, and the peak corresponding to the conjugate was integrated using LabSolutions software. The data was then plotted on Prism (GraphPad Software) using one-phase exponential decay.

***P. falciparum* Culture.** *P. falciparum* strain 3D7 was cultured as a 2.5% hematocrit solution by mixing O^+ human RBCs (300 μL) with complete culture medium (CCM, 12 mL), composed of RPMI 1640 supplemented with 8.8 mM D-glucose, 22 mM HEPES, 208 nM hypoxanthine, 46.1 nM gentamicin, 2.8 mM L-glutamine (all from Sigma-Aldrich, Castle Hill, Australia), 2.1 g/L AlbuMAX I (Thermo Fisher Scientific, Australia), and 4.2% (v/v) O^+ human serum. The RBCs and serum were provided by the Australian Red Cross Lifeblood, obtained from anonymous blood donors (aged 18−60 years). Cultures were maintained in 25 cm^3 flasks filled with a low oxygen gas mixture (1% O_2/3% CO_2/96% N_2) and kept in an orbital shaking incubator at 50 rpm at 37 °C. Culture parasitemia was maintained between 0.2 and 10% and CCM was changed every 2−3 days.

Growth Inhibition Assays. Treatment of parasites was conducted using solutions of each drug diluted in CCM to 5× the highest concentration required for the assay, followed by twofold serial dilutions. One day prior to assays, parasites were synchronized at the ring stage by incubating in 5% (w/v) D-sorbitol for 10 min at room temperature, followed by washing twice with warm red cell wash (10 mM sodium phosphate buffer, 160 mM NaCl, pH 7.4) and adding the cells into fresh CCM (12 mL) in a new flask. After a further 18−24 h incubation, the enriched rings developed into synchronized trophozoites, ready for use in the growth assays. An aliquot (10 μL) of each drug dilution and controls (10 μL CCM) were gently mixed with the 0.2% parasite culture (40 μL) in duplicate in a 96-well plate, to create a fivefold dilution of the drug. Parasites were incubated with the treatments at 37 °C for 48 h in an airtight box filled with a low oxygen gas mixture (1% O_2/3% CO_2/96% N_2). Cells were subsequently fixed in 1% (w/v) formaldehyde (1:3 v/v Cytofix (BD Biosciences, Australia) diluted with phosphate-buffered saline (PBS; 137 mM NaCl, 2.7 mM KCl, 10 mM Na_2HPO_4, 1.8 mM KH_2PO_4)) for at least 24 h at 4 °C.

Parasitemia levels in the fixed cells were determined using flow cytometry. Fixed cells were washed twice with PBS containing 1% (w/v) bovine serum albumin (BSA) and stained with 5 μg/mL Hoechst 33342 (Life Technologies, Australia) in 1% BSA/PBS for at least 15 min at 4 °C. Fluorescence signals of stained cells were measured using an LSR Fortessa cell analyzer (BD Biosciences) with at least 200,000 events (cells) collected per sample. Percentages of infected cells (*i.e.*, parasitemia) were identified and computed using FlowJo software (BD Biosciences). The IC_{50} data was determined for each treatment with Prism (GraphPad Software) using nonlinear regression of a dose−response curve.

■ ASSOCIATED CONTENT

Supporting Information

The Supporting Information is available free of charge at https://pubs.acs.org/doi/10.1021/acs.bioconjchem.3c00147.

Supplementary figures and schemes, detailed experimental procedures and characterization data for compounds **3**−**21** (PDF)

■ AUTHOR INFORMATION

Corresponding Authors

Brendan J. McMorran − *The John Curtin School of Medical Research, Australian National University, Canberra 2601 ACT, Australia*; Email: brendan.mcmorran@anu.edu.au

Lara R. Malins − *Research School of Chemistry, Australian National University, Canberra 2601 ACT, Australia; Australian Research Council Centre of Excellence for Innovations in Peptide and Protein Science, Australian National University, Canberra 2601 ACT, Australia*; orcid.org/0000-0002-7691-6432; Email: lara.malins@anu.edu.au

Authors

Isabella R. Palombi − *Research School of Chemistry, Australian National University, Canberra 2601 ACT, Australia; Australian Research Council Centre of Excellence for Innovations in Peptide and Protein Science, Australian National University, Canberra 2601 ACT, Australia*; orcid.org/0000-0002-7958-500X

Nicole Lawrence − *Institute for Molecular Bioscience, The University of Queensland, Brisbane 4072 QLD, Australia; Australian Research Council Centre of Excellence for Innovations in Peptide and Protein Science, The University of Queensland, Brisbane 4072 QLD, Australia*

Andrew M. White − *Research School of Chemistry, Australian National University, Canberra 2601 ACT, Australia; Australian Research Council Centre of Excellence for Innovations in Peptide and Protein Science, Australian National University, Canberra 2601 ACT, Australia*

Caitlin L. Gare − *Research School of Chemistry, Australian National University, Canberra 2601 ACT, Australia; Australian Research Council Centre of Excellence for Innovations in Peptide and Protein Science, Australian National University, Canberra 2601 ACT, Australia;* orcid.org/0009-0002-4916-7314

David J. Craik − *Institute for Molecular Bioscience, The University of Queensland, Brisbane 4072 QLD, Australia; Australian Research Council Centre of Excellence for Innovations in Peptide and Protein Science, The University of Queensland, Brisbane 4072 QLD, Australia;* orcid.org/0000-0003-0007-6796

Complete contact information is available at: https://pubs.acs.org/10.1021/acs.bioconjchem.3c00147

Author Contributions

I.R.P., N.L., A.M.W., and C.L.G. carried out the experimental work in this manuscript. N.L., B.J.M., and L.R.M. conceived of the study, and D.J.C., B.J.M., and L.R.M. provided laboratory resources and infrastructure to support peptide synthesis, parasite growth assays, and synthetic chemistry, respectively. I.R.P. and L.R.M. wrote the manuscript, which was further edited by A.M.W., N.L., and B.J.M. All authors reviewed the final version of the manuscript.

Funding

This work was supported by the National Health and Medical Research Council (Ideas Grant, APP1183927 to L.R.M., N.L., and B.J.M.; Leadership Grant, GNT2009564 to D.J.C.), the Australian Research Council Centre of Excellence for Innovations in Peptide and Protein Science (CE200100012), and the Australian Government Research Training Program PhD Scholarship scheme (I.R.P.).

Notes

The authors declare no competing financial interest.

Experimental procedures involving human blood were approved by the Australian National University Human Research Ethics Committee, approval number 2018/398.

■ ACKNOWLEDGMENTS

The authors thank Megan Sawbridge, Kiran Javed, and Huma Sohail (ANU) for assistance with parasite assays; Dr. Hideki Onagi and Daniel Bartkus (ANU) for technical assistance; Anitha Jeyasingham and Joseph Boileau (ANU) for assistance with mass spectrometry; Dr. Doug Lawes and Dr. Chris Blake (ANU) for support with NMR spectroscopy; Dr. Harpreet Vohra and Michael Devoy (ANU) for help with flow cytometry; and Dr. Yen-Hua Huang, Dr. Lai Yue Chan, and Dr. Simon de Veer (UQ) for assistance with peptide synthesis. Australian Red Cross Lifeblood is acknowledged for providing RBCs and sera.

■ ABBREVIATIONS

PDC, peptide−drug conjugate; RBC, red blood cell; PDIP, platelet factor 4-derived internalization peptide; PQ, primaquine; CuAAC, copper(I)-catalyzed azide−alkyne cycloaddition; SPAAC, strain-promoted azide−alkyne cycloaddition

■ REFERENCES

(1) Siciliano, G.; Alano, P. Enlightening the Malaria Parasite Life Cycle: Bioluminescent *Plasmodium* in Fundamental and Applied Research. *Front. Microbiol.* **2015**, *6*, No. 391.

(2) World Health Organization. *World Malaria Report*, 2022.

(3) Blasco, B.; Leroy, D.; Fidock, D. A. Antimalarial Drug Resistance: Linking *Plasmodium falciparum* Parasite Biology to the Clinic. *Nat. Med.* **2017**, *23*, 917−928.

(4) Wicht, K. J.; Mok, S.; Fidock, D. A. Molecular Mechanisms of Drug Resistance in *Plasmodium falciparum* Malaria. *Annu. Rev. Microbiol.* **2020**, *74*, 431−454.

(5) Uwimana, A.; Umulisa, N.; Venkatesan, M.; Svigel, S. S.; Zhou, Z.; Munyaneza, T.; Habimana, R. M.; Rucogoza, A.; Moriarty, L. F.; Sandford, R.; et al. Association of *Plasmodium falciparum* Kelch13 R561H Genotypes with Delayed Parasite Clearance in Rwanda: An Open-Label, Single-Arm, Multicentre, Therapeutic Efficacy Study. *Lancet Infect. Dis.* **2021**, *21*, 1120−1128.

(6) Balikagala, B.; Fukuda, N.; Ikeda, M.; Katuro, O. T.; Tachibana, S.-I.; Yamauchi, M.; Opio, W.; Emoto, S.; Anywar, D. A.; Kimura, E.; et al. Evidence of Artemisinin-Resistant Malaria in Africa. *N. Engl. J. Med.* **2021**, *385*, 1163−1171.

(7) Haldar, K.; Bhattacharjee, S.; Safeukui, I. Drug Resistance in *Plasmodium*. *Nat. Rev. Microbiol.* **2018**, *16*, 156−170.

(8) Rao, M. S.; Gupta, R.; Liguori, M. J.; Hu, M.; Huang, X.; Mantena, S. R.; Mittelstadt, S. W.; Blomme, E. A.; Van Vleet, T. R. Novel Computational Approach to Predict Off-Target Interactions for Small Molecules. *Front. Big Data* **2019**, *2*, No. 25.

(9) He, R.; Finan, B.; Mayer, J. P.; DiMarchi, R. D. Peptide Conjugates with Small Molecules Designed to Enhance Efficacy and Safety. *Molecules* **2019**, *24*, No. 1855.

(10) Lawrence, N.; Dennis, A. S. M.; Lehane, A. M.; Ehmann, A.; Harvey, P. J.; Benfield, A. H.; Cheneval, O.; Henriques, S. T.; Craik, D. J.; McMorran, B. J. Defense Peptides Engineered from Human Platelet Factor 4 Kill *Plasmodium* by Selective Membrane Disruption. *Cell Chem. Biol.* **2018**, *25*, 1140−1150.

(11) McMorran, B. J.; Wieczorski, L.; Drysdale, K. E.; Chan, J. A.; Huang, H. M.; Smith, C.; Mitiku, C.; Beeson, J. G.; Burgio, G.; Foote, S. J. Platelet Factor 4 and Duffy Antigen Required for Platelet Killing of *Plasmodium falciparum*. *Science* **2012**, *338*, 1348−1351.

(12) Love, M. S.; Millholland, M. G.; Mishra, S.; Kulkarni, S.; Freeman, K. B.; Pan, W.; Kavash, R. W.; Costanzo, M. J.; Jo, H.; Daly, T. M.; et al. Platelet Factor 4 Activity against *P. falciparum* and Its Translation to Nonpeptidic Mimics as Antimalarials. *Cell Host Microbe* **2012**, *12*, 815−823.

(13) Kho, S.; Barber, B. E.; Johar, E.; Andries, B.; Poespoprodjo, J. R.; Kenangalem, E.; Piera, K. A.; Ehmann, A.; Price, R. N.; William, T.; et al. Platelets Kill Circulating Parasites of All Major *Plasmodium* Species in Human Malaria. *Blood* **2018**, *132*, 1332−1344.

(14) Engelbrecht, D.; Coetzer, T. L. *Plasmodium falciparum* Exhibits Markers of Regulated Cell Death at High Population Density in Vitro. *Parasitol. Int.* **2016**, *65*, 715−727.

(15) Tsuchikama, K.; An, Z. Antibody-Drug Conjugates: Recent Advances in Conjugation and Linker Chemistries. *Protein Cell* **2018**, *9*, 33−46.

(16) Lawrence, N.; Philippe, G.; Harvey, P. J.; Condon, N. D.; Benfield, A. H.; Cheneval, O.; Craik, D. J.; Henriques, S. T. Cyclic Peptide Scaffold with Ability to Stabilize and Deliver a Helical Cell-Impermeable Cargo across Membranes of Cultured Cancer Cells. *RSC Chem. Biol.* **2020**, *1*, 405−420.

(17) Philippe, G. J. B.; Mittermeier, A.; Lawrence, N.; Huang, Y. H.; Condon, N. D.; Loewer, A.; Craik, D. J.; Henriques, S. T. Angler Peptides: Macrocyclic Conjugates Inhibit P53:MDM2/X Interactions and Activate Apoptosis in Cancer Cells. *ACS Chem. Biol.* **2021**, *16*, 414−428.

(18) Fu, C.; Yu, L.; Miao, Y.; Liu, X.; Yu, Z.; Wei, M. Peptide−Drug Conjugates (PDCs): A Novel Trend of Research and Development on Targeted Therapy, Hype or Hope? *Acta Pharm. Sin. B* **2023**, *13*, 498−516.

(19) (a) Aguiar, L.; Biosca, A.; Lantero, E.; Gut, J.; Vale, N.; Rosenthal, P. J.; Nogueira, F.; Andreu, D.; Fernàndez-Busquets, X.; Gomes, P. Coupling the Antimalarial Cell Penetrating Peptide TP10 to Classical Antimalarial Drugs Primaquine and Chloroquine Produces Strongly Hemolytic Conjugates. *Molecules* **2019**, *24*, No. 4559. Note: to the best of our knowledge, refs 19−21 are the only reported antimalarial PDCs (following the strict definition of a peptide used as a targeting device conjugated to a small molecule drug). For an example of PDCs that do not follow the above definition, see: (b) Panda, S. S.; Ibrahim, M. A.; Küçükbay, H.; Meyers, M. J.; Sverdrup, F. M.; El-Feky, S. A.; Katritzky, A. R. Synthesis and Antimalarial Bioassay of Quinine − Peptide Conjugates. *Chem. Biol. Drug Des.* **2013**, *82*, 361−366.
(20) Aguiar, L.; Machado, M.; Sanches-Vaz, M.; Prudêncio, M.; Vale, N.; Gomes, P. Coupling the Cell-Penetrating Peptides Transportan and Transportan 10 to Primaquine Enhances Its Activity against Liver-Stage Malaria Parasites. *MedChemComm* **2019**, *10*, 221−226.
(21) Aguiar, L.; Pinheiro, M.; Neves, A. R.; Vale, N.; Defaus, S.; Andreu, D.; Reis, S.; Gomes, P. Insights into the Membranolytic Activity of Antimalarial Drug-Cell Penetrating Peptide Conjugates. *Membranes* **2021**, *11*, No. 4.
(22) Cappellini, M.; Fiorelli, G. Glucose-6-Phosphate Dehydrogenase Deficiency. *Lancet* **2008**, *371*, 64−74.
(23) Howes, R. E.; Battle, K. E.; Satyagraha, A. W.; Baird, J. K.; Hay, S. I. G6PD Deficiency: Global Distribution, Genetic Variants and Primaquine Therapy. *Adv. Parasitol.* **2013**, *81*, 133−201.
(24) Teixeira, C.; Vale, N.; Pérez, B.; Gomes, A.; Gomes, J. R. B.; Gomes, P. "Recycling" Classical Drugs for Malaria. *Chem. Rev.* **2014**, *114*, 11164−11220.
(25) Rostovtsev, V. V.; Green, L. G.; Fokin, V. V.; Sharpless, K. B. A Stepwise Huisgen Cycloaddition Process: Copper(I)-Catalyzed Regioselective "Ligation" of Azides and Terminal Alkynes. *Angew. Chem., Int. Ed.* **2002**, *41*, 2596−2599.
(26) Tornøe, C. W.; Christensen, C.; Meldal, M. Peptidotriazoles on Solid Phase: [1,2,3]-Triazoles by Regiospecific Copper(I)-Catalyzed 1,3-Dipolar Cycloadditions of Terminal Alkynes to Azides. *J. Org. Chem.* **2002**, *67*, 3057−3064.
(27) Agard, N. J.; Prescher, J. A.; Bertozzi, C. R. A Strain-Promoted [3 + 2] Azide-Alkyne Cycloaddition for Covalent Modification of Biomolecules in Living Systems. *J. Am. Chem. Soc.* **2004**, *126*, 15046−15047.
(28) Kularatne, S. A.; Venkatesh, C.; Santhapuram, H. K. R.; Wang, K.; Vaitilingam, B.; Henne, W. A.; Low, P. S. Synthesis and Biological Analysis of Prostate-Specific Membrane Antigen-Targeted Anticancer Prodrugs. *J. Med. Chem.* **2010**, *53*, 7767−7777.
(29) Müller, S. Redox and Antioxidant Systems of the Malaria Parasite *Plasmodium falciparum*. *Mol. Microbiol.* **2004**, *53*, 1291−1305.
(30) Mahajan, S. S.; Deu, E.; Lauterwasser, E. M.; Leyva, M. J.; Ellman, J. A.; Bogyo, M.; Renslo, A. R. A Fragmenting Hybrid Approach for Targeted Delivery of Multiple Therapeutic Agents to the Malaria Parasite. *ChemMedChem* **2011**, *6*, 415−419.
(31) Deu, E.; Chen, I. T.; Lauterwasser, E. M. W.; Valderramos, J.; Li, H.; Edgington, L. E.; Renslo, A. R.; Bogyo, M. Ferrous Iron-Dependent Drug Delivery Enables Controlled and Selective Release of Therapeutic Agents in Vivo. *Proc. Natl. Acad. Sci. U.S.A.* **2013**, *110*, 18244−18249.
(32) Spangler, B.; Kline, T.; Hanson, J.; Li, X.; Zhou, S.; Wells, J. A.; Sato, A. K.; Renslo, A. R. Toward a Ferrous Iron-Cleavable Linker for Antibody−Drug Conjugates. *Mol. Pharm.* **2018**, *15*, 2054−2059.
(33) Hong, V.; Presolski, S. I.; Ma, C.; Finn, M. G. Analysis and Optimization of Copper-Catalyzed Azide-Alkyne Cycloaddition for Bioconjugation. *Angew. Chem., Int. Ed.* **2009**, *48*, 9879−9883.
(34) Lau, Y. H.; Wu, Y.; Rossmann, M.; Tan, B. X.; De Andrade, P.; Tan, Y. S.; Verma, C.; McKenzie, G. J.; Venkitaraman, A. R.; Hyvönen, M.; Spring, D. R. Double Strain-Promoted Macrocyclization for the Rapid Selection of Cell-Active Stapled Peptides. *Angew. Chem., Int. Ed.* **2015**, *54*, 15410−15413.
(35) Jones, L. R.; Goun, E. A.; Shinde, R.; Rothbard, J. B.; Contag, C. H.; Wender, P. A. Releasable Luciferin-Transporter Conjugates: Tools for the Real-Time Analysis of Cellular Uptake and Release. *J. Am. Chem. Soc.* **2006**, *128*, 6526−6527.
(36) Henne, W. A.; Doorneweerd, D. D.; Hilgenbrink, A. R.; Kularatne, S. A.; Low, P. S. Synthesis and Activity of a Folate Peptide Camptothecin Prodrug. *Bioorg. Med. Chem. Lett.* **2006**, *16*, 5350−5355.
(37) Vennerstrom, J. L.; Arbe-Barnes, S.; Brun, R.; Charman, S. A.; Chiu, F. C. K.; Chollet, J.; Dong, Y.; Dorn, A.; Hunziker, D.; Matile, H.; et al. Identification of an Antimalarial Synthetic Trioxolane Drug Development Candidate. *Nature* **2004**, *430*, 900−904.
(38) Forman, H. J.; Zhang, H.; Rinna, A. Glutathione: Overview of Its Protective Roles, Measurement, and Biosynthesis. *Mol. Aspects Med.* **2009**, *30*, 1−12.
(39) Müller, S. Role and Regulation of Glutathione Metabolism in *Plasmodium falciparum*. *Molecules* **2015**, *20*, No. 10511.
(40) Bargh, J. D.; Isidro-Llobet, A.; Parker, J. S.; Spring, D. R. Cleavable Linkers in Antibody-Drug Conjugates. *Chem. Soc. Rev.* **2019**, *48*, 4361−4374.
(41) Camarda, G.; Jirawatcharadech, P.; Priestley, R. S.; Saif, A.; March, S.; Wong, M. H.; Leung, S.; Miller, A. B.; Baker, D. A.; Alano, P.; et al. Antimalarial Activity of Primaquine Operates via a Two-Step Biochemical Relay. *Nat. Commun.* **2019**, *10*, No. 3226.

https://doi.org/10.1021/acs.bioconjchem.3c00147
Bioconjugate Chem. 2023, 34, 1105−1113

Concluding Remarks

The published study presented in this chapter highlights the utility of PDCs as promising alternatives to small molecule drugs for malaria treatment and the outcomes warrant the continued exploration of antimalarial PDCs. Through the exploration of six PQ-containing PDCs—with three different linker types (non-cleavable, Fe(II)-sensitive and reducible disulfide) and two PDIP analogues—the value of using PDC design to maintain the potency of PQ and PDIP was realised. Based on the results of this study, we have already extended our PDIP-based PDCs to include other drug cargoes, including tafenoquine (**2.10**), artesunate (**2.6**) and methotrexate (a DHFR inhibitor that has reported antiplasmodial activity[44,45]), a project led by PhD student Caitlin Gare.[46] Alternate peptide scaffolds, such as CPPs with limited or no antiplasmodial activity, were also used in the production of PQ and artesunate PDCs. Analogous to the study presented in this chapter, the activity of our next generation PDCs was largely driven by the drug cargo, however, contributions from the peptide component were also evident as a PDC containing an antiplasmodial peptide scaffold (**2.11**) was more potent than PDCs comprising CPPs with limited or no intrinsic activity (**2.12** and **2.13**) (Figure 2.6).[46] This implies that PDCs with a dual mechanism of action may have an advantage over PDCs with a single mechanism, even if potency enhancements are not realised. While some of our PDCs induced minor haemolysis at high drug concentrations (> 32 μM), this is in contrast to previously published PQ-containing PDCs where extensive haemolysis occurred (so no activity data could be obtained),[38,39] further indicating the important role of the peptide scaffold and the requirement for careful design to ensure the mechanisms of the drug and peptide components are not impaired following conjugation.

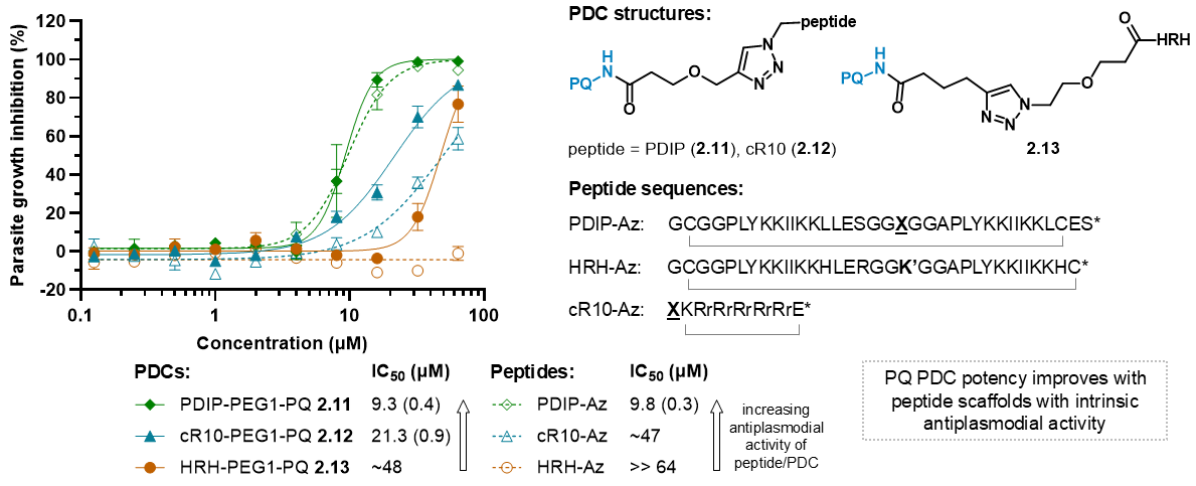

Figure 2.6. Summary of the results from our follow up study of non-cleavable PQ-containing PDCs. The role of the peptide scaffold was examined by conjugating PQ onto three CPP scaffolds, one with antiplasmodial activity (PDIP), one with moderate antiplasmodial activity (cR10) and one with no activity (HRH). For the peptide sequences, the amino acid sites for drug conjugation are bolded and the cyclisation junctions (either disulfide or amide linkage) are displayed with grey lines. * = amidated C-terminus; r = D-arginine; X = azidoalanine; K' = lysine side chain modified with propargyl-PEG1-acid. Note: IC_{50} values from this study were obtained from a 72 h high-throughput imaging assay against blood stage parasites.[47] Figure adapted from Gare *et al.*[46]

Since the contribution of the peptide scaffold to overall PDC activity appears to be more subtle than the contribution from the drug cargo, future mechanistic studies should explore the role of the peptide. This could be achieved using similar methods to those used to determine the mechanism of action for PDIP,[41] allowing for direct comparison with the PDCs. We are interested in understanding whether PDIP-based PDCs are still able to lyse the parasite digestive vacuole with an appended drug cargo, which can be investigated using fluorescence imaging following treatment of RBCs infected with a *P. falciparum* strain that expresses a GFP-tagged enzyme found in the digestive vacuole.[48] We also aim to understand the membrane binding properties of the PDCs by using surface plasmon resonance to analyse their association to different lipid bilayer models representative of the membranes of the parasite (anionic),[49] infected RBCs (anionic)[50,51] or uninfected RBCs (neutral).[52] This could provide knowledge about whether the addition of hydrophobic drugs and linkers changes the preferential binding of PDIP to membranes containing anionic lipid headgroups and therefore its selectivity for infected cells. Additional insight into the membrane-disruptive properties of the PDCs can be obtained by measuring leakage of a fluorescent molecule from vesicles composed of lipids representative of infected or uninfected cells.

Despite the PDIP-PQ PDCs not having additive activity against blood stage parasites, they may provide the potential benefit of enhanced safety profiles in G6PD deficient individuals. It may be possible to gain insights into this selectivity by incubating the PDCs and relevant drug and peptide controls with G6PD deficient RBCs and analysing the cells for markers of haemotoxicity, such as the formation of methaemoglobin and reactive oxygen species.[53] Such experiments may require the inclusion of human liver microsomes to generate the oxidative metabolites of PQ (*via* cytochrome P450 enzymes) that are proposed to be responsible for its toxicity.[26,53] If obtaining G6PD deficient blood is challenging, normal RBCs could be pretreated with a small molecule G6PD inhibitor,[54] to mimic deficient RBCs. Ideally, if the PDCs are selective, limited haemotoxicity towards G6PD deficient cells should be observed for these treatments relative to PQ.

For the PDIP-PQ PDCs discussed in this chapter, traceless cleavable linkers capable of releasing unmodified PQ from the peptide were determined to produce the most potent PDCs. This indicated the importance of the amine moiety of PQ for its activity or that it cannot achieve its intended mechanism of action while tethered to a peptide. Therefore, the exploration of alternative cleavable linkers could be useful in the design of future triazole linked, PQ-containing PDCs. Protease-sensitive linkers including the Val-Cit or Val-Ala dipeptide sequences could be useful in the context of malaria, as the parasite contains several proteases involved in haemoglobin degradation (*e.g.* plasmepsin and falcipain) that could potentially cleave dipeptide linkers.[55] Synthesis of the dipeptide linkers **2.15** could be achieved from

commercially available **2.14** (Scheme 2.1A), or alternatively by construction on a solid-phase support as recently described by Ahangarpour *et al.* (synthetic route not shown).[56] The acidic pH of the parasite digestive vacuole[14] could also enable investigation of a cleavable linker that contains an acid-labile hydrazone functional group. A possible synthetic route towards hydrazone linker **2.18** entails the modification of PQ to contain a ketone handle (**2.16**) and subsequent hydrazone formation with Boc-protected hydrazide **2.17** (Scheme 2.1B). It should be noted that following hydrazone linker cleavage an appendage remains on the drug,[57] so modifications to install a ketone moiety onto PQ should be minimal, for example by using pyruvic acid. In our hands, synthetic efforts towards this linker have not yet been successful due to hydrazone hydrolysis during purification with flash column chromatography or with HPLC containing an acidic eluent. Future efforts may benefit from purification with HPLC containing a basic eluent, such as ammonium bicarbonate.

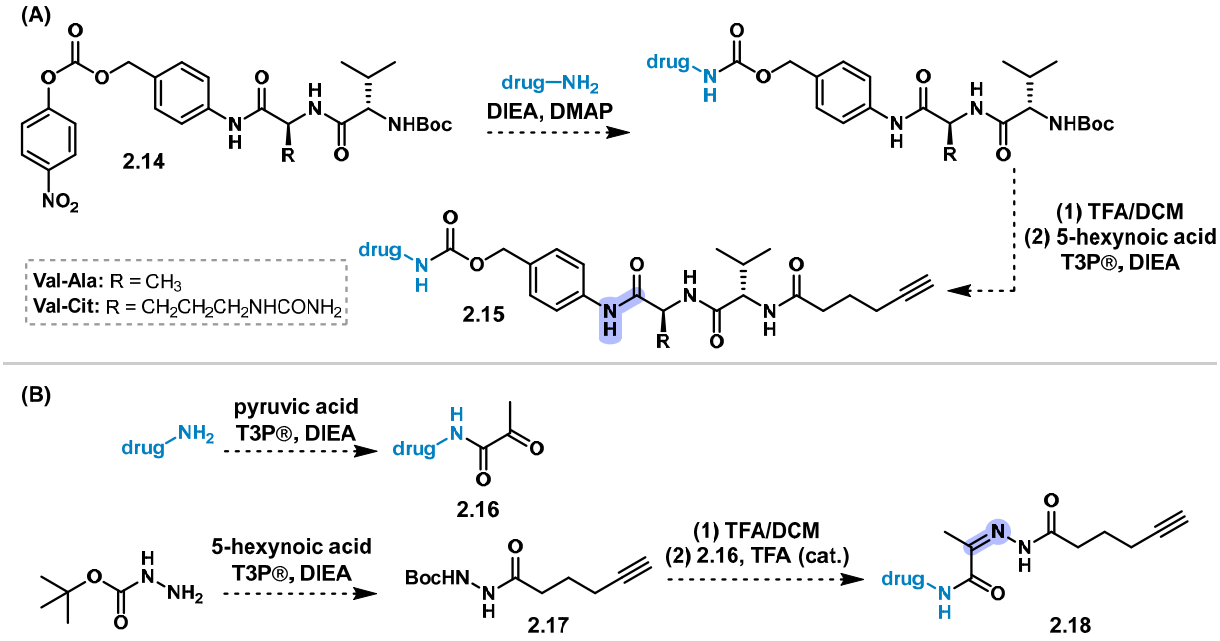

Scheme 2.1. Proposed synthetic pathways towards (A) protease-sensitive and (B) acid-sensitive cleavable linkers that could be utilised in future generations of antimalarial PDCs.

To be useful as antimalarial treatment, PDIP-PQ PDCs should preferably be active against multiple parasite life cycle stages (see ideal criteria in Section 2.2.1). In our studies, we only examined the activity of PQ-containing PDCs on asexual blood stage parasites, however, PQ is active on multiple life cycle stages, including liver and gametocyte forms of the parasite. Future studies would thus benefit from the exploration of PDC activity against other parasite stages. To this end, preliminary studies have been initiated into the killing ability of lead non-cleavable and cleavable PDIP-PQ PDCs, along with PDIP, against gametocyte (McMorran lab, Australian National University) and mosquito stage (Sutherland lab, London School of Hygiene and Tropical Medicine) parasites (Figure 2.7A).

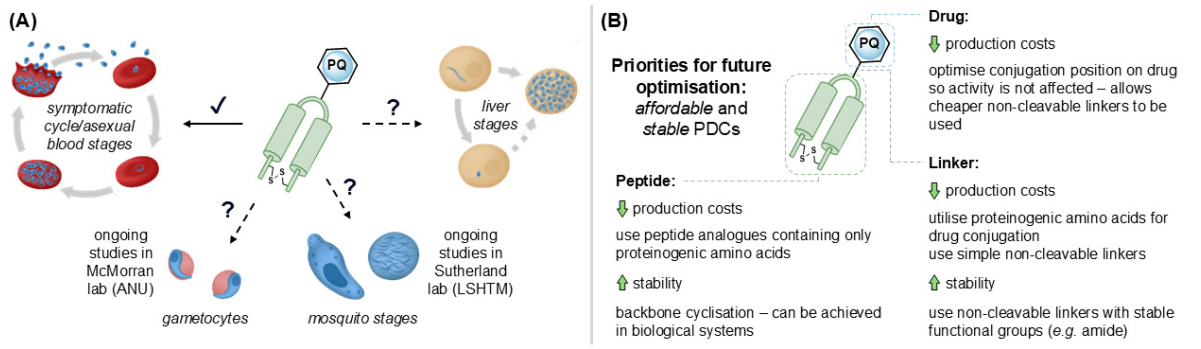

Figure 2.7. Optimisation of PDIP-PQ PDCs required for enhanced practicality of this modality for antimalarial treatments. (A) Exploration of the killing ability of PDIP-PQ PDCs against other parasite life cycle stages. (B) Priorities for the design of future generations of PDIP-PQ PDCs that are more affordable and stable.

Alongside targeting multiple parasite stages, PDIP-PQ PDCs will need to be affordable, stable during transport and easy to administer, to be a feasible approach for malaria treatment in low-income countries. With our proof-of-principle studies suggesting that PDCs are a viable way to kill *Plasmodium* parasites, future PDC optimisation should aim to enhance their practicality as antimalarial treatments (Figure 2.7B). Peptide scaffolds that are composed of only proteinogenic amino acids can be produced by cheaper chemical synthesis and recombinant expression methods, so should be prioritised in subsequent generations of PDCs. This will require a conjugation strategy that utilises a proteinogenic amino acid. The preliminary development of a PDC containing a backbone cyclised PDIP analogue with a single cysteine conjugated to PQ *via* a disulfide bond supports the potential for more affordable future synthetic routes. Peptide backbone macrocyclisation, which is thought to enhance stability, can be achieved in biological systems using asparaginyl endopeptidase enzymes,[58] potentially enabling the production of cyclic PDIP analogues *via* biosynthetic methods. Additional cost reductions could be achieved if drug cargoes are conjugated in a way that does not hinder their mechanism of action, as then cleavable linkers with extensive syntheses can be avoided. Alternatively, cargoes that are inherently cleavable can be utilised,[46] such as artesunate (**2.6**), a prodrug that contains an ester linkage labile to esterases.[59] Finally, improved stability of the PDIP scaffold[60] and linkers will be important to prolong PDC stability during circulation but also will be essential for successful storage and distribution without refrigeration. It is likely that a non-cleavable linkage will provide better stability compared to a cleavable linker, so future PDCs should prioritise modifications on PQ for conjugation that do not impede on its activity when tethered to the peptide.

With many avenues for further studies, PDIP-PQ PDCs are promising alternatives to traditional antimalarial drugs. Altogether, our initial and follow up studies on antimalarial PDCs demonstrate that PDCs with a dual mechanism of bioactivity and targeted delivery of drugs to infected RBCs could be a promising approach which renews interest in drugs with resistance

or toxicity issues. The future experiments outlined in this section could provide greater understanding of the mechanism of antimalarial PDCs and provide insight into the broader applicability of PDCs as antimalarial drugs.

References

(1) World Health Organisation. *World Malaria Report 2023*; Geneva, 2023.

(2) Schofield, L.; Grau, G. E. *Nat. Rev. Immunol.* **2005**, *5*, 722–735.

(3) Ashley, E. A.; Phyo, A. P. *Drugs* **2018**, *78*, 861–879.

(4) Malaria Atlas Project, https://data.malariaatlas.org/ (accessed Sep 6, 2024).

(5) Bryan, J. H.; Foley, D. H.; Sutherst, R. W. *Med. J. Aust.* **1996**, *164*, 345–347.

(6) Sohail, A.; Barry, A.; Auburn, S.; Cheng, Q.; Lau, C. L.; Lee, R.; Price, R. N.; Furuya-Kanamori, L.; Bareng, P.; McGuinness, S. L.; Leder, K. *J. Travel Med.* **2024**, *31*, 1–11.

(7) Aly, A. S.; Vaughan, A. M.; Kappe, S. H. *Annu. Rev. Microbiol.* **2009**, *63*, 195–221.

(8) Siciliano, G.; Alano, P. *Front. Microbiol.* **2015**, *6*, 391.

(9) Klein, E. Y. *Int. J. Antimicrob. Agents* **2013**, *41*, 311–317.

(10) Blasco, B.; Leroy, D.; Fidock, D. A. *Nat. Med.* **2017**, *23*, 917–928.

(11) Wellcome Genome Campus: yourgenome. What is malaria? https://www.yourgenome.org/theme/what-is-malaria/ (accessed Sep 11, 2024).

(12) Basore, K.; Cheng, Y.; Kushwaha, A. K.; Nguyen, S. T.; Desai, S. A. *Front. Pharmacol.* **2015**, *6*, 91.

(13) Sullivan, D. J.; Gluzman, I. Y.; Russell, D. G.; Goldberg, D. E. *Proc. Natl. Acad. Sci. USA* **1996**, *93*, 11865–11870.

(14) Lehane, A. M.; Hayward, R.; Saliba, K. J.; Kirk, K. *J. Cell Sci.* **2008**, *121*, 1624–1632.

(15) Haldar, K.; Bhattacharjee, S.; Safeukui, I. *Nat. Rev. Microbiol.* **2018**, *16*, 156–170.

(16) Tse, E. G.; Korsik, M.; Todd, M. H. *Malar. J.* **2019**, *18*, 93.

(17) Rudrapal, M.; Chetia, D. *Drug Des. Devel. Ther.* **2016**, *10*, 3575–3590.

(18) Kung, S. H.; Lund, S.; Murarka, A.; McPhee, D.; Paddon, C. J. *Front. Plant Sci.* **2018**, *9*, 87.

(19) Meshnick, S. R. *Int. J. Parasitol.* **2002**, *32*, 1655–1660.

(20) Wang, J.; Xu, C.; Wong, Y. K.; Li, Y.; Liao, F.; Jiang, T.; Tu, Y. *Engineering* **2019**, *5*, 32–39.

(21) Uwimana, A.; Umulisa, N.; Venkatesan, M.; Svigel, S. S.; Zhou, Z.; Munyaneza, T.;

Habimana, R. M.; Rucogoza, A.; Moriarty, L. F.; Sandford, R.; Piercefield, E.; Goldman, I.; Ezema, B.; Talundzic, E.; Pacheco, M. A.; Escalante, A. A.; Ngamije, D.; Mangala, J.-L. N.; Kabera, M.; Munguti, K.; Murindahabi, M.; Brieger, W.; Musanabaganwa, C.; Mutesa, L.; Udhayakumar, V.; Mbituyumuremyi, A.; Halsey, E. S.; Lucchi, N. W. *Lancet Infect. Dis.* **2021**, *21*, 1120–1128.

(22) Balikagala, B.; Fukuda, N.; Ikeda, M.; Katuro, O. T.; Tachibana, S.-I.; Yamauchi, M.; Opio, W.; Emoto, S.; Anywar, D. A.; Kimura, E.; Palacpac, N. M. Q.; Odongo-Aginya, E. I.; Ogwang, M.; Horii, T.; Mita, T. *N. Engl. J. Med.* **2021**, *385*, 1163–1171.

(23) Ashley, E. A.; Recht, J.; White, N. J. *Malar. J.* **2014**, *13*, 418.

(24) Pukrittayakamee, S.; Chotivanich, K.; Chantra, A.; Clemens, R.; Looareesuwan, S.; White, N. J. *Antimicrob. Agents Chemother.* **2004**, *48*, 1329–1334.

(25) Uyoga, S.; Ndila, C. M.; Macharia, A. W.; Nyutu, G.; Shah, S.; Peshu, N.; Clarke, G. M.; Kwiatkowski, D. P.; Rockett, K. A.; Williams, T. N. *Lancet Haematol.* **2015**, *2*, e437–e444.

(26) Camarda, G.; Jirawatcharadech, P.; Priestley, R. S.; Saif, A.; March, S.; Wong, M. H.; Leung, S.; Miller, A. B.; Baker, D. A.; Alano, P.; Paine, M. J.; Bhatia, S. N.; O'Neill, P. M.; Ward, S. A.; Biagini, G. A. *Nat. Commun.* **2019**, *10*, 3226.

(27) Howes, R. E.; Piel, F. B.; Patil, A. P.; Nyangiri, O. A.; Gething, P. W.; Dewi, M.; Hogg, M. M.; Battle, K. E.; Padilla, C. D.; Baird, J. K.; Hay, S. I. *PLoS Med.* **2012**, *9*, e1001339.

(28) He, R.; Finan, B.; Mayer, J. P.; DiMarchi, R. D. *Molecules* **2019**, *24*, 1855.

(29) Vale, N.; Aguiar, L.; Gomes, P. *Front. Pharmacol.* **2014**, *5*, 275.

(30) Fu, C.; Yu, L.; Miao, Y.; Liu, X.; Yu, Z.; Wei, M. *Acta Pharm. Sin. B* **2023**, *13*, 498–516.

(31) Dean, T. T.; Jelú-Reyes, J.; Allen, A. C.; Moore, T. W. *J. Med. Chem.* **2024**, *67*, 1641–1661.

(32) Todorovski, T.; Kalafatovic, D.; Andreu, D. *Pharmaceutics* **2023**, *15*, 351.

(33) Reinhardt, A.; Neundorf, I. *Int. J. Mol. Sci.* **2016**, *17*, 701.

(34) Kalimuthu, K.; Srinivasan, N. R.; Govindarajan, G. *Int. J. Pept. Res. Ther.* **2023**, *29*, 91.

(35) Rząd, K.; Paluszkiewicz, E.; Neubauer, D.; Olszewski, M.; Kozłowska-Tylingo, K.; Kamysz, W.; Gabriel, I. *Int. J. Mol. Sci.* **2021**, *22*, 13190.

(36) Brankiewicz, W.; Okońska, J.; Serbakowska, K.; Lica, J.; Drab, M.; Ptaszyńska, N.; Łęgowska, A.; Rolka, K.; Szweda, P. *Pharmaceutics* **2022**, *14*, 693.

(37) Aguiar, L.; Machado, M.; Sanches-Vaz, M.; Prudêncio, M.; Vale, N.; Gomes, P. *MedChemComm* **2019**, *10*, 221–226.

(38) Aguiar, L.; Biosca, A.; Lantero, E.; Gut, J.; Vale, N.; Rosenthal, P. J.; Nogueira, F.; Andreu, D.; Fernàndez-Busquets, X.; Gomes, P. *Molecules* **2019**, *24*, 4559.

(39) Aguiar, L.; Pinheiro, M.; Neves, A. R.; Vale, N.; Defaus, S.; Andreu, D.; Reis, S.; Gomes, P. *Membranes* **2021**, *11*, 4.

(40) Costa, N. C. S.; dos Anjos, L. R.; de Souza, J. V. M.; Brasil, M. C. O. de A.; Moreira, V. P.; Graminha, M. A. S.; Lubec, G.; Gonzalez, E. R. P.; Cilli, E. M. *ACS Omega* **2023**, *8*, 34008–34016.

(41) Lawrence, N.; Dennis, A. S.; Lehane, A. M.; Ehmann, A.; Harvey, P. J.; Benfield, A. H.; Cheneval, O.; Henriques, S. T.; Craik, D. J.; McMorran, B. J. *Cell Chem. Biol.* **2018**, *25*, 1140–1150.

(42) Teixeira, C.; Vale, N.; Pérez, B.; Gomes, A.; Gomes, J. R. B.; Gomes, P. *Chem. Rev.* **2014**, *114*, 11164–11220.

(43) Palombi, I. R.; Lawrence, N.; White, A. M.; Gare, C. L.; Craik, D. J.; McMorran, B. J.; Malins, L. R. *Bioconjug. Chem.* **2023**, *34*, 1105–1113.

(44) Sheehy, T. W.; Dempsey, H. *JAMA* **1970**, *214*, 109–114.

(45) Imwong, M.; Russell, B.; Suwanarusk, R.; Nzila, A.; Leimanis, M. L.; Sriprawat, K.; Kaewpongsri, S.; Phyo, A. P.; Snounou, G.; Nosten, F.; Renia, L. *J. Infect. Dis.* **2011**, *203*, 207–210.

(46) Gare, C. L.; Palombi, I. R.; White, A. M.; Chavchich, M.; Edstein, M. D.; Lock, A. A.; Avery, V. M.; Craik, D. J.; McMorran, B. J.; Lawrence, N.; Malins, L. R. *ChemMedChem* **2025**, *20*, e202400637.

(47) Duffy, S.; Avery, V. M. *Am. J. Trop. Med. Hyg.* **2012**, *86*, 84–92.

(48) Klonis, N.; Tan, O.; Jackson, K.; Goldberg, D.; Klemba, M.; Tilley, L. *Biochem. J.* **2007**, *407*, 343–354.

(49) Tawk, L.; Chicanne, G.; Dubremetz, J. F.; Richard, V.; Payrastre, B.; Vial, H. J.; Roy, C.; Wengelnik, K. *Eukaryot. Cell* **2010**, *9*, 1519–1530.

(50) Engelbrecht, D.; Coetzer, T. L. *Parasitol. Int.* **2016**, *65*, 715–727.

(51) Eda, S.; Sherman, I. W. *Cell. Physiol. Biochem.* **2002**, *12*, 373–384.

(52) Himbert, S.; Rheinstädter, M. C. *Front. Physiol.* **2022**, *13*, 953257.

(53) Ganesan, S.; Chaurasiya, N. D.; Sahu, R.; Walker, L. A.; Tekwani, B. L. *Toxicology* **2012**, *294*, 54–60.

(54) Ghergurovich, J. M.; García-Cañaveras, J. C.; Wang, J.; Schmidt, E.; Zhang, Z.; TeSlaa, T.; Patel, H.; Chen, L.; Britt, E. C.; Piqueras-Nebot, M.; Gomez-Cabrera, M. C.; Lahoz, A.; Fan, J.; Beier, U. H.; Kim, H.; Rabinowitz, J. D. *Nat. Chem. Biol.* **2020**, *16*, 731–739.

(55) Mishra, M.; Singh, V.; Singh, S. *Front. Microbiol.* **2019**, *10*, 394.

(56) Ahangarpour, M.; Brimble, M. A.; Kavianinia, I. *Bioconjug. Chem.* **2024**, *35*, 1007–1014.

(57) Tsuchikama, K.; An, Z. *Protein Cell* **2018**, *9*, 33–46.

(58) Jackson, M. A.; Gilding, E. K.; Shafee, T.; Harris, K. S.; Kaas, Q.; Poon, S.; Yap, K.; Jia, H.; Guarino, R.; Chan, L. Y.; Durek, T.; Anderson, M. A.; Craik, D. J. *Nat. Commun.* **2018**, *9*, 2411.

(59) Morris, C. A.; Duparc, S.; Borghini-Fuhrer, I.; Jung, D.; Shin, C. S.; Fleckenstein, L. *Malar. J.* **2011**, *10*, 263.

(60) Lawrence, N.; Handley, T. N. G.; de Veer, S. J.; Harding, M. D.; Andraszek, A.; Hall, L.; Raven, K. D.; Duffy, S.; Avery, V. M.; Craik, D. J.; Malins, L. R.; McMorran, B. J. *ACS Infect. Dis.* **2024**, *10*, 2899–2912.

Chapter 3:

Camptothecin PDCs – a case study for reducing anticancer drug toxicity

Introduction

Drug conjugate development began as an important alternative to traditional chemotherapy drugs for the treatment of cancer. Cancer encompasses a collection of diseases caused by uncontrolled proliferation of cells that have acquired changes which provide an abnormal growth advantage.[1] As a result, many conventional chemotherapeutics target rapidly dividing cells, however, this also kills healthy proliferative cells, leading to patient side effects.[2] Therefore, drug conjugates are suited to cancer treatment because cytotoxic chemotherapeutics can be directly targeted to cancer cells, thereby minimising their interaction with healthy tissues. As many ADCs and PDCs have been developed with the aim of safely delivering non-selective cytotoxic drug cargoes, we were interested to explore the ability of our cell-penetrating, anticancer peptide PDIP as a delivery vehicle to potentially improve the safety of the cytotoxic drug camptothecin.

3.1 Factors limiting the clinical use of camptothecin

Camptothecin (CPT, **3.1**) is an alkaloid natural product that was originally isolated from the bark of the *Camptotheca accuminata* tree.[3] It has a unique anticancer mechanism of action that involves the poisoning of topoisomerase I, an enzyme that relaxes supercoiled DNA during replication and transcription.[4,5] Inhibition of this enzyme causes an accumulation of DNA damage which ultimately results in cell death. Unfortunately, treatment with CPT is limited due to severe systemic toxicity.[6] While the lactone moiety in the CPT E-ring is important for its binding to topoisomerase I,[7,8] at physiological (and basic) pH this pharmacophore is converted *via* hydrolysis into an inactive carboxylate species (**3.2**, Figure 3.1), which is thought to contribute to the non-specific toxicity of CPT. Furthermore, CPT (lactone form) is insoluble in many biologically relevant solvents. These three factors—off-target toxicity, instability of the lactone and poor solubility—have prevented the clinical use of CPT.[6]

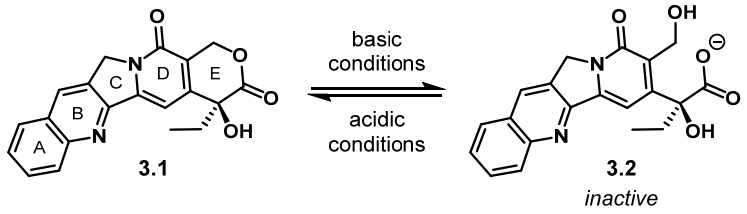

Figure 3.1. The structure of camptothecin (CPT, **3.1**) and the inactive carboxylate form present at physiological pH (and basic pH). The lactone form is favoured under acidic conditions.

3.1.1 Improving the safety of camptothecin

In an effort to improve on the aforementioned limitations, many structural derivatives have been developed, ultimately resulting in three clinically approved CPT analogues—irinotecan (**3.3**), topotecan (**3.4**) and belotecan[a] (**3.5**) (Figure 3.2A).[9,10] Alternatively, utilising CPT as the drug cargo in a drug conjugate has emerged as a viable method to enhance CPT selectivity

[a] Belotecan is only approved for clinical use in South Korea.

and improve its safety profile. This is exemplified by the recent approval of trastuzumab deruxtecan **3.6** (Enhertu®) and commencement of clinical trials for raludotatug deruxtecan (developed by Merck), both of which are ADCs that contain a CPT derivative payload (Figure 3.2B).[11,12] The interest in peptide targeting vehicles as an alternative to expensive antibodies has motivated the exploration of PDCs for CPT-based therapies.[13] While multiple studies of CPT-containing PDCs have utilised cell-targeting peptides as the peptide partner, relatively few have explored the utility of cell-penetrating peptides (CPPs).[14,15]

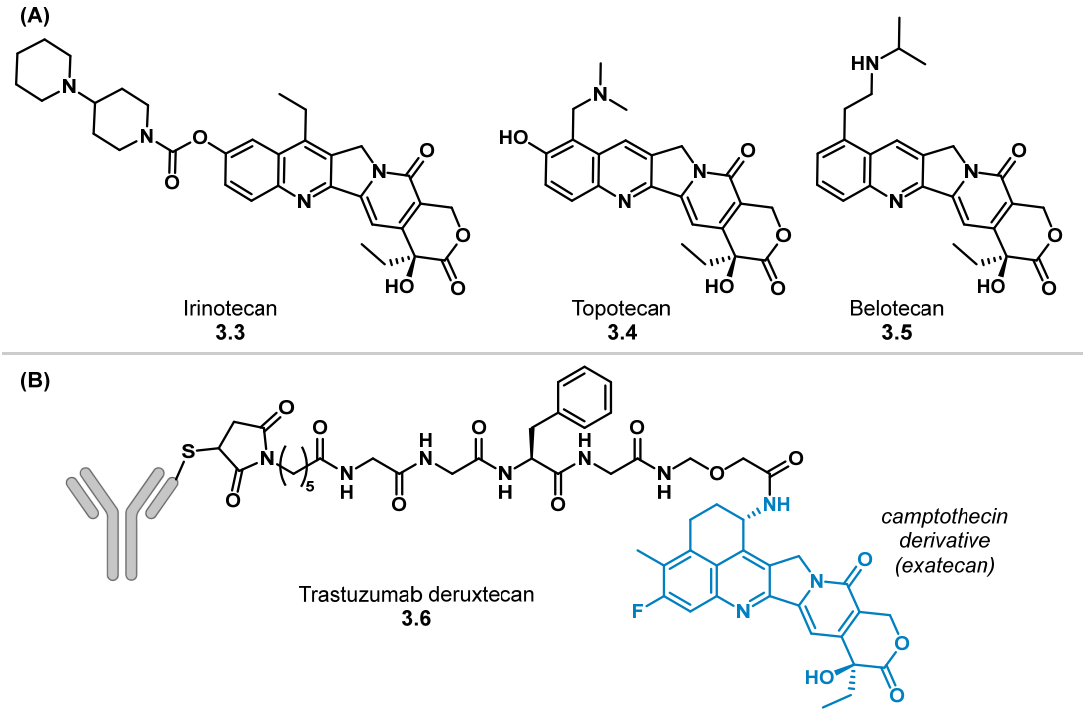

Figure 3.2. (A) The structures of three approved CPT derivatives. (B) The structure of trastuzumab deruxtecan, an approved ADC containing a camptothecin derivative payload.

Previous CPT-containing PDCs with CPPs have employed cationic amphipathic peptides including a cyclic peptide with alternating tryptophan and arginine residues ([W(WR)$_4$K])[14,16] and a linear antimicrobial peptide derived from a wasp venom toxin (KM8-Aib) (Table 3.1).[15] As these scaffolds were shown to be suitable for the production of active CPT PDCs, we postulated that the cell-penetrating peptide PDIP could also be a viable alternative scaffold to deliver CPT to cancer cells. With the demonstrated ability of PDIP to selectively enter and kill cells of melanoma—a deadly form of skin cancer—we explored the suitability of PDIP-CPT PDCs as a melanoma treatment.[17]

Table 3.1. Examples of cell-penetrating peptide scaffolds utilised in previous CPT-containing PDCs within the literature.

Entry	Peptide Name/Sequence	Notes	Ref.
1	**[W(WR)$_4$K]:** c[WRWRWRWRWK]	• Peptide scaffold with no antitumour activity[18] • Disulfide-reducible PDC more potent than a PDC with a pH-labile carbonate linker • Drug conjugated onto lysine side chain	El-Sayed *et al*. (14)
2	**KM8-Aib:** KLLKKNLKXLAALAKKIL*	• Peptide scaffold with low micromolar antitumour activity • All 8 PDCs contained a disulfide-reducible linker • Peptide modified to incorporate cysteine onto the N- or C-terminus, to allow for drug conjugation onto cysteine side chain	Zhang *et al.* (15)

c[ ] = backbone cyclised, X = 2-aminoisobutyric acid (Aib), * = C-terminal amide.

3.2 Informed PDIP-based PDC design

The design insights obtained from the PDIP-PQ PDC studies presented in Chapter 2 were used to inform the construction of PDIP-CPT PDCs. Cleavable linkers that could release PQ from the peptide were deemed to be important for PQ to carry out its mechanism of action, which likely extends to any drug whose mechanism is impeded by conjugation to a peptide. As CPT has an intranuclear enzyme target, it likely cannot localise in the nucleus while tethered to a peptide. Furthermore, previous studies of CPT-containing PDCs with CPP scaffolds highlighted the benefit of a disulfide-reducible cleavable linker to retain the potency of CPT (Table 3.1).[14,15] The majority of PDIP-CPT PDCs were thus designed to contain a cleavable linker—including disulfide-reducible and protease-cleavable linkers—with one non-cleavable PDC constructed for comparison.

The conjugation site on PDIP was also determined to be important for maintaining the activity of PDIP-based PDCs. The PDIP analogue that contained an azide conjugation handle in the spacer region between the two α-helices resulted in more active PDCs, compared to an analogue with an N-terminal conjugation handle. As such, only the former azide-modified PDIP analogue was used for CPT-containing PDCs. The promising activity observed in Chapter 2 for a PDC containing a backbone cyclised PDIP analogue that comprised a single cysteine residue for conjugation, prompted exploration of a similar PDIP analogue in this study, in which the drug was appended using an alternative conjugation strategy to azide–alkyne cycloaddition.

This chapter, presented as a published manuscript,[19] outlines the design and synthesis of PDIP-CPT PDCs and their subsequent biological evaluation against a melanoma cell line. Through cytotoxicity screening, membrane permeability studies and analysis of cellular uptake, valuable insights into the distinct roles of the peptide, linker and drug components were gained. PDC design was established as a crucial requirement for maintaining the selective properties of the PDIP scaffold.

Australian National University

Statement of Contribution

This thesis is submitted as a Thesis by Compilation in accordance with https://policies.anu.edu.au/ppl/document/ANUP_003405

I declare that the research presented in this Thesis represents original work that I carried out during my candidature at the Australian National University, except for contributions to multi-author papers incorporated in the Thesis where my contributions are specified in this Statement of Contribution.

Title: Synthesis and Investigation of Peptide–Drug Conjugates Comprising Camptothecin and a Human Protein-Derived Cell-Penetrating Peptide

Authors: Isabella R. Palombi, Andrew M. White, Yasuko Koda, David J. Craik, Nicole Lawrence,* Lara R. Malins*

Publication outlet: Chemical Biology & Drug Design

Current status of paper: Not Yet Submitted/**Submitted**/Under Revision/Accepted/Published

Contribution to paper: Conducted the majority (over 90%) of the planning, experimental work (both synthetic chemistry and biology testing) and data analysis/compound characterisation. Wrote the original draft of the manuscript and the accompanying Supporting Material and incorporated edits from other authors. Chemistry components were conducted at the RSC, ANU, and the biology component was completed at the Institute of Molecular Biology, University of Queensland.

Senior author or collaborating authors endorsement: The above statement is accurate. The candidate performed the experimental work as indicated, including biological experiments at the University of Queensland. The candidate wrote the original manuscript and Supporting Information file.

Isabella Palombi		25/10/2024
Candidate – Print Name	Signature	Date

Endorsed

Nicole Lawrence		25/10/2024
Primary Supervisor – Print Name	Signature	Date
Mark Humphrey		25/10/2024
Delegated Authority – Print Name	Signature	Date

Chemical Biology & Drug Design

WILEY

RESEARCH ARTICLE OPEN ACCESS

Synthesis and Investigation of Peptide–Drug Conjugates Comprising Camptothecin and a Human Protein-Derived Cell-Penetrating Peptide

Isabella R. Palombi[1,2] | Andrew M. White[1,2] | Yasuko Koda[3,4] | David J. Craik[3,4] | Nicole Lawrence[3,4] | Lara R. Malins[1,2]

[1]Research School of Chemistry, Australian National University, Canberra, Australian Capital Territory, Australia | [2]Australian Research Council Centre of Excellence for Innovations in Peptide and Protein Science, Australian National University, Canberra, Australian Capital Territory, Australia | [3]Institute for Molecular Bioscience, The University of Queensland, Brisbane, Queensland, Australia | [4]Australian Research Council Centre of Excellence for Innovations in Peptide and Protein Science, The University of Queensland, Brisbane, Queensland, Australia

Correspondence: Nicole Lawrence (n.lawrence@imb.uq.edu.au) | Lara R. Malins (lara.malins@anu.edu.au)

Received: 4 October 2024 | **Revised:** 13 December 2024 | **Accepted:** 6 January 2025

Funding: This work was supported by funding from the Australian Research Council Centre of Excellence for Innovations in Peptide and Protein Science (CE200100012), the US Department of Defense Congressionally Directed Medical Research Programs (W81XWH2210219 to D.J.C. and N.L.), the National Health and Medical Research Council (NHMRC) Australia (Leadership Fellowship, GNT2009564 to D.J.C), and the Australian Government Research Training Program PhD Scholarship scheme (I.R.P).

Keywords: camptothecin | cell-penetrating peptide | cleavable linker | melanoma | peptide–drug conjugate

ABSTRACT

Drug targeting strategies, such as peptide–drug conjugates (PDCs), have arisen to combat the issue of off-target toxicity that is commonly associated with chemotherapeutic small molecule drugs. Here we investigated the ability of PDCs comprising a human protein-derived cell-penetrating peptide—platelet factor 4-derived internalization peptide (PDIP)—as a targeting strategy to improve the selectivity of camptothecin (CPT), a topoisomerase I inhibitor that suffers from off-target toxicity. The intranuclear target of CPT allowed exploration of PDC design features required for optimal potency. A suite of PDCs with various structural characteristics, including alternative conjugation strategies (such as azide–alkyne cycloaddition and disulfide conjugation) and linker types (non-cleavable or cleavable), were synthesized and investigated for their anticancer activity. Membrane permeability and cytotoxicity studies revealed that intact PDIP-CPT PDCs can cross membranes, and that PDCs with disulfide- and protease-cleavable linkers liberated free CPT and killed melanoma cells with nanomolar potency. However, selectivity of the PDIP carrier peptide for melanoma compared to noncancerous epidermal cells was not maintained for the PDCs. This study emphasizes the distinct role of the peptide, linker, and drug for optimal PDC activity and highlights the need to carefully match components when assembling PDCs as targeted therapies.

1 | Introduction

Cancer poses a serious global health burden, with nearly 20 million new cases and 10 million deaths worldwide in 2022—statistics that are expected to increase in the coming decades (Ferlay et al. 2024; IARC 2024). Surgery, chemotherapy, radiotherapy, and immunotherapy are the conventional methods for treating the disease, but new therapies and treatment approaches will be required to address increasing cancer incidence (Rizvi et al. 2024). Many chemotherapeutic agents target rapidly dividing cells, resulting in systemic toxicity against healthy proliferative cells. This manifests as patient side effects, a hallmark of small molecule anticancer treatments (Hoppenz, Els-Heindl, and Beck-Sickinger 2020).

Camptothecin (CPT), originally isolated from the bark of the *Camptotheca accuminata* tree, is an alkaloid with antitumor activity against diverse cancer types (Botella and Rivero-Buceta 2017; Wall et al. 1966). Its mechanism of action involves inhibition of topoisomerase I, an enzyme that relaxes supercoiled DNA during replication and transcription, leading to DNA damage and cell apoptosis (Chen and Liu 1994; Pommier 2006). Unfortunately, the clinical use of CPT has been hindered by off-target toxicity, poor solubility of its rigid fused-ring system and instability of the lactone moiety—which produces an inactive carboxylate species after hydrolysis at physiological pH (Botella and Rivero-Buceta 2017). With these limitations in mind, a variety of CPT derivatives with structural modifications have been developed over the last few decades, ultimately resulting in three clinically approved analogues—irinotecan, topotecan, and belotecan (Venditto and Simanek 2010; Wang et al. 2023).

Recent research has examined alternative methods of improving CPT safety, for example by attaching the drug onto a cancer cell targeting device—such as an antibody (Conilh et al. 2023) or peptide (Fang and Wang 2022; Rizvi et al. 2024)—or by utilizing self-assembling nanostructures (Botella and Rivero-Buceta 2017) as drug carriers. The approval of trastuzumab deruxtecan (Enhertu®) in 2019, an antibody–drug conjugate (ADC) containing a CPT derivative payload attached to an anti-HER2 monoclonal antibody (Ogitani et al. 2016; Xu et al. 2019), highlighted targeted drug delivery as a promising treatment approach for improving CPT safety. Although ADCs have the advantage of reducing the side effects of cytotoxic drugs, they are costly to produce, can have limited tumor penetration and can induce an immune response. Due to their smaller size, peptide–drug conjugates (PDCs) are often able to overcome the limitations of ADCs, while maintaining selectivity for specific intracellular targets (Wang et al. 2018, 2024). In a PDC approach, CPT has been paired with cell-penetrating (El-Sayed et al. 2019; Zhang et al. 2023) and cell-targeting (Fuselier et al. 2003; Henne et al. 2006; Hou et al. 2022; Moody et al. 2004; Redko et al. 2017; Sun, Fuselier, and Coy 2004; Zhou et al. 2020, 2021, 2022;) peptides, with continued interest in the exploration of peptide scaffolds that utilize diverse drug delivery mechanisms.

We previously designed a human protein-derived cell-penetrating peptide (CPP) capable of delivering cargo into diseased cells via direct translocation across the plasma membrane (Lawrence et al. 2020; Palombi et al. 2023; Philippe et al. 2021). The peptide, platelet factor 4-derived internalization peptide (PDIP; see Figure 1 for sequence), is a structural mimic of the amphipathic C-terminal domain from the human defense protein platelet factor 4. PDIP comprises an alpha-helical hairpin structure that is cyclized via a disulfide bond. Along with having CPP properties, it has low micromolar anticancer activity (Lawrence et al. 2020). In melanoma and leukemia cancer cells, this activity is attributed to disruption and impairment of the function of mitochondrial membranes. Furthermore, PDIP can selectively interact with and traverse negatively charged membranes, a property conferred by the cationic residues within its two helical domains (Lawrence et al. 2020). The exposure of anionic phosphatidylserine (PS) lipid headgroups on the surface of cancer cell membranes (Vallabhapurapu et al. 2015) provides a unique opportunity for the selective entry of a cationic CPP into cancer cells. Comparatively, healthy cells have neutrally charged outer membranes, due to PS lipids being maintained in the inner leaflet by flippase enzymes (Nagata et al. 2016; Seigneuret and Devaux 1984). Thus, a PDIP-containing PDC could provide intracellular delivery of cytotoxic drugs into negatively charged cancer cells, while preventing interaction of the drug with healthy tissues.

PDIP has been shown to act as a tool to deliver peptide cargos into cancer cells (Lawrence et al. 2020; Philippe et al. 2021), but here we investigated its ability to selectively deliver a small

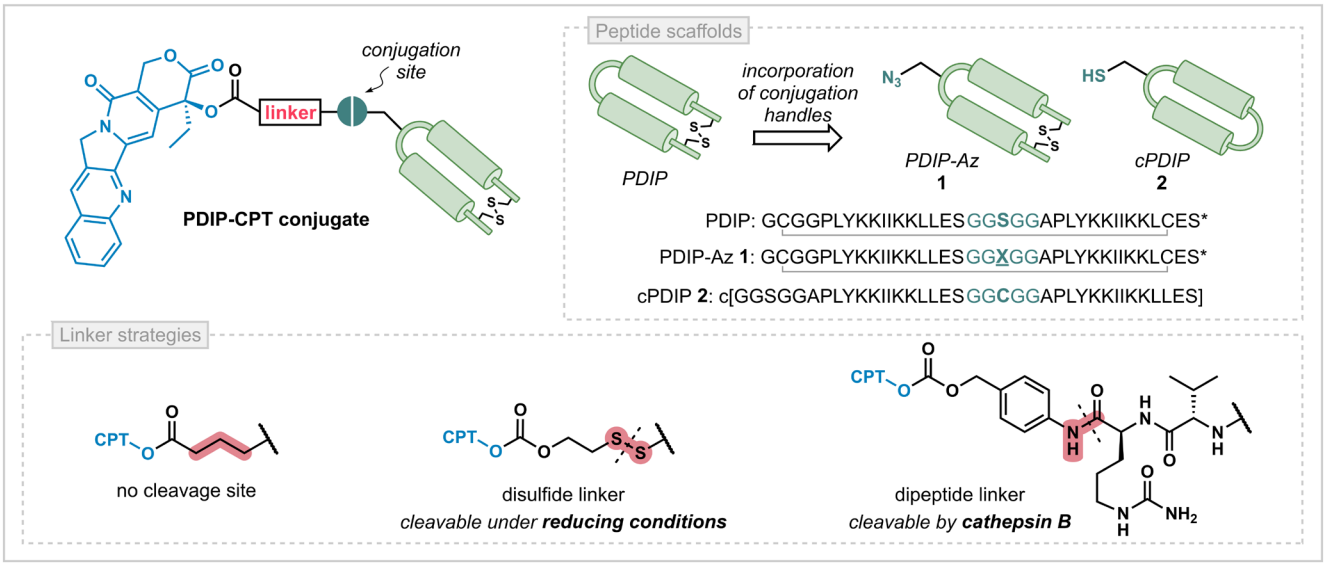

FIGURE 1 | The proposed characteristics varied to generate a suite of PDIP-CPT PDCs, including the peptide conjugation handle and linker type (colored pink). For cleavable linkers, the cleavage site is indicated with a dotted black line. For the peptide sequences, disulfide bonds are indicated with a grey line and the residues in the spacer region are colored teal; c[ ] = backbone cyclized; X = azidoalanine; *amidated C-terminus.

molecule anticancer drug. CPT was identified as a model drug because its potent toxicity could be used to distinguish peptide versus drug cargo activity of PDCs against diseased cells, and its intranuclear target could be used to probe the requirement for release of CPT from the PDC. We hypothesized that PDIP-CPT PDCs could improve the selectivity of the small molecule drug, and would likely require intracellular release of CPT from PDIP to allow CPT to inhibit topoisomerase I. Accordingly, we synthesized four PDIP-CPT PDCs, incorporating distinct conjugation strategies and the ability to liberate the CPT drug cargo via reductive or enzymatic cleavage, with the aim of understanding how PDC components and design features influence biological activity, membrane permeability, and cellular uptake. This work demonstrates that PDIP-CPT conjugates can cross membranes and kill melanoma cells with nanomolar potency when a traceless cleavable linker is included in the PDC design. However, selectivity of the PDIP carrier peptide for melanoma compared to noncancerous cells was not maintained for the CPT-containing PDCs. The insights provided by this study highlight the distinct roles of the peptide, linker, and drug components and emphasize that PDC design is crucial for a successful targeted therapeutic approach.

2 | Results and Discussion

2.1 | Design of PDIP-CPT Conjugates

A modular strategy for PDC synthesis was utilized to probe how specific components and design characteristics influence potency. Two PDIP analogues with different conjugation handles were proposed to understand the role of the peptide scaffold. The sequences and schematic representations of the peptide structures are shown in Figure 1 and they were synthesized as previously described (Lawrence et al. 2020; Palombi et al. 2023). The first analogue, PDIP-Az (**1**), is similar to the parent peptide (PDIP) as it is cyclized via a disulfide bond. It contains an azide handle in the spacer region between the two helices, primed for drug conjugation via azide-alkyne cycloaddition chemistry. The second analogue is a backbone cyclized variant containing only proteinogenic amino acids, herein referred to as cPDIP (**2**), providing a scaffold that does not require incorporation of bioorthogonal functionalities, such as an azide. The single cysteine residue in the spacer region enables macrocyclization via native chemical ligation during synthesis (Dawson et al. 1994), while also providing a reactive handle for downstream drug conjugation.

CPT-linker constructs were designed to contain either an alkyne or activated disulfide moiety for PDC formation with the two PDIP analogues. Three alternative linkers, encompassing the region between CPT and the peptide, were proposed to identify whether CPT release is required to provide potent PDCs (Figure 1). A non-cleavable linker is straightforward to install so is beneficial if drug and/or peptide activity is maintained following PDC construction. However, it is possible that this irreversible modification might prevent CPT from reaching or inhibiting topoisomerase I in the nucleus, requiring a linker that allows for traceless release of CPT from PDIP. Accordingly, two self-immolative linkers were envisioned (Edupuganti, Tyndall, and Gamble 2021), bearing either a disulfide linkage that is reducible by intracellular glutathione (Henne et al. 2006; Kularatne et al. 2010) or a dipeptide moiety that is cleavable by the protease cathepsin B (Dubowchik et al. 2002) (Figure 1).

2.2 | Modification of CPT With Cleavable or Non-Cleavable Linkers and PDC Synthesis

The construction of PDIP-CPT PDCs first required modification of CPT to install the linkers and handles necessary for conjugation to peptides **1** and **2**. The hydroxyl group of CPT was chosen as an ideal site for linker attachment because modifications such as alkylation or acylation at this position are accessible and have been shown to improve stability of the lactone (Venditto and Simanek 2010; Zhao et al. 2000). CPT was thus modified at the tertiary alcohol to install a non-cleavable linker by reacting it with 5-hexynoic acid, in the presence of the coupling reagent EDC•HCl, to produce **3** in 40% yield (Scheme 1A).

The synthesis of CPT with a cleavable disulfide linker began with treatment of HOBt-activated compound **4** (Kularatne et al. 2010) with CPT under basic conditions and in the presence of DMAP, forming carbonate **5** in 26% yield (Scheme 1B). Compound **5** served the dual purpose of providing an activated disulfide for conjugation to thiol-containing cPDIP (**2**) and a viable precursor to a second disulfide linker containing an alkyne handle for conjugation to PDIP-Az (**1**). To accomplish the latter objective, activated disulfide **5** was reacted with thiol-containing DBCO analogue **7**, following the acidic deprotection of methyltrityl-protected precursor **6**. Disulfide exchange under mildly basic conditions (pH 8) afforded CPT-linker construct **8** (28% yield over two steps) (Palombi et al. 2023).

The construction of a protease-sensitive linker first involved installation of CPT onto commercially available Boc-Val-Cit-PAB-PNP (**9**) via a carbonate linkage (Scheme 1C). Removal of the Boc group on **10** allowed for subsequent amide formation at the deprotected amine with propargyl-PEG1-acid, aided by the coupling reagent T3P®, providing alkyne-containing CPT-linker construct **11** (46% yield over two steps).

With CPT-linker constructs in hand (**3**, **5**, **8**, and **11**), four water soluble PDCs were synthesized, the structures and yields of which are displayed in Figure 2 (see Supporting Information for analytical traces confirming product identity and purity). Two of these PDCs (**12**, **13**) were generated via a copper(I)-catalyzed azide–alkyne cycloaddition (CuAAC) (Rostovtsev et al. 2002; Tornøe, Christensen, and Meldal 2002) reaction employing $CuSO_4$, sodium ascorbate, and the water-soluble ligand tris(3-hydroxypropyltriazolylmethyl)amine (THPTA) (Hong et al. 2009). PDC **12** contains a non-cleavable linker, formed by reacting terminal alkyne **3** with PDIP-Az (**1**), and PDC **13** contains a protease-sensitive linker, produced instead by reacting linker construct **11** with PDIP-Az (**1**). Finally, two PDCs with a reducible disulfide linker were prepared, with each of the PDIP scaffold peptides. PDC **14** was generated via strain-promoted azide–alkyne cycloaddition (SPAAC) (Agard, Prescher, and

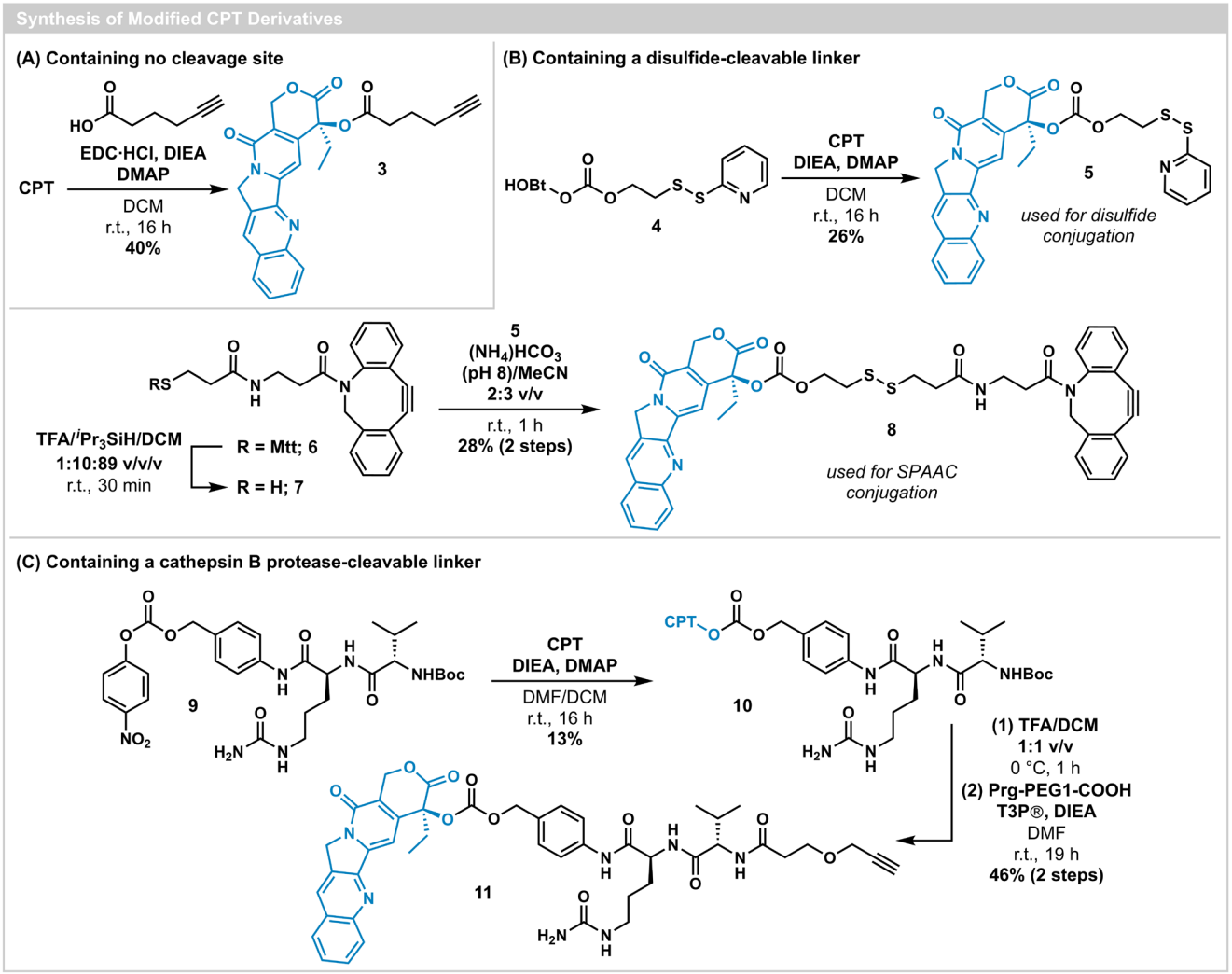

SCHEME 1 | Modification of CPT to produce constructs with (A) a non-cleavable linker, (B) a disulfide-cleavable linker, and (C) a cathepsin B protease-sensitive linker.

Bertozzi 2004) between cyclooctyne **8** and PDIP-Az (**1**), to avoid the use of copper and excess reducing agents—which are required for CuAAC—in the presence of the disulfide-cleavable functionality. In an alternative approach, PDC **15** was prepared by reacting reduced cPDIP (**2**) with the activated disulfide **5**, allowing for disulfide exchange under mildly basic conditions (pH 8).

2.3 | Cytotoxicity and Hemolytic Activity of PDIP-CPT Conjugates

PDIP is a membrane-active CPP that has been shown to have low micromolar activity toward a melanoma cell line, with selectivity over noncancerous skin cells (Lawrence et al. 2020). Thus, the in vitro cytotoxicity of the four PDIP-CPT conjugates was analyzed against melanoma (HT144) and noncancerous (HaCaT) cell lines. Cytotoxic activity of the PDCs was compared to the activity of CPT and the scaffold peptides—PDIP and c[A]PDIP—where the latter is a desulfurized variant of cPDIP (**2**) (see Supporting Information for synthetic details), produced to prevent dimerization of cPDIP via disulfide bonds formed between the sulfhydryl groups in physiological solutions.

2.3.1 | CPT Release From PDCs Is Required for Anticancer Activity

Cytotoxicity testing of the four PDCs against the HT144 melanoma cell line, where cells were incubated with the treatments for 72 h, revealed nanomolar or low micromolar half maximal cytotoxicity concentration (CC_{50}) values for the three cleavable PDCs **13** (1.21 μM), **14** (0.44 μM), and **15** (0.36 μM) (Figure 3A,D). In contrast, the non-cleavable PDC **12** had no activity in the concentration range tested (16 nM—2 μM), supporting our hypothesis that release of CPT from PDIP is required before the drug can inhibit its intranuclear target, topoisomerase I. Finally, treatment of the melanoma cells with an equimolar mixture of unconjugated CPT and PDIP resulted in similar activity to CPT itself, indicating that while PDIP does not appear to enhance the activity of CPT, it probably does not interfere with the mechanism of action of the free drug or its ability to interact with topoisomerase I.

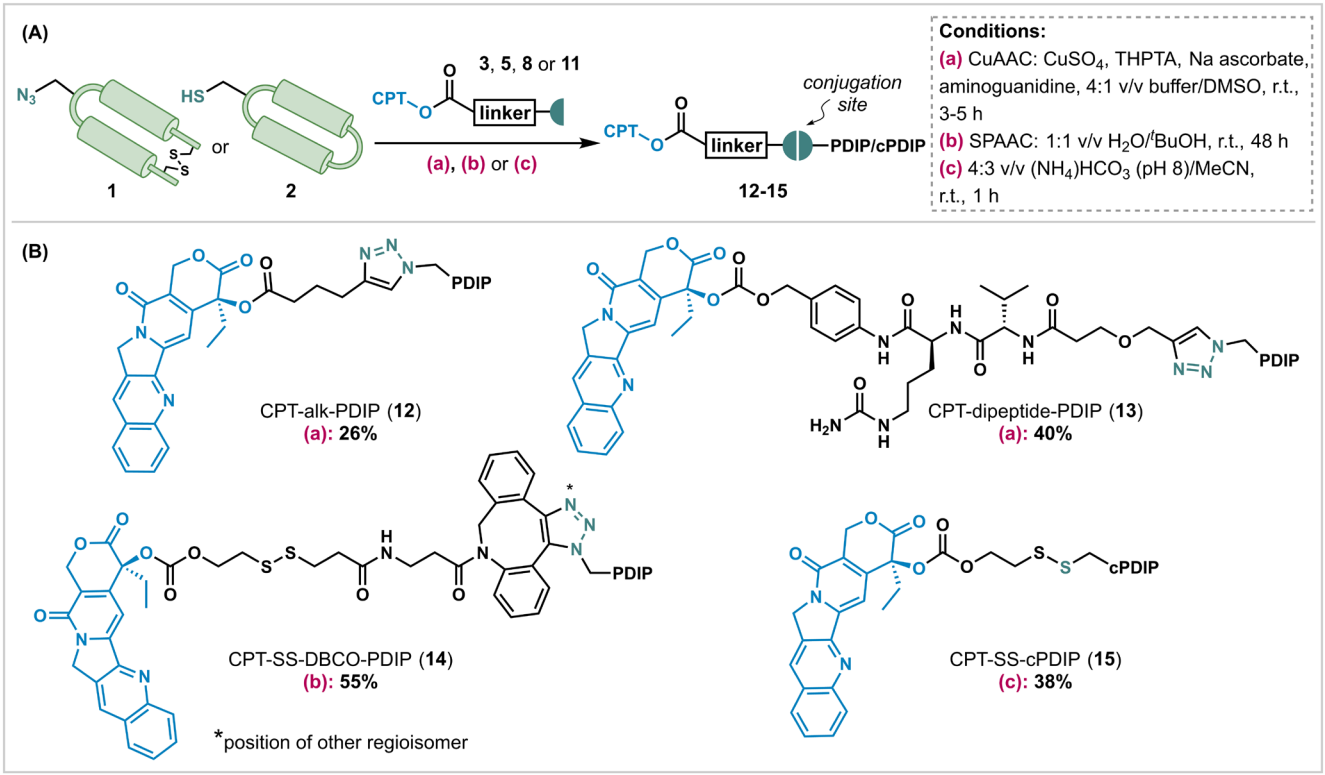

FIGURE 2 | (A) General scheme and conditions for PDC synthesis. (B) Structures and yields of the four PDCs. The yields were determined using the molecular weight of the TFA salt, assuming all basic residues, the terminal amine (if present) and the quinoline moiety within CPT are protonated.

2.3.2 | PDC Potency Is Cargo Driven But Non-Selective

The cleavable PDCs (**13**–**15**) had similar levels of cytotoxicity toward the melanoma cell line as CPT alone (CC_{50} = 0.38 μM), especially the conjugates with disulfide linkers (**14**–**15**) (Figure 3A,D). Comparatively, the two peptides were less potent (PDIP CC_{50} = 4.83 μM; c[A]PDIP CC_{50} = 9.35 μM), suggesting that CPT is the main component contributing to PDC activity at sublethal peptide concentrations. To further investigate whether the CPT cargo drives PDC potency, activity was examined following a shorter incubation time (24 h) but with the same concentration range (16 nM to 2 μM) where the PDCs but not PDIP were shown to be active after 72 h incubation (Figure 3A, Supporting Information, Figure S1). The absence of activity observed for CPT and the PDCs at concentrations below the effective range for PDIP and c[A]PDIP, and at a time point (24 h) that was too short to detect CPT toxicity (Supporting Information, Figure S1), confirms that the observed activity of PDCs at 72 h was driven by the CPT cargo. Comparison of PDIP and c[A]PDIP activity at concentrations up to 32 μM revealed similar activity ranges at both 24 h (Supporting Information, Figure S1) and 72 h (Figure 3A,D), which agrees with our previous observations of the rapid action of PDIP analogues against melanoma cells (Lawrence et al. 2020).

Although displaying favorable activity against the melanoma cell line, the cleavable PDCs (**13**–**15**) had similar toxicity against the control, noncancerous cell line (HaCaT) at nanomolar to low micromolar concentrations (Figure 3B,D). This was an unexpected result because PDIP and c[A]PDIP have $CC_{50} \geq 32$ μM toward HaCaT cells. Therefore, it is possible that the addition of a hydrophobic drug and linker to the cationic peptide reduced the selectivity of PDIP for the anionic membranes present in cancer cells (see Supporting Information, Table S1, for relative hydrophobicity of PDIP and PDCs). However, since CPT itself is cell permeable, we cannot rule out the possibility that the observed toxicity resulted from gradual extracellular cleavage or degradation of PDCs **13**–**15** before cell internalization (Balamkundu and Liu 2023; Lei et al. 2021). Cleavable PDC **15** with the cPDIP scaffold was the most toxic PDC (CC_{50} = 84 nM against HaCaT, Figure 3B), suggesting that constraining the peptide via backbone cyclization may alter the interactions of charged and hydrophobic residues with membrane phospholipids required for selective cell entry.

To determine whether the PDCs showed toxicity toward cells with neutral membranes that were not immortalized for continuous culture, hemolysis assays were conducted with human RBCs (Figure 3C,D). The four PDCs (**12**–**15**) and CPT did not lyse RBCs within the same concentration range that they were active against the cell lines (16 nM—2 μM). PDIP displayed some hemolytic activity at the top concentration tested, with a minimal hemolytic concentration (HC_{10}) of ~32 μM, whereas the control hemolytic peptide, melittin (Asthana, Yadav, and Ghosh 2004), had a HC_{10} of 1.8 μM and completely lysed the RBCs at 8 μM. Nevertheless, the lack of selectivity against a noncancerous cell line accentuates the importance of careful conjugate design to ensure that overall changes in the physiochemical properties (e.g., increased hydrophobicity) of the PDC compared to the peptide do not affect the safety window. Preserving the

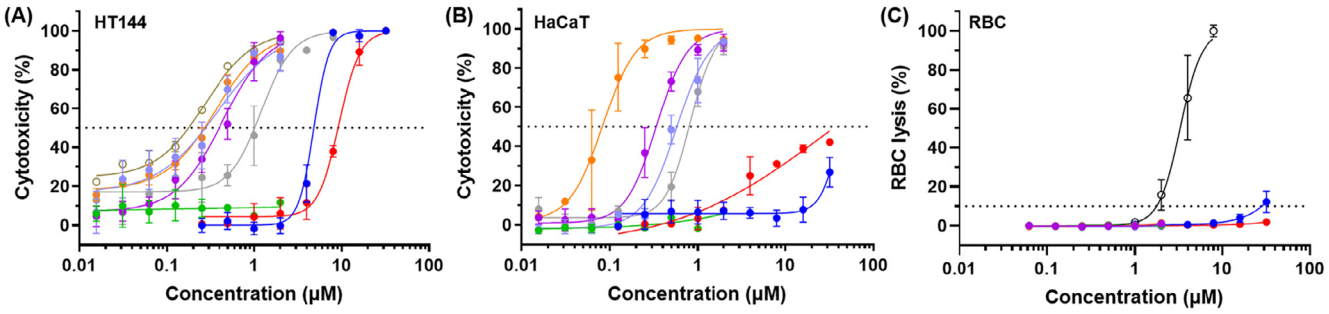

(D)

Compound	CC_{50} (μM) HT144	CC_{50} (μM) HaCaT	HC_{10} (μM) RBC	Compound	CC_{50} (μM) HT144	CC_{50} (μM) HaCaT	HC_{10} (μM) RBC
CPT-alk-PDIP **12**	>>2	>>2	>2	PDIP	4.83 (0.14)	>32	~32
CPT-dipeptide-PDIP **13**	1.21 (0.14)	0.82 (0.03)	>2	c[A]PDIP	9.35 (0.43)	~32	>32
CPT-SS-DBCO-PDIP **14**	0.44 (0.03)	0.34 (0.02)	>2	CPT	0.38 (0.07)	0.57 (0.03)	>2
CPT-SS-cPDIP **15**	0.36 (0.03)	0.084 (0.02)	>2	CPT + PDIP	0.27 (0.02)	n.d.	n.d.
				Melittin	n.d.	n.d.	1.8

FIGURE 3 | (A) and (B) Cytotoxicity of PDCs, CPT, and peptides against cultured HT144 (melanoma) and HaCaT (noncancerous) cells, following incubation for 72 h. Cell death was measured using resazurin, with 0.1% (v/v) Triton X-100 as a control for 100% cell death. Data points are expressed as mean ± SD for at least two biological replicates. Dose response curves were fitted using [inhibitor] versus response with variable slope, Graphpad Prism v10. (C) Hemolysis of human RBCs (0.25% v/v) following incubation with PDCs, CPT, and peptides for 72 h. RBC lysis was determined by measuring released hemoglobin, with 0.1% (v/v) Triton X-100 as a control for 100% cell lysis. Melittin was included as a membranolytic control. Data points are expressed as mean ± SD for two technical replicates. Dose response curves were fitted using [inhibitor] versus response with variable slope, Graphpad Prism v10. (D) Half maximal cytotoxicity concentration (CC_{50}) and minimal hemolytic concentration (HC_{10}) values of PDCs, CPT, and peptides. CC_{50} values are expressed as mean (SEM). The legend applies to all three graphs. c[A]PDIP is a desulfurized variant of cPDIP **2** (see Table S1) to prevent the presence of free thiol during assays. n.d., not determined.

selectivity of PDIP for diseased cells over noncancerous cells after drug attachment is a high priority for future PDC design.

2.4 | Membrane Permeability and Cell Uptake and Fate of PDIP-CPT Conjugates

Membrane permeability, cellular uptake, and intracellular liberation of CPT were investigated alongside the cytotoxicity studies to provide an understanding of how PDC design influences compound internalization and potency.

2.4.1 | PDCs Are Membrane Permeable and Remain Intact

To determine whether intact peptides and PDCs could cross membranes, we used the parallel artificial membrane permeability assay (PAMPA) to report apparent permeability (Papp) because of passive movement through membranes, and mass spectrometric analysis of peptides and PDCs recovered from treated and washed HT144 cells to report on internalized compounds (passive or active transport). It should be noted that the latter method detects any sample that is associated with the harvested cells so can include both membrane-associated and internalized compounds. Graphical representations of each assay are provided in Figure 4.

For the first assay, the PDCs (**12**–**15**), scaffold peptides and CPT (4 μM) were added to the apical side of PAMPA monolayers and incubated for 4 h. Analysis of the apical and basolateral sides of the membrane using liquid chromatography–mass spectrometry (LC–MS) revealed the Papp (movement from apical to basolateral fractions) and % recovery (amount of recovered sample in combined soluble fractions) for each compound (Figure 4A). PDIP, CPT, and PDCs **12** and **14** had high permeability (Papp $\geq 2\times10^{-6}$ cm/s), highlighting that these PDCs maintain membrane permeability with the CPT cargo attached. However, both PDCs **12** and **14** had diminished recovery rates (58% and 33%, respectively) compared to CPT and PDIP (>90%), suggesting that some membrane association or compound aggregation occurred during the assay. PDC **15** was less permeable (Papp ~9×10^{-7} cm/s), consistent with the lower permeability of the cyclic scaffold peptide c[A]PDIP (Papp ~4×10^{-7} cm/s). Furthermore, PDC **15** and c[A]PDIP had reduced recovery from the soluble fractions (40% and 34%, respectively), suggesting aggregation or membrane association during the assay. Reliable permeability data were not obtained for PDC **13** because of poor recovery of the PDC from soluble fractions, and degradation during the 4 h PAMPA experiment. Analysis of the degradation products revealed possible hydrolysis of **13** at the benzyl carbonate linkage, releasing CPT and CO_2 from the dipeptide linker (see Supporting Information, Scheme S1). Negligible degradation was observed for the other two PDCs containing a carbonate linkage (**14** and **15**); these are probably more stable as the alkyl alcohol liberated upon carbonate hydrolysis is a poorer leaving group than the benzyl alcohol liberated from PDC **13**. Instability of the carbonate linkage within CPT conjugates containing a dipeptide linker has been previously reported (Walker et al. 2002), highlighting the potential incompatibility of this drug–linker combination for CPT PDCs. Considering the observed degradation of **13** in the cell-free assay, it is also possible that extracellular degradation occurred during the cytotoxicity assays.

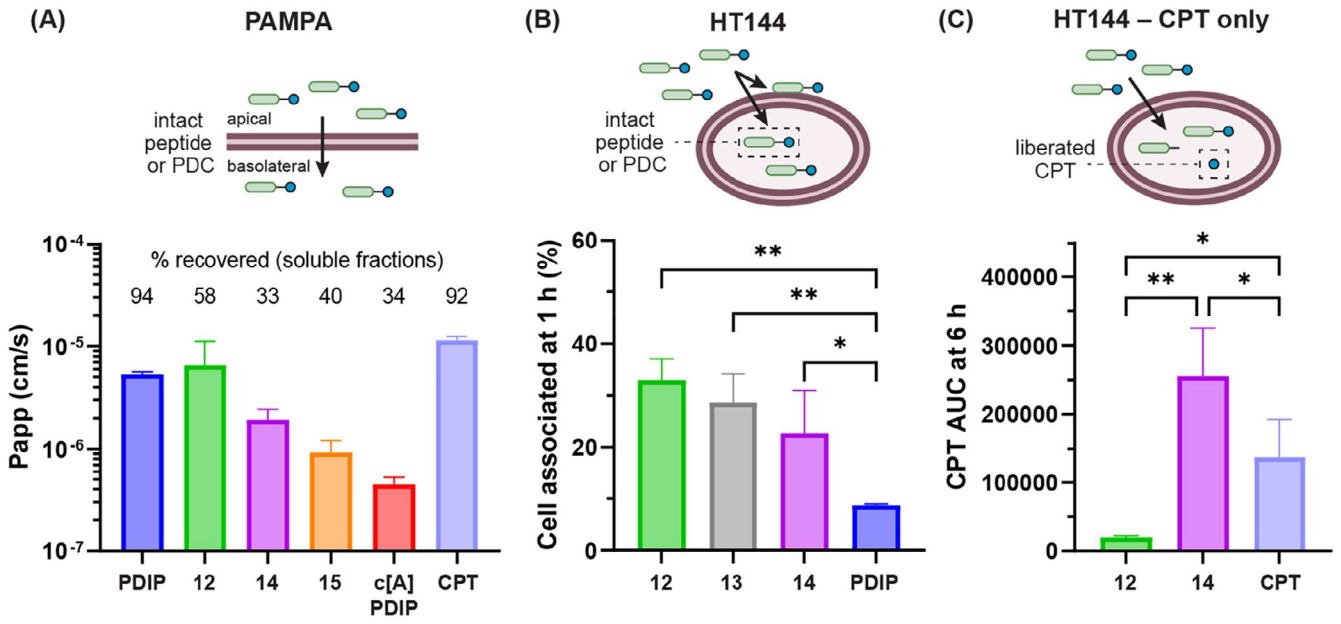

FIGURE 4 | (A) Membrane permeability and cellular uptake of PDCs, scaffold peptides, and CPT. Compounds were added to PAMPA wells (4 μM) and incubated for 4 h. Supernatant from apical and basolateral sides of the membrane were collected and analyzed using LC–MS. The amount in the combined soluble fractions was compared to the starting amount to determine % recovery, and the apparent permeability (Papp) was calculated as before (Sevin et al. 2013). Data is expressed as mean ± SD from a single experiment with three technical replicates. (B) Internalization/cell membrane association of PDCs **12**–**14** and PDIP with HT144 cells. Cells were treated with PDIP or PDCs (4 μM) for 1 h, washed to remove extracellular compound, then extracted with 75% (v/v) MeCN in mQH_2O (containing 1.75% (v/v) TFA), to recover soluble peptide or PDC from precipitated cell proteins. The relative amount of internalized peptide or PDC was determined by integrating area under the curve (AUC) for the $[M + 6H]^{6+}$ m/z peak (for the intact mass) using time of flight–mass spectrometry (see Figure S2). The amount of internalized compound was compared to the AUC present when 4 μM of each analogue was added to untreated cells after addition of the extraction solution, to determine the percentage of internalized compound. Data is expressed as mean ± SD from a single experiment with three technical replicates for each treatment and control and was analyzed with ANOVA (Tukey multiple comparisons; $^{**}p < 0.01$, $^{*}p < 0.05$). (C) Detection of intracellular CPT following 6 h treatment of HT144 cells with CPT and PDCs **12** and **14**. Cells were treated with CPT, **12** or **14** (4 μM) for 6 h, washed to remove extracellular compound, and the relative amount of CPT was compared by determining AUC from targeted multiple reaction monitoring using tandem mass spectrometry (see Figure S3). Data is expressed as mean ± SD from a single experiment with three technical replicates for each treatment and was analyzed with ANOVA (Fisher multiple paired comparisons; $^{**}p < 0.01$, $^{*}p < 0.05$).

Representative cleavable (**13**–**14**) and non-cleavable (**12**) PDCs, along with PDIP, were next examined to understand whether intact PDCs could be detected in HT144 cell extracts. Cells were treated with each compound (4 μM) for 1 h, followed by mass spectrometric analysis of washed and harvested cells. The area under the curve (AUC) values for each sample were compared to controls (untreated cells with compounds added post harvesting) to determine the total recovered PDC or peptide (see Supporting Information, Figure S2). A 1 h time point was chosen because it has been shown that PDIP enters cells within this time frame (Lawrence et al. 2020), and the concentration used to provide adequate detection (4 μM) is within the expected membrane-active concentration range. The amount of recovered intact conjugate after 1 h for PDCs **12** (33%), **13** (29%), and **14** (23%) was significantly greater than that of the PDIP scaffold (9%) (Figure 4B), indicating rapid internalization and/or cell membrane association that may be aided by addition of the drug and linker to the peptide. This observed increase for the PDCs in the cell-based assay was not consistent with the Papp determined from PAMPA. It is possible that active transport mechanisms contributed to PDC entry into the HT144 cells, but it is also likely that a proportion of the PDCs remained associated with cell membranes, which is consistent with the lower amounts recovered from the soluble fractions in the PAMPA experiment.

2.4.2 | Cleavable PDC 14 Releases CPT

To determine whether the CPT drug cargo is liberated from PDCs once inside melanoma cells, the amount of intracellular CPT was determined via tandem mass spectrometry. HT144 cells were treated with either CPT, the non-cleavable PDC **12** or the disulfide-cleavable PDC **14** for 6 h—a time point expected to allow for some linker cleavage on the basis of our previous work on disulfide linker fragmentation from PDIP conjugates (Palombi et al. 2023)—followed by the detection of relative amounts of CPT inside cells that had been washed and extracted as above (see Supporting Information, Figure S3). CPT was observed in the extract of HT144 cells treated with the disulfide-cleavable PDC **14** (Figure 4C), suggesting that some intracellular cleavage had occurred within this time frame to release CPT from the PDIP carrier. In comparison, negligible amounts of CPT were detected for cells treated with the non-cleavable PDC **12** (Figure 4C), indicating that the ester linkage to the drug is not hydrolyzed during this time frame (e.g., by

intracellular esterases), in contrast to other reported potent non-cleavable CPT conjugates (Hou et al. 2022). Since intact **12** was observed to cross membranes and enter cells (Figure 4A,B), the lack of activity for this PDC is likely not explained by the PDC being unable to enter the cell but rather by the inability for CPT to access its intranuclear target while tethered to a peptide.

Altogether, the permeability and uptake assays demonstrate that PDCs **12** and **14** maintained the high membrane permeability observed for PDIP and remained intact when inside and/or associated with melanoma cells. It is likely that the PDCs entered HT144 cells predominantly via a passive mechanism, but a portion of these conjugates may be aggregating/associating with the cell membrane. Association with membranes in a non-selective manner (e.g., PAMPA) is consistent with the increased hydrophobicity of **12** and **14** relative to PDIP (see comparative HPLC retention times in Table S1), and their observed toxicity toward noncancerous HaCaT cells. Although PDC **13** degraded in the conditions of the PAMPA experiment, the intact mass was detected in treated HT144 cell extracts, suggesting that the conjugate did not completely degrade prior to cell entry/association in the shorter 1 h experiment. It is also possible that this PDC—containing a linker known for its hydrophobicity (Bargh et al. 2019; Jeffrey et al. 2006)—aggregates to a greater extent than the other cleavable PDCs (**14**–**15**) thereby affecting the ability of intact PDC or liberated CPT to enter cells.

3 | Conclusions

In summary, a suite of CPT-containing PDCs was successfully produced by conjugating CPT to two analogues of PDIP, a CPP derived from the innate defense molecule human platelet factor 4. The modular PDC design strategy enabled flexible installation of the CPT drug cargo using a collection of different conjugation strategies (CuAAC, SPAAC, and disulfide conjugation chemistry) and facilitated the synthesis of four PDCs in moderate yields. Three synthetically accessible linker technologies were explored including a non-cleavable alkane, a disulfide-cleavable linker, and a cathepsin B (dipeptide)-cleavable linker. The intranuclear target of CPT enabled comparison of the three linker types and emphasized the crucial requirement for a cleavable linker when peptide attachment interferes with drug localization.

The combination of CPT, PDIP, and a cleavable linker produced PDCs with cargo driven and nanomolar activity against a melanoma cell line, with potency that was comparable to CPT alone. The three cleavable PDCs did not retain the selectivity for melanoma cells observed for the parent peptides, as they were toxic to the noncancerous HaCaT cell line. However, the PDCs were not hemolytic to human RBCs within the concentration range where they were active against HT144 and HaCaT cell lines, suggesting they do not exert an effect on neutral mammalian cell membranes at the tested concentrations.

Investigation of membrane permeability and cell uptake showed that PDIP is a highly membrane permeable peptide that can carry CPT cargo across membranes and was a superior carrier peptide relative to its backbone cyclic analogue, cPDIP. Despite the high apparent permeability of PDCs **12** and **14**, a degree of aggregation/membrane association likely affected the uptake of these PDCs into cells compared to the parent peptide. Intact PDCs were detected in extracts of HT144 cells after treatment for 1 h, even for PDC **13** with the dipeptide linker, which showed evidence of degradation over longer assays because of the unstable carbonate linkage. However, programmed drug release under reductive conditions was confirmed with liberated CPT observed for the disulfide-cleavable PDC **14** after 6 h.

Future PDIP-CPT PDCs should explore alternative linker types and conjugation strategies to improve PDC activity and selectivity. Cleavable linkers that are acid-labile or iron(II)-sensitive (Goldenberg et al. 2015; Spangler et al. 2018) and conjugation strategies such as oxime ligation (Lang and Chin 2014) are examples of alternative approaches that could be applied in the context of cancer treatment. The design of subsequent PDCs should take care to minimize hydrophobicity added to the peptide.

In conclusion, this study provided insight into the role of the peptide, linker, and drug components of PDCs for potential applications as targeted cancer therapies. PDIP-CPT PDCs maintained the high membrane permeability of the carrier PDIP peptide, and liberation of the CPT drug cargo to access an intranuclear target was achieved through incorporating a disulfide-cleavable linker. However, the loss of PDC selectivity for melanoma cells compared to the carrier PDIP peptide needs to be addressed when designing future PDCs, especially when the cargo is a cell-permeable, cytotoxic drug.

4 | Experimental Procedures

Detailed experimental and compound characterization data can be found in the Supporting Information file, along with figures, schemes, and tables.

Acknowledgements

This work was supported by funding from the Australian Research Council Centre of Excellence for Innovations in Peptide and Protein Science (CE200100012), the US Department of Defense Congressionally Directed Medical Research Programs (W81XWH2210219 to D.J.C. and N.L.), the National Health and Medical Research Council (NHMRC) Australia (Leadership Fellowship, GNT2009564 to D.J.C), and the Australian Government Research Training Program PhD Scholarship scheme (I.R.P). The authors thank Anitha Jeyasingham and Joseph Boileau (ANU) for assistance with mass spectrometry; Kuok Yap (UQ) for assistance in developing mass spectrometry methods and for establishing the conditions required for CPT quantification; Dr. Doug Lawes (ANU) for support with NMR spectroscopy; and Dr. Yen-Hua Huang, Dr. Lai Yue Chan, and Dr. Simon de Veer (UQ) for assistance with peptide synthesis. Open access publishing facilitated by Australian National University, as part of the Wiley - Australian National University agreement via the Council of Australian University Librarians.

Ethics Statement

RBC lysis assays (using human RBC and serum) were performed in accordance with the University of Queensland Human Research Ethics Approval number 2022/HE000300.

Conflicts of Interest

The authors declare no conflicts of interest.

Data Availability Statement

The data that supports the findings of this study are available in the Supporting Information of this article.

References

Agard, N. J., J. A. Prescher, and C. R. Bertozzi. 2004. "A Strain-Promoted [3 + 2] Azide-Alkyne Cycloaddition for Covalent Modification of Biomolecules in Living Systems." *Journal of the American Chemical Society* 126: 15046–15047. https://doi.org/10.1021/ja044996f.

Asthana, N., S. P. Yadav, and J. K. Ghosh. 2004. "Dissection of Antibacterial and Toxic Activity of Melittin." *Journal of Biological Chemistry* 279: 55042–55050. https://doi.org/10.1074/JBC.M408881200.

Balamkundu, S., and C. F. Liu. 2023. "Lysosomal-Cleavable Peptide Linkers in Antibody–Drug Conjugates." *Biomedicines* 11: 3080. https://doi.org/10.3390/BIOMEDICINES11113080.

Bargh, J. D., A. Isidro-Llobet, J. S. Parker, and D. R. Spring. 2019. "Cleavable Linkers in Antibody-Drug Conjugates." *Chemical Society Reviews* 48: 4361–4374. https://doi.org/10.1039/c8cs00676h.

Botella, P., and E. Rivero-Buceta. 2017. "Safe Approaches for Camptothecin Delivery: Structural Analogues and Nanomedicines." *Journal of Controlled Release* 247: 28–54. https://doi.org/10.1016/J.JCONREL.2016.12.023.

Chen, A. Y., and L. F. Liu. 1994. "DNA Topoisomerases: Essential Enzymes and Lethal Targets." *Annual Review of Pharmacology and Toxicology* 34: 191–218. https://doi.org/10.1146/ANNUREV.PA.34.040194.001203.

Conilh, L., L. Sadilkova, W. Viricel, and C. Dumontet. 2023. "Payload Diversification: A Key Step in the Development of Antibody–Drug Conjugates." *Journal of Hematology & Oncology* 16: 3. https://doi.org/10.1186/S13045-022-01397-Y.

Dawson, P. E., T. W. Muir, I. Clark-Lewis, and S. B. H. Kent. 1994. "Synthesis of Proteins by Native Chemical Ligation." *Science* 266: 776–779. https://doi.org/10.1126/SCIENCE.7973629.

Dubowchik, G. M., R. A. Firestone, L. Padilla, et al. 2002. "Cathepsin B-Labile Dipeptide Linkers for Lysosomal Release of Doxorubicin From Internalizing Immunoconjugates: Model Studies of Enzymatic Drug Release and Antigen-Specific In Vitro Anticancer Activity." *Bioconjugate Chemistry* 13: 855–869. https://doi.org/10.1021/bc025536j.

Edupuganti, V. V. S. R., J. D. A. Tyndall, and A. B. Gamble. 2021. "Self-Immolative Linkers in Prodrugs and Antibody Drug Conjugates in Cancer Treatment." *Recent Patents on Anti-Cancer Drug Discovery* 16: 479–497. https://doi.org/10.2174/1574892816666210509001139.

El-Sayed, N. S., A. Nasrolahi Shirazi, M. I. Sajid, S. E. Park, K. Parang, and R. K. Tiwari. 2019. "Synthesis and Antiproliferative Activities of Conjugates of Paclitaxel and Camptothecin With a Cyclic Cell-Penetrating Peptide." *Molecules* 24: 1427. https://doi.org/10.3390/MOLECULES24071427.

Fang, Y., and H. Wang. 2022. "Molecular Engineering of Peptide–Drug Conjugates for Therapeutics." *Pharmaceutics* 14: 212. https://doi.org/10.3390/PHARMACEUTICS14010212.

Ferlay, J., M. Ervik, F. Lam, et al. 2024. *Global Cancer Observatory: Cancer Today*. Lyon, France: International Agency for Research on Cancer. https://gco.iarc.who.int/today.

Fuselier, J. A., L. Sun, S. N. Woltering, W. A. Murphy, N. Vasilevich, and D. H. Coy. 2003. "An Adjustable Release Rate Linking Strategy for Cytotoxin–Peptide Conjugates." *Bioorganic & Medicinal Chemistry Letters* 13: 799–803. https://doi.org/10.1016/S0960-894X(03)00016-7.

Goldenberg, D. M., T. M. Cardillo, S. V. Govindan, E. A. Rossi, and R. M. Sharkey. 2015. "Trop-2 Is a Novel Target for Solid Cancer Therapy With Sacituzumab Govitecan (IMMU-132), an Antibody-Drug Conjugate (ADC)." *Oncotarget* 6: 22496–22512. https://doi.org/10.18632/ONCOTARGET.4318.

Henne, W. A., D. D. Doorneweerd, A. R. Hilgenbrink, S. A. Kularatne, and P. S. Low. 2006. "Synthesis and Activity of a Folate Peptide Camptothecin Prodrug." *Bioorganic & Medicinal Chemistry Letters* 16: 5350–5355. https://doi.org/10.1016/j.bmcl.2006.07.076.

Hong, V., S. I. Presolski, C. Ma, and M. G. Finn. 2009. "Analysis and Optimization of Copper-Catalyzed Azide-Alkyne Cycloaddition for Bioconjugation." *Angewandte Chemie International Edition* 48: 9879–9883. https://doi.org/10.1002/anie.200905087.

Hoppenz, P., S. Els-Heindl, and A. G. Beck-Sickinger. 2020. "Peptide-Drug Conjugates and Their Targets in Advanced Cancer Therapies." *Frontiers in Chemistry* 8: 571. https://doi.org/10.3389/fchem.2020.00571.

Hou, L., Y. Hou, Y. Liang, et al. 2022. "Anti-Tumor Effects of P-LPK-CPT, a Peptide-Camptothecin Conjugate, in Colorectal Cancer." *Communications Biology* 5: 1248. https://doi.org/10.1038/s42003-022-04191-1.

IARC. 2024. *Cancer Tomorrow*. Lyon, France: International Agency for Research on Cancer. https://gco.iarc.fr/tomorrow/en.

Jeffrey, S. C., M. T. Nguyen, J. B. Andreyka, D. L. Meyer, S. O. Doronina, and P. D. Senter. 2006. "Dipeptide-Based Highly Potent Doxorubicin Antibody Conjugates." *Bioorganic & Medicinal Chemistry Letters* 16: 358–362. https://doi.org/10.1016/J.BMCL.2005.09.081.

Kularatne, S. A., C. Venkatesh, H. K. R. Santhapuram, et al. 2010. "Synthesis and Biological Analysis of Prostate-Specific Membrane Antigen-Targeted Anticancer Prodrugs." *Journal of Medicinal Chemistry* 53: 7767–7777. https://doi.org/10.1021/jm100729b.

Lang, K., and J. W. Chin. 2014. "Bioorthogonal Reactions for Labeling Proteins." *ACS Chemical Biology* 9: 16–20. https://doi.org/10.1021/cb4009292.

Lawrence, N., G. Philippe, P. J. Harvey, et al. 2020. "Cyclic Peptide Scaffold With Ability to Stabilize and Deliver a Helical Cell-Impermeable Cargo Across Membranes of Cultured Cancer Cells." *RSC Chemical Biology* 1: 405–420. https://doi.org/10.1039/d0cb00099j.

Lei, J., Q. Zhang, X. Jin, et al. 2021. "Drug Release From Disulfide-Linked Prodrugs: Role of Thiol Agents." *Molecular Pharmaceutics* 18: 2777–2785. https://doi.org/10.1021/ACS.MOLPHARMACEUT.1C00326.

Moody, T. W., S. A. Mantey, T. K. Pradhan, et al. 2004. "Development of High Affinity Camptothecin-Bombesin Conjugates That Have Targeted Cytotoxicity for Bombesin Receptor-Containing Tumor Cells." *Journal of Biological Chemistry* 279: 23580–23589. https://doi.org/10.1074/JBC.M401938200.

Nagata, S., J. Suzuki, K. Segawa, and T. Fujii. 2016. "Exposure of Phosphatidylserine on the Cell Surface." *Cell Death and Differentiation* 23: 952–961. https://doi.org/10.1038/cdd.2016.7.

Ogitani, Y., T. Aida, K. Hagihara, et al. 2016. "DS-8201a, a Novel HER2-Targeting ADC With a Novel DNA Topoisomerase I Inhibitor, Demonstrates a Promising Antitumor Efficacy With Differentiation From T-DM1." *Clinical Cancer Research* 22: 5097–5108. https://doi.org/10.1158/1078-0432.CCR-15-2822.

Palombi, I. R., N. Lawrence, A. M. White, et al. 2023. "Development of Antiplasmodial Peptide-Drug Conjugates Using a Human Protein-Derived Cell-Penetrating Peptide With Selectivity for Infected Cells." *Bioconjugate Chemistry* 34: 1105–1113. https://doi.org/10.1021/acs.bioconjchem.3c00147.

Philippe, G. J. B., A. Mittermeier, N. Lawrence, et al. 2021. "Angler Peptides: Macrocyclic Conjugates Inhibit p53:MDM2/X Interactions and Activate Apoptosis in Cancer Cells." *ACS Chemical Biology* 16: 414–428. https://doi.org/10.1021/acschembio.0c00988.

Pommier, Y. 2006. "Topoisomerase I Inhibitors: Camptothecins and Beyond." *Nature Reviews Cancer* 6: 789–802. https://doi.org/10.1038/nrc1977.

Redko, B., H. Tuchinsky, T. Segal, et al. 2017. "Toward the Development of a Novel Non-RGD Cyclic Peptide Drug Conjugate for Treatment of Human Metastatic Melanoma." *Oncotarget* 8: 757–768. https://doi.org/10.18632/ONCOTARGET.12748.

Rizvi, S. F. A., L. Zhang, H. Zhang, and Q. Fang. 2024. "Peptide-Drug Conjugates: Design, Chemistry, and Drug Delivery System as a Novel Cancer Theranostic." *ACS Pharmacology & Translational Science* 7: 309–334. https://doi.org/10.1021/ACSPTSCI.3C00269.

Rostovtsev, V. V., L. G. Green, V. V. Fokin, and K. B. Sharpless. 2002. "A Stepwise Huisgen Cycloaddition Process: Copper(I)-Catalyzed Regioselective 'Ligation' of Azides and Terminal Alkynes." *Angewandte Chemie International Edition* 41: 2596–2599. https://doi.org/10.1002/1521-3773(20020715)41:14<2596::AID-ANIE2596>3.0.CO;2-4.

Seigneuret, M., and P. F. Devaux. 1984. "ATP-Dependent Asymmetric Distribution of Spin-Labeled Phospholipids in the Erythrocyte Membrane: Relation to Shape Changes." *Proceedings of the National Academy of Sciences of the United States of America* 81: 3751–3755. https://doi.org/10.1073/PNAS.81.12.3751.

Sevin, E., L. Dehouck, A. Fabulas-da Costa, et al. 2013. "Accelerated CaCo-2 Cell Permeability Model for Drug Discovery." *Journal of Pharmacological and Toxicological Methods* 68: 334–339. https://doi.org/10.1016/J.VASCN.2013.07.004.

Spangler, B., T. Kline, J. Hanson, et al. 2018. "Toward a Ferrous Iron-Cleavable Linker for Antibody–Drug Conjugates." *Molecular Pharmaceutics* 15: 2054–2059. https://doi.org/10.1021/acs.molpharmaceut.8b00242.

Sun, L., J. A. Fuselier, and D. H. Coy. 2004. "Effects of Camptothecin Conjugated to a Somatostatin Analog Vector on Growth of Tumor Cell Lines in Culture and Related Tumors in Rodents." *Drug Delivery* 11: 231–238. https://doi.org/10.1080/10717540490446125.

Tornøe, C. W., C. Christensen, and M. Meldal. 2002. "Peptidotriazoles on Solid Phase: [1,2,3]-Triazoles by Regiospecific Copper(I)-Catalyzed 1,3-Dipolar Cycloadditions of Terminal Alkynes to Azides." *Journal of Organic Chemistry* 67: 3057–3064. https://doi.org/10.1021/jo011148j.

Vallabhapurapu, S. D., V. M. Blanco, M. K. Sulaiman, et al. 2015. "Variation in Human Cancer Cell External Phosphatidylserine Is Regulated by Flippase Activity and Intracellular Calcium." *Oncotarget* 6: 34375–34388. https://doi.org/10.18632/ONCOTARGET.6045.

Venditto, V. J., and E. E. Simanek. 2010. "Cancer Therapies Utilizing the Camptothecins: A Review of the In Vivo Literature." *Molecular Pharmaceutics* 7: 307–349. https://doi.org/10.1021/mp900243b.

Walker, M. A., G. M. Dubowchik, S. J. Hofstead, P. A. Trail, and R. A. Firestone. 2002. "Synthesis of an Immunoconjugate of Camptothecin." *Bioorganic & Medicinal Chemistry Letters* 12: 217–219. https://doi.org/10.1016/S0960-894X(01)00707-7.

Wall, M. E., M. C. Wani, C. E. Cook, K. H. Palmer, A. T. McPhail, and G. A. Sim. 1966. "Plant Antitumor Agents. I. The Isolation and Structure of Camptothecin, a Novel Alkaloidal Leukemia and Tumor Inhibitor From *Camptotheca acuminata*." *Journal of the American Chemical Society* 88: 3888–3890. https://doi.org/10.1021/ja00968a057.

Wang, M., J. Liu, M. Xia, et al. 2024. "Peptide-Drug Conjugates: A New Paradigm for Targeted Cancer Therapy." *European Journal of Medicinal Chemistry* 265: 116119. https://doi.org/10.1016/j.ejmech.2023.116119.

Wang, M., K. P. Rakesh, J. Leng, et al. 2018. "Amino Acids/Peptides Conjugated Heterocycles: A Tool for the Recent Development of Novel Therapeutic Agents." *Bioorganic Chemistry* 76: 113–129. https://doi.org/10.1016/J.BIOORG.2017.11.007.

Wang, X., Y. Zhuang, Y. Wang, M. Jiang, and L. Yao. 2023. "The Recent Developments of Camptothecin and Its Derivatives as Potential Anti-Tumor Agents." *European Journal of Medicinal Chemistry* 260: 115710. https://doi.org/10.1016/J.EJMECH.2023.115710.

Xu, Z., D. Guo, Z. Jiang, et al. 2019. "Novel HER2-Targeting Antibody-Drug Conjugates of Trastuzumab Beyond T-DM1 in Breast Cancer: Trastuzumab Deruxtecan (DS-8201a) and (Vic-)Trastuzumab Duocarmazine (SYD985)." *European Journal of Medicinal Chemistry* 183: 111682. https://doi.org/10.1016/J.EJMECH.2019.111682.

Zhang, C., H. Zhong, X. Li, et al. 2023. "Design, Synthesis and Bioactivity Investigation of Peptide-Camptothecin Conjugates as Anticancer Agents With a Potential to Overcome Drug Resistance." *International Journal of Pharmaceutics* 645: 123402. https://doi.org/10.1016/J.IJPHARM.2023.123402.

Zhao, H., C. Lee, P. Sai, et al. 2000. "20-O-Acylcamptothecin Derivatives: Evidence for Lactone Stabilization." *Journal of Organic Chemistry* 65: 4601–4606. https://doi.org/10.1021/jo000221n.

Zhou, J., X. Bian, Z. Kan, et al. 2022. "In Silico Exploration and Biological Evaluation of Bispecific Peptides Derived From Anti-HER2 Antibodies and Peptide-Camptothecin Conjugates for HER2-Positive Breast Cancer." *Journal of Medicinal Chemistry* 65: 15123–15139. https://doi.org/10.1021/acs.jmedchem.2c00968.

Zhou, J., Y. Zou, Y. Cai, et al. 2021. "A Designed Cyclic Peptide Based on Trastuzumab Used to Construct Peptide-Drug Conjugates for Its HER2-Targeting Ability." *Bioorganic Chemistry* 117: 105453. https://doi.org/10.1016/J.BIOORG.2021.105453.

Zhou, Y., S. Mowlazadeh Haghighi, Z. Liu, L. Wang, V. J. Hruby, and M. Cai. 2020. "Development of Ligand-Drug Conjugates Targeting Melanoma Through the Overexpressed Melanocortin 1 Receptor." *ACS Pharmacology & Translational Science* 3: 921–930. https://doi.org/10.1021/acsptsci.0c00072.

Supporting Information

Additional supporting information can be found online in the Supporting Information section.

Concluding Remarks

The findings presented in the manuscript within this Chapter highlight the imperative nature of PDC design. Analogous to the PDIP-PQ PDCs presented in Chapter 2, the PDIP-CPT PDCs required a cleavable linker that could release the drug for optimal cargo-driven potency and the superior carrier peptide was the disulfide-cyclised PDIP analogue. The utility of disulfide-reducible and protease-sensitive cleavable linkers that are commonly employed in ADC and PDC research was explored and detection of intracellular release of CPT was accomplished without the requirement for labels or fluorescent tags that can alter the properties of the conjugate. Undesired toxicity against a noncancerous control cell line emphasised the requirement for further optimisation of PDC design to maintain the properties of the peptide scaffold. Future exploration into the membrane binding properties of the PDIP-CPT PDCs using surface plasmon resonance or vesicle leakage experiments, as described in Chapter 2, could provide additional insight regarding their non-selective activity against noncancerous cells.

It is possible that CPPs with AMP-like properties (*e.g.* PDIP) are less optimal targeting devices for cytotoxic drugs such as CPT, compared to cell-targeting peptides, and may explain why fewer literature studies utilise this type of peptide scaffold. With an AMP-like CPP, any modification needs to maintain the overall structural (*e.g.* helicity), hydrophobic and amphipathic properties of the peptide, as these are important for its membrane-selective mechanism.[20] For a cell-targeting peptide, modifications acquired from PDC construction may have less impact on the ability of the peptide to bind to its cell-surface target, assuming that the site required for target binding is not altered. CPT-containing PDCs developed by Zhang *et al.*[15] illustrate that it is possible to utilise a lysine-rich AMP-like CPP as the peptide vehicle and retain selectivity for killing of cancerous over noncancerous cell lines. We are therefore optimistic that further optimisation of the PDIP-CPT PDC design could result in future generations of selective PDCs.

As the linker type and conjugation strategy were important for PDC activity and selectivity, future generations of PDIP-CPT PDCs should explore alternative linkers and conjugation methods. An additional linker that could be examined is the iron(II)-sensitive trioxolane linker that was explored in Chapter 2, as it has previously been applied to both malaria and cancer treatment contexts.[21–23] While this linker could add additional unwanted hydrophobicity to PDIP, as did the disulfide and dipeptide linkers, it has a cleavage mechanism that is specific for cancer cells.[23] Tumour cells often have abnormal iron regulation to support rapid proliferation, resulting in elevated unbound ferrous iron levels. In healthy cells, iron homeostasis is tightly regulated to prevent ferrous iron from damaging cells through the production of reactive oxygen species.[24] Therefore, the trioxolane linker could help to minimise

drug release within noncancerous cells if PDC selectivity cannot be improved, which could reduce PDC toxicity against noncancerous cell lines.

The synthesis of a cleavable CPT-trioxolane linker (**3.7**) could occur using a similar reaction sequence to the trioxolane scaffolds described by Mahajan *et al*.[20] or Spangler *et al*.[21] (as used in the manuscript presented in Chapter 2). As a measure to minimise additional hydrophobicity, a bicyclononyne (BCN) handle can be used in place of the dibenzocyclooctyne (DBCO) applied in Chapter 2 for SPAAC conjugation. Additionally, incorporation of a hydroxylamine handle (*e.g.* see **3.8**) instead of an alkyne could allow for oxime ligation with a previously developed PDIP analogue containing an acetone bridged disulfide bond (**3.9**).[24] Such a PDC could also provide understanding into whether alternative conjugation strategies provide better outcomes for PDC selectivity.

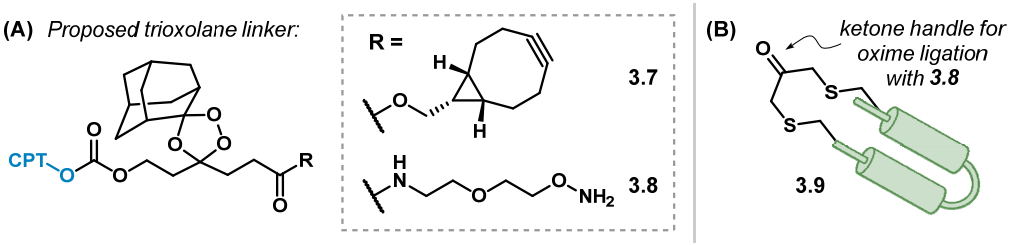

Figure 3.3. (A) An iron(II)-sensitive trioxolane linker could be a viable alternative cleavable linker for PDIP-CPT PDCs. **3.7** has an alkyne handle for SPAAC and **3.8** comprises a hydroxylamine handle for oxime ligation. (B) Cartoon representation of a PDIP analogue that contains an acetone bridged disulfide, which can be used for oxime conjugation.

Altogether, our efforts towards antimelanoma PDIP-CPT PDCs reinforce the requirement for PDC design to match a drug cargo with the correct carrier peptide and linker type. The potential for further optimisation of these PDCs as outlined in this section could result in improved PDC selectivity in the future.

References

(1) Brown, J. S.; Amend, S. R.; Austin, R. H.; Gatenby, R. A.; Hammarlund, E. U.; Pienta, K. J. *Mol. Cancer Res.* **2023**, *21*, 1142–1147.

(2) Hoppenz, P.; Els-Heindl, S.; Beck-Sickinger, A. G. *Front. Chem.* **2020**, *8*, 571.

(3) Wall, M. E.; Wani, M. C.; Cook, C. E.; Palmer, K. H.; McPhail, A. T.; Sim, G. A. *J. Am. Chem. Soc.* **1966**, *88*, 3888–3890.

(4) Chen, A. Y.; Liu, L. F. *Annu. Rev. Pharmacol. Toxicol.* **1994**, *34*, 191–218.

(5) Pommier, Y. *Nat. Rev. Cancer* **2006**, *6*, 789–802.

(6) Botella, P.; Rivero-Buceta, E. *J. Control. Release* **2017**, *247*, 28–54.

(7) Redinbo, M. R.; Stewart, L.; Kuhn, P.; Champoux, J. J.; Hol, W. G. J. *Science* **1998**, *279*, 1504–1513.

(8) Laco, G. S.; Collins, J. R.; Luke, B. T.; Kroth, H.; Sayer, J. M.; Jerina, D. M.; Pommier, Y. *Biochemistry* **2002**, *41*, 1428–1435.

(9) Venditto, V. J.; Simanek, E. E. *Mol. Pharm.* **2010**, *7*, 307–349.

(10) Wang, X.; Zhuang, Y.; Wang, Y.; Jiang, M.; Yao, L. *Eur. J. Med. Chem.* **2023**, *260*, 115710.

(11) Ogitani, Y.; Aida, T.; Hagihara, K.; Yamaguchi, J.; Ishii, C.; Harada, N.; Soma, M.; Okamoto, H.; Oitate, M.; Arakawa, S.; Hirai, T.; Atsumi, R.; Nakada, T.; Hayakawa, I.; Abe, Y.; Agatsuma, T. *Clin. Cancer Res.* **2016**, *22*, 5097–5108.

(12) Suzuki, H.; Nagase, S.; Saito, C.; Takatsuka, A.; Nagata, M.; Honda, K.; Kaneda, Y.; Nishiya, Y.; Honda, T.; Ishizaka, T.; Nakamura, K.; Nakada, T.; Abe, Y.; Agatsuma, T. *Mol. Cancer Ther.* **2024**, *23*, 257–271.

(13) Rizvi, S. F. A.; Zhang, L.; Zhang, H.; Fang, Q. *ACS Pharmacol. Transl. Sci.* **2024**, *7*, 309–334.

(14) El-Sayed, N. S.; Nasrolahi Shirazi, A.; Sajid, M. I.; Park, S. E.; Parang, K.; Tiwari, R. K. *Molecules* **2019**, *24*, 1427.

(15) Zhang, C.; Zhong, H.; Li, X.; Xing, Z.; Liu, J.; Yu, R.; Deng, X. *Int. J. Pharm.* **2023**, *645*, 123402.

(16) Mandal, D.; Nasrolahi Shirazi, A.; Parang, K. *Angew. Chem. Int. Ed.* **2011**, *50*, 9633–9637.

(17) Lawrence, N.; Philippe, G.; Harvey, P. J.; Condon, N. D.; Benfield, A. H.; Cheneval, O.; Craik, D. J.; Henriques, S. T. *RSC Chem. Biol.* **2020**, *1*, 405–420.

(18) Nasrolahi Shirazi, A.; Tiwari, R.; Chhikara, B. S.; Mandal, D.; Parang, K. *Mol. Pharm.*

2013, *10*, 488–499.

(19) Palombi, I. R.; White, A. M.; Koda, Y.; Craik, D. J.; Lawrence, N.; Malins, L. R. *Chem. Biol. Drug Des.* **2025**, *105*, e70051.

(20) Matthyssen, T.; Li, W.; Holden, J. A.; Lenzo, J. C.; Hadjigol, S.; O'Brien-Simpson, N. M. *Front. Chem.* **2022**, *9*, 795433.

(21) Mahajan, S. S.; Deu, E.; Lauterwasser, E. M.; Leyva, M. J.; Ellman, J. A.; Bogyo, M.; Renslo, A. R. *ChemMedChem* **2011**, *6*, 415–419.

(22) Spangler, B.; Kline, T.; Hanson, J.; Li, X.; Zhou, S.; Wells, J. A.; Sato, A. K.; Renslo, A. R. *Mol. Pharm.* **2018**, *15*, 2054–2059.

(23) Spangler, B.; Fontaine, S. D.; Shi, Y.; Sambucetti, L.; Mattis, A. N.; Hann, B.; Wells, J. A.; Renslo, A. R. *J. Med. Chem.* **2016**, *59*, 11161–11170.

(24) Torti, S. V.; Torti, F. M. *Nat. Rev. Cancer* **2013**, *13*, 342–355.

(25) Lawrence, N.; Dennis, A. S. M.; Lehane, A. M.; Ehmann, A.; Harvey, P. J.; Benfield, A. H.; Cheneval, O.; Henriques, S. T.; Craik, D. J.; McMorran, B. J. *Cell Chem. Biol.* **2018**, *25*, 1140–1150.

Chapter 4:

Vemurafenib PDCs – a case study for combating anticancer drug resistance

Introduction

A dual-acting PDC, comprising a peptide and drug that each have anticancer activity, could improve outcomes against acquired drug resistance, a challenge that is often encountered during the treatment of cancer with monotherapies.[1,2] Melanoma is no exception, with many patients experiencing disease relapse when tumour cells acquire mechanisms to evade drug treatment. Melanoma occurs in pigment-producing cells called melanocytes and is often the result of damage caused by exposure to ultraviolet light.[3] More than half of melanomas contain mutations in BRAF, a kinase involved in the mitogen activated protein kinase (MAPK) pathway that controls cell growth and division.[4] Mutations that lead to constituent activation of BRAF, such as the replacement of valine with glutamic acid at codon 600 (V600E), may contribute to uncontrolled cell growth and tumour development.[5] As a result, mutant BRAF is an oncoprotein that can be targeted for melanoma treatment.

Two inhibitors of BRAF-V600E, vemurafenib (Vem, **4.1**) and dabrafenib (Dab, **4.2**), are currently approved for melanoma treatment (Figure 4.1).[6] While these inhibitors have improved survival outcomes for melanoma patients, many develop drug resistance within six to eight months of starting treatment.[7] To address this, concurrent therapy with BRAF-V600E inhibitors and drugs that target MEK—a kinase downstream of BRAF—has become an important part of the melanoma treatment regimen. The current approved combination therapies include Vem with cobimetinib (**4.3**) and Dab with trametinib (**4.4**, Figure 4.1).[6] While such combinations typically exhibit delayed resistance acquisition compared to monotherapies, resistance is often still inevitable.[8] Combination therapies that instead pair two compounds with distinct killing mechanisms may make it more difficult for melanoma cells to develop resistance, compared to current combination therapies with drug targets in the same pathway.

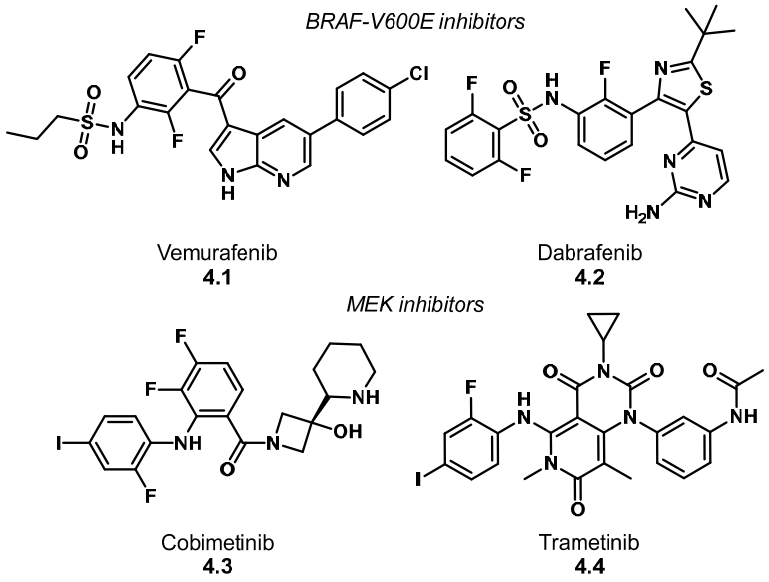

Figure 4.1. The structures of two BRAF-V600E inhibitors, vemurafenib (Vem, **4.1**) and dabrafenib (Dab, **4.2**), and the MEK inhibitors (**4.3**, **4.4**) they are often paired with for combination therapy.

4.1 Combining vemurafenib with anticancer peptides

Anticancer peptides represent an alternative modality that could be used alongside a BRAF inhibitor, such as Vem (**4.1**), as a combination therapy. A small number of studies have highlighted the utility of pairing Vem with a peptide, including using a peptide to facilitate the transdermal delivery of Vem[9] or to resensitise resistant tumour cells to Vem treatment by targeting signalling pathways involved in resistance.[10–12] However, to the best of our knowledge, Vem has rarely been paired with a peptide that has anticancer activity itself. We rationalised that the anticancer peptides PDIP and cGm6 could be paired with Vem because their membrane-active mechanisms (see Section 1.3.2) are distinct from the cell signalling pathway targeted by the BRAF inhibitors. We opted to combine Vem with the two peptide scaffolds in the form of PDCs, envisioning that this could also improve the poor water solubility of the drug.[13] Vem (**4.1**) was chosen in preference to Dab (**4.2**) for initial PDC studies because commercially available precursors enable modification of its drug core,[14] allowing the accessible installation of a conjugation handle onto the drug for subsequent attachment to the peptides.

A dual-acting therapy comprising Vem and PDIP/cGm6, each with distinct anticancer killing mechanisms, could make it harder for cancer cells to acquire resistance to both components and may ensure that cancer cells with resistance to one compound can still be killed by the other. We therefore aimed to understand whether Vem-containing PDCs were active against two distinct melanoma cell lines: one that was sensitive to drug treatment and a second that was resistant to treatment with Vem (Figure 4.2). Ensuring the anticancer peptide within prospective PDCs can kill drug-resistant cells that will not respond to the activity of the drug cargo will be an important factor for successful dual-acting PDCs. As a result, modifications to the peptide during PDC construction must not affect the function or killing mechanism of the peptide scaffold.

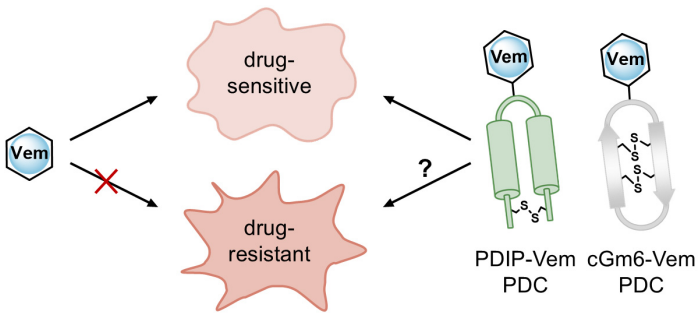

Figure 4.2. Proposed ability of PDIP-Vem and cGm6-Vem PDCs to kill melanoma cells that are sensitive and resistant to treatment with Vem. The drug-resistant cell line is unable to be killed by Vem alone.

4.2 Prior development of a drug-resistant melanoma cell line

A melanoma cell line with acquired resistance to Dab (**4.2**) was previously developed in the Henriques lab,[15] by continuously growing drug-sensitive cells in the presence of Dab at a clinically relevant concentration (100 nM). Initially, slow-cycling cells can survive Dab treatment

(known as drug-tolerant persisters) and eventually these cells evolve to have permanent drug resistance (> 105 days), meaning they can replicate in the presence of the drug (CC_{50} >> 1 μM) (Figure 4.3). Notably, cGm, the parent analogue of cGm6, was able to kill the Dab-resistant cells (CC_{50} = 3.4 μM, Figure 4.3), providing important precedent for efficacious combination therapies comprising similar anticancer peptides and BRAF inhibitors. Since Dab is a BRAF inhibitor, this cell line is expected to also have inherent resistance to treatment with Vem.

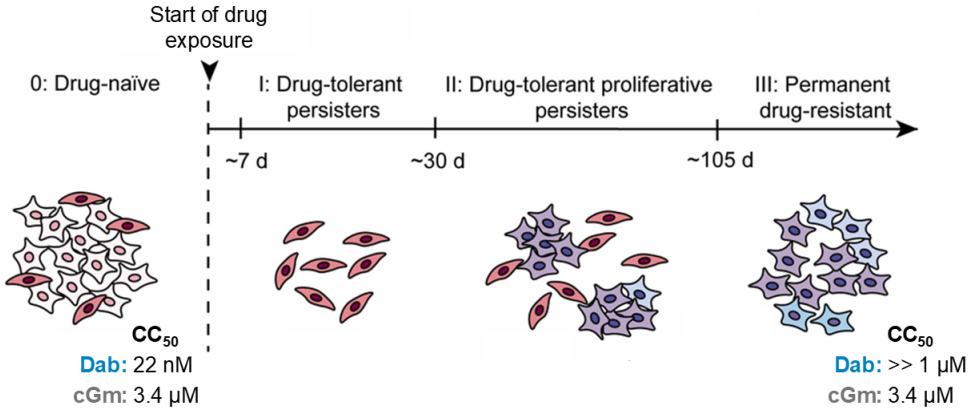

Figure 4.3. Schematic illustrating the prior development of a melanoma cell line (HT144) that was initially sensitive to drug treatment and resulted in acquired resistance to Dab. The CC_{50} values shown correspond to the activity of compounds tested on the drug-naïve and drug-resistant cell lines. Figure adapted from Benfield *et al.*[15]

This chapter, presented as a final draft of a manuscript for submission, details the synthesis of five Vem-containing PDCs and their bioactivity against Dab-sensitive and Dab-resistant melanoma cell lines. While prior chapters evaluated the ability of PDIP to improve the selectivity of a small molecule drug, here we aimed to understand whether the distinct killing mechanism of PDIP, and a second anticancer peptide cGm6, is beneficial for treatment against melanoma cell lines with expected resistance to Vem. Contributions of the drug, linker and peptide towards PDC bioactivity were analysed and the peptide carrier was revealed to be important for optimal activity against both drug-sensitive and resistant cells.

Australian National University

Statement of Contribution

This thesis is submitted as a Thesis by Compilation in accordance with https://policies.anu.edu.au/ppl/document/ANUP_003405

I declare that the research presented in this Thesis represents original work that I carried out during my candidature at the Australian National University, except for contributions to multi-author papers incorporated in the Thesis where my contributions are specified in this Statement of Contribution.

Title: Combining Bioactive Cell-Penetrating Peptides and Vemurafenib to Produce Peptide–Drug Conjugates with Activity Against Drug-Resistant Melanoma Cells

Authors: Isabella R. Palombi, Andrew M. White, Yasuko Koda, David J. Craik, Sónia Troeira Henriques, Nicole Lawrence,* Lara R. Malins*

Publication outlet:

Current status of paper: **Not Yet Submitted**/Submitted/Under Revision/Accepted/Published

Contribution to paper: Conducted the majority (over 85%) of the planning, experimental work (both synthetic chemistry and biology testing) and data analysis/compound characterisation. Most of the biology experiments were conducted by myself (with assistance from Nicole Lawrence) on lab exchanges to the University of Queensland, however, additional testing was conducted by Nicole after my departure. Wrote the original draft of the manuscript and the accompanying Supporting Material and incorporated edits from other authors. Chemistry components were conducted at the Research School of Chemistry, ANU, and the biology component was completed at the Institute of Molecular Biology, University of Queensland.

Senior author or collaborating authors endorsement: The above statement of contribution is accurate. The candidate performed the experimental work as indicated, including biological experiments which were carried out at the University of Queensland. The candidate wrote the original manuscript and Supporting Information file.

Isabella Palombi		25/10/2024
Candidate – Print Name	Signature	Date

Endorsed

Nicole Lawrence		25/10/2024
Primary Supervisor – Print Name	Signature	Date
Mark Humphrey		25/10/2024
Delegated Authority – Print Name	Signature	Date

Combining Bioactive Cell-Penetrating Peptides and Vemurafenib to Produce Peptide–Drug Conjugates with Activity Against Drug-Resistant Melanoma Cells

Isabella R. Palombi,[a,b] Andrew M. White,[a,b] Yasuko Koda,[c,d] David J. Craik,[c,d] Sónia Troeira Henriques,[d,e] Nicole Lawrence,[c,d*] Lara R. Malins[a,b*]

[a]Research School of Chemistry, Australian National University, Canberra 2601 ACT, Australia; [b]Australian Research Council Centre of Excellence for Innovations in Peptide and Protein Science, Australian National University, Canberra 2601 ACT, Australia; [c]Institute for Molecular Bioscience, The University of Queensland, Brisbane 4072 QLD, Australia; [d]Australian Research Council Centre of Excellence for Innovations in Peptide and Protein Science, The University of Queensland, Brisbane 4072 QLD, Australia; [e]School of Biomedical Sciences, Faculty of Health, Queensland University of Technology, Translational Research Institute, Brisbane 4102 QLD, Australia.

Email: lara.malins@anu.edu.au; n.lawrence@imb.uq.edu.au.

Abstract

Acquired drug resistance remains an ongoing challenge for the treatment of melanoma, a deadly form of skin cancer. Monotherapies used for melanoma treatment such as vemurafenib and dabrafenib, which target a mutant form of BRAF kinase, become ineffective within six months of starting treatment due to acquired resistance. Combination therapies—which pair multiple drugs that target the same signaling pathway—for the treatment of melanoma have emerged as a viable strategy to reduce drug resistance development, however, further benefits could be achieved if anticancer compounds with distinct killing mechanisms are combined. We sought to pair vemurafenib with bioactive peptides in the form of peptide–drug conjugates (PDCs) to establish whether this combination could kill melanoma cells that were sensitive or resistant to the related drug dabrafenib. We synthesized a suite of PDCs containing vemurafenib attached to three cell-penetrating peptides including two anticancer peptides with selective membrane-disruptive activity and one non-disruptive peptide. The five PDCs killed melanoma cells with improved activity relative to the free drug and were able to cross membranes with the drug cargo attached, however, the peptide carrier impacted PDC potency and selectivity. One peptide scaffold was determined to be the optimal partner for the drug and a PDC containing this peptide remained active against a melanoma cell line with acquired resistance to dabrafenib, highlighting the benefit of pairing BRAF inhibitors with a peptide that acts on a distinct cellular target.

Introduction

Skin cancers are the most diagnosed type of cancer, with over 1.5 million new cases worldwide in 2020. Melanoma, the deadliest form of skin cancer, resulted in an estimated 57 000 fatalities in the same year.[1] Over half of melanomas contain mutations in the BRAF protein, a kinase involved in the mitogen activated protein kinase (MAPK) pathway that controls cell growth and division.[2,3] The most common mutation occurs in codon 600, resulting in the replacement of a valine with a glutamic acid (V600E). This amino acid is in the activation loop of BRAF, resulting in increased kinase activity and thus cell proliferation when mutated.[2]

The prevalence of BRAF-V600E mutants in melanoma cancers provides a tumor marker that can be exploited for targeted drug therapy. Approval has been granted for two small molecule BRAF-V600E kinase inhibitors for melanoma treatment: vemurafenib (Vem) and dabrafenib (Dab).[4] While these inhibitors have improved survival outcomes for melanoma patients, many develop drug resistance within six to eight months of starting monotherapy, through an array of acquired resistance mechanisms.[5] Furthermore, some patients have intrinsic resistance so do not initially respond to BRAF inhibitors.[5] Continued research into alternative treatment strategies for melanoma is vital to prevent disease relapse associated with drug resistance and provide additional treatment options for patients who do not respond to current therapies.

Reactivation of the MAPK pathway is one of the predominant routes to BRAF inhibitor resistance, for example through mutations in other proteins involved in the signaling cascade, such as RAS or MEK, or activation of proteins that can bypass the BRAF kinase.[6] One solution to address MAPK reactivation consists of concurrent treatment with multiple inhibitors of the pathway, including the approved combination of Vem and cobimetinib, which target BRAF and MEK, respectively.[4] Current combination therapies typically exhibit delayed resistance acquisition compared to monotherapies, but resistance still occurs in many cases.[4,7] As an

alternative approach, combination therapies that utilize multiple anticancer compounds with distinct killing mechanisms—rather than targets in the same pathway—may make it more difficult for cancer cells to acquire resistance to both drugs.[8] Several studies have explored alternative combination strategies to improve the efficacy of existing BRAF kinase inhibitors, including; pairing Vem with an inhibitor that locks BRAF in an inactive conformation,[9,10] conjugating Vem to a ligand that targets BRAF-V600E for proteolytic degradation,[11] targeting other signaling pathways with a peptide to resensitize resistant cells to Vem therapy,[12–14] and cotreatment of melanoma with Dab and an antibody–drug conjugate.[15,16]

Inspired by these combination therapy approaches, we sought to couple Vem with bioactive peptides, an approach which has been scarcely explored in the literature.[12–14,17] Bioactive peptides are a class of molecules derived from diverse animal and plant sources and can exhibit anti-inflammatory, antimicrobial and anticancer properties.[18] Many are amphipathic, consisting of both positively charged and hydrophobic amino acids, and are promising candidates for anticancer treatment because they have inherent selectivity for anionic cancer cell membranes. Selectivity is conferred by electrostatic interactions between the positively charged residues of the bioactive peptide and the surface-exposed negatively charged phosphatidylserine lipid headgroups in cancer cell membranes, which are maintained in the inner membrane leaflet of healthy cells.[18,19]

We have previously engineered anticancer peptides from naturally occurring amphipathic bioactive peptides or protein domains. The first peptide, platelet factor 4-derived internalization peptide (PDIP),[20] is a structural mimic of the bioactive C-terminal domain from the human defense protein platelet factor 4 (see Figure 1A for sequence). PDIP comprises an α-helical hairpin structure that is cyclized *via* a disulfide bond. The second peptide, [G1K,K8R]cGm[21]—herein referred to as cGm6—is a cyclic analogue derived from gomesin (Gm), a host defense peptide produced in the hemocytes of the Brazilian spider *Acanthoscurria gomesiana*.[22,23] cGm6 has a β-hairpin structure that is stabilized by two disulfide bonds, with an additional cationic residue (lysine), and an arginine replacing the naturally occurring lysine of Gm (see Figure 1A for sequence).[21] Both PDIP and cGm6 have low micromolar potency against melanoma cell lines, attributed to the targeted disruption of membranes, including the mitochondrial membrane (PDIP) or cell membrane (cGm6).[21,24] Notably, the killing mechanism of the peptides is distinct from the cell signaling pathways targeted by BRAF kinase inhibitors, potentially making it harder for the cancer cells to acquire resistance to both the drug and peptide when used in combination.[25]

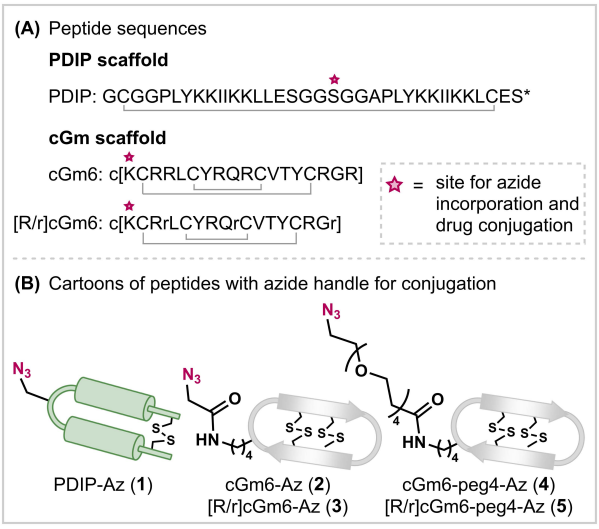

Figure 1. (A) Sequences of the PDIP, cGm6 and [R/r]cGm6 peptides utilized in this study. The disulfide bonds are represented by gray lines and the amino acid site for azide incorporation and subsequent drug conjugation is indicated with a pink star. c[ ] = backbone cyclized; * = amidated C-terminus; r = D-arginine. (B) Cartoon representation of azide-modified PDIP, cGm6 and [R/r]cGm6 peptides. For PDIP, the azide is incorporated *via* substitution of the serine with an azide modified alanine residue (azidoalanine). For cGm6 and [R/r]cGm6, the azide is incorporated by modifying the lysine side chain *via* amide bond ligation with either a short azide handle or longer handle containing a peg4 spacer.

PDIP and cGm6 are bioactive cell-penetrating peptides (CPPs), able to translocate membranes to deliver cargo into cells.[24,26,27] Furthermore, a less potent analogue of cGm6 that replaces three L-arginine residues with

D-arginine ([G1K,R4r,K8R,R10r,R18r]cGm), herein referred to as [R/r]cGm6, provides a CPP that can enter cancer cells without disrupting membranes (see Figure 1A for sequence).[27] We postulated that peptide–drug conjugates (PDCs) that combine Vem with each of the three CPPs could improve the efficacy of Vem and have additional benefits such as improving its poor water solubility and membrane permeability.[17,28]

Herein, a suite of Vem-containing PDCs utilizing the PDIP, cGm6 and [R/r]cGm6 peptides was synthesized and evaluated for activity against melanoma cell lines that were sensitive or resistant to the related drug Dab. Notably, the contribution of the peptide and drug components to overall PDC activity was able to be examined with PDCs containing the non-disruptive [R/r]cGm6 peptide (*i.e.* limited contribution from the peptide) and testing the PDCs against drug-resistant cells (*i.e.* limited contribution from the drug). This work demonstrates that Vem-containing PDCs have improved cytotoxicity towards melanoma cells relative to the drug itself, with the CPP scaffold having an impact on PDC activity. PDIP was found to be the optimal scaffold, resulting in the most potent PDC against both drug-sensitive and drug-resistant cells. Overall, Vem-containing PDCs are showcased as a viable alternative strategy for melanoma treatment.

Results and Discussion

Design and synthesis of Vem-containing PDCs

To produce a suite of Vem-containing PDCs, strain promoted azide−alkyne cycloaddition (SPAAC)[29] was envisioned as a conjugation strategy, to remain orthogonal to the disulfide linkages within the PDIP and cGm peptide scaffolds. As such, azide-containing peptides (see Figure 1B for cartoon representations) were designed to provide a chemoselective handle for conjugation to an alkyne-modified Vem analogue. PDIP-Az (**1**) contains an azide modified alanine residue within the spacer region between the two helices that was incorporated during automated solid-phase peptide synthesis (SPPS), as previously described.[24,26] Late-stage azide installation was instead used to produce cGm6-Az (**2**) and [R/r]cGm6-Az (**3**). Peptides precursors were synthesized using automated SPPS, then backbone cyclized using native chemical ligation.[30] Orthogonal folding of cysteine pairs, first in 0.1 M ammonium bicarbonate then with iodine oxidation in 20% (v/v) acetonitrile was performed to produce cGm6 and [R/r]cGm6. Next, the azide handle was appended *via* an amide bond onto the side chain of the single lysine residue within the cGm6 and [R/r]cGm6 sequences (see Supporting Information for further details). Since cGm6 and [R/r]cGm6 are small CPPs, we synthesized two additional analogues, cGm6-peg4-Az (**4**) and [R/r]cGm6-peg4-Az (**5**), containing a four-unit poly(ethyleneglycol) (peg4) linkage between the peptide and azide (Figure 1B), to probe whether increased spacing between PDC components is required for optimal activity of Vem and/or the peptide partner. The additional peg4 linkage was not included for PDIP, as we have previously shown that altering linker length does not affect activity for PDIP-containing PDCs.[26]

An alkyne-modified Vem analogue was designed to provide a non-cleavable linkage between the drug and peptide following drug installation, meaning the PDCs will not have programmed release of Vem from the peptide once inside target cells. We hypothesized that non-cleavable PDCs would not impair the activity of Vem, if modified in a position that is not essential for its mechanism of action or binding to BRAF. Modifications at the *para* position on the chlorophenyl ring of Vem are well tolerated because this part of the phenyl ring is solvent exposed when bound to BRAF, providing an ideal position for linker attachment.[11,31,32] Including a non-cleavable linker has the additional benefit of maintaining simplicity in PDC synthesis.

To this end, a commercially available Vem precursor (**6**) was modified *via* a Suzuki–Miyaura cross-coupling reaction to install a Boc protected *p*-benzylamine moiety in place of the *p*-chlorophenyl structure of the Vem core (Scheme 1A).[11,32] Removal of the Boc group produced Vem-NH_2 (**7**, 66% yield over two steps), providing a free primary amine for further modification. Amide formation with dibenzocyclooctyne-acid (DBCO-COOH), aided by the coupling reagent T3P®, generated Vem-DBCO (**8**), an alkyne modified Vem analogue primed for peptide conjugation, in 46% yield.

With the strained alkyne Vem-DBCO (**8**) in hand, PDCs **10**-**14** were synthesized *via* a SPAAC reaction with each of the azide-modified peptides (Table 1). SPAAC was utilized as a preferred conjugation tool because we found the alternate click chemistry approach of copper-catalyzed azide–alkyne cycloaddition to be incompatible with Vem without extensive reaction optimization.[33] Five Vem-containing PDCs were

successfully synthesized in good yield (63–88%, entries 1–5), including one PDC with the PDIP scaffold (**10**) and four with the cGm scaffold. Two of the cGm PDCs (**11-12**) contained the cGm6 and [R/r]cGm6 analogues with the shorter linkage between Vem and the corresponding peptide. The remaining two PDCs (**13-14**) comprised the longer peg4 linkage. Notably, all PDCs were soluble in aqueous solution, as opposed to Vem which is insoluble in water.

Scheme 1. (A) Synthesis of a Vem analogue containing an alkyne conjugation handle. (B) Modification of DBCO-COOH to produce DBCO-amide.

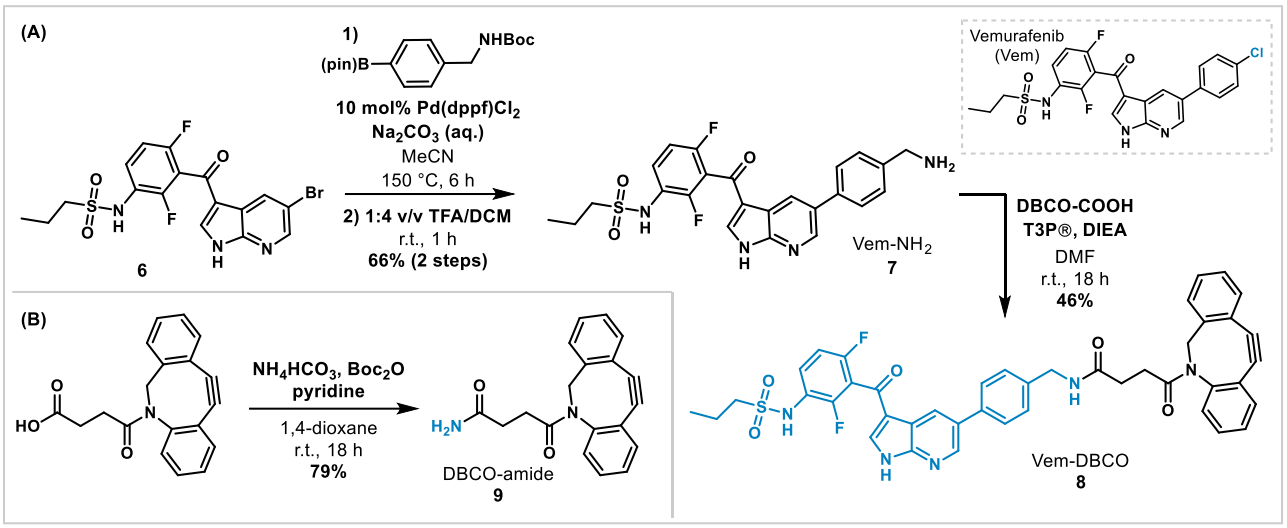

Table 1. PDC and peptide-DBCO linker construct synthesis *via* SPAAC conjugation.

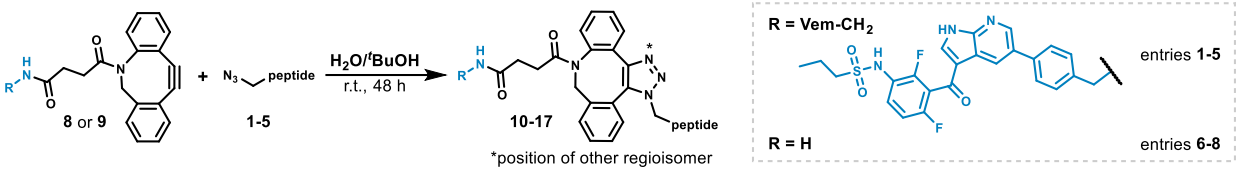

Entry	Alkyne	Azide	Product	Yield[a]	Entry	Alkyne	Azide	Product	Yield[a]
1	Vem-DBCO **8**	PDIP-Az **1**	PDIP-DBCO-Vem **10**	81%	5	Vem-DBCO **8**	[R/r]cGm6-peg4-Az **5**	[R/r]cGm6-peg4-DBCO-Vem **14**	64%
2	Vem-DBCO **8**	cGm6-Az **2**	cGm6-DBCO-Vem **11**	87%	6	DBCO-amide **9**	PDIP-Az **1**	PDIP-DBCO-amide **15**	70%
3	Vem-DBCO **8**	[R/r]cGm6-Az **3**	[R/r]cGm6-DBCO-Vem **12**	88%	7	DBCO-amide **9**	cGm6-Az **2**	cGm6-DBCO-amide **16**	94%
4	Vem-DBCO **8**	cGm6-peg4-Az **4**	cGm6-peg4-DBCO-Vem **13**	63%	8	DBCO-amide **9**	[R/r]cGm6-Az **3**	[R/r]cGm6-DBCO-amide **17**	95%

[a] Isolated yields were calculated using the molecular weight of the TFA salt, assuming all basic amino acids, the terminal amine (if present) and the 7-azaindole moiety within Vem were protonated.

Synthesis of peptide-DBCO linker controls

The requirement of a strained cyclooctyne reagent for SPAAC conjugation meant incorporation of a bulky DBCO moiety into the PDCs. Concerned that the additional hydrophobicity provided by the linker could influence the activity and selectivity of the peptides, especially the smaller cGm6 and [R/r]cGm6 peptides, we sought to evaluate peptide-DBCO linker constructs as additional controls. These constructs were designed to mimic the structure of the Vem PDCs but without the drug itself, containing only the peptide and DBCO linker components. Towards this objective, the carboxylic acid of DBCO-COOH was converted into an amide in the presence of ammonium bicarbonate, Boc anhydride and pyridine,[34,35] producing DBCO-amide (**9**) in 79% yield (Scheme 1B). We predicted that an amide moiety would be an inert functional group in the physiological conditions required for subsequent biological testing.[36] Finally, DBCO-amide was conjugated onto the azide

modified PDIP, cGm6 and [R/r]cGm6 peptides *via* SPAAC (Table 1) to generate peptide-DBCO linker constructs **15**, **16** and **17**, respectively (70–95% yields, entries 6–8).

Vem PDCs are active against drug-sensitive and drug-resistant cell lines

The *in vitro* cytotoxicity of the Vem PDCs (**10**-**14**) was evaluated against two melanoma cell lines and a noncancerous epidermal cell line and compared to the activity of the parent peptides, peptide-DBCO linker controls (**15**-**17**) and modified (Vem-NH_2, **7**) and unmodified Vem (Table 2). Dabrafenib (Dab) was included as a control to distinguish between HT144, a melanoma cell line with a V600E mutation in BRAF, that is sensitive to Dab (and Vem) treatment, and a HT144-derived cell line (Dab-PDRC) that was previously developed in the Henriques lab[25] with permanent drug-resistant cells (PDRCs) comprising acquired resistance to Dab. As Dab and Vem are both BRAF-V600E inhibitors,[37] the Dab-resistant cells are expected to also be resistant to Vem. Cytotoxicity against the Dab-PDRC cell line was examined to determine whether PDCs remained active against drug-resistant cells. As the drug portion of the PDCs was expected to be inactive against this cell line, its use also provided insight into peptide versus drug contributions to PDC activity. HaCaT, a noncancerous cell line with wildtype BRAF, was utilized as a control to determine whether PDCs were selective for cancerous over noncancerous cells. Each cell line was incubated with the treatments for 72 h to determine the concentration required to inhibit the growth of 50% of cells (CC_{50}). The ratio of CC_{50} values for HaCaT compared to the two melanoma cell lines was also determined to understand relative selectivity for killing of cancer cells for each compound. Treatments with higher selectivity ratios were considered preferable.

Table 2. Cytotoxic activity of Vem-containing PDCs compared to peptides, peptide-DBCO controls, and drugs against Dab-sensitive and resistant HT144 (melanoma) and HaCaT (noncancerous) cells.[a]

Compound	CC_{50} (μM)			Selectivity[c]	
	HT144	Dab-PDRC[b]	HaCaT	CC_{50} HaCaT/ CC_{50} HT144	CC_{50} HaCaT/ CC_{50} Dab-PDRC
PDIP	4.5 ± 0.1	5.1 ± 0.3	> 32	> 7	> 6
PDIP-DBCO-amide **15**	3.4 ± 0.3	4.3 ± 0.3	19.2 ± 1.1	5.6	4.5
PDIP-DBCO-Vem **10**	1.0 ± 0.1	3.4 ± 0.2	15.5 ± 1.4	15.5	4.6
PDIP + Vem (unconjugated, equimolar)	5.0 ± 0.6	n.d.	n.d.		
cGm6	1.9 ± 0.1	2.8 ± 0.2	8.3 ± 0.2	4.4	3.0
cGm6-DBCO-amide **16**	9.4 ± 1.1	10.4 ± 1.4	27.5 ± 1.9	2.9	2.6
cGm6-DBCO-Vem **11**	3.9 ± 0.1	8.6 ± 0.6	12.8 ± 0.9	3.3	1.5
cGm6-peg4-DBCO-Vem **13**	6.8 ± 0.4	24.8 ± 1.6	24.0 ± 1.4	3.5	0.97
cGm6 + Vem (unconjugated, equimolar)	2.8 ± 0.2	n.d.	n.d.		
[R/r]cGm6	19.5 ± 0.9	21.5 ± 1.4	> 64	> 3	> 3
[R/r]cGm6-DBCO-amide **17**	> 32	> 32	> 32		
[R/r]cGm6-DBCO-Vem **12**	6.1 ± 0.3	20.7 ± 1.6	24.2 ± 1.9	4.0	1.2
[R/r]cGm6-peg4-DBCO-Vem **14**	8.7 ± 0.8	~ 24	42.5 ± 3.3	4.9	~1.8
Vem	10.5 ± 1.5	no activity	>> 64	>> 6	
Vem-NH_2 **7**	0.33 ± 0.03	19.8 ± 1.3	13.1 ± 1.5	39.7	0.66
Dab	< 0.008	no activity	> 2		

[a] Cells were incubated with serial dilutions of each compound for 72 h. Cell death was measured using resazurin, with 0.1% (v/v) Triton X-100 as a control for 100% cell death. Half maximal cytotoxic concentration (CC_{50}) values are expressed as mean ± SEM and were determined from dose response curves that were fitted using [inhibitor] *vs* response with variable slope (Graphpad Prism v10) for at least three biological replicates. [b] Dab-PDRC is a HT144 cell line, previously developed in the Henriques lab,[25] with permanent drug resistance to the BRAF-V600E inhibitor dabrafenib (Dab) and inherent resistance to Vem. [c] HaCaT CC_{50} relative to HT144 or Dab-PDRC CC_{50} was used to establish selectivity for killing of cancer cells over noncancerous cells. n.d. = not determined.

Cytotoxicity and selectivity of the drugs, peptides and peptide-DBCO controls

Vem (free drug) had moderate cytotoxicity against the HT144 melanoma cell line (CC_{50} = 10.5 μM) but had no activity against the Dab-resistant cell line, confirming that the Dab-PDRCs are inherently resistant to Vem treatment. Interestingly, the modified Vem analogue, Vem-NH_2 (**7**; CC_{50} = 0.33 μM), was far more potent than Vem against the drug-sensitive HT144 melanoma cells and was selective for HT144 cells over the noncancerous HaCaT cells. This confirms that modifications of Vem at the *para* position on the phenyl ring are not detrimental to its activity. The enhanced activity of Vem-NH_2 may be explained by improved solubility (relative to Vem) due to the incorporation of an ionizable amine into the structure of Vem[38] and/or improved

binding to BRAF through additional hydrogen bonds between the benzylamine moiety of the drug and residues within the enzyme.[11] Analogous to Vem, Vem-NH_2 was substantially less active against Dab-resistant PDRCs than HT144 (drug-sensitive) cells.

The three parent peptides had selective activity against HT144 that agreed with our previously reported findings for melanoma cell lines.[24,25,27] cGm6 was the most potent peptide (CC_{50} = 1.9 μM), followed by PDIP (CC_{50} = 4.5 μM), then [R/r]cGm6 as the least active peptide (CC_{50} = 19.5 μM). All peptides retained similar selective potency for the drug-resistant Dab-PDRCs, with the most active being cGm6 (2.8 μM), followed by PDIP (5.1 μM), then [R/r]cGm6 (21.5 μM).

The three peptide-DBCO controls had varied activity against the HT144 cell line. PDIP-DBCO-amide **15** had similar potency (CC_{50} = 3.4 μM) to PDIP itself, suggesting that the addition of the bulky DBCO moiety to the peptide did not affect its activity. However, introducing DBCO into the peptide structure may promote nonselective membrane binding, as **15** was more active than PDIP against HaCaT cells with the HaCaT/HT144 CC_{50} difference reducing from > 7 to 5.6. In contrast, the DBCO-modified cGm6 and [R/r]cGm6 (**16** and **17**) had reduced activity relative to their parent peptides, suggesting that these peptides did not tolerate the addition of a bulky hydrophobic moiety to the same extent as PDIP. The same trend was also reflected in the drug-resistant Dab-PDRC cell line.

Cytotoxicity and selectivity of the Vem PDCs

Collectively, the five Vem PDCs (**10**-**14**) had low micromolar activity against drug-sensitive HT144 melanoma cells and were more potent than Vem as a free drug, with CC_{50} values ranging from 1–9 μM. As these PDCs contain a non-cleavable linker, these results support our hypothesis that the Vem drug core can interact with and bind to its BRAF-V600E target while tethered to a peptide, and corroborate the findings of previous studies where Vem was modified at the same position.[9,11,32] Here, the maintained activity of Vem with a fixed linker between the drug and peptide contrasts our previous observations for PDIP-based PDCs containing the anticancer drug camptothecin, where optimal activity required a cleavable linker to release the drug from the peptide.[39] Interestingly, Vem-NH_2 (**7**) was substantially more potent than the five PDCs, despite the PDCs containing this modified Vem analogue as the drug cargo. This suggests that the amine functional group—which is converted to an amide in the PDCs—may be important in the enhanced activity of Vem-NH_2. The different CPPs appeared to affect overall PDC activity, as different potencies were observed against melanoma cells that were sensitive or resistant to the related drug Dab, despite the five PDCs containing the same drug cargo and similar linker regions.

PDIP-based PDC. PDIP-DBCO-Vem (**10**) was the most potent PDC tested and had enhanced activity against HT144 (CC_{50} = 1.0 μM) compared to PDIP and Vem alone, or an equimolar mixture of unconjugated PDIP and Vem (CC_{50} = 5.0 μM). This improvement was further enhanced by PDC **10** maintaining the selective killing observed for the parent PDIP peptide (HaCaT/HT144 CC_{50} difference = 15.5), despite being more active than PDIP against HaCaT (CC_{50} = 15.5 μM). The favorable activity of PDC **10** may be explained by improved solubility and passage of Vem through cell membranes to access the intracellular BRAF target. PDIP-DBCO-Vem (**10**) was also the most potent and selective PDC against the drug-resistant Dab-PDRC cell line, with a CC_{50} value (3.4 μM) representative of the activity of PDIP. These results suggest that the peptide portion of the PDC can still kill melanoma cells when the Vem drug component is ineffective due to acquired resistance to Dab. The activity of PDC **10** against a drug-resistant melanoma cell line accentuates the benefit of pairing Vem with another modality that acts on a distinct cellular target.[12–14,16]

cGm6-based PDCs. cGm6-DBCO-Vem (**11**) was also a potent PDC (HT144 CC_{50} = 3.9 μM) that retained similar selectivity for melanoma over noncancerous HaCaT cells as the parent peptide. However, increasing the spacing between cGm6 and Vem with a peg4 linkage reduced PDC activity against HT144 cells (CC_{50} = 6.8 μM for PDC **13**). Whilst displaying low micromolar potency that was better than Vem as a free drug, PDCs **11** and **13** were less potent than cGm6 and further worsening of activity and selectivity was observed against the drug-resistant Dab-PDRC cell line.

The decreased activity of the cGm6-based PDCs compared to the parent peptide suggests that the addition of a drug and linker affected the membrane-disruptive activity of cGm6. Peptide structure is crucial for the

activity and function of bioactive peptides,[40] including for β-sheet containing AMPs such as cGm6, where peptides with higher amphipathicity often exhibit better antimicrobial activity,[41,42] which may also extend to their anticancer activity. Appending a hydrophobic linker and drug cargo onto cGm6 may have altered the overall amphipathicity of the peptide within the PDC, compared to the original peptide, and reduced the key electrostatic and nonpolar interactions—between the peptide residues and cell membrane lipids—that were required for the mechanism of the peptide.[21,27] The five-fold lower activity of cGm6-DBCO-amide **16** (CC_{50} = 9.4 μM) compared to cGm6 suggests that even the addition of smaller hydrophobic moieties may affect the peptide activity. Furthermore, in contrast to PDIP, the cGm6-containing PDCs did not appear to provide a benefit compared to coadministration of unconjugated cGm6 and Vem (HT144 CC_{50} = 2.8 μM). Therefore, the combination of cGm6 and Vem may benefit less from the PDC format and indeed previous *in vivo* studies have indicated that cotreatment of mice with xenografted tumors using an unconjugated BRAF inhibitor and β-hairpin peptide improved their survival compared to monotherapy.[25]

[R/r]cGm6-based PDCs. The two [R/r]cGm6-based PDCs (**12** and **14**) had moderate activity against HT144 cells (CC_{50} = 6.1 μM and 8.7 μM, respectively), despite containing the least potent peptide analogue. The improved potency of **12** and **14** compared to [R/r]cGm6 may signify that the activity for these PDCs is driven by the attached Vem cargo. This contrasts with the PDIP- and cGm6-based PDCs, which appear to have contributions from both the drug and peptide towards PDC bioactivity. Both PDCs **12** and **14** lost activity when tested against the drug-resistant Dab-PDRC cell line, emphasizing the benefit of pairing Vem with a potent anticancer peptide to kill cells with existing or acquired resistance to the drug cargo.

Altogether, the CPP that was paired with Vem in the PDC design was important as it influenced PDC activity and selectivity. While the PDC containing the PDIP scaffold had favorable activity against drug-sensitive and drug-resistant melanoma cells, the cGm scaffold did not benefit from a PDC format to the same extent. Future iterations of cGm6-based PDCs may require further optimization in PDC design (*e.g.* alternative conjugation sites or strategies) to maintain the cell-penetrating and membrane-disruptive activity of cGm6. Additionally, studies that evaluate whether HT144 melanoma cells acquire resistance to Vem as a PDC cargo—compared to as a free drug or as an unconjugated mixture with the peptide—could indicate whether PDCs are an optimal format for combination therapy with Vem and cGm6.[25] As the activity of PDCs **10**-**14** was better than Vem as a free drug but not Vem-NH_2 (**7**), future Vem-containing PDCs may benefit from cleavable linkers[43] that can release the cargo inside melanoma cells to retain the potency of Vem-NH_2.

Vem PDCs utilize different cell internalization methods depending on the peptide carrier

We employed two assays to evaluate how the different CPPs and PDCs moved through membranes, with compounds **10**-**13** chosen as representative PDCs for the assays. The parallel artificial membrane permeability assay (PAMPA) was used to report apparent permeability (Papp) due to passive movement through membranes, whereas mass spectrometric analysis of peptides and PDCs recovered from treated and washed HT144 cells was used to report on cell entry (passive or active transport) and/or association of compounds with cell membranes. Graphical representations of each assay are shown in Figure 2.

For the PAMPA experiment, the PDCs (**10**-**13**), parent peptides and modified Vem (**7**) were added to the apical side of PAMPA monolayers and incubated for 4 h. Analysis of the apical and basolateral sides of the membrane using liquid chromatography–mass spectrometry (LC–MS) determined the Papp (movement from apical to basolateral fractions) and % recovery (amount of recovered sample in combined soluble fractions) for each treatment. Good membrane permeability ($> 1 \times 10^{-6}$ cm/s) in this assay indicated passive movement across the artificial membrane, and high proportions of recovered sample signified that the compound remained soluble and did not aggregate or associate with the membrane. For the cell internalization assay, HT144 cells were treated with the PDCs (**10**-**13**), parent peptides and modified Vem-NH_2 (**7**) (4 μM) for 1 h, followed by mass spectrometric analysis of washed and harvested cells. The area under the curve (AUC) values for each sample were compared to controls (untreated cells with compounds added post harvesting) to determine the total recovered PDC or peptide.

Membrane permeability and internalization of the parent drugs and peptides

The three parent peptides had high membrane permeability (Papp ≥ 2 × 10^{-6} cm/s) and recovery (> 80%) (Figure 2A), indicating passive movement across the membrane that is consistent with previous observations for similar peptide analogues.[27,39] Intact peptides were detected in HT144 cell extracts, with cGm6 having the highest degree of internalization/cell association (16%), followed by [R/r]cGm6 (9%) and PDIP (8%) (Figure 2B).

Vem-NH_2 (**7**) had moderate permeability (Papp ~8 × 10^{-7} cm/s) and was more soluble than Vem (not shown), which was too insoluble to obtain reliable permeability data at the tested concentration of 4 µM. Also, Vem-NH_2 was not completely recovered from the soluble fractions (37%) after the assay, suggesting that while the compound could passively move through the membrane, the modified drug likely aggregated during the assay. Vem-NH_2 (7%) was detected in HT144 cell extracts after 1 h incubation, but it is likely that solubility affected cell uptake, similar to the observations from PAMPA.

Membrane permeability and internalization of the Vem PDCs

The three PDCs containing the shorter linker (**10**-**12**) had good solubility as they were readily recovered (>99%) from the PAMPA assay (Figure 2A). cGm6-DBCO-Vem (**11**) had similar permeability (Papp ~2 × 10^{-6} cm/s) to its parent peptide, however, the equivalent [R/r]cGm6 and PDIP PDCs (**12**, **10**) had minimal to no movement through the artificial membrane. Interestingly, cGm6-peg4-DBCO-Vem (**13**) had reduced recovery (59%) despite having moderate permeability (Papp ~7 × 10^{-7} cm/s). This is surprising as incorporation of peg units into PDCs is generally considered to improve solubility.[44] Intact PDC was detected for all four tested PDCs (**10**-**13**) in HT144 cell extracts at significantly higher proportions than the corresponding parent peptides, except for cGm6-DBCO-Vem (**11**) which was detected in comparable amounts to cGm6 (Figure 2B).

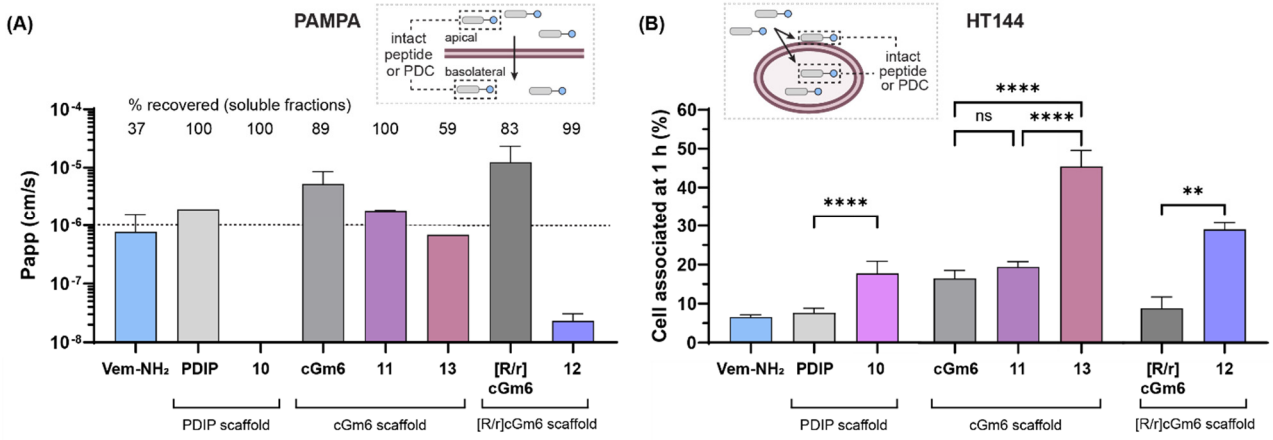

Figure 2. (A) Membrane permeability of PDCs, parent peptides, and Vem-NH_2. Compounds were added to PAMPA wells (4 µM) and incubated for 4 h. Supernatant from apical and basolateral sides of the membrane were collected and analyzed using LC–MS. The amount in the combined soluble fractions was compared to the starting amount to determine % recovery, and the apparent permeability (Papp) was calculated as before.[45] Data is expressed as mean ± SD from a single experiment with three technical replicates. (B) Internalization/cell membrane association of PDCs, parent peptides, and Vem-NH_2 with HT144 cells. Cells were treated with each sample (4 µM) for 1 h, washed to remove extracellular compound, then extracted with 75% (v/v) MeCN in mQH_2O (containing 1.75% (v/v) TFA), to recover soluble peptide or PDC from precipitated cell proteins. The relative amount of internalized peptide or PDC was determined by integrating area under the curve (AUC) for the $[M+6H]^{6+}$ m/z peak (for the intact mass) using time of flight–mass spectrometry. The amount of internalized compound was compared to the AUC present when 4 µM of each analogue was added to untreated cells after addition of the extraction solution, to determine the percentage of internalized compound. Data is expressed as mean ± SD from a single experiment with three technical replicates for each treatment and control. Each peptide subgroup was analyzed with ANOVA (Tukey multiple comparisons; **** $p < 0.0001$, ** $p < 0.01$, ns $p > 0.05$). Graphical representations of each assay type are shown in the inserts.

The permeability and uptake assays demonstrate that the cGm6 PDCs **11** and **13** can move through an artificial membrane *via* a passive mechanism, similar to the peptides, so are likely able to move into HT144 cells using a similar mechanism. However, these experiments do not rule out that alternate pathways (*e.g.* endocytosis)

could also contribute to the cell entry of PDCs **11** and **13**, as such pathways have been previously shown to be utilized by cGm analogues.[27] Despite these PDCs having reduced activity compared to cGm6 (Table 2), the data depicted in Figure 2 reveals that the cGm6-based PDCs retained the ability to traverse membranes with the drug cargo attached, highlighting that this is likely not the cause of the decrease in activity.

The minimal permeability of the PDIP and [R/r]cGm6 PDCs (**10, 12**) suggests they do not cross membranes *via* passive transport mechanisms. Since these PDCs were observed intact in HT144 cell extracts (Figure 2B) and had cargo driven activity (Table 2), these PDCs likely rely on alternate cell entry routes such as active transport pathways (*e.g.* endocytosis). While the higher cell-association of PDCs **10** and **12** compared to PDIP and [R/r]cGm6 could also occur because of increased association of the PDCs with the cell membrane, this is not consistent with the complete recovery of these PDCs after the PAMPA assay (Figure 2). To gain a better understanding of PDC transport mechanisms, permeability assays with Caco-2 monolayers could be used to support transport of these PDCs *via* active pathways.[45] Finally, as the HT144 experiments utilized a 1 h timeframe, only rapid cell entry and membrane permeation was detected so may not wholly represent what occurs during the 72 h cytotoxicity assay.

Conclusions

In summary, we produced five synthetically tractable and high yielding PDCs by covalently attaching Vem to three CPPs including PDIP, derived from an innate human defense molecule, cGm6, derived from a spider defense peptide, and [R/r]cGm6, a less potent analogue of cGm6 with maintained cell-penetrating properties. These PDCs selectively killed HT144 melanoma cells compared to noncancer HaCaT cells, all with improved activity relative to Vem as a free drug. Furthermore, PDC **10** remained active against and selective for a melanoma cell line with acquired resistance to Dab, a drug with the same intracellular target as Vem.

The low micromolar activity of the PDCs highlighted that the drug portion of the conjugate was likely able to interact with its target enzyme while tethered to a peptide *via* a non-cleavable DBCO linker. In comparison, analysis of the peptide-DBCO controls revealed that altering the peptide was detrimental for cGm6 and [R/r]cGm6, even though changes were tolerated by PDIP. Despite having similar linkers and the same drug cargo, differences in relative PDC activity highlighted the importance of the peptide for overall PDC potency. PDIP-DBCO-Vem (**10**) was the most potent PDC with activity that was enhanced compared to the parent peptide and drug alone or administration of the peptide and drug as an equimolar cotreatment, highlighting the benefit of utilizing peptides to deliver BRAF-V600E inhibitors to tumor cells.[17,46,47] This PDC was also potent towards Dab-PDRC melanoma cells, providing proof-of-principle that PDIP-based PDCs could be promising candidates for developing treatments against drug-resistant cells or heterogenous tumors containing a mixture of drug-sensitive and drug-resistant melanoma cells.

The two cGm6-based PDCs (**11** and **13**) also had potent activity against HT144 melanoma cells, but the effects of modifying the smaller cGm6 peptide on its activity were more pronounced compared to PDIP. This was further evidenced by the poor activity of these PDCs against the drug-resistant Dab-PDRC cell line. The improved activity of the two [R/r]cGm6-based PDCs (**12** and **14**) relative to the inactive parent peptide indicates that non-disruptive CPPs can be successfully used as carrier peptides,[48,49] but they are less beneficial than active peptides for treating drug-resistant cells. While the [R/r]cGm6-based PDCs likely have cargo driven activity, the activity of the more potent PDIP- and cGm6-based PDCs benefited from contributions from both the drug and peptide.

Membrane permeability and cell internalization assays confirmed that the three CPPs can carry the Vem cargo across membranes. The cGm6-based PDCs (**11** and **13**) maintained the high membrane permeability of their parent peptide, so likely can move passively through membranes. In contrast, the PDIP- and [R/r]cGm6-based PDCs (**10** and **12**) likely require active transport to deliver the Vem drug cargo into the cell. Further exploration into passive versus active transport mechanisms would provide a better understanding of the role that different CPPs play in delivering intact PDCs such that their drug cargoes can access intracellular targets.

Overall, combining Vem with bioactive peptides produced PDCs with improved activity relative to the free drug, validating this strategy as a promising avenue to improving the efficacy of Vem. PDCs that pair drugs with membrane disruptive peptides, which have distinct killing mechanisms to that of most small molecule

chemotherapies,[50] could make it difficult for cancer cells to acquire resistance. Accordingly, further exploration of this promising therapeutic modality with alternative drugs and bioactive peptides is an exciting future direction.

Acknowledgements

This work was supported by funding from the Australian Research Council Centre of Excellence for Innovations in Peptide and Protein Science (CE200100012), the US Department of Defense (PR210354 to D.J.C. and N.L.), the National Health and Medical Research Council (NHMRC) Australia (Leadership Fellowship, GNT2009564 to D.J.C), and the Australian Government Research Training Program PhD Scholarship scheme (I.R.P).

The authors thank Anitha Jeyasingham and Joseph Boileau (ANU) for assistance with mass spectrometry; Dr. Doug Lawes (ANU) for support with NMR spectroscopy; and Dr. Simon de Veer and Alicja Andraszek (UQ) for assistance with peptide synthesis.

Author contributions

I.R.P., N.L. and Y.K. carried out the experimental work in this manuscript. I.R.P., A.M.W., S.T.H, N.L. and L.R.M. conceived of the study, and D.J.C. and L.R.M. provided laboratory resources and infrastructure to support experimental work. I.R.P. wrote the manuscript, which was further edited by L.R.M. and N.L.

Conflicts of Interest

The authors declare no conflict of interest.

References

(1) Arnold, M.; Singh, D.; Laversanne, M.; Vignat, J.; Vaccarella, S.; Meheus, F.; Cust, A. E.; De Vries, E.; Whiteman, D. C.; Bray, F. *JAMA Dermatology* **2022**, *158*, 495–503.

(2) Owsley, J.; Stein, M. K.; Porter, J.; In, G. K.; Salem, M.; O'Day, S.; Elliott, A.; Poorman, K.; Gibney, G.; VanderWalde, A. *Exp. Biol. Med.* **2021**, *246*, 31–39.

(3) Davies, H.; Bignell, G. R.; Cox, C.; Stephens, P.; Edkins, S.; Clegg, S.; Teague, J.; Woffendin, H.; Garnett, M. J.; Bottomley, W.; Davis, N.; Dicks, E.; Ewing, R.; Floyd, Y.; Gray, K.; Hall, S.; Hawes, R.; Hughes, J.; Kosmidou, V.; Menzies, A.; Mould, C.; Parker, A.; Stevens, C.; Watt, S.; Hooper, S.; Jayatilake, H.; Gusterson, B. A.; Cooper, C.; Shipley, J.; Hargrave, D.; Pritchard-Jones, K.; Maitland, N.; Chenevix-Trench, G.; Riggins, G. J.; Bigner, D. D.; Palmieri, G.; Cossu, A.; Flanagan, A.; Nicholson, A.; Ho, J. W. C.; Leung, S. Y.; Yuen, S. T.; Weber, B. L.; Seigler, H. F.; Darrow, T. L.; Paterson, H.; Wooster, R.; Stratton, M. R.; Futreal, P. A. *Nature* **2002**, *417*, 949–954.

(4) Gouda, M. A.; Subbiah, V. *ESMO Open* **2023**, *8*, 100788.

(5) Manzano, J. L.; Layos, L.; Bugés, C.; De los Llanos Gil, M.; Vila, L.; Martínez-Balibrea, E.; Martínez-Cardús, A. *Ann. Transl. Med.* **2016**, *4*, 237.

(6) Poulikakos, P. I.; Rosen, N. *Cancer Cell* **2011**, *19*, 11–15.

(7) Villanueva, J.; Infante, J. R.; Krepler, C.; Reyes-Uribe, P.; Samanta, M.; Chen, H. Y.; Li, B.; Swoboda, R. K.; Wilson, M.; Vultur, A.; Fukunaba-Kalabis, M.; Wubbenhorst, B.; Chen, T. Y.; Liu, Q.; Sproesser, K.; DeMarini, D. J.; Gilmer, T. M.; Martin, A. M.; Marmorstein, R.; Schultz, D. C.; Speicher, D. W.; Karakousis, G. C.; Xu, W.; Amaravadi, R. K.; Xu, X.; Schuchter, L. M.; Herlyn, M.; Nathanson, K. L. *Cell Rep.* **2013**, *4*, 1090–1099.

(8) Al-Lazikani, B.; Banerji, U.; Workman, P. *Nat. Biotechnol.* **2012**, *30*, 679–692.

(9) Grasso, M.; Estrada, M. A.; Ventocilla, C.; Samanta, M.; Maksimoska, J.; Villanueva, J.; Winkler, J. D.; Marmorstein, R. *ACS Chem. Biol.* **2016**, *11*, 2876–2888.

(10) Gunderwala, A. Y.; Nimbvikar, A. A.; Cope, N. J.; Li, Z.; Wang, Z. *ACS Chem. Biol.* **2019**, *14*, 1471–1480.

(11) Han, X. R.; Chen, L.; Wei, Y.; Yu, W.; Chen, Y.; Zhang, C.; Jiao, B.; Shi, T.; Sun, L.; Zhang, C.; Xu, Y.; Lee, M. R.; Luo, Y.; Plewe, M. B.; Wang, J. *J. Med. Chem.* **2020**, *63*, 4069–4080.

(12) Laurenzana, A.; Margheri, F.; Biagioni, A.; Chillà, A.; Pimpinelli, N.; Ruzzolini, J.; Peppicelli, S.; Andreucci, E.; Calorini, L.; Serratì, S.; Del Rosso, M.; Fibbi, G. *EBioMedicine* **2019**, *39*, 194–206.

(13) Kim, T. W.; Kim, Y.; Keum, H.; Jung, W.; Kang, M.; Jon, S. *Mol. Ther. Oncolytics* **2022**, *26*, 1–14.

(14) Guzzetti, C.; Corno, C.; Vergani, E.; Mirra, L.; Ciusani, E.; Rodolfo, M.; Perego, P.; Beretta, G. L. *Front. Oncol.* **2023**, *13*, 1182853.

(15) Li, W.; Zheng, C.; Xu, X.; Xia, Y.; Zhang, K.; Huang, A.; Zhang, X.; Zheng, Y.; Chen, G.; Zhang, S. *Cell. Mol. Biol. Lett.* **2024**, *29*, 50.

(16) Rose, A. A. N.; Annis, M. G.; Frederick, D. T.; Biondini, M.; Dong, Z.; Kwong, L.; Chin, L.; Keler, T.; Hawthorne, T.; Watson, I. R.; Flaherty, K. T.; Siegel, P. M. *Clin. Cancer Res.* **2016**, *22*, 6088–6098.

(17) Zou, L.; Ding, W.; Zhang, Y.; Cheng, S.; Li, F.; Ruan, R.; Wei, P.; Qiu, B. *Biomaterials* **2018**, *182*, 1–12.

(18) Zhang, Y.; Wang, C.; Zhang, W.; Li, X. *Biomater. Transl.* **2023**, *4*, 5–17.

(19) Vallabhapurapu, S. D.; Blanco, V. M.; Sulaiman, M. K.; Vallabhapurapu, S. L.; Chu, Z.; Franco, R. S.; Qi, X. *Oncotarget* **2015**, *6*, 34375–34388.

(20) Lawrence, N.; Dennis, A. S.; Lehane, A. M.; Ehmann, A.; Harvey, P. J.; Benfield, A. H.; Cheneval, O.; Henriques, S. T.; Craik, D. J.; McMorran, B. J. *Cell Chem. Biol.* **2018**, *25*, 1140–1150.

(21) Henriques, S. T.; Lawrence, N.; Chaousis, S.; Ravipati, A. S.; Cheneval, O.; Benfield, A. H.; Elliott, A. G.; Kavanagh, A. M.; Cooper, M. A.; Chan, L. Y.; Huang, Y. H.; Craik, D. J. *ACS Chem. Biol.* **2017**, *12*, 2324–2334.

(22) Silva, P. I.; Daffre, S.; Bulet, P. *J. Biol. Chem.* **2000**, *275*, 33464–33470.

(23) Chan, L. Y.; Zhang, V. M.; Huang, Y. H.; Waters, N. C.; Bansal, P. S.; Craik, D. J.; Daly, N. L. *ChemBioChem* **2013**, *14*, 617–624.

(24) Lawrence, N.; Philippe, G.; Harvey, P. J.; Condon, N. D.; Benfield, A. H.; Cheneval, O.; Craik, D. J.; Henriques, S. T. *RSC Chem. Biol.* **2020**, *1*, 405–420.

(25) Benfield, A. H.; Vernen, F.; Young, R. S. E.; Nadal-Bufí, F.; Lamb, H.; Hammerlindl, H.; Craik, D. J.; Schaider, H.; Lawrence, N.; Blanksby, S. J.; Henriques, S. T. *Pharmacol. Res.* **2024**, *207*, 107298.

(26) Palombi, I. R.; Lawrence, N.; White, A. M.; Gare, C. L.; Craik, D. J.; McMorran, B. J.; Malins, L. R. *Bioconjug. Chem.* **2023**, *34*, 1105–1113.

(27) Benfield, A. H.; Defaus, S.; Lawrence, N.; Chaousis, S.; Condon, N.; Cheneval, O.; Huang, Y. H.; Chan, L. Y.; Andreu, D.; Craik, D. J.; Henriques, S. T. *Biochim. Biophys. Acta Biomembr.* **2021**, *1863*, 183480.

(28) Gala, U. H.; Miller, D. A.; Williams, R. O. *Biochim. Biophys. Acta Rev. Cancer* **2020**, *1873*, 188319.

(29) Agard, N. J.; Prescher, J. A.; Bertozzi, C. R. *J. Am. Chem. Soc.* **2004**, *126*, 15046–15047.

(30) Dawson, P. E.; Muir, T. W.; Clark-Lewis, I.; Kent, S. B. H. *Science* **1994**, *266*, 776–779.

(31) Bollag, G.; Hirth, P.; Tsai, J.; Zhang, J.; Ibrahim, P. N.; Cho, H.; Spevak, W.; Zhang, C.; Zhang, Y.; Habets, G.; Burton, E. A.; Wong, B.; Tsang, G.; West, B. L.; Powell, B.; Shellooe, R.; Marimuthu, A.; Nguyen, H.; Zhang, K. Y. J.; Artis, D. R.; Schlessinger, J.; Su, F.; Higgins, B.; Iyer, R.; Dandrea, K.; Koehler, A.; Stumm, M.; Lin, P. S.; Lee, R. J.; Grippo, J.; Puzanov, I.; Kim, K. B.; Ribas, A.; McArthur, G. A.; Sosman, J. A.; Chapman, P. B.; Flaherty, K. T.; Xu, X.; Nathanson, K. L.; Nolop, K. *Nature* **2010**, *467*, 596–599.

(32) Mikula, H.; Stapleton, S.; Kohler, R. H.; Vinegoni, C.; Weissleder, R. *Theranostics* **2017**, *7*, 1257–1265.

(33) Presolski, S. I.; Hong, V. P.; Finn, M. G. *Curr. Protoc. Chem. Biol.* **2011**, *3*, 153–162.

(34) Sayers, J.; Thompson, R. E.; Perry, K. J.; Malins, L. R.; Payne, R. J. *Org. Lett.* **2015**, *17*, 4902–4905.

(35) Hung, K. Y.; Harris, P. W. R.; Brimble, M. A. *Synlett* **2009**, *2009*, 1233–1236.

(36) Pattabiraman, V. R.; Bode, J. W. *Nature* **2011**, *480*, 471–479.

(37) Zhong, L.; Li, Y.; Xiong, L.; Wang, W.; Wu, M.; Yuan, T.; Yang, W.; Tian, C.; Miao, Z.; Wang, T.; Yang, S. *Signal Transduct. Target. Ther.* **2021**, *6*, 201.

(38) Das, B.; Baidya, A. T. K.; Mathew, A. T.; Yadav, A. K.; Kumar, R. *Bioorg. Med. Chem.* **2022**, *56*, 116614.

(39) Palombi, I. R.; White, A. M.; Koda, Y.; Craik, D. J.; Lawrence, N.; Malins, L. R. *Chem. Biol. Drug Des.* **2025**, *105*, e70051.

(40) Chen, N.; Jiang, C. *Eur. J. Med. Chem.* **2023**, *255*, 115377.

(41) Edwards, I. A.; Elliott, A. G.; Kavanagh, A. M.; Zuegg, J.; Blaskovich, M. A. T.; Cooper, M. A. *ACS Infect. Dis.* **2016**, *2*, 442–450.

(42) Matthyssen, T.; Li, W.; Holden, J. A.; Lenzo, J. C.; Hadjigol, S.; O'Brien-Simpson, N. M. *Front. Chem.* **2022**, *9*, 795433.

(43) Edupuganti, V. V. S. R.; Tyndall, J. D. A.; Gamble, A. B. *Recent Pat. Anticancer. Drug Discov.* **2021**, *16*, 479–497.

(44) Fu, C.; Yu, L.; Miao, Y.; Liu, X.; Yu, Z.; Wei, M. *Acta Pharm. Sin. B* **2023**, *13*, 498–516.

(45) Sevin, E.; Dehouck, L.; Fabulas-da Costa, A.; Cecchelli, R.; Dehouck, M. P.; Lundquist, S.; Culot, M. *J. Pharmacol. Toxicol. Methods* **2013**, *68*, 334–339.

(46) Aasen, S. N.; Espedal, H.; Holte, C. F.; Keunen, O.; Karlsen, T. V.; Tenstad, O.; Maherally, Z.; Miletic, H.; Hoang, T.; Eikeland, A. V.; Baghirov, H.; Olberg, D. E.; Pilkington, G. J.; Sarkar, G.; Jenkins, R. B.; Sundstrøm, T.; Bjerkvig, R.; Thorsen, F. *Mol. Cancer Ther.* **2019**, *18*, 2171–2181.

(47) Chen, P.; Cai, X.; Mu, G.; Duan, Y.; Jing, C.; Yang, Z.; Yang, C.; Wang, X. *Theranostics* **2023**, *13*, 2140–2153.

(48) Madani, F.; Lindberg, S.; Langel, Ü.; Futaki, S.; Gräslund, A. *J. Biophys.* **2011**, *2011*, 414729.

(49) Gong, L.; Zhao, H.; Liu, Y.; Wu, H.; Liu, C.; Chang, S.; Chen, L.; Jin, M.; Wang, Q.; Gao, Z.; Huang, W. *Acta Pharm. Sin. B* **2023**, *13*, 3659–3677.

(50) Tornesello, A. L.; Borrelli, A.; Buonaguro, L.; Buonaguro, F. M.; Tornesello, M. L. *Molecules* **2020**, *25*, 2850.

Concluding Remarks

The study presented in this chapter illustrates that PDCs which combine anticancer peptides and Vem are a promising approach to reinvigorating Vem for melanoma treatment. The exploration of five Vem-containing PDCs—which had improved activity against a drug-sensitive cell line relative to the free drug—highlighted that the drug cargo remained active without the requirement of a cleavable linker, in contrast to the PDCs described in Chapters 2 and 3. However, the PDCs were substantially less potent than the modified Vem analogue (Vem-NH_2) that was used in the PDC design, accentuating that the amine could have an important role in the enhanced activity of this analogue or that binding affinity to its enzyme target is reduced with the attached peptide. Incorporation of cleavable linkers (see Section 1.2.3) into the PDC design is therefore an essential avenue for future work to understand if PDC activity can match or exceed the potency of Vem-NH_2.

The peptide carrier also had an important contribution to PDC potency. While PDIP remained active and selective when incorporated into a PDC, the cGm6 and [R/r]cGm6 peptides did not tolerate alterations to their structure. The favourable activity of the PDIP-based PDC against a Dab-resistant melanoma cell line emphasises PDCs as a valuable strategy for improving the efficacy of Vem, alongside other approaches that pair Vem with a peptide for the treatment of drug-resistant cells.[10–12] Furthermore, it showcases the ability of PDIP to be used as both a tool for selective drug delivery (*e.g.* Chapter 2) or as an anticancer partner to a drug in a dual-acting treatment (this Chapter).

While the same benefits were not observed for the cGm6-based PDCs, we are optimistic that future optimisation of the design of these PDCs could retain the potent activity of the cGm6 peptide within the PDC. The reduced activity of the cGm6-linker control and cGm6-based PDCs compared to the peptide indicate the requirement for conjugation and linker strategies that minimise hydrophobicity. Therefore, conjugation approaches that do not require the hydrophobic DBCO linker moiety should be prioritised. For example, conjugation *via* an amide bond could instead be utilised by coupling a modified drug-linker construct containing an activated acyl group (**4.5**) directly onto the lysine side chain of cGm6 to form PDC **4.6** (Figure 4.4).

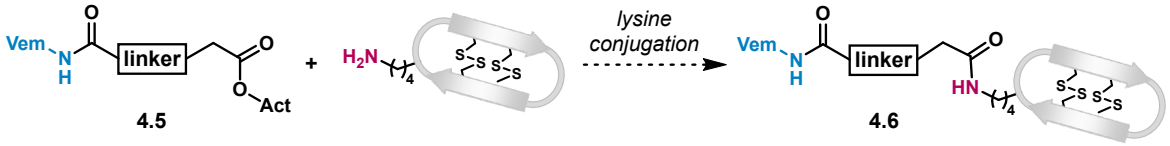

Figure 4.4. Proposed alternative conjugation strategy to minimise added hydrophobicity to the peptide, involving amide bond formation with the lysine side chain of cGm6. An example of an activating acyl group for **4.5** is an *N*-hydroxysuccinimide ester.

Going forward, it is vital to understand whether the PDC modality is an optimal format for Vem combination therapy, especially for the cGm6-based PDCs. While cotreatment with an

unconjugated mixture of peptide and Vem is operationally simpler, in our study we saw the benefit of tethering Vem to a peptide carrier through improved water solubility and cell entry compared to Vem or Vem-NH_2. However, the true utility of Vem-containing PDCs will be realised if it is more difficult for melanoma cells to acquire resistance to Vem as a PDC cargo, in comparison to as a free drug or as an unconjugated cotreatment with the peptide. As such, future work should examine the effects of the long-term treatment of melanoma cells with Vem-containing PDCs, which can be achieved using a similar experimental procedure to that displayed in Figure 4.3.[15,16] Here, the peptide may serve to prevent the development of Vem-resistant cells by eliminating the drug-tolerant persisters that are not able to be killed by the drug cargo. Studies conducted by Henriques and co-workers[15] have exemplified that a similar membrane-active anticancer peptide, also developed from a host defence peptide (tachyplesin I),[17] is able to kill drug-tolerant persister cells. Furthermore, melanoma cell lines did not develop resistance to this peptide, despite continuous exposure during growth, providing insight that the distinct killing mechanism provided by membrane-active peptides could help to prevent resistance development against Vem-containing PDCs.

Altogether, pairing Vem with bioactive cell-penetrating peptides provided PDCs with low micromolar activity against drug-sensitive melanoma cells. However, only the PDIP-based PDC was effective at killing cells with acquired resistance to Dab, a drug with the same intracellular target as Vem. The future experiments outlined in this section aim to optimise PDC potency, especially for the cGm6-based PDCs, so the benefits of coupling Vem with an anticancer peptide can be realised. Overall, the Vem-containing PDCs explored within this chapter are showcased as an alternative strategy to improve the efficacy of Vem and the promising outcomes warrant the continued exploration of these PDCs as combination therapies for melanoma treatment.

References

(1) Vasan, N.; Baselga, J.; Hyman, D. M. *Nature* **2019**, *575*, 299–309.

(2) Mokhtari, R. B.; Homayouni, T. S.; Baluch, N.; Morgatskaya, E.; Kumar, S.; Das, B.; Yeger, H. *Oncotarget* **2017**, *8*, 38022–38043.

(3) Robertson, B. M.; Fane, M. E.; Weeraratna, A. T.; Rebecca, V. W. *Nat. Cancer* **2024**, *5*, 964–982.

(4) Davies, H.; Bignell, G. R.; Cox, C.; Stephens, P.; Edkins, S.; Clegg, S.; Teague, J.; Woffendin, H.; Garnett, M. J.; Bottomley, W.; Davis, N.; Dicks, E.; Ewing, R.; Floyd, Y.; Gray, K.; Hall, S.; Hawes, R.; Hughes, J.; Kosmidou, V.; Menzies, A.; Mould, C.; Parker, A.; Stevens, C.; Watt, S.; Hooper, S.; Jayatilake, H.; Gusterson, B. A.; Cooper, C.; Shipley, J.; Hargrave, D.; Pritchard-Jones, K.; Maitland, N.; Chenevix-Trench, G.; Riggins, G. J.; Bigner, D. D.; Palmieri, G.; Cossu, A.; Flanagan, A.; Nicholson, A.; Ho, J. W. C.; Leung, S. Y.; Yuen, S. T.; Weber, B. L.; Seigler, H. F.; Darrow, T. L.; Paterson, H.; Wooster, R.; Stratton, M. R.; Futreal, P. A. *Nature* **2002**, *417*, 949–954.

(5) Owsley, J.; Stein, M. K.; Porter, J.; In, G. K.; Salem, M.; O'Day, S.; Elliott, A.; Poorman, K.; Gibney, G.; VanderWalde, A. *Exp. Biol. Med.* **2021**, *246*, 31–39.

(6) Gouda, M. A.; Subbiah, V. *ESMO Open* **2023**, *8*, 100788.

(7) Manzano, J. L.; Layos, L.; Bugés, C.; De los Llanos Gil, M.; Vila, L.; Martínez-Balibrea, E.; Martínez-Cardús, A. *Ann. Transl. Med.* **2016**, *4*, 237.

(8) Villanueva, J.; Infante, J. R.; Krepler, C.; Reyes-Uribe, P.; Samanta, M.; Chen, H. Y.; Li, B.; Swoboda, R. K.; Wilson, M.; Vultur, A.; Fukunaba-Kalabis, M.; Wubbenhorst, B.; Chen, T. Y.; Liu, Q.; Sproesser, K.; DeMarini, D. J.; Gilmer, T. M.; Martin, A. M.; Marmorstein, R.; Schultz, D. C.; Speicher, D. W.; Karakousis, G. C.; Xu, W.; Amaravadi, R. K.; Xu, X.; Schuchter, L. M.; Herlyn, M.; Nathanson, K. L. *Cell Rep.* **2013**, *4*, 1090–1099.

(9) Zou, L.; Ding, W.; Zhang, Y.; Cheng, S.; Li, F.; Ruan, R.; Wei, P.; Qiu, B. *Biomaterials* **2018**, *182*, 1–12.

(10) Laurenzana, A.; Margheri, F.; Biagioni, A.; Chillà, A.; Pimpinelli, N.; Ruzzolini, J.; Peppicelli, S.; Andreucci, E.; Calorini, L.; Serratì, S.; Del Rosso, M.; Fibbi, G. *EBioMedicine* **2019**, *39*, 194–206.

(11) Kim, T. W.; Kim, Y.; Keum, H.; Jung, W.; Kang, M.; Jon, S. *Mol. Ther. Oncolytics* **2022**, *26*, 1–14.

(12) Guzzetti, C.; Corno, C.; Vergani, E.; Mirra, L.; Ciusani, E.; Rodolfo, M.; Perego, P.; Beretta, G. L. *Front. Oncol.* **2023**, *13*, 1182853.

(13) Bollag, G.; Tsai, J.; Zhang, J.; Zhang, C.; Ibrahim, P.; Nolop, K.; Hirth, P. *Nat. Rev. Drug Discov.* **2012**, *11*, 873–886.

(14) Han, X. R.; Chen, L.; Wei, Y.; Yu, W.; Chen, Y.; Zhang, C.; Jiao, B.; Shi, T.; Sun, L.; Zhang, C.; Xu, Y.; Lee, M. R.; Luo, Y.; Plewe, M. B.; Wang, J. *J. Med. Chem.* **2020**, *63*, 4069–4080.

(15) Benfield, A. H.; Vernen, F.; Young, R. S. E.; Nadal-Bufí, F.; Lamb, H.; Hammerlindl, H.; Craik, D. J.; Schaider, H.; Lawrence, N.; Blanksby, S. J.; Henriques, S. T. *Pharmacol. Res.* **2024**, *207*, 107298.

(16) Ravindran Menon, D.; Das, S.; Krepler, C.; Vultur, A.; Rinner, B.; Schauer, S.; Kashofer, K.; Wagner, K.; Zhang, G.; Bonyadi Rad, E.; Haass, N. K.; Soyer, H. P.; Gabrielli, B.; Somasundaram, R.; Hoefler, G.; Herlyn, M.; Schaider, H. *Oncogene* **2015**, *34*, 4448–4459.

(17) Vernen, F.; Harvey, P. J.; Dias, S. A.; Veiga, A. S.; Huang, Y. H.; Craik, D. J.; Lawrence, N.; Henriques, S. T. *Int. J. Mol. Sci.* **2019**, *20*, 4184.

Chapter 5:

Conclusions and outlook

Conclusions

The three manuscripts presented in this thesis showcase PDCs containing bioactive cell-penetrating peptides (CPPs)—including PDIP and cGm6—for use as targeted treatments in two different disease contexts, malaria and cancer. To demonstrate the utility of a PDC approach comprising our bioactive peptides, three drugs—primaquine (PQ), camptothecin (CPT) and vemurafenib (Vem)—each with toxicity or resistance issues, were explored as the PDC cargo. Small libraries of PDCs with varying linkers, conjugation strategies and peptide scaffolds were produced with each drug cargo, to understand how certain design features influenced PDC potency.

Chapter Two explored whether PQ, an antimalarial drug with limited widespread use due to off-target toxicity in some individuals, could be successfully conjugated onto an antiplasmodial peptide. Six PDIP-PQ PDCs were synthesised, comprising three linker types (non-cleavable, Fe(II)-sensitive and reducible disulfide) and two PDIP analogues with different conjugation positions on the peptide (Figure 5.1).[1] Analysis of PDC activity against *Plasmodium* parasites in the asexual blood stages revealed PDCs with low micromolar and cargo-driven potency, that required the incorporation of a cleavable linker and a PDIP analogue with an internal conjugation site in the PDC design for optimal activity (gold boxes, Figure 5.1). Furthermore, follow-up studies highlighted the important contribution of the antiplasmodial peptide (PDIP) to overall PDC activity, validating the use of PDCs with a dual mechanism of bioactivity.[2]

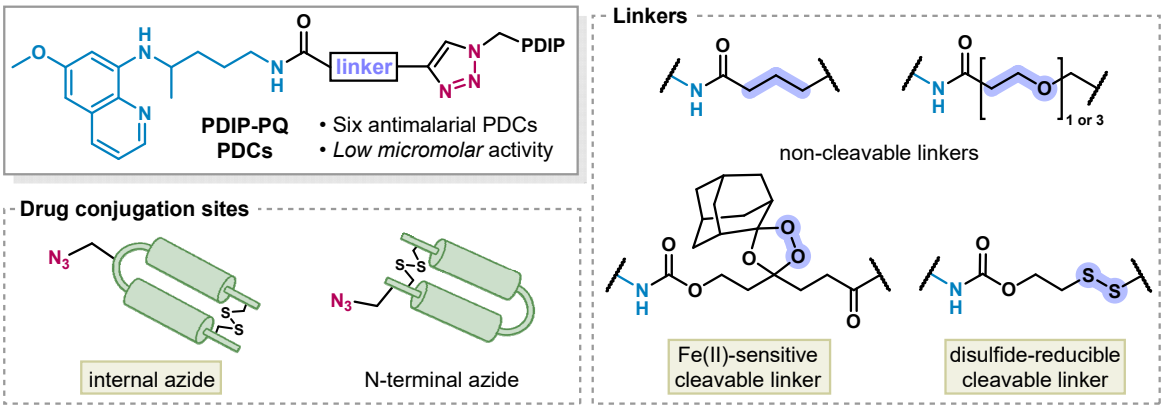

Figure 5.1. In Chapter 2, six PDIP-PQ PDCs were synthesised and biologically evaluated against blood stage *Plasmodium* parasites. The design features modified are displayed in the dotted grey boxes and those that provided optimal PDC potency are indicated with a gold box.

Although this proof-of-concept study did not result in PDCs with enhanced activity relative to PQ, the prospect of improved safety profiles in G6PD deficient individuals warrants future exploration into their selectivity. Additional studies into the role of the peptide in PDC activity and whether these PDCs are potent against other parasite stages are required to cement these treatments as feasible alternatives to traditional antimalarial therapies.

Chapter Three investigated whether the safety of CPT, a non-selective chemotherapy drug, could be improved by conjugation to a peptide carrier, PDIP. Based on the design–activity

knowledge gained from the previous chapter, four PDIP-CPT PDCs were synthesised, comprising three linker types (non-cleavable, reducible disulfide and cathepsin B-sensitive dipeptide) and two PDIP analogues with different conjugation handles (Figure 5.2).[3] Evaluation of PDC bioactivity against a melanoma cell line revealed cargo-driven potency in the nanomolar to low micromolar range, with a cleavable linker essential in the PDC design for maximal potency (gold boxes, Figure 5.2). Membrane permeability and cell internalisation studies revealed that intact PDCs could passively cross membranes and highlighted that the disulfide-cyclised PDIP analogue (gold box, Figure 5.2) was a superior carrier peptide relative to the backbone cyclic PDIP analogue.

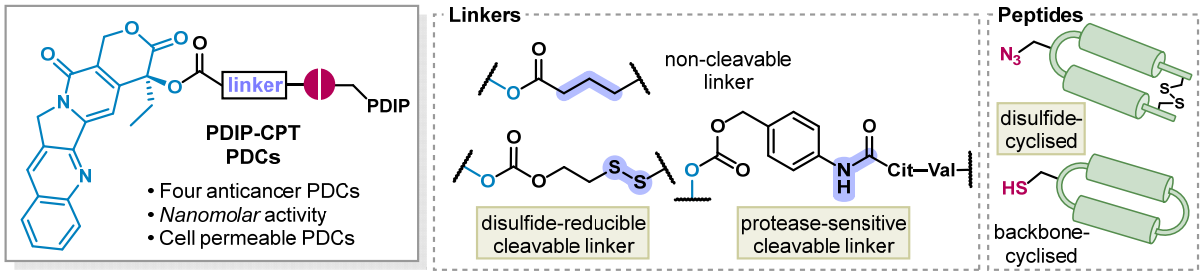

Figure 5.2. In Chapter 3, four PDIP-CPT PDCs were synthesised and biologically evaluated against a melanoma cell line. The design features modified are displayed in the dotted grey boxes and those that provided optimal PDC potency and function are indicated with a gold box.

The loss of selectivity of these PDCs for melanoma cells compared to the parent PDIP peptide needs to be addressed in the design of ensuing generations of PDIP-CPT PDCs. Future PDCs should explore alternative linkers and conjugation strategies that minimise additional hydrophobicity appended onto the peptide to maintain the crucial amphipathic properties of the peptide carrier. The insight obtained into PDC design in this chapter reinforced how it is crucial to match a drug cargo with an appropriate carrier peptide and linker type.

Chapter Four examined whether Vem, an antimelanoma drug with solubility and acquired resistance issues, would benefit from conjugation to peptides with distinct anticancer mechanisms. Five non-cleavable Vem-containing PDCs were synthesised with three different CPP carriers, two with anticancer activity (PDIP and cGm6) and one with poor anticancer activity ([R/r]cGm6) (Figure 5.3). Evaluation of PDC activity against a drug-sensitive melanoma cell line highlighted that the PDCs had low micromolar activity that was enhanced relative to Vem treatment alone. Furthermore, PDIP (gold box, Figure 5.3) was identified as the optimal peptide partner as the PDIP-based PDC was the most potent and was also able to kill melanoma cells that had acquired resistance to dabrafenib, a drug with the same enzyme target as Vem. Membrane permeability and cell internalisation studies validated that the peptides could carry the Vem cargo across membranes, however, the PDCs appeared to utilise different modes of cell entry (*e.g.* active versus passive entry).

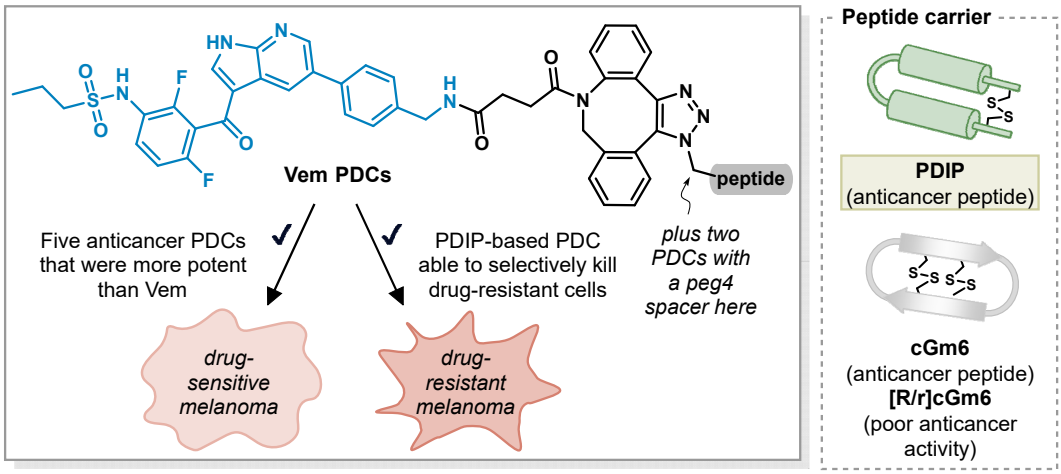

Figure 5.3. In Chapter 4, five Vem-containing PDCs were synthesised and biologically evaluated against dabrafenib-sensitive and resistant melanoma cell lines. The three peptide carriers utilised are displayed in the dotted grey box and the optimal scaffold is indicated with a gold box.

The use of dual-acting PDCs was illustrated as a promising alternative for the treatment of resistant melanoma cells, however, future optimisation of PDCs containing the cGm6 peptide is required for the same benefits to be observed as PDCs containing the PDIP peptide. Further exploration into whether melanoma cells can acquire resistance to these PDCs is essential to determine if a PDC modality is optimal for combination therapy compared to the coadministration of a drug and peptide.

Overall, the three projects presented in this thesis emphasise the importance of design to produce PDCs with potent bioactivity. Regardless of the disease context, design optimisation was imperative to maintain the function and properties of the drug cargo and peptide carrier, to ensure that each component could successfully undertake its mechanism of action while conjugated together. The conjugation site on the drug/peptide and linker type needed to be considered consistently throughout the three projects. Ultimately, optimal design was found to be unique for each drug and peptide combination, demonstrating the importance of PDC structure optimisation.

Outlook

Targeted therapeutics such as PDCs continue to serve as valuable alternatives to traditional small molecule treatments. Throughout this thesis, three drugs were incorporated into a PDC modality to integrate the benefits of selectivity and a distinct killing mechanism provided by bioactive CPPs that are derived from host defence molecules. The PDIP and cGm6 peptides studied were found to be useful peptide partners to the drugs in most contexts, however, modifications to their overall structure and physiochemical properties—factors that are important for the correct function and activity of bioactive CPPs—had a detrimental effect in some circumstances.[4] Therefore, investigation into how the structure and membrane selectivity of the peptides is altered following drug conjugation is vital to understand how to

prevent this in the design of future generations of PDIP- and cGm6-based PDCs. For example, structural information could be acquired with circular dichroism and may provide understanding about how peptide secondary structure changes with an attached linker and drug.[5] Membrane selectivity insights could be obtained by examining the binding affinity of the PDCs to different lipid bilayer models, representative of either diseased or healthy cells, and comparing this to the affinity of the parent peptides.[6]

With the proof-of-principle studies presented in this thesis highlighting the ability to synthesise PDIP- and cGm6-based PDCs that have potent activity, we next aim to understand what happens to these PDCs during treatment, to gain insight into their mechanism of action. The preliminary mechanistic studies regarding membrane permeability and cell entry that have already been explored can be expanded to further investigate the role of the peptide in PDC activity. For example, assessing the membrane-disruptive activity of the PDCs could indicate the contribution of the peptide to PDC activity.[7] Fluorescent imaging would also be a useful tool to understand PDC localisation inside cells and can be used to further probe linker cleavage in a biological context.[8]

Future analysis of the *in vivo* activity of the PDIP- and cGm6-based PDCs will be important to determine their feasibility as treatments. It is possible that the stability of PDCs during circulation will be a challenge, as seen with many therapeutic peptides, meaning PDC stability should be explored prior to *in vivo* testing.[9] If stability is not optimal, future generations of PDCs could employ known methods of improving peptide stability, such as peptide lipidation. Lipidation is often used to prevent the clearance of peptide drugs during circulation by promoting the binding of albumin and thereby restricting the access of proteases to the peptide.[10] Additional strategies regarding the improvement of these PDCs for feasible therapeutic application, including efforts towards affordable production for use as malaria treatments, were discussed in Chapter 2.

Ultimately, the promising outcomes of the PDCs disclosed in this thesis and the multiple avenues for future PDC optimisation highlight the capability of PDIP and cGm6 to be effective peptide partners to selected small molecule drugs. Through the exploration of PDCs containing these peptide scaffolds in both malaria and cancer contexts, they are showcased as versatile tools for both targeted treatments and dual-acting therapies. Furthermore, the utility of the PDIP and cGm6 peptides in multiple disease contexts prompts the future exploration of PDCs containing these peptides in alternate treatment scenarios, such as bacterial and viral infections.[11] Given that design optimisation is vital for potent PDCs, we hope that the collective insights from these studies will serve to accelerate the future development and synthesis of PDCs containing bioactive cell-penetrating peptides.

References

(1) Palombi, I. R.; Lawrence, N.; White, A. M.; Gare, C. L.; Craik, D. J.; McMorran, B. J.; Malins, L. R. *Bioconjug. Chem.* **2023**, *34*, 1105–1113.

(2) Gare, C. L.; Palombi, I. R.; White, A. M.; Chavchich, M.; Edstein, M. D.; Lock, A. A.; Avery, V. M.; Craik, D. J.; McMorran, B. J.; Lawrence, N.; Malins, L. R. *ChemMedChem* **2025**, *20*, e202400637.

(3) Palombi, I. R.; White, A. M.; Koda, Y.; Craik, D. J.; Lawrence, N.; Malins, L. R. *Chem. Biol. Drug Des.* **2025**, *105*, e70051.

(4) Matthyssen, T.; Li, W.; Holden, J. A.; Lenzo, J. C.; Hadjigol, S.; O'Brien-Simpson, N. M. *Front. Chem.* **2022**, *9*, 795433.

(5) Lawrence, N.; Handley, T. N. G.; de Veer, S. J.; Harding, M. D.; Andraszek, A.; Hall, L.; Raven, K. D.; Duffy, S.; Avery, V. M.; Craik, D. J.; Malins, L. R.; McMorran, B. J. *ACS Infect. Dis.* **2024**, *10*, 2899–2912.

(6) Henriques, S. T.; Pattenden, L. K.; Aguilar, M. I.; Castanho, M. A. R. B. *Biophys. J.* **2008**, *95*, 1877–1889.

(7) Huang, Y. H.; Colgrave, M. L.; Daly, N. L.; Keleshian, A.; Martinac, B.; Craik, D. J. *J. Biol. Chem.* **2009**, *284*, 20699–20707.

(8) Lee, B.-C.; Chalouni, C.; Doll, S.; Nalle, S. C.; Darwish, M.; Tsai, S. P.; Kozak, K. R.; Del-Rosario, G.; Yu, S. F.; Erickson, H.; Vandlen, R. *Bioconjug. Chem.* **2018**, *29*, 2468–2477.

(9) Wang, M.; Liu, J.; Xia, M.; Yin, L.; Zhang, L.; Liu, X.; Cheng, Y. *Eur. J. Med. Chem.* **2024**, *265*, 116119.

(10) Menacho-Melgar, R.; Decker, J. S.; Hennigan, J. N.; Lynch, M. D. *J. Control. Release* **2019**, *295*, 1–12.

(11) Dean, T. T.; Jelú-Reyes, J.; Allen, A. C.; Moore, T. W. *J. Med. Chem.* **2024**, *67*, 1641–1661.

Supporting Information for Chapter 2:

Primaquine PDCs

Supporting Information

Development of Antiplasmodial Peptide–Drug Conjugates Using a Human Protein Derived Cell-Penetrating Peptide with Selectivity for Infected Cells

Isabella R. Palombi,[1,2] Nicole Lawrence,[3,4] Andrew M. White,[1,2] Caitlin, L. Gare,[1,2] David J. Craik,[3,4] Brendan J. McMorran,*[,5] Lara R. Malins*[,1,2]

[1]Research School of Chemistry, Australian National University, Canberra, ACT 2601, Australia

[2]Australian Research Council Centre of Excellence for Innovations in Peptide and Protein Science, Australian National University, Canberra, ACT 2601, Australia

[3]Institute for Molecular Bioscience, The University of Queensland, Brisbane, QLD 4072, Australia

[4]Australian Research Council Centre of Excellence for Innovations in Peptide and Protein Science, The University of Queensland, Brisbane, QLD 4072, Australia

[5]The John Curtin School of Medical Research, Australian National University, Canberra, ACT 2601, Australia

*Email: lara.malins@anu.edu.au, brendan.mcmorran@anu.edu.au

Table of Contents

Supplementary Figures

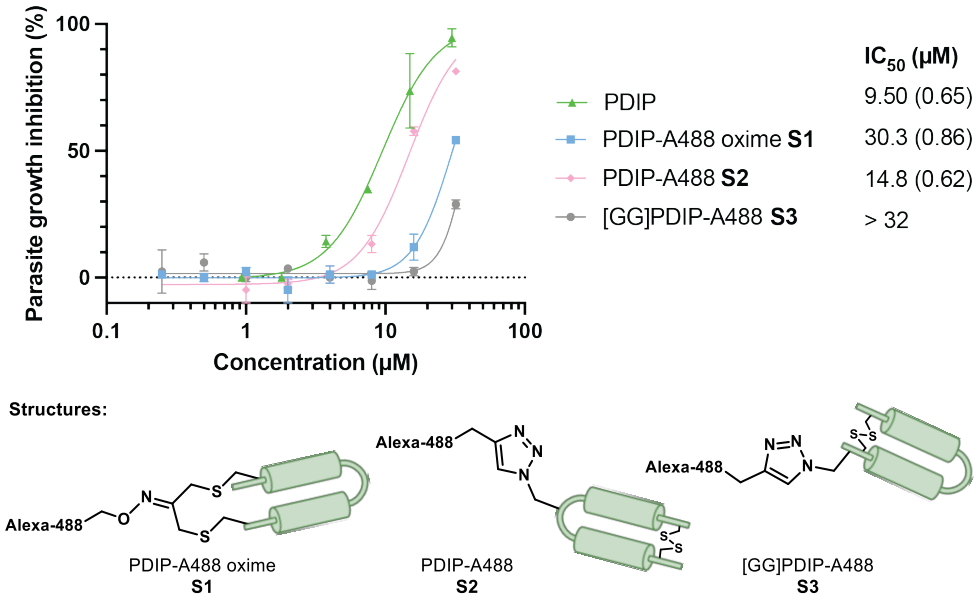

Figure S1. *In vitro* inhibition of *P. falciparum* growth in human RBCs by increasing concentrations of Alexa Fluor 488 (A488) PDCs comprising different conjugation strategies, compared to the parent PDIP peptide. Data points are expressed as mean ± SD for at least two biological replicates. IC_{50} values are given as mean (SEM). Note: PDIP-A488 oxime (**S1**) contains Alexa Fluor 488 conjugated to PDIP *via* an oxime ligation to an acetone linkage between the two cysteines, see prior work for further peptide and synthesis details (PDIP was formerly known as cPF4DP).[1]

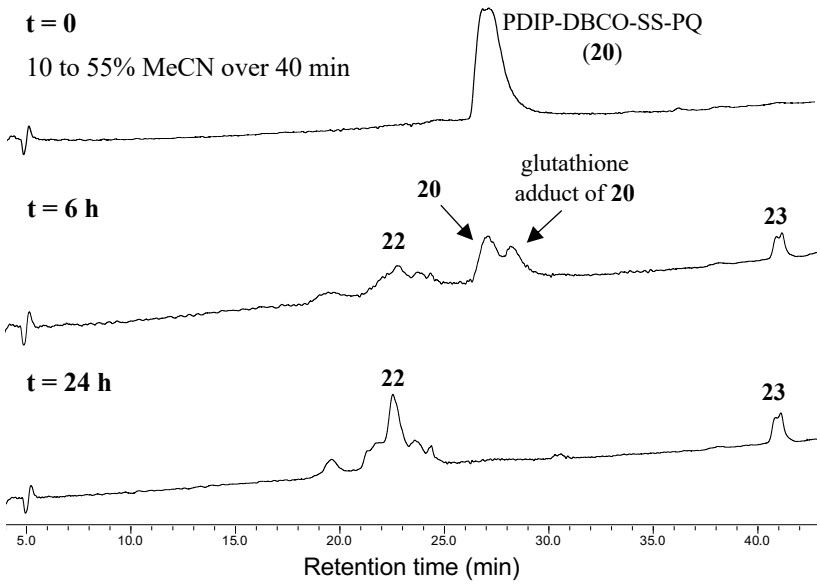

Figure S2. Consumption of PDIP-DBCO-SS-PQ (**20**) over 24 hours by disulfide reduction. Fragmentation of the PDC was monitored using analytical reverse-phase LCMS (10 to 55% MeCN over 40 min, λ = 214 nm). Glutathione adduct **22** (see Figure 3A for structure) was observed to form within 6 hours followed by depletion of all starting PDC by 24 hours. Free primaquine (PQ) was not observed under these conditions, however, thiol modified primaquine **23** was observed within 6 hours. The glutathione adduct of PDC **20** is thought to be formed by reaction of glutathione with the disulfide of PDIP, leaving the disulfide linker intact. In cases where both **20** and the glutathione adduct of **20** were present, both peaks were accounted for in the integration of the PDC, as presented in Figure 3B.

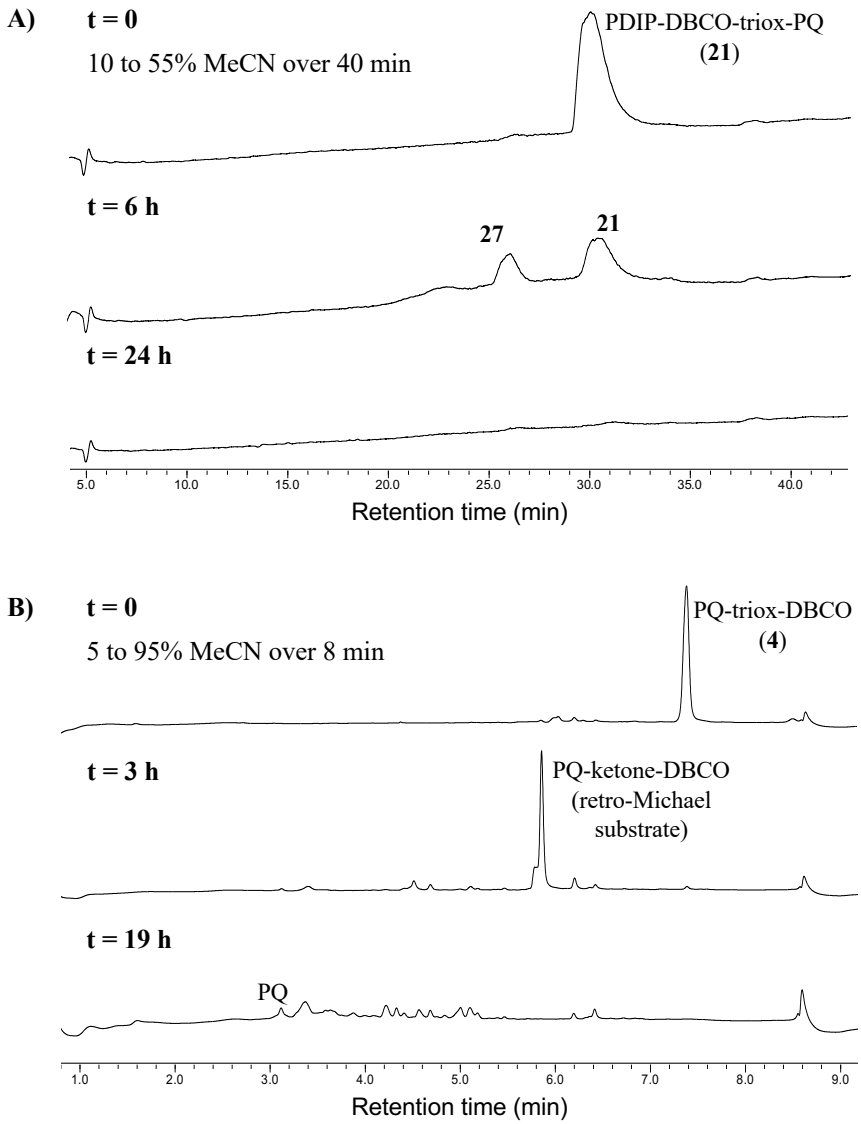

Figure S3. A) Consumption of PDIP-DBCO-triox-PQ (**21**) over 24 hours by treatment with $FeCl_2$. Fragmentation of the PDC was monitored using analytical reverse-phase LCMS (10 to 55% MeCN over 40 min, $\lambda = 214$ nm). Ketone intermediate **27** (see Figure 3A for structure) was observed to form within 6 hours followed by depletion of all starting PDC and intermediates by 24 hours. Free primaquine was not observed under these conditions. B) Consumption of linker PQ-triox-DBCO (**4**) over 19 hours by treatment with $FeCl_2$. Fragmentation of the drug-linker construct was monitored using analytical reverse-phase LCMS (5 to 95% MeCN over 8 min, $\lambda = 214$ nm). After 3 hours, **4** had converted into the corresponding retro-Michael substrate (analogous to ketone intermediate **27**). Primaquine (PQ) was only observed as a small peak at 19 hours, at which point the starting drug-linker construct and all other intermediates had been consumed.

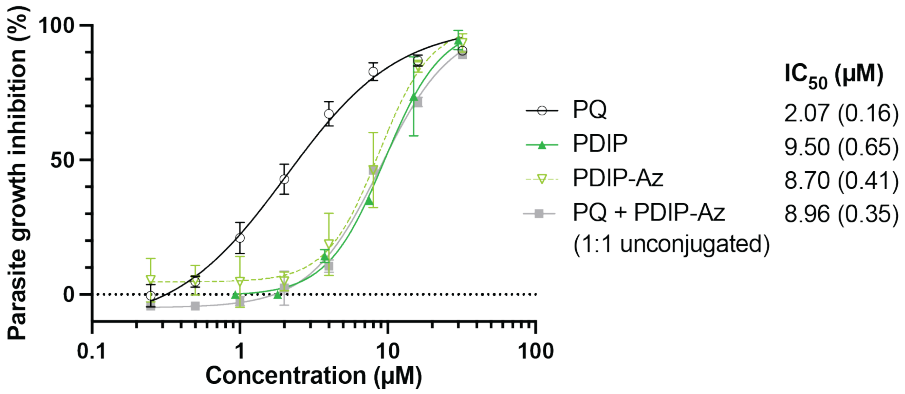

Figure S4. *In vitro* inhibition of *P. falciparum* growth in human RBCs by increasing concentrations of an equimolar mixture of unconjugated PQ and PDIP-Az, compared to PQ, PDIP and PDIP-Az **1**. Data points are expressed as mean ± SD for at least two biological replicates. IC_{50} values are given as mean (SEM).

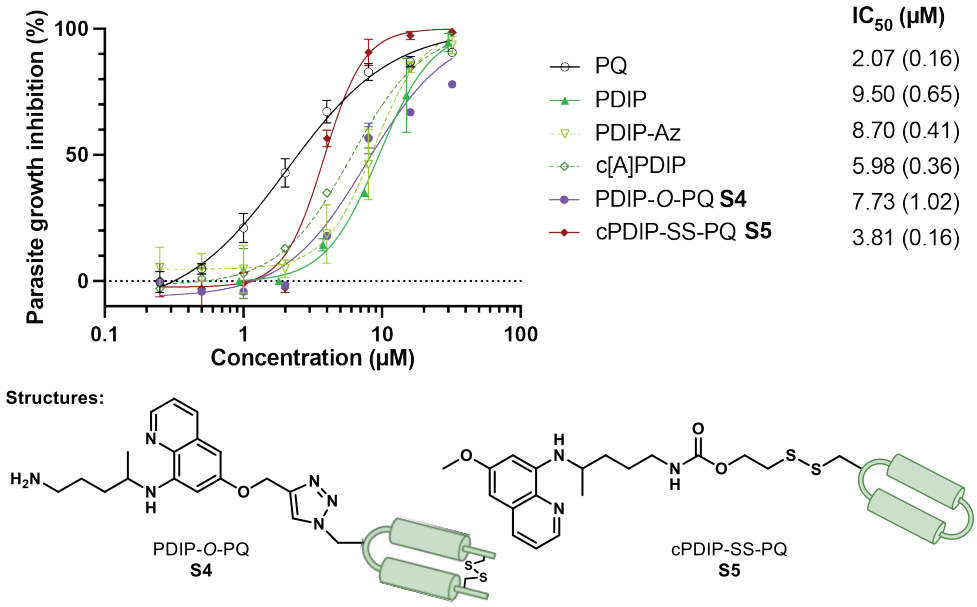

Figure S5. *In vitro* inhibition of *P. falciparum* growth in human RBCs by increasing concentrations of a cleavable disulfide PDC containing a backbone cyclized peptide (**S5**) and a non-cleavable *O*-modified PQ PDC (**S4**). Data points are expressed as mean ± SD for at least two biological replicates. IC_{50} values are given as mean (SEM). Note: for detailed peptide sequence information, see Table S1, p. 6.

Scheme S1. Synthesis of A) PDIP-*O*-PQ and B) cPDIP-SS-PQ conjugates.

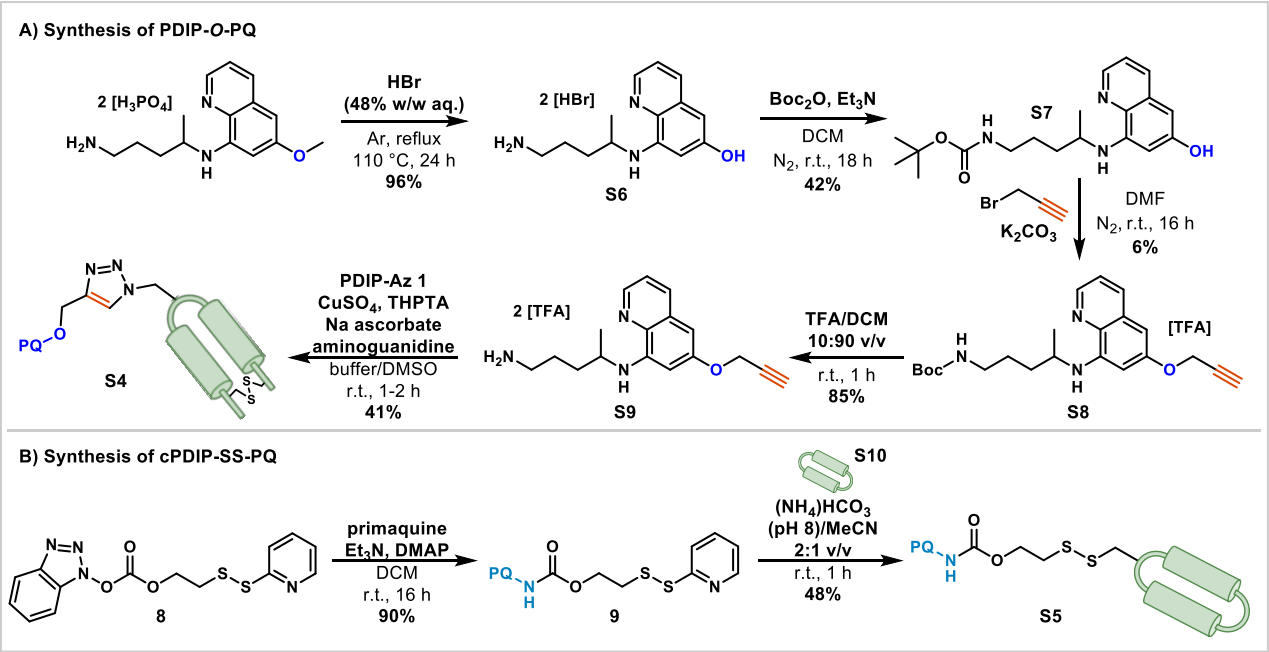

Table S1. Peptide sequences and properties of PDIP analogues.

Peptide	Sequence	MW (Da)[a]	MW (Da) TFA salt[b]
PDIP	GCGGPLYKKIIKKLLESGGSGGAPLYKKIIKKLCES*	3775.6	4801.8
PDIP-Az **1**	GCGGPLYKKIIKKLLESGGXGGAPLYKKIIKKLCES*	3800.6	4826.8
[GG]PDIP-Az **2**	xGGGCQAPLYKKIIKKLLESGGSGGAPLYKKIIKKLCES*	4057.9	5084.1
cPDIP **S10**	c[GGCGGAPLYKKIIKKLAKSGAQAPLYKKIIKKLLES]	3796.7	4822.9
c[A]PDIP[c]	c[GG**A**GGAPLYKKIIKKLAKSGAQAPLYKKIIKKLLES]	3764.7	4790.9

X = azidoalanine

x = azidoacetic acid

* denotes an amidated C-terminus

[a] Oxidized molecular weight is provided for PDIP, PDIP-Az and [GG]PDIP-Az

[b] TFA salt molecular weight includes the mass of TFA counterions resulting from protonation of basic residues and the N-terminal amine during HPLC purification with acidic eluent (0.1% TFA)

[c] A desulfurized variant of cPDIP was employed in growth inhibition assays to prevent the presence of a free thiol during assays.

General Chemistry Procedures

^{1}H and $^{13}C\{^{1}H\}$ NMR spectra were recorded on a Bruker AVANCE spectrometer (400/700 MHz) at 298 K, in the solvents specified. $CDCl_3$ was treated with K_2CO_3(s) and 4 Å molecular sieves prior to use. For ^{1}H NMR and ^{13}C NMR spectra, signals arising from the residual protio-form and deutero-form of the solvent, respectively, were used as an internal reference. These correspond to δ_H 7.26 and δ_C 77.16 for $CDCl_3$, δ_H 1.94 and δ_C 1.32 for CD_3CN and δ_H 3.31 and δ_C 49.00 for CD_3OD. ^{1}H NMR data were recorded as follows: chemical shift (δ) [multiplicity, coupling constant(s) *J* (Hz), relative integral] where multiplicity was defined as: s = singlet; d = doublet; t = triplet; m = multiplet or combinations of the above. Coupling constants are quoted to the nearest 0.1 Hz.

Low-resolution mass spectrometry (LRMS) was carried out using positive or negative electrospray ionisation (ESI) on a Waters LCT ToF Premier XE or Agilent 6120 Single Quadrupole mass spectrometer. High-resolution mass spectrometry (HRMS) was carried out using positive ESI on a Waters Synapt G2-Si mass spectrometer. Infrared (IR) spectra were performed on a Perkin-Elmer UATR Two spectrometer as a solid and analyzed using Essential FTIR software. Preparative high-performance liquid chromatography (HPLC) was performed on a Waters 600 Controller with a Waters 717 plus Autosampler and a Waters 2996 Photodiode Array Detector running Empower Pro Empower 3 software. Liquid chromatography mass spectrometry (LCMS) was performed on an Agilent 6120 Single Quadrupole mass spectrometer with an Agilent 1260 HPLC component, using an Agilent Poroshell C18 column, or a Shimadzu LCMS-2050 mass spectrometer with a Shimadzu LC40Dx3 UHPLC system, using either a Shimadzu Shim-pack XR-ODS III column or an Agilent Zorbax SB-C18 column. Analytical HPLC was performed on an Agilent 1100 Analytical HPLC with an Agilent Zorbax SB-C18 column. Linear gradients of water (solvent A) and MeCN (solvent B) were used for LCMS, preparative and analytical HPLC with eluents containing 0.1% TFA for HPLC, 0.1% formic acid for LCMS or 0.01% formic acid for UHPLC. When specified, dry solvents were obtained from a Glass Contour solvent purification system.

Peptide and PDC masses for yields were determined on a Mettler Toledo UMX2 microbalance to 0.001 mg accuracy. Azide containing PDIP analogues were synthesized either by published protocols[1,2] (PDIP was formerly known as cPF4PD) or manufactured by Wuxi AppTec (see Table S1 for sequences). Fmoc-azido-alanine was manufactured by Combi-Blocks, other amino acids by GL Biochem or AK Scientific, and PEG-alkynes from Ambeed and BroadPharm. All other chemicals were purchased from major suppliers. Syntheses for cleavable linkers were based off reported methods.[3–6]

General procedure: T3P® coupling for amide bond formation

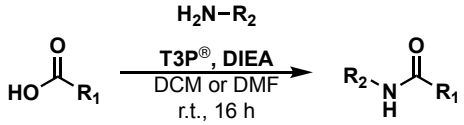

A magnetically stirred mixture of amine (1.0 equiv.), carboxylic acid (1.0 equiv.) and DIEA (6.0 equiv.) in DCM or DMF (0.05–0.1 M) maintained under an atmosphere of nitrogen was treated with T3P® (50% in EtOAc, 1.5 equiv.). The mixture was stirred at room temperature for 16 h. Reaction work-up and purification were conducted using either of the following methods:

Method A: The mixture was diluted with DCM (50 mL) and washed sequentially with saturated aqueous $NaHCO_3$ (10 mL) and brine (10 mL). The organic phase was dried (Na_2SO_4), filtered and concentrated under reduced pressure to give a crude product that was subjected to purification by flash column chromatography under the solvent conditions specified to afford the desired product.

Method B: The mixture was diluted in MeCN/H_2O and subjected to purification by reverse-phase semi-preparative HPLC using the specified gradient to afford the desired product.

*PQ-alkyne **5** (N-(4-((6-methoxyquinolin-8-yl)amino)pentyl)hex-5-ynamide)*

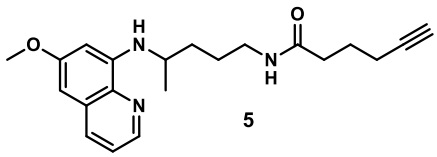

Synthesized according to the general procedure on a 110 µmol scale using primaquine bisphosphate (50 mg) and 5-hexynoic acid (12 µL) in DCM (2 mL). Purified according to method A (3% methanol/DCM) to afford **5** (16 mg, 40%) as a dark-brown oil.

^{1}H NMR: (400 MHz, $CDCl_3$) δ 8.51 (dd, *J* = 4.2, 1.7 Hz, 1H), 7.91 (dd, *J* = 8.3, 1.7 Hz, 1H), 7.28 (dd, *J* = 8.3, 4.2 Hz, 1H), 6.32 (d, *J* = 2.5 Hz, 1H), 6.27 (d, *J* = 2.5 Hz, 1H), 6.03 – 5.95 (m, 1H), 5.82 – 5.73 (m, 1H), 3.86 (s, 3H), 3.65 – 3.54 (m, 1H), 3.32 – 3.15 (m, 2H), 2.25 – 2.16 (m, 4H), 1.95 (t, *J* = 2.7 Hz, 1H), 1.85 – 1.74 (m, 2H), 1.73 – 1.54 (m, 4H), 1.27 (d, *J* = 6.4 Hz, 3H).ppm; **^{13}C NMR:** (101 MHz, $CDCl_3$) δ 171.9, 159.2, 144.7, 144.2, 135.2, 134.6, 129.7, 121.7, 96.7, 91.6, 83.4, 69.0, 55.0, 47.7, 39.3, 34.9, 33.8, 26.1, 24.0, 20.5, 17.6 ppm; **HRMS:** (ESI+) *m/z* found 354.2188, calcd for $C_{21}H_{28}N_3O_2$ $[M+H]^+$ 354.2176; **IR:** 3290, 2935, 2118, 1645, 1615, 1519 cm^{-1}.

*PQ-PEG1-alkyne **6** (N-(4-((6-methoxyquinolin-8-yl)amino)pentyl)-3-(prop-2-yn-1-yloxy)propan amide)*

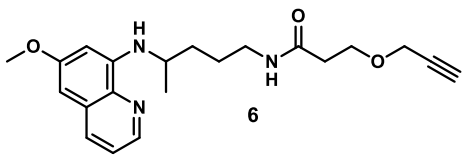

Synthesized according to the general procedure on a 78 µmol scale using primaquine bisphosphate (36 mg) and propargyl-PEG1-acid (10 mg) in DCM (1 mL). Purified according to method B (50 to 85% MeCN over 20 min) to afford **6** (7.1 mg, 18%) as a yellow oil (TFA salt).

^{1}H NMR: (400 MHz, CD_3CN) δ 8.67 (dd, *J* = 4.8, 1.6 Hz, 1H), 8.38 (dd, *J* = 8.4, 1.6 Hz, 1H), 7.60 (dd, *J* = 8.4, 4.8 Hz, 1H), 6.71 – 6.63 (m, 1H), 6.59 (br s, 1H), 6.53 – 6.46 (m, 1H), 5.96 (br s, 1H), 4.09 (d, *J* = 2.4 Hz, 2H), 3.89 (s, 3H), 3.76 – 3.64 (m, 3H), 3.26 – 3.11 (m, 2H), 2.67 (t, *J* = 2.4 Hz, 1H), 2.35 (t, *J* = 6.1 Hz, 2H), 1.78 – 1.51 (m, 4H), 1.26 (d, *J* = 6.3 Hz, 3H) ppm; **^{13}C NMR:** (101 MHz, CD_3CN) δ 171.8, 161.5, 143.6, 142.7, 141.0, 132.3, 131.0, 122.9, 100.9, 94.1, 80.8, 75.7, 66.9, 58.6, 56.3, 49.2, 39.8, 37.2, 34.1, 26.9, 20.4; **HRMS:** (ESI+) *m/z* found 370.2135, calcd for $C_{21}H_{28}N_3O_3$ $[M+H]^+$ 370.2123; found 392.1949, calcd for $C_{21}H_{27}N_3O_3Na$ $[M+Na]^+$ 392.1944; **IR:** 3300, 2937, 2118, 1647, 1597 cm^{-1}.

PQ-PEG3-alkyne 7 (N-(4-((6-methoxyquinolin-8-yl)amino)pentyl)-3-(2-(2-(prop-2-yn-1-yloxy) ethoxy)ethoxy)propanamide)

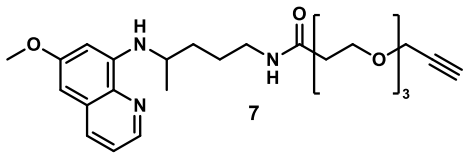

Synthesized according to the general procedure on a 50 µmol scale using primaquine bisphosphate (23 mg) and propargyl-PEG3-acid (11 mg) in DMF (0.7 mL). Purified according to method B (50 to 85% MeCN over 20 min) to afford **7** (3.4 mg, 12%) as a yellow oil (TFA salt).

^{1}H NMR: (700 MHz, $CDCl_3$) *one N–H not observed* δ 8.81 (dd, *J* = 4.9, 1.6 Hz, 1H), 8.32 (dd, *J* = 8.4, 1.6 Hz, 1H), 7.57 (dd, *J* = 8.4, 4.9 Hz, 1H), 6.66 (br s, 1H), 6.51 – 6.48 (m, 2H), 4.17 (d, *J* = 2.4 Hz, 2H), 3.93 (s, 3H), 3.71 (t, *J* = 5.8 Hz, 2H), 3.67 – 3.60 (m, 9H), 3.33 – 3.24 (m, 2H), 2.48 (t, *J* = 5.8 Hz, 2H), 2.42 (t, *J* = 2.4 Hz, 1H), 1.83 – 1.62 (m, 4H), 1.32 (d, *J* = 6.4 Hz, 3H) ppm; **^{13}C NMR:** (176 MHz, $CDCl_3$) δ 172.2, 161.2, 142.3, 141.0, 140.5, 131.8, 129.1, 121.4, 101.1, 92.9, 79.7, 74.8, 70.4 (2C), 70.3, 69.2, 67.4, 58.5, 55.7, 48.7, 39.4, 36.9, 33.5, 26.2, 20.0 ppm; **HRMS:** (ESI+) *m/z* found 458.2658, calcd for $C_{25}H_{36}N_3O_5$ $[M+H]^+$ 458.2650; found 480.2480, calcd for $C_{25}H_{35}N_3O_5Na$ $[M+Na]^+$ 480.2469, **IR:** 3213, 2921, 2113, 1651, 1520 cm^{-1}.

PQ-*O*-alkyne (S9) synthesis

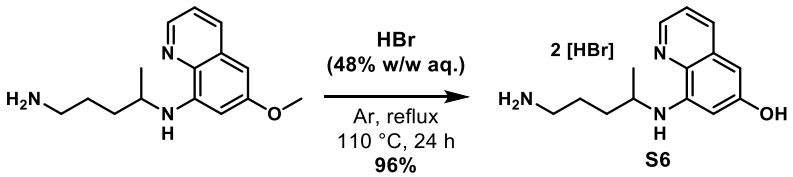

PQ bisphosphate (1.038 g, 2.28 mmol, 1.0 equiv.) was combined with aqueous hydrobromic acid (4 mL, 48% w/w, 73.7 mmol, 32 equiv.) at reflux under an atmosphere of argon for 24 h. Remaining hydrobromic acid was evaporated under a stream of nitrogen and gases quenched by scrubbing with ammonium bicarbonate. The orange crude product was purified with flash column chromatography (1:5 v/v methanol/DCM) and afforded the product **S6** (0.889 g, 96%) as a bright orange oil (HBr salt).

^{1}H NMR: (400 MHz, CD_3OD) *O–H, N–H, and exchangeable Ar C–H not observed*[i] δ 8.81 – 8.65 (m, 2H), 7.86 (dd, *J* = 8.5, 5.3 Hz, 1H), 6.85 (s, 1H), 3.89 – 3.75 (m, 1H), 3.11 – 2.92 (m, 2H), 2.06 – 1.74 (m, 4H), 1.40 (d, *J* = 6.3 Hz, 3H) ppm; **^{13}C NMR:** (101 MHz, CD_3OD) δ 161.1, 145.6, 140.7, 139.6, 133.9, 125.7, 122.7, 106.2, 101.4, 50.6, 40.7, 33.7, 25.3, 19.9 ppm; **HRMS:** (ESI+) *m/z* found 246.1613, calcd for $C_{14}H_{20}N_3O$ $[M+H]^+$ 246.1606; **IR:** 3321, 3023, 2969, 2924, 1594, 1578, 1451, 1440 cm^{-1}.

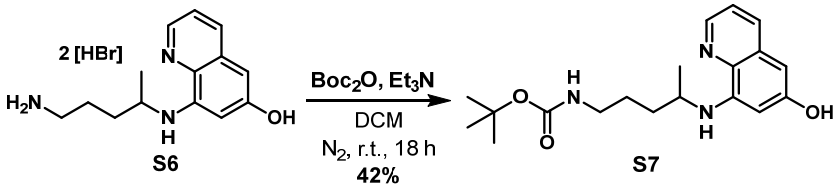

Compound **S6** (0.555 g, 1.36 mmol, 1.0 equiv.) in DCM (5 mL) was combined with Boc anhydride (0.590 g, 2.70 mmol, 2.0 equiv.) and triethylamine (0.631 mL, 4.53 mmol, 3.3 equiv.), and stirred under an atmosphere of nitrogen for 18 h. The crude mixture was concentrated under reduced pressure and purified with flash column chromatography (1:5 to 1:0 v/v ethyl acetate/PS), to afford **S7** (0.198 g, 42%) as a bright orange oil.

^{1}H NMR: (400 MHz, CD_3OD) *Exchangeable Ar C–H, O–H and N–Hs not observed* δ 8.63 (dd, *J* = 4.8, 1.5 Hz, 1H), 8.43 (d, *J* = 8.3 Hz, 1H), 7.64 (dd, *J* = 8.5, 4.8 Hz, 1H), 6.74 (s, 1H), 3.78 – 3.68 (m, 1H), 3.14 – 3.01 (m, 2H), 1.84 – 1.55 (m, 4H), 1.41 (s, 9H), 1.34 (d, *J* = 6.4 Hz, 3H) ppm; **^{13}C NMR:** (101 MHz, CD_3OD) δ 158.3, 158.2, 146.4, 144.6, 135.7, 135.6, 131.9, 122.8, 98.4, 96.2, 79.8, 49.0 (from 2D), 41.3, 34.9, 28.8 (3C), 27.6, 20.8 ppm; **HRMS:** (ESI+) *m/z* found 346.2137, calcd for $C_{19}H_{28}N_3O_3$ $[M+H]^+$ 346.2131; **IR:** 3317, 2972, 2933, 1688, 1522 cm^{-1}.

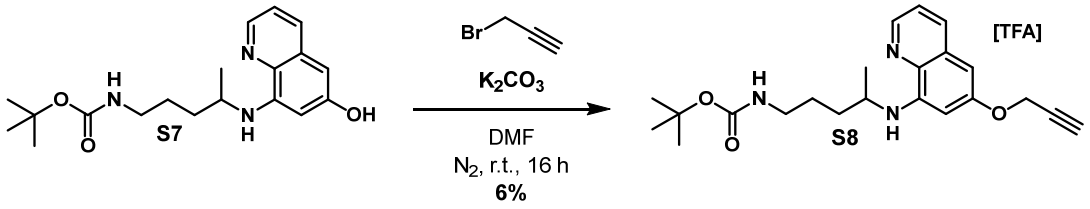

Compound **S7** (0.198 g, 0.574 mmol, 1.0 equiv.) was stirred with potassium carbonate (0.086 g, 0.622 mmol, 1.1 equiv.) in DMF (5 mL) for 30 min under an atmosphere of nitrogen. Propargyl bromide (43.5 µL, 0.574 mmol, 1.0 equiv.) was added and the reaction continued for 16 h. The mixture was diluted in DCM (30 mL) and washed with water (30 mL). The aqueous layer was extracted with DCM (2 × 30 mL), and the combined organic layers washed with brine (1 × 20 mL), lithium chloride (10 mL, 1 M), dried with magnesium sulfate and concentrated under reduced

[i] Fast exchange of proton at C5 position of PQ has previously been noted in NMR studies.[10]

pressure. The crude residue was purified by preparative HPLC (30 to 90% MeCN over 30 min), to afford **S8** (15.9 mg, 6%) as an orange oil (TFA salt).

^{1}H NMR: (400 MHz, $CDCl_3$) *one N–H not observed* δ 8.92 (dd, *J* = 5.1, 1.6 Hz, 1H), 8.43 (dd, *J* = 8.4, 1.6 Hz, 1H), 7.64 (dd, *J* = 8.4, 5.0 Hz, 1H), 6.63 (d, *J* = 2.4 Hz, 1H), 6.58 (d, *J* = 2.4 Hz, 1H), 4.82 (d, *J* = 2.4 Hz, 2H), 4.67 (br s, 1H), 3.67 – 3.58 (m, 1H), 3.17 – 3.12 (m, 2H), 2.61 (t, *J* = 2.4 Hz, 1H), 1.85 – 1.55 (m, 4H), 1.42 (s, 9H), 1.32 (d, *J* = 6.4 Hz, 3H) ppm; **^{13}C NMR:** (101 MHz, $CDCl_3$) δ 159.3, 156.3, 142.4, 142.0, 140.4, 131.8, 128.0, 121.4, 101.7, 94.3, 79.2, 77.9, 76.6, 56.2, 49.0, 40.6, 33.3, 28.5 (3C), 26.8, 19.8 ppm; **HRMS:** (ESI+) *m/z* found 384.2288, calcd for $C_{22}H_{30}N_3O_3$ $[M+H]^+$ 384.2287; **IR:** 3378, 3311, 2974, 2933, 2870, 2122, 1694, 1514 cm^{-1}.

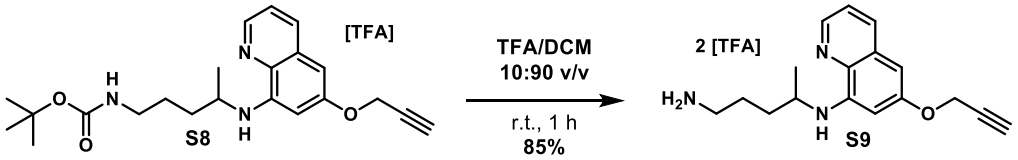

Compound **S8** (15.9 mg, 33.1 µmol, 1.0 equiv.) was stirred with TFA/DCM (2 mL, 1:9 v/v) for 1 h. The solution was concentrated under a stream of nitrogen and then purified by flash column chromatography (1:10 to 1:5 v/v methanol/DCM) to afford **S9** (14.4 mg, 85%) as a brown oil (TFA salt).

^{1}H NMR: (400 MHz, $CDCl_3$) δ 8.52 (dd, *J* = 4.3, 1.6 Hz, 1H), 7.92 (dd, *J* = 8.3, 1.6 Hz, 1H), 7.68 (br s, 2H), 7.28 (dd, *J* = 8.2, 4.3 Hz, 1H), 6.42 (s, 1H), 6.30 (d, *J* = 2.5 Hz, 1H), 5.95 (br s, 1H), 4.74 (d, *J* = 2.4 Hz, 2H), 3.59 – 3.48 (m, 1H), 2.87 (t, *J* = 7.1 Hz, 2H), 2.55 (t, *J* = 2.4 Hz, 1H), 1.79 – 1.49 (m, 4H), 1.21 (d, *J* = 6.3 Hz, 3H) ppm; **^{13}C NMR:** (101 MHz, $CDCl_3$) δ 157.5, 144.8, 144.7, 135.7, 135.1, 129.8, 122.1, 97.6, 93.7, 78.7, 75.8, 55.9, 47.9, 40.1, 33.3, 24.3, 20.1 ppm; **HRMS:** (ESI+) *m/z* found 284.1765, calcd for $C_{17}H_{22}N_3O$ $[M+H]^+$ 284.1763; **IR:** 3287, 2966, 2931, 2123, 1673, 1517 cm^{-1}.

Disulfide linker (3) synthesis

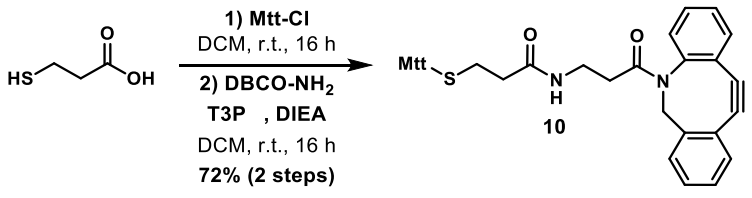

A magnetically stirred solution of 4-methyltrityl chloride (14 mg, 50 µmol, 1.0 equiv.) in DCM (0.5 mL) maintained under an atmosphere of nitrogen was treated with 3-mercaptopropionic acid (4.4 µL, 50 µmol, 1.0 equiv.). The resulting bright yellow mixture was stirred at room temperature

overnight for 16 h. The mixture was concentrated under a stream of nitrogen and the crude material obtained was used without further purification.

LRMS: (ESI−) *m/z* found 361.1, calcd for $C_{23}H_{21}O_2S$ $[M-H]^-$ 361.1.

Subsequent amide bond formation was conducted according to the T3P® coupling general procedure on a 40 µmol scale using DBCO-NH_2 (11 mg, 1.0 equiv.) and the crude Mtt-protected 3-mercaptopropionic acid (1.3 equiv.) in DCM (0.5 mL). Purified according to method A (3% methanol/DCM) to afford **10** (18 mg, 72% over two steps) as a clear oil.

^{1}H NMR: (400 MHz, $CDCl_3$) δ 7.66 (d, *J* = 7.5 Hz, 1H), 7.47 – 7.27 (m, 15H), 7.26 – 7.15 (m, 4H), 7.09 (d, *J* = 8.0 Hz, 2H), 5.87 (t, *J* = 6.2 Hz, 1H), 5.04 (d, *J* = 14.0 Hz, 1H), 3.64 (d, *J* = 14.0 Hz, 1H), 3.38 – 3.29 (m, 1H), 3.17 – 3.07 (m, 1H), 2.56 – 2.45 (m, 2H), 2.44 – 2.34 (m, 1H), 2.31 (s, 3H), 1.98 – 1.81 (m, 2H), 1.80 – 1.70 (m, 1H) ppm; **^{13}C NMR:** (101 MHz, $CDCl_3$) δ 172.3, 170.9, 151.1, 148.2, 145.1, 141.9, 136.4, 132.1, 129.8 (4C), 129.7 (2C), 129.3, 128.8 (2C), 128.8, 128.5 (2C), 128.1, 128.0 (4C), 128.0, 127.3, 126.8 (2C), 125.8, 123.1, 122.7, 114.9, 107.8, 66.6, 55.7, 35.6, 35.2, 34.8, 28.0, 21.1 ppm; **HRMS:** (ESI+) *m/z* found 643.2394, calcd for $C_{41}H_{36}N_2O_2SNa$ $[M+Na]^+$ 643.2390.

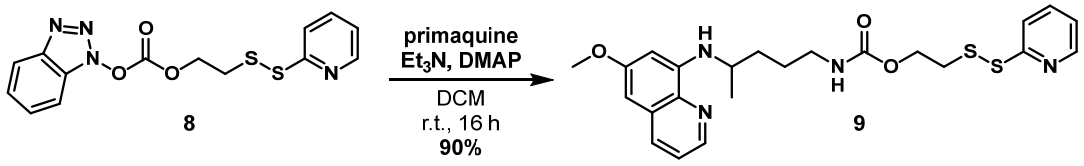

A magnetically stirred mixture of carbonate **8**[5] (36 mg, 0.10 mmol, 1.0 equiv.) and primaquine bisphosphate (55 mg, 0.12 mmol, 1.2 equiv.) in DCM (5 mL) maintained under an atmosphere of nitrogen was treated with DIEA (35 µL, 0.20 mmol, 2.0 equiv.). The mixture was stirred at room temperature for 16 h, then concentrated under a stream of nitrogen and purified by reverse-phase preparative HPLC (40 to 90% MeCN over 20 min) to afford **9** (44 mg, 90%) as an orange oil (TFA salt).

^{1}H NMR: (400 MHz, $CDCl_3$) *one N–H not observed* δ 8.96 – 8.83 (m, 1H), 8.69 – 8.39 (m, 2H), 8.02 – 7.48 (m, 4H), 6.64 – 6.55 (m, 2H), 5.17 (br s, 1H), 4.26 (t, *J* = 6.0 Hz, 2H), 3.95 (s, 3H), 3.69 – 3.59 (m, 1H), 3.24 – 3.11 (m, 2H), 3.05 (t, *J* = 6.0 Hz, 2H), 1.85 – 1.57 (m, 4H), 1.37 – 1.27 (m, 3H) ppm; **^{13}C NMR:** (101 MHz, $CDCl_3$) *peaks associated with compound **9** reported*[ii] δ 161.9, 161.2, 160.9, 156.4, 144.1, 140.7, 138.6, 132.5, 125.9, 121.2, 117.3, 114.4, 111.6, 103.3, 93.6, 62.5, 55.9, 49.2, 41.0, 38.4, 33.1, 26.4, 19.6 ppm; **HRMS:** (ESI+) *m/z* found 473.1679, calcd for $C_{23}H_{29}N_4O_3S_2$ $[M+H]^+$ 473.1676.

[ii] Note: Compound **9** gradually decomposes in solution to form a mercaptopyridine adduct (substitution of a proton on the aminoquinoline backbone of PQ), as indicated by the emergence of additional peaks in the ^{13}C NMR spectrum.

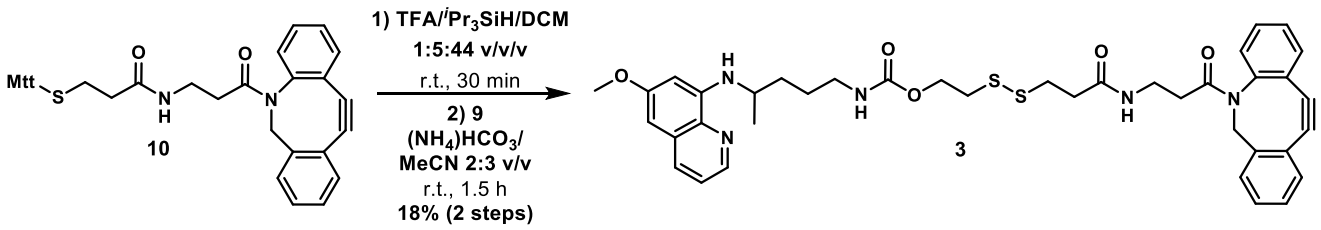

Compound **10** (8 mg, 13 μmol, 1.0 equiv.) was suspended in a mixture of TFA/^{i}Pr$_3$SiH/DCM (1:5:44 v/v/v, 0.6 mL total) and magnetically stirred at room temperature for 30 min. The mixture was concentrated under a stream of nitrogen and the resulting residue was redissolved in argon purged MeCN (1.5 mL). This solution was transferred to a flask containing **9** (8 mg, 17 μmol, 1.3 equiv.), followed by the addition of an argon purged 200 mM ammonium bicarbonate solution (pH 8, 1 mL). The mixture was magnetically stirred at room temperature for 1.5 h, then concentrated under a stream of nitrogen. Purification with reverse-phase semi-preparative HPLC (40 to 90% MeCN over 20 min, 5 mL/min, containing 0.1% TFA) followed by further purification with reverse-phase analytical HPLC (20 to 80% MeCN over 30 min, 1 mL/min, containing 0.1% formic acid) afforded **3** (1.6 mg, 18%) as a yellow oil (formic acid salt).

^{1}H NMR: (700 MHz, $CDCl_3$) *one N–H not observed, isolated with an unknown impurity* δ 9.03 – 8.98 (m, 1H), 8.52 (dd, *J* = 4.2, 1.6 Hz, 1H), 7.98 – 7.87 (m, 2H), 7.55 (apparent t, *J* = 7.1 Hz, 1H), 7.48 (apparent t, *J* = 7.4 Hz, 1H), 7.44 – 7.27 (m, 5H), 6.67 – 6.57 (m, 1H), 6.36 – 6.24 (m, 2H), 5.43 – 5.36 (m, 1H), 5.15 – 5.11 (m, 2H), 4.32 – 4.19 (m, 2H), 3.91 – 3.84 (m, 3H), 3.83 – 3.77 (m, 2H), 3.65 – 3.56 (m, 1H), 3.40 – 3.29 (m, 2H), 3.24 – 3.14 (m, 2H), 2.98 (t, *J* = 7.4 Hz, 2H), 2.93 – 2.86 (m, 2H), 2.57 (t, *J* = 7.5 Hz, 2H), 1.75 – 1.61 (m, 4H), 1.28 (d, *J* = 6.4 Hz, 3H) ppm; **HRMS:** (ESI+) *m/z* found 726.2783, calcd for $C_{39}H_{44}N_5O_5S_2$ $[M+H]^+$ 726.2778.

UPLC trace:

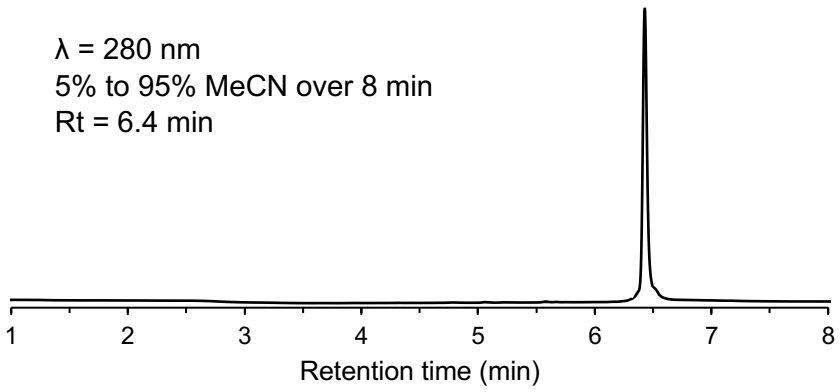

Trioxolane linker (4) synthesis

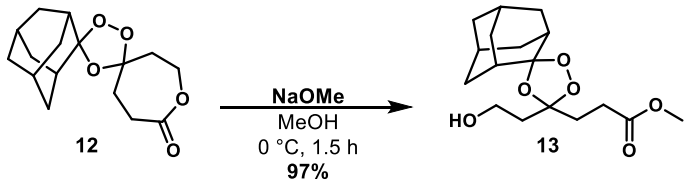

NaOMe (18 mg, 0.34 mmol, 1.0 equiv.) was suspended in methanol (0.7 mL) under an atmosphere of nitrogen and cooled to 0 °C (ice bath). This NaOMe solution was added dropwise to a flask containing lactone **12**[3] (0.10 g, 0.34 mmol, 1.0 equiv.) and the mixture was magnetically stirred in an ice bath for 1.5 h. The reaction was neutralized with the addition of 1M HCl, diluted with DCM (10 mL) and washed with brine (10 mL). The organic phase was dried (Na_2SO_4), filtered and concentrated under reduced pressure to afford **13** (0.11 g, 97%) as a clear oil, which was used without further purification.

^{1}H NMR: (400 MHz, $CDCl_3$) *O–H not observed* δ 3.87 – 3.73 (m, 2H), 3.69 (s, 3H), 2.53 – 2.38 (m, 2H), 2.27 – 2.07 (m, 2H), 2.06 – 1.67 (m, 16H) ppm; **^{13}C NMR:** (101 MHz, $CDCl_3$) δ 173.5, 112.7, 110.7, 58.6, 51.9, 37.7, 36.7, 36.4, 36.4, 35.1, 34.9, 34.9, 34.9, 31.0, 28.8, 26.8, 26.4 ppm; **HRMS:** (ESI+) *m/z* found 349.1629, calcd for $C_{17}H_{26}O_6Na$ $[M+Na]^+$ 349.1622.

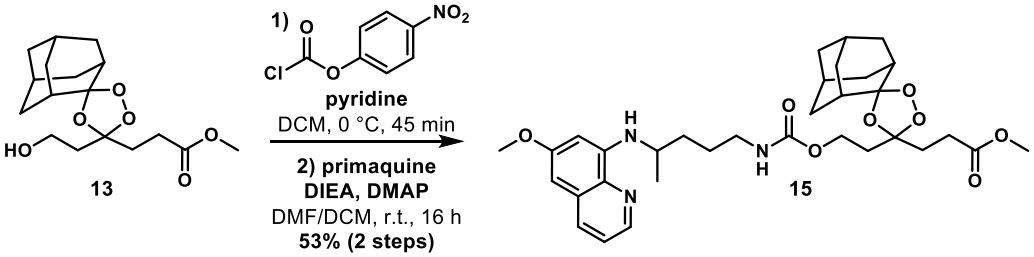

A magnetically stirred mixture of alcohol **13** (38 mg, 0.12 mmol, 1.0 equiv.) and pyridine (14 µL, 0.17 mmol, 1.5 equiv.) in DCM (1.5 mL) maintained under an atmosphere of nitrogen was cooled to 0 °C (ice bath). *p*-nitrophenylchloroformate (46 mg, 0.24 mmol, 2.0 equiv.) was added and the mixture stirred in an ice bath for 45 min. The reaction mixture was concentrated and subjected to purification by flash column chromatography (15% EtOAc/petroleum spirits) to afford carbonate **14** (45 mg) as a yellow oil. The product was isolated with an impurity (*p*-nitrophenol) but was used without further purification, owing to its instability.

^{1}H NMR: (400 MHz, $CDCl_3$) δ 8.31 – 8.25 (m, 2H), 7.42 – 7.36 (m, 2H), 4.43 (t, J = 6.8 Hz, 2H), 3.69 (s, 3H), 2.57 – 2.41 (m, 2H), 2.31 – 2.08 (m, 4H), 2.04 – 1.67 (m, 14H) ppm; **LRMS:** (ESI+) *m/z* found 514.2, calcd for $C_{24}H_{29}NO_{10}Na$ $[M+Na]^+$ 514.2.

A magnetically stirred solution of carbonate **14** (45 mg, 1.0 equiv.) and primaquine bisphosphate (77 mg, 0.17 mmol, 1.5 equiv.) maintained under an atmosphere of nitrogen in DCM (0.5 mL) and

DMF (0.5 mL) was treated with DIEA (81 µL, 0.46 mmol, 4.0 equiv.) and DMAP (9 mg, 0.07 mmol, 0.6 equiv.). The mixture was stirred at room temperature for 16 h, then concentrated to remove DCM and subjected to purification by reverse-phase semi-preparative HPLC (40 to 90% MeCN over 20 min) to afford **15** (45 mg, 53% over two steps) as an orange oil (TFA salt).

^{1}H NMR: (700 MHz, $CDCl_3$) *one N–H not observed* δ 8.94 (d, *J* = 5.3 Hz, 1H), 8.50 (dd, *J* = 8.5, 1.5 Hz, 1H), 7.69 (dd, *J* = 8.5, 5.3 Hz, 1H), 6.59 (d, *J* = 2.4 Hz, 1H), 6.57 (d, *J* = 2.4 Hz, 1H), 4.99 (s, 1H), 4.16 (t, *J* = 6.7 Hz, 2H), 3.95 (s, 3H), 3.68 – 3.62 (m, 4H), 3.24 – 3.17 (m, 2H), 2.54 – 2.37 (m, 2H), 2.24 – 1.55 (m, 22H), 1.32 (d, *J* = 6.3 Hz, 3H) ppm; **^{13}C NMR:** (176 MHz, $CDCl_3$) δ 173.7, 161.8, 156.7, 143.6, 141.1, 139.1, 132.5, 126.5, 121.2, 112.5, 109.4, 102.9, 93.4, 60.6, 55.9, 51.9, 49.1, 40.9, 36.8, 36.5, 36.4, 35.4, 35.1, 34.9 (2C), 34.7, 33.1, 30.9, 28.8, 26.9, 26.6, 26.5, 19.7 ppm; **HRMS:** (ESI+) *m/z* found 612.3284, calcd for $C_{33}H_{46}N_3O_8$ $[M+H]^+$ 612.3279.

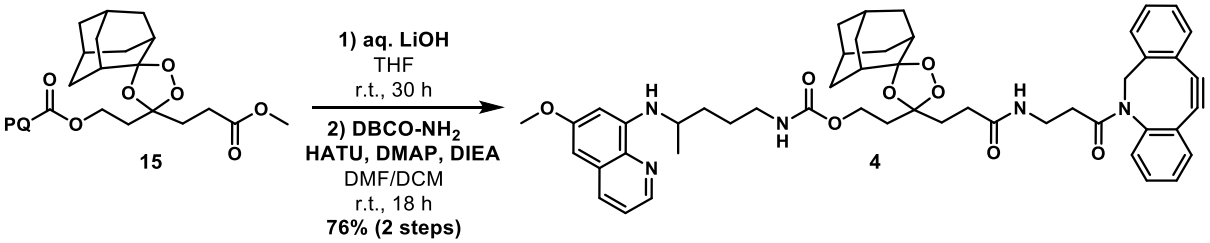

A magnetically stirred solution of methyl ester **15** (22 mg, 30 µmol, 1.0 equiv.) in THF (3 mL) was treated with a 1 M solution of LiOH in water (0.39 mL, 0.39 mmol, 13 equiv.). The mixture was stirred at room temperature for 30 h, then diluted in DCM (10 mL) and water (10 mL). The pH of the aqueous layer was decreased (pH ~4) with 1 M HCl and the product extracted with DCM (3 × 5 mL). The combined organic layers were washed with brine (10 mL), dried (Na_2SO_4), filtered and concentrated under reduced pressure to afford the corresponding carboxylic acid compound (19 mg) as a yellow oil, which was used without further purification.

HRMS: (ESI+) *m/z* found 598.3145, calcd for $C_{32}H_{44}N_3O_8$ $[M+H]^+$ 598.3129.

A magnetically stirred solution of the aforementioned carboxylic acid (19 mg, 1.0 equiv.), DBCO-NH_2 (9.1 mg, 33 µmol, 1.1 equiv.) and HATU (48 mg, 0.14 mmol, 4.6 equiv.) maintained under an atmosphere of nitrogen in DCM (0.4 mL) and DMF (0.4 mL) was treated with DIEA (52 µL, 0.30 mmol, 10 equiv.) and DMAP (2 mg, 16 µmol, 0.5 equiv.). The mixture was stirred at room temperature for 18 h, then concentrated to remove DCM and subjected to purification by reverse-phase semi-preparative HPLC (40 to 90% MeCN over 20 min) to afford **4** (22 mg, 76% over two steps) as an orange oil (TFA salt).

^{1}H NMR: (700 MHz, $CDCl_3$) *one N–H not observed* δ 8.94 – 8.87 (m, 1H), 8.50 (d, *J* = 8.4 Hz, 1H), 7.70 – 7.66 (m, 1H), 7.66 – 7.62 (m, 1H), 7.43 – 7.35 (m, 4H), 7.34 – 7.30 (m, 2H), 7.29 – 7.27 (m,

1H), 6.61 – 6.59 (m, 1H), 6.59 – 6.56 (m, 1H), 6.45 (d, *J* = 14.1 Hz, 1H), 5.38 (br s, 1H), 5.12 (d, *J* = 14.0 Hz, 1H), 4.20 – 4.12 (m, 2H), 3.94 (s, 3H), 3.71 (d, *J* = 14.0 Hz, 1H), 3.66 – 3.60 (m, 1H), 3.38 – 3.28 (m, 1H), 3.22 – 3.13 (m, 3H), 2.51 – 2.41 (m, 1H), 2.22 – 2.16 (m, 2H), 2.12 – 1.56 (m, 23H), 1.31 (d, *J* = 6.3 Hz, 3H) ppm; **HRMS:** (ESI+) *m/z* found 856.4294, calcd for $C_{50}H_{58}N_5O_8$ $[M+H]^+$ 856.4280.

UPLC trace:

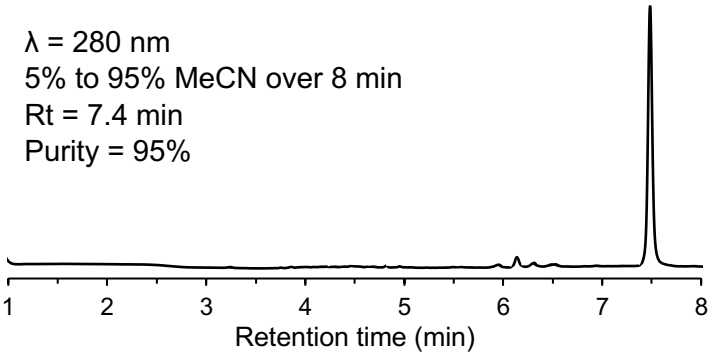

Synthesis of cPDIP (S10) and c[A]PDIP

Preparation and loading of 2-Cl-Trt-NHNH$_2$ resin

2-chlorotrityl chloride resin (1.0 g, 1.0 equiv., substitution = 1.4 mmol/g) was swollen in dry DCM for 30 min, followed by washing with DCM (5 × 5 mL) and DMF (5 × 5 mL). The resin was treated twice with hydrazine monohydrate (5% in DMF v/v, 4 mL) and agitated at room temperature for 45 min each time. The resin was washed with DMF (5 × 5 mL), DCM (5 × 5 mL) and DMF (5 × 5 mL) and unreacted resin sites were capped with MeOH/DMF (1:4 v/v) for 1 h. A solution of Fmoc-Gly-OH (1.7 g, 5.6 mmol, 4.0 equiv.), PyBOP (2.9 g, 5.6 mmol, 4.0 equiv.) and DIEA (1.95 mL, 11.2 mmol, 8.0 equiv.) in DMF (5 mL) was added to the resin and agitated at room temperature for 18 h. The resin was washed with DMF (5 × 5 mL) and DCM (5 × 5 mL) and dried under vacuum for 2 h.

Quantification of loading efficiency

The loading efficiency was quantified by measuring the removal of the Fmoc protecting group with 20% piperidine/DMF. Three samples of dry Fmoc-Gly loaded resin (5-10 mg) were weighed into Eppendorf tubes. Each sample was swelled in DMF (800 μL) for 15 min, followed by the addition of piperidine (200 μL) and agitation for 15 min. Aliquots from each sample (30 μL) were diluted in DMF (3 mL) in a quartz cuvette and the UV absorbance of the piperidine-fulvene adduct was measured (λ = 301 nm, ε = 7800 M^{-1} cm^{-1}) to quantify the amount of amino acid loaded onto the resin. The loading efficiency of the three replicates was averaged to determine a resin substitution for the

Fmoc-Gly loaded hydrazine resin (0.816 mmol/g). The theoretical maximum for the reported yield of synthesized peptide is based on the 0.816 mmol/g substitution from the resin loading.

General iterative peptide assembly (Fmoc-SPPS)

cPDIP (**S10**, see Table S1 for sequence) was synthesized on a 0.2 mmol scale using automated solid phase peptide synthesis (SPPS) according to the following protocols:

Deprotection: The resin was treated with 20% piperidine/DMF (3 mL, 2 × 5 min) and washed with DMF (5 × 5 mL).

General amino acid coupling: A solution of Fmoc-amino acid (4.0 equiv.), Oxyma® (4.0 equiv.) and *N,N'*-diisopropylcarbodiimide (DIC, 4.0 equiv.) in DMF (final concentration 0.15 M) was added to the resin. The resin was heated under microwave conditions (50 °C) for 30 min before washing with DMF (5 × 5 mL). Each coupling was repeated two times.

Capping: A solution of acetic anhydride/DMF (1:4 v/v) and DIEA (8 equiv.) was added to the resin and agitated for 10 min. The resin was washed with DMF (5 × 5 mL).

Cleavage: A mixture of TFA/$^{i}Pr_3SiH/H_2O$ (95:2.5:2.5 v/v/v) was added to the resin. After 2 hours, the resin was washed with TFA (3 × 2 mL) and DCM (3 × 2 mL). The combined cleavage solution and TFA and DCM washes were concentrated under a stream of N_2. The residue was treated with cold Et_2O (15 mL) to precipitate the peptide. The precipitate was centrifuged to form a pellet, the Et_2O was removed, and the pellet redissolved in MeCN/H_2O (containing 0.1% TFA), filtered and purified by reverse-phase preparative HPLC.

Backbone cyclization

The semi-purified linear peptide bearing an N-terminal cysteine residue and a C-terminal acyl hydrazide (14 mg, 1.0 equiv., containing 60% peptide impurity (~5.6 mg of linear peptide)) was subjected to backbone cyclization using intramolecular native chemical ligation.[7] The linear peptide hydrazide was prepared as a 1 mM solution in ligation buffer A (6.0 M Gn·HCl, pH 3.0) with a suspension of MPAA (200 equiv.). Acetyl acetone (2.0 equiv., 0.5 M stock solution in H_2O) was added and the resulting mixture was shaken for 2 h, followed by a 2-fold dilution with ligation buffer B (6.0 M Gn·HCl, 0.2 M NaH_2PO_4, pH 8.8) containing TCEP (50 equiv.). The pH was adjusted to 7.0 with 1 M NaOH and shaken for 18 h before LCMS was used to confirm the formation of the cyclic product. The sample was diluted with MeCN/H_2O, acidified with 1 M HCl and purified by reverse-phase semi-preparative HPLC (25 to 40% MeCN over 40 minutes) to afford **S10** as a white solid (2.9 mg, 5.4% based on initial resin loading).

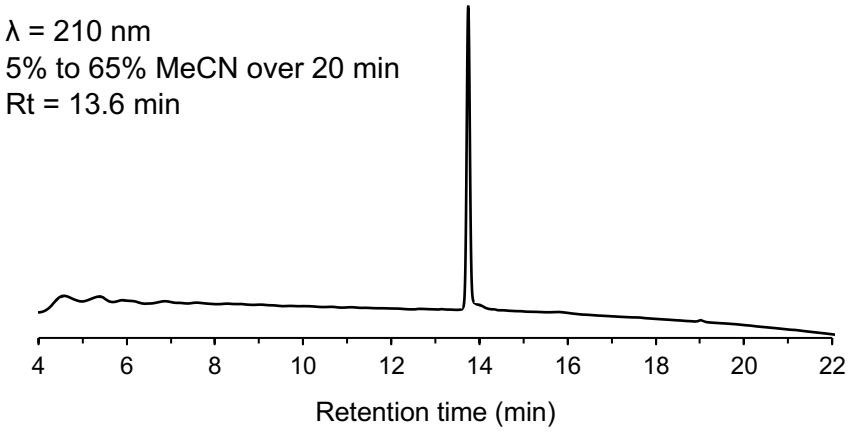

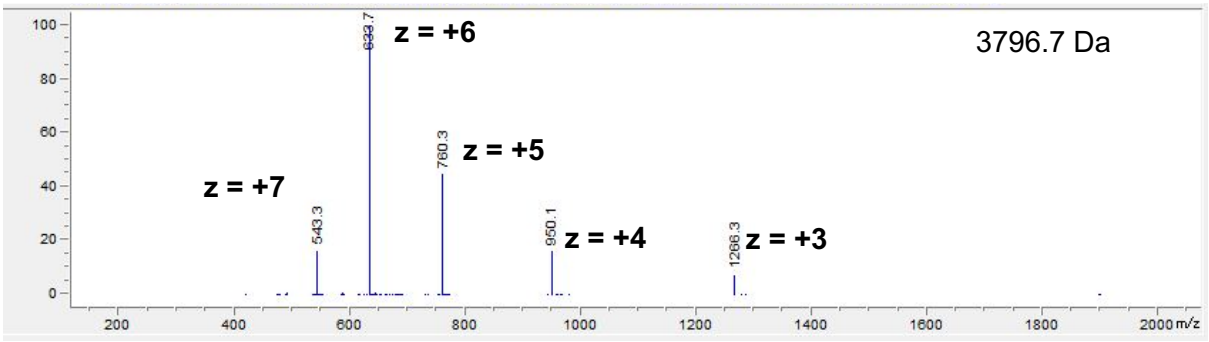

Desulfurization of S10

Stock solutions of reduced glutathione (GSH, 40 mM) and VA-044 (200 mM) were prepared in water and a stock solution of TCEP (0.5 M) was prepared in buffer (pH 6.5) containing Gn·HCl (6.0 M) and NaH_2PO_4 (0.1 M). Each stock solution was sparged with argon for 5 min prior to use. The cyclic peptide (4.3 mg, 1.1 µmol, 1.0 equiv.) was dissolved in degassed water (7.5 mM) and GSH (20 µL), VA-044 (20 µL) and TCEP (100 µL) were added sequentially to the mixture. The headspace of the reaction vessel was purged with argon, the vial was sealed and heated at 70 °C for 5 h. The sample was diluted with water (containing 0.1% TFA) and purified by reverse-phase semi-preparative HPLC (25 to 40% MeCN over 40 minutes) to afford c[A]PDIP as a white solid (2.3 mg, 54%).

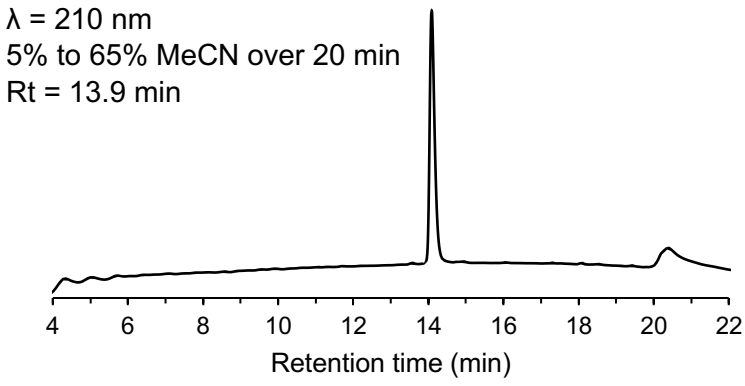

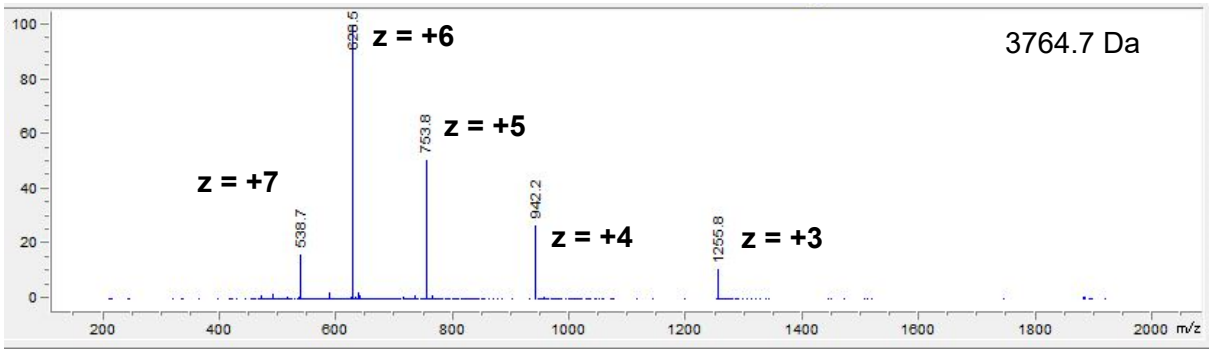

General procedure: CuAAC conjugation

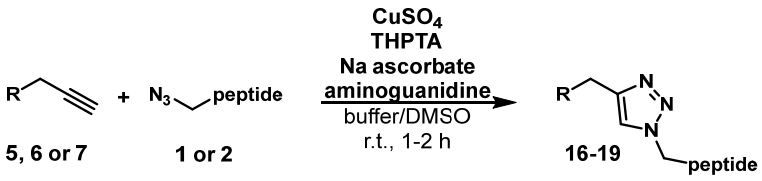

Following a procedure adapted from Hong and co-workers.[8] All reagent stock solutions were prepared in water, unless otherwise specified, to the following concentrations: aminoguanidine hydrochloride 100 mM, copper(II) sulfate 20 mM, tris(3-hydroxypropyltriazolylmethyl)amine (THPTA) 50 mM, sodium ascorbate 100 mM (freshly prepared), ethylenediaminetetraacetic acid (EDTA) 100 mM and drug-alkyne (**5**, **6**, **7**) 20 mM (in DMSO).

Peptide-azide (**1** or **2**, 1.0 equiv.) was dissolved in 100 mM sodium phosphate buffer (prepared by mixing 100 mM Na_2HPO_4 with 100 mM NaH_2PO_4 until pH = 7) to produce a final peptide concentration of 200 µM (based on total reaction volume including reagents to be added). An aliquot of DMSO was included to make the conjugation reaction mixture 10-20% organic/80-90% aqueous by volume, depending on solubility of the drug-alkyne used. The following reagents were then added sequentially to the reaction vial and magnetically stirred after each new addition: aminoguanidine hydrochloride (5 mM[iii], 25 equiv.), drug-alkyne (400 µM, 2.0 equiv.), copper(II) sulfate (100 µM, 0.5 equiv.) pre-mixed with THPTA (500 µM, 2.5 equiv.), and sodium ascorbate (5 mM, 25 equiv.). The conjugation mixture was magnetically stirred at room temperature for 1 – 2 h. The reaction was quenched with EDTA (5.0 equiv.) and purified by reverse-phase semi-preparative HPLC. Reported yields were determined by weight on a microbalance and were calculated using the mass of the TFA salt of the product (assuming all basic residues and the N-terminal amine are protonated).

[iii] Concentration of each component refers to the final concentration in the reaction mixture

*[GG]PDIP-alkane-PQ (**16**)*

Prepared with [GG]PDIP-Az **2** and primaquine-alkyne **5** on a 0.51 µmol scale (2.6 mg peptide) and 10% DMSO/90% aqueous conjugation conditions. Purification with semi-preparative HPLC (30 to 50% MeCN over 40 minutes) yielded **16** (1.25 mg, 45%) as a light-yellow solid.

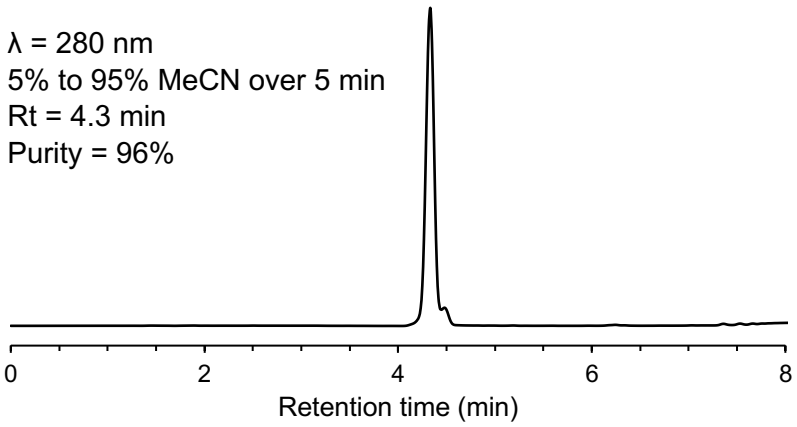

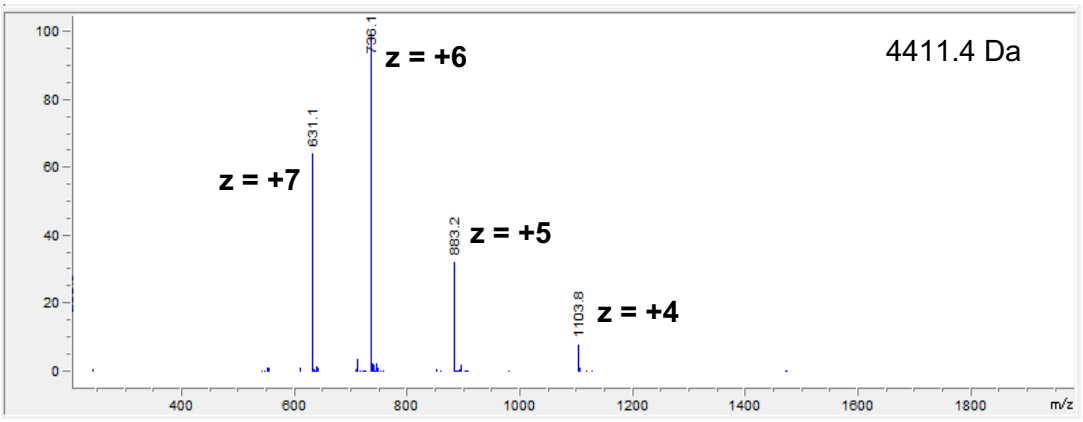

*PDIP-alkane-PQ (**17**)*

Prepared with PDIP-Az **1** and primaquine-alkyne **5** on a 0.68 µmol scale (3.3 mg peptide) and 10% DMSO/90% aqueous conjugation conditions. Purification with semi-preparative HPLC (30 to 60% MeCN over 40 minutes) yielded **17** (1.57 mg, 43%) as a light-yellow solid.

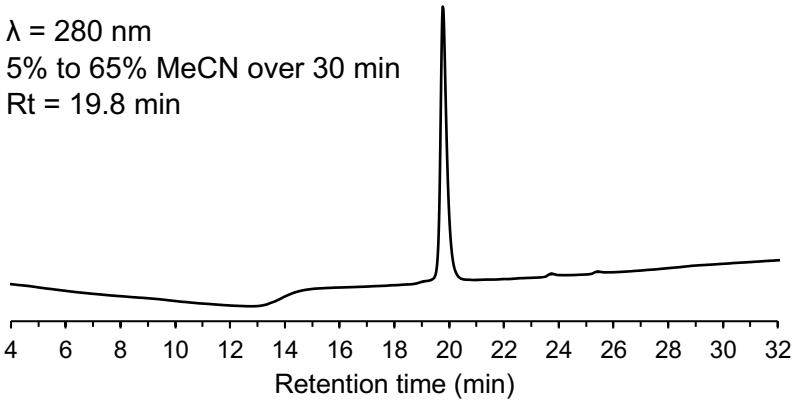

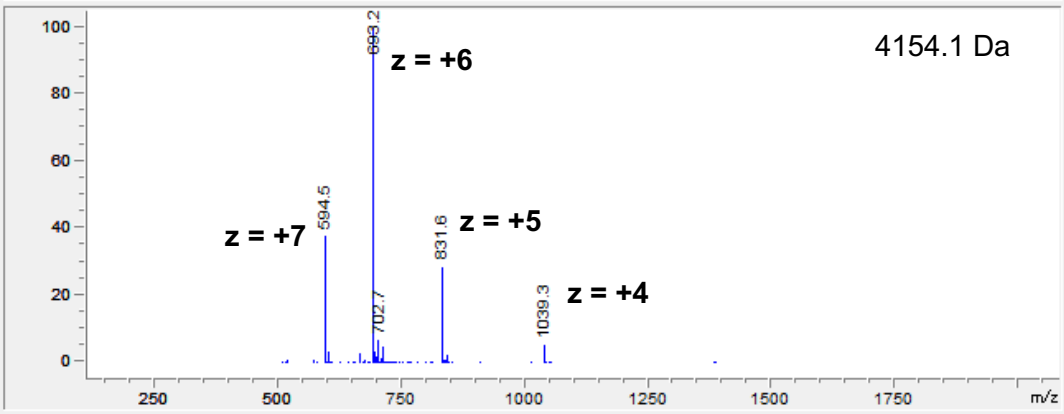

*PDIP-PEG1-PQ (**18**)*

Prepared with PDIP-Az **1** and primaquine-PEG1-alkyne **6** on a 0.89 µmol scale (4.3 mg peptide) and 10% DMSO/90% aqueous conjugation conditions. Purification with semi-preparative HPLC (20 to 65% MeCN over 40 minutes) yielded **18** (1.81 mg, 38%) as a light-yellow solid.

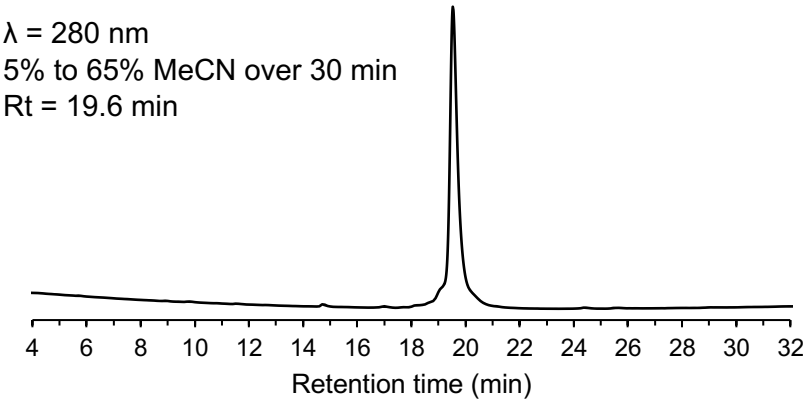

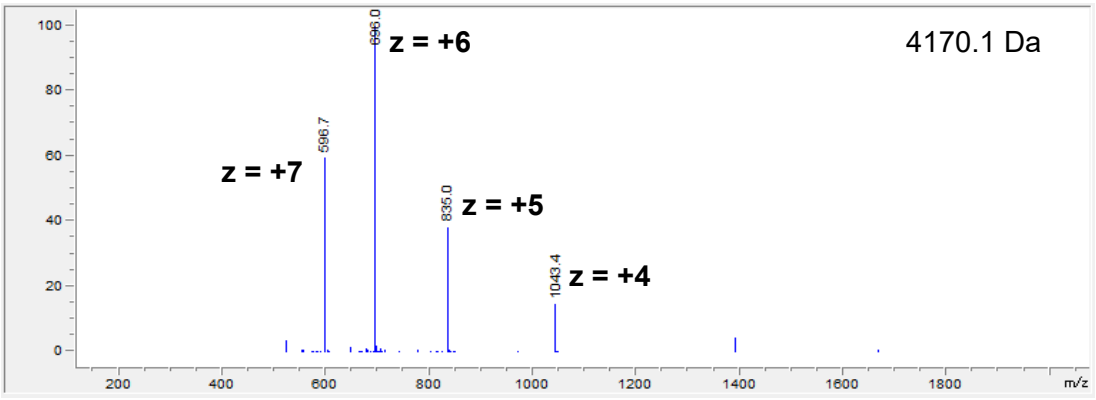

*PDIP-PEG3-PQ (**19**)*

Prepared with PDIP-Az **1** and primaquine-PEG3-alkyne **7** on a 0.85 µmol scale (4.1 mg peptide) and 10% DMSO/90% aqueous conjugation conditions. Purification with semi-preparative HPLC (10 to 50% MeCN over 40 minutes) yielded **19** (1.10 mg, 24%) as a light-yellow solid.

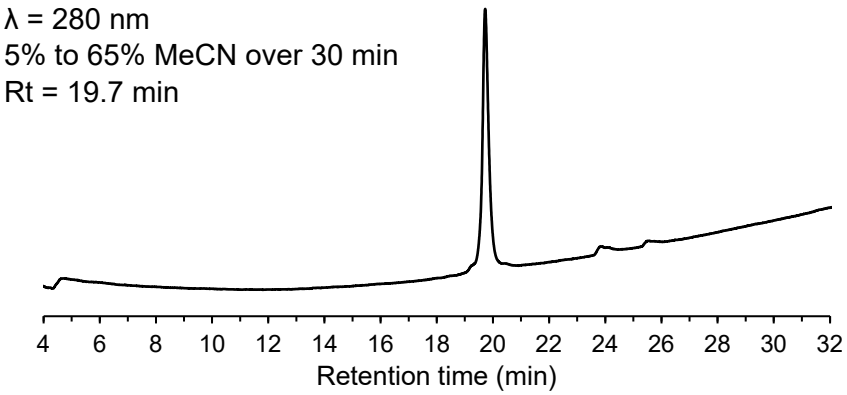

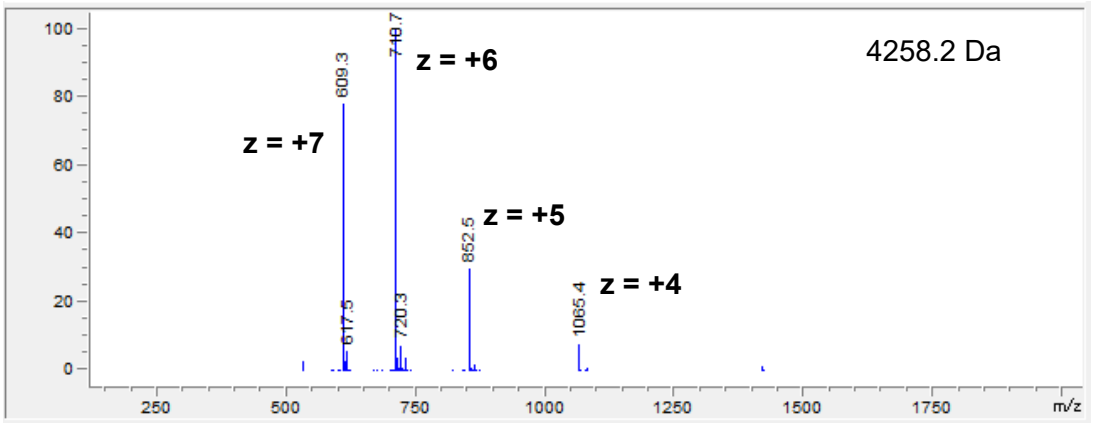

*PDIP-O-PQ (**S4**)*

Prepared with PDIP-Az **1** and primaquine-*O*-alkyne **S9** on a 0.44 µmol scale (2.1 mg peptide) and 10% DMSO/90% aqueous conjugation conditions. Purification with semi-preparative HPLC (20 to 50% MeCN over 40 minutes) yielded **S4** (0.96 mg, 41%) as a light-yellow solid.

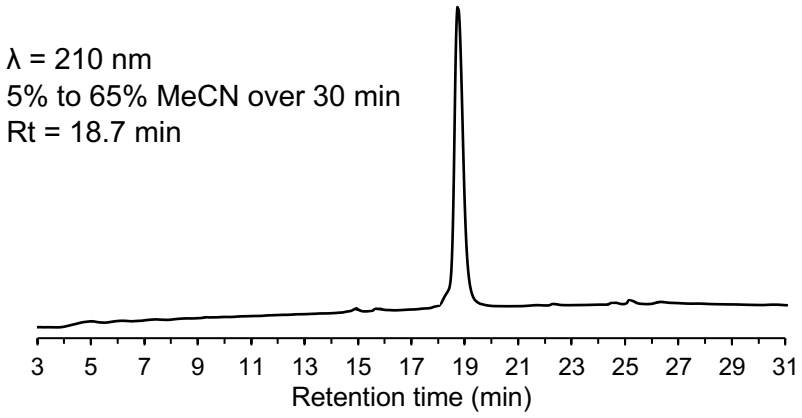

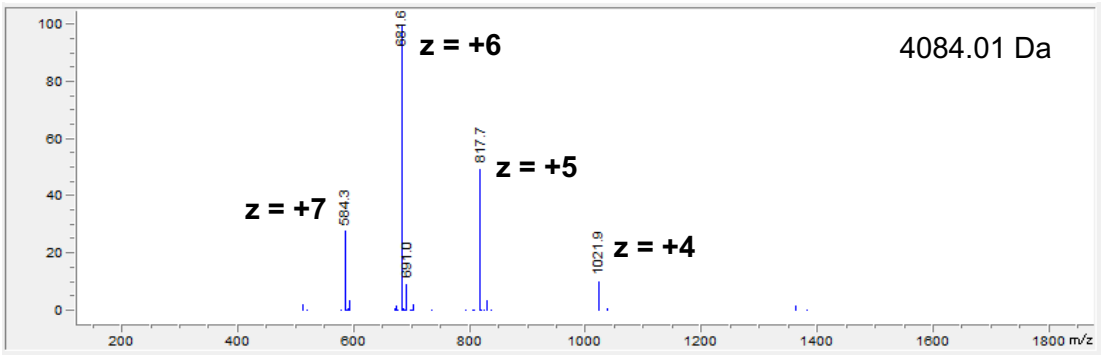

General procedure: SPAAC conjugation

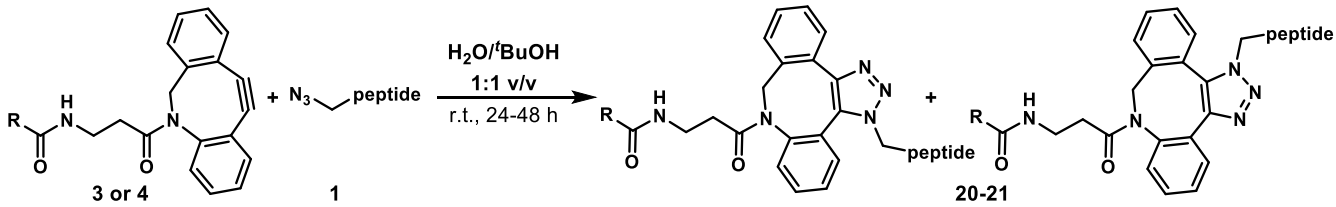

Following a procedure adapted from Lau *et al.*:[9] PDIP-Az **1** (1.0 equiv.) and drug-alkyne (**3** or **4**, 2.0 equiv.) were dissolved in water/*t*-butanol (1:1 v/v, 0.7-0.8 mM with respect to the peptide). The mixture was stirred for 24 – 48 h to produce two regioisomers that were purified by reverse-phase semi-preparative HPLC. Reported yields were determined by weight on a microbalance and were calculated using the mass of the TFA salt of the product (assuming all basic residues and the N-terminal amine are protonated).

*PDIP-DBCO-SS-PQ (**20**)*

Prepared with PDIP-Az **1** and PQ-SS-DBCO **3** on a 0.31 µmol scale (1.5 mg peptide). Purification with semi-preparative HPLC (20 to 65% MeCN over 40 minutes) yielded **20** (1.15 mg, 65%) as a light-yellow solid. The two regioisomers were collected together.

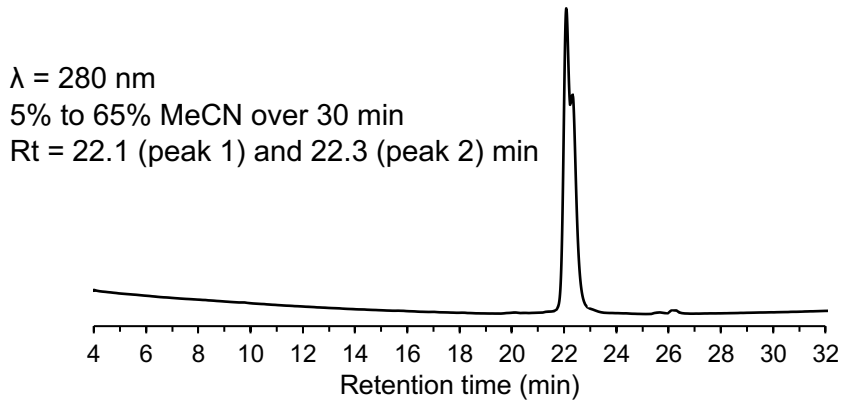

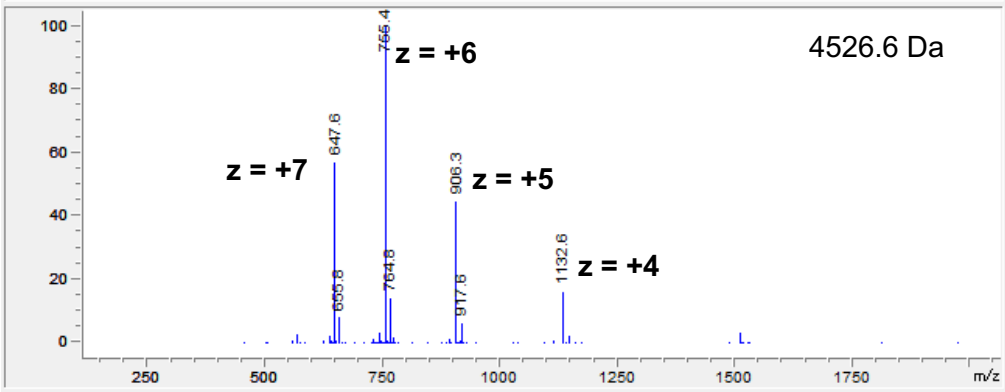

*PDIP-DBCO-trioxolane-PQ (**21**)*

Prepared with PDIP3-Az **1** and PQ-triox-DBCO **4** on a 0.87 µmol scale (4.2 mg peptide). Purification with semi-preparative HPLC (20 to 65% MeCN over 40 minutes) yielded **21** (3.64 mg, 72%) as a light-yellow solid. The two regioisomers were collected together.

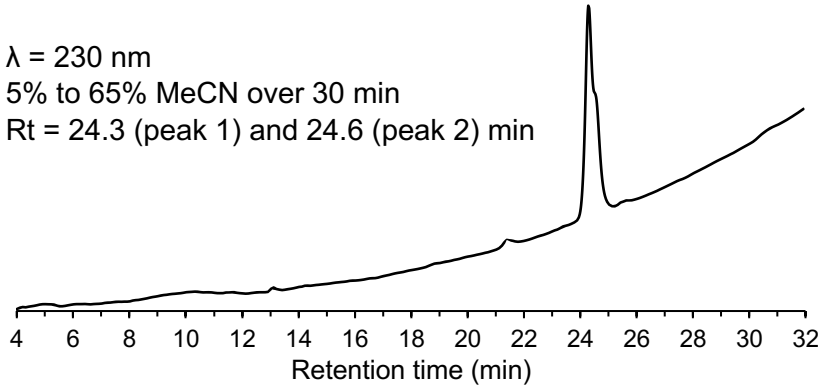

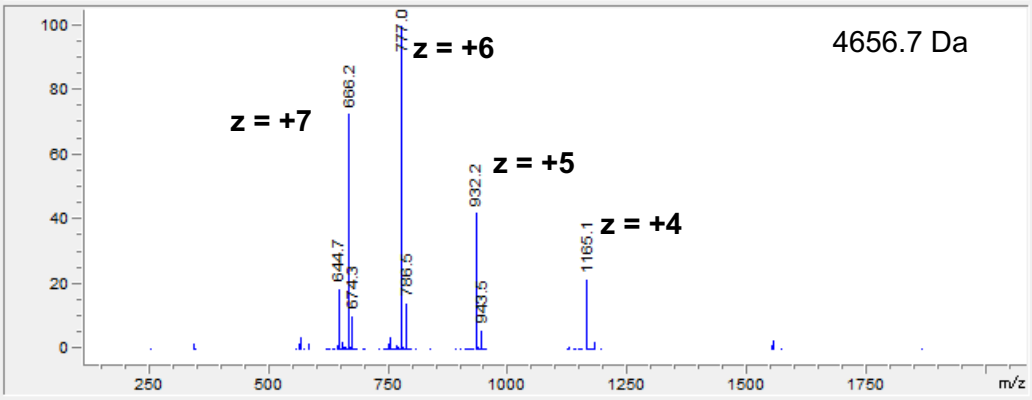

cPDIP-SS-PQ (S5) synthesis

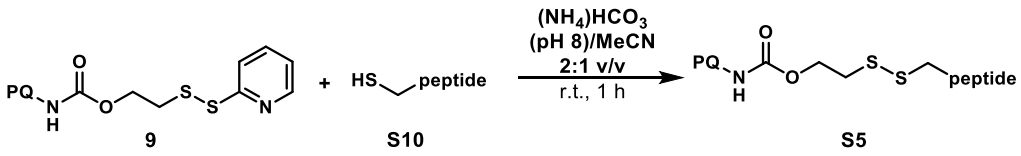

Following a procedure adapted from Zhou *et al.*:[6] cPDIP **S10** (3.2 mg, 0.66 µmol, 1.0 equiv.) was dissolved in argon purged H_2O (2 mL). This solution was transferred to a flask containing **9** (0.8 mg, 1.7 µmol, 2.5 equiv.) in argon purged MeCN (2 mL), followed by the addition of an argon purged 200 mM ammonium bicarbonate solution (pH 8, 2 mL). The mixture was magnetically stirred at room temperature for 1 h, then concentrated under a stream of nitrogen and purified by reverse-phase semi-preparative HPLC (25 to 50% MeCN over 40 min) to afford **S5** (1.7 mg, 48%) as a light-yellow solid.

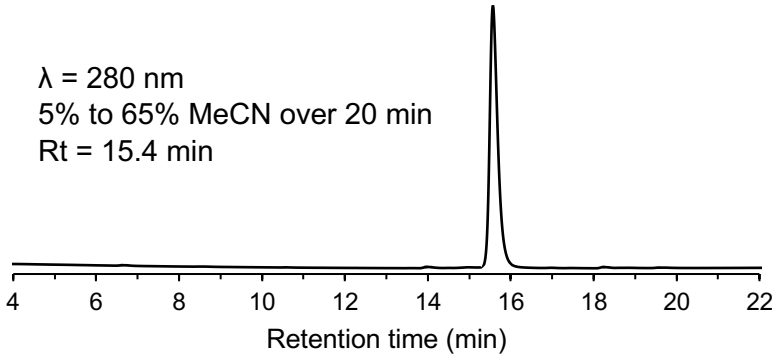

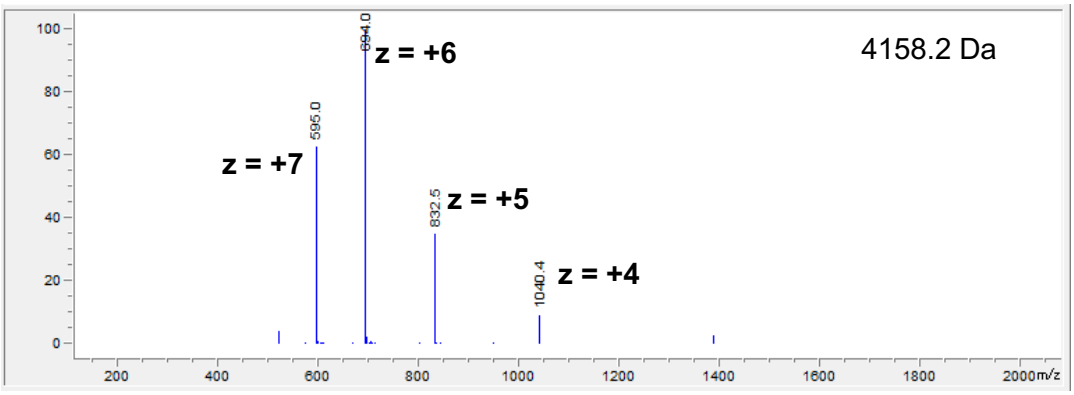

Cleavage studies to monitor drug release

A solution of **20** or **21** (20 µM, 1.0 equiv.) in phosphate buffer (1 mM, pH 7) was treated with either reduced glutathione (100 equiv.) or $Fe(II)Cl_2$ (100 equiv.), respectively. The solutions were incubated at 37 °C and aliquots were quenched at various time intervals with either MeCN (containing 0.1% formic acid) for tests containing **20** or EDTA (100 mM) for tests containing **21**. Samples were analyzed with reverse-phase LCMS (10 to 55% MeCN over 40 minutes, 0.01% formic acid) at λ = 214 nm and the peak corresponding to the conjugate was integrated using LabSolutions software. The data were then plotted on Prism (GraphPad Software) using one phase exponential decay.

***Plasmodium falciparum* culturing**

P. falciparum strain 3D7 was cultured as a 2.5% haematocrit solution by mixing O^+ human RBCs (300 µL) with complete culture medium (CCM, 12 mL), comprised of RPMI 1640 supplemented with 8.8 mM D-glucose, 22 mM HEPES, 208 nM hypoxanthine, 46.1 nM gentamicin, 2.8 mM L-glutamine (all from Sigma-Aldrich, Castle Hill, Australia), 2.1 g/L AlbuMAX® I (ThermoFisher Scientific, Australia) and 4.2% (v/v) O^+ human serum. The RBCs and serum were provided by the Australian Red Cross Lifeblood, obtained from anonymous blood donors (aged 18-60 years). Cultures were maintained in 25 cm^3 flasks filled with a low oxygen gas mixture ($1\%O_2/3\%CO_2/96\%N_2$) and

kept in an orbital shaking incubator at 50 rpm at 37 °C. Culture parasitaemia was maintained between 0.2% and 10% and CCM was changed every 2-3 days.

Growth inhibition assays

Stock solutions of drug treatments were prepared in water (e.g., 1 mM). Treatment of parasites was conducted using solutions of each drug diluted in CCM to 5× the highest concentration required for the assay, followed by 2-fold serial dilutions. One day prior to assays, parasites were synchronized at the ring stage by incubating in 5% (w/v) D-sorbitol for 10 minutes at room temperature, followed by washing twice with warm red cell wash (10 mM sodium phosphate buffer, 160 mM NaCl, pH 7.4) and adding the cells into fresh CCM (12 mL) in a new flask. After a further 18-24 h incubation, the enriched rings developed into synchronized trophozoites, ready for use in the growth assays. An aliquot (10 µL) of each drug dilution and controls (10 µL CCM) were gently mixed with the 0.2% parasite culture (40 µL) in duplicate in a 96-well plate, to create a 5-fold dilution of the drug. Parasites were incubated with the treatments at 37 °C for 48 h in an airtight box filled with a low oxygen gas mixture (1%O_2/3%CO_2/96%N_2). Cells were subsequently fixed in 1% (w/v) formaldehyde (1:3 v/v Cytofix™ (BD Biosciences, Australia) diluted with phosphate buffered saline (PBS; 137 mM NaCl, 2.7 mM KCl, 10 mM Na_2HPO_4, 1.8 mM KH_2PO_4)) for at least 24 h at 4 °C.

Parasitemia levels in the fixed cells were determined using flow cytometry. Fixed cells were washed twice with PBS containing 1% (w/v) bovine serum albumin (BSA) and stained with 5 µg/mL Hoechst 33342 (Life Technologies, Australia) in 1% BSA/PBS for at least 15 minutes at 4 °C. Fluorescence signals of stained cells were measured using a LSR Fortessa cell analyzer (BD Biosciences) with at least 200,000 events (cells) collected per sample. Percentages of infected cells (i.e., parasitaemia) were identified and computed using FlowJo software (BD Biosciences). Percentage parasite growth inhibition was determined from parasitaemia counts using the formula:

$$\text{Parasite growth inhibition (\%)} = 100 - \left(\frac{\text{treatment parasitaemia}}{\text{untreated parasitaemia}} \times 100\right)$$

The IC_{50} data was determined for each treatment with Prism (GraphPad Software) using nonlinear regression of a dose-response curve.

^{1}H and $^{13}C\{^{1}H\}$ NMR

400 MHz ^{1}H NMR in $CDCl_3$

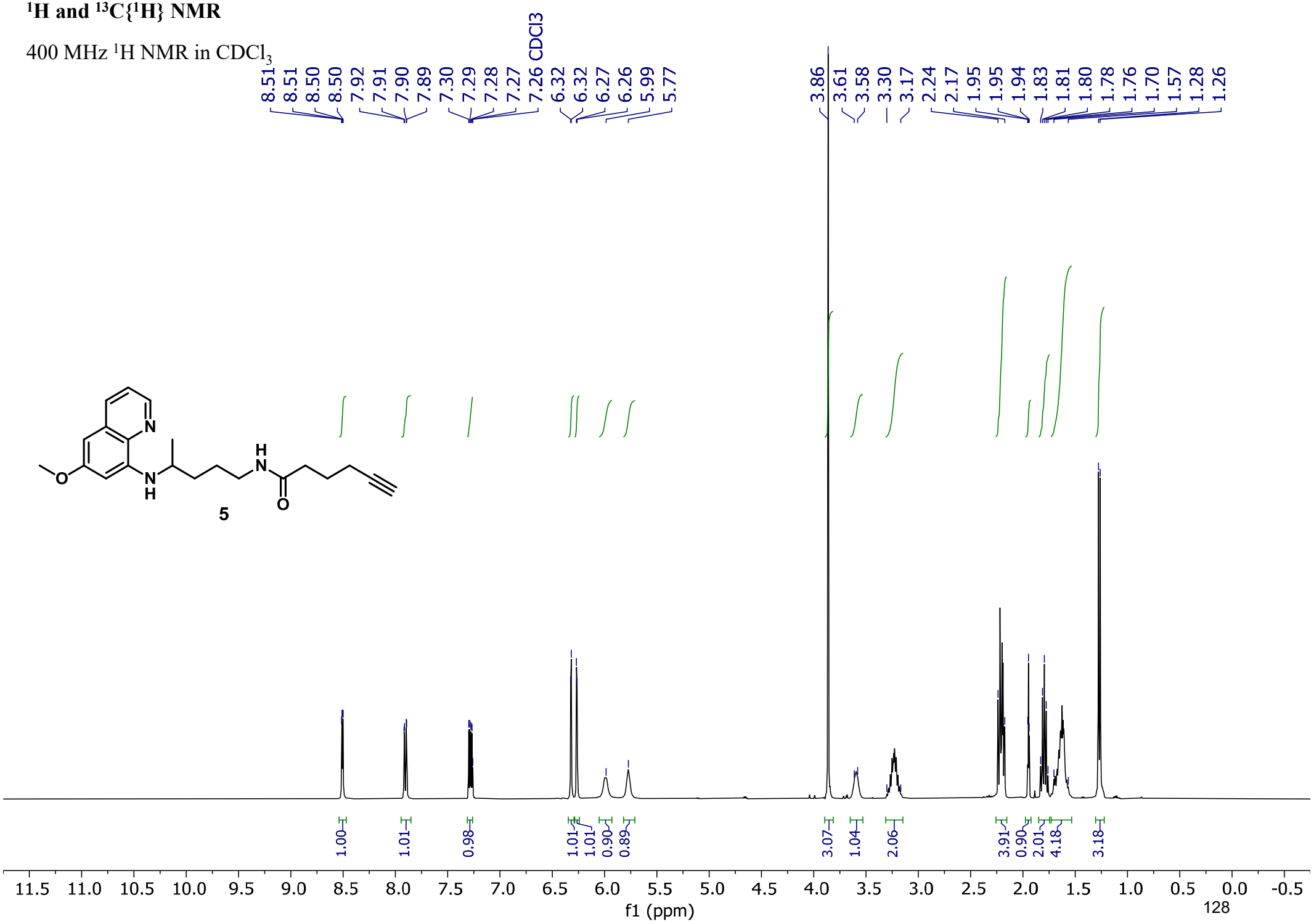

5

101 MHz ^{13}C NMR in $CDCl_3$

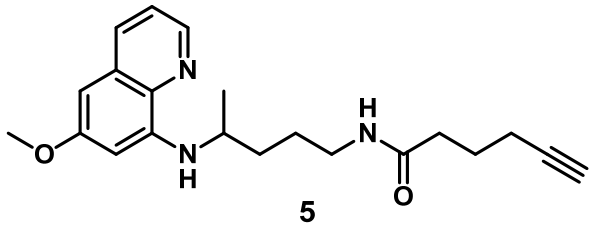

5

400 MHz ^{1}H NMR in CD_3CN

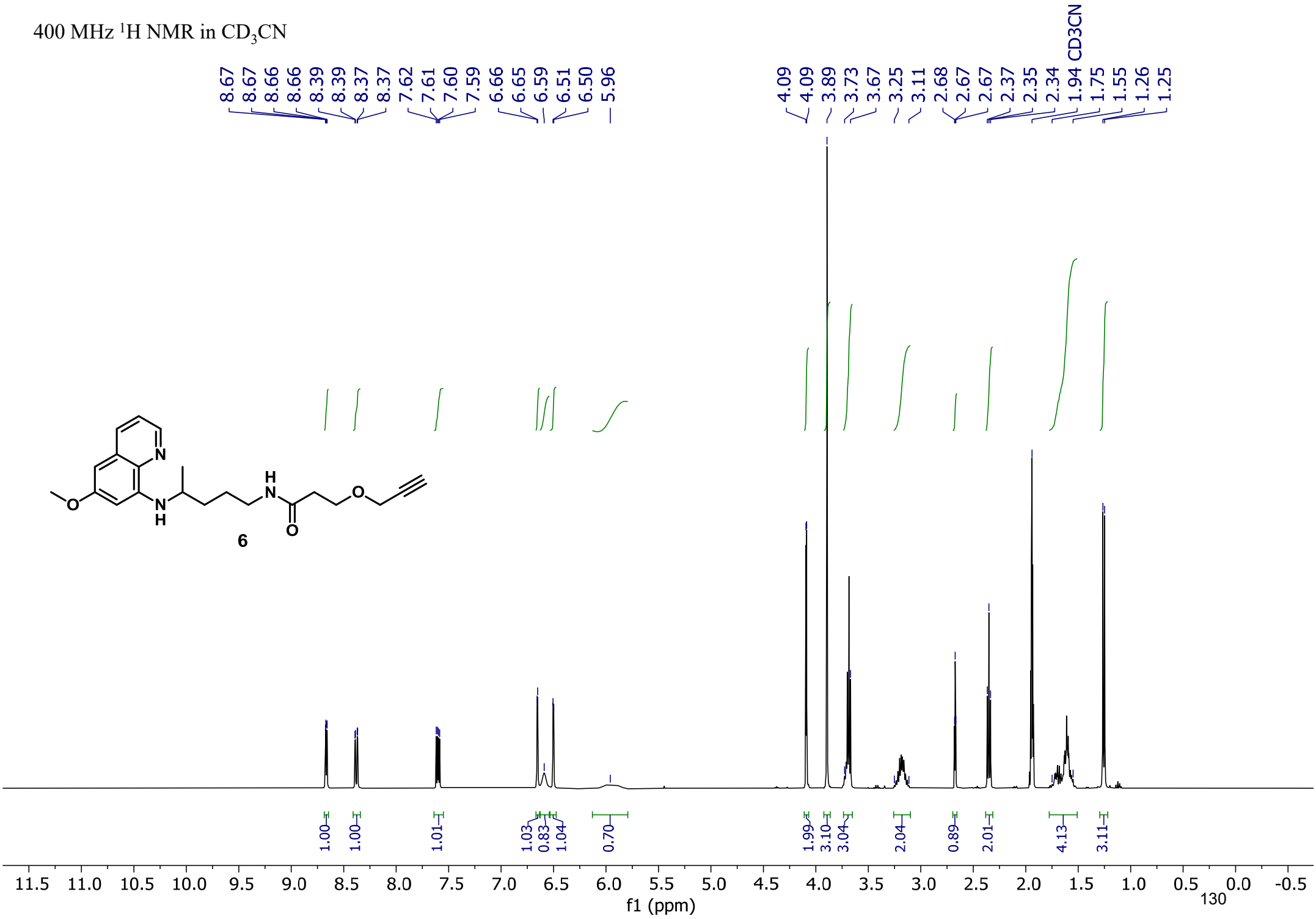

151 MHz ^{13}C NMR in CD_3CN

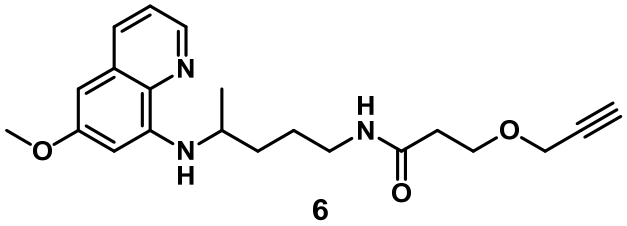

6

700 MHz ^{1}H NMR in $CDCl_3$

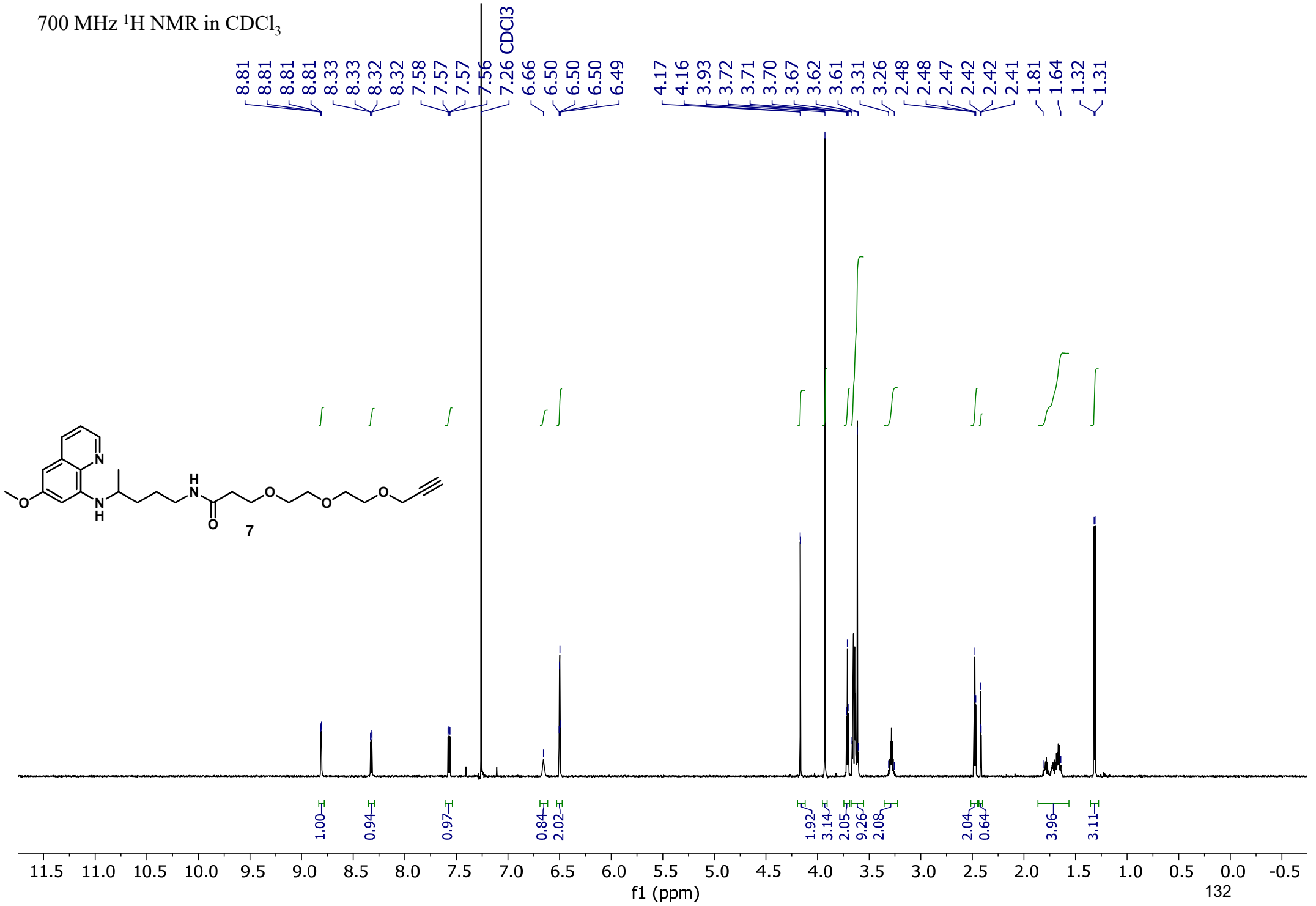

7

176 MHz ^{13}C NMR in $CDCl_3$

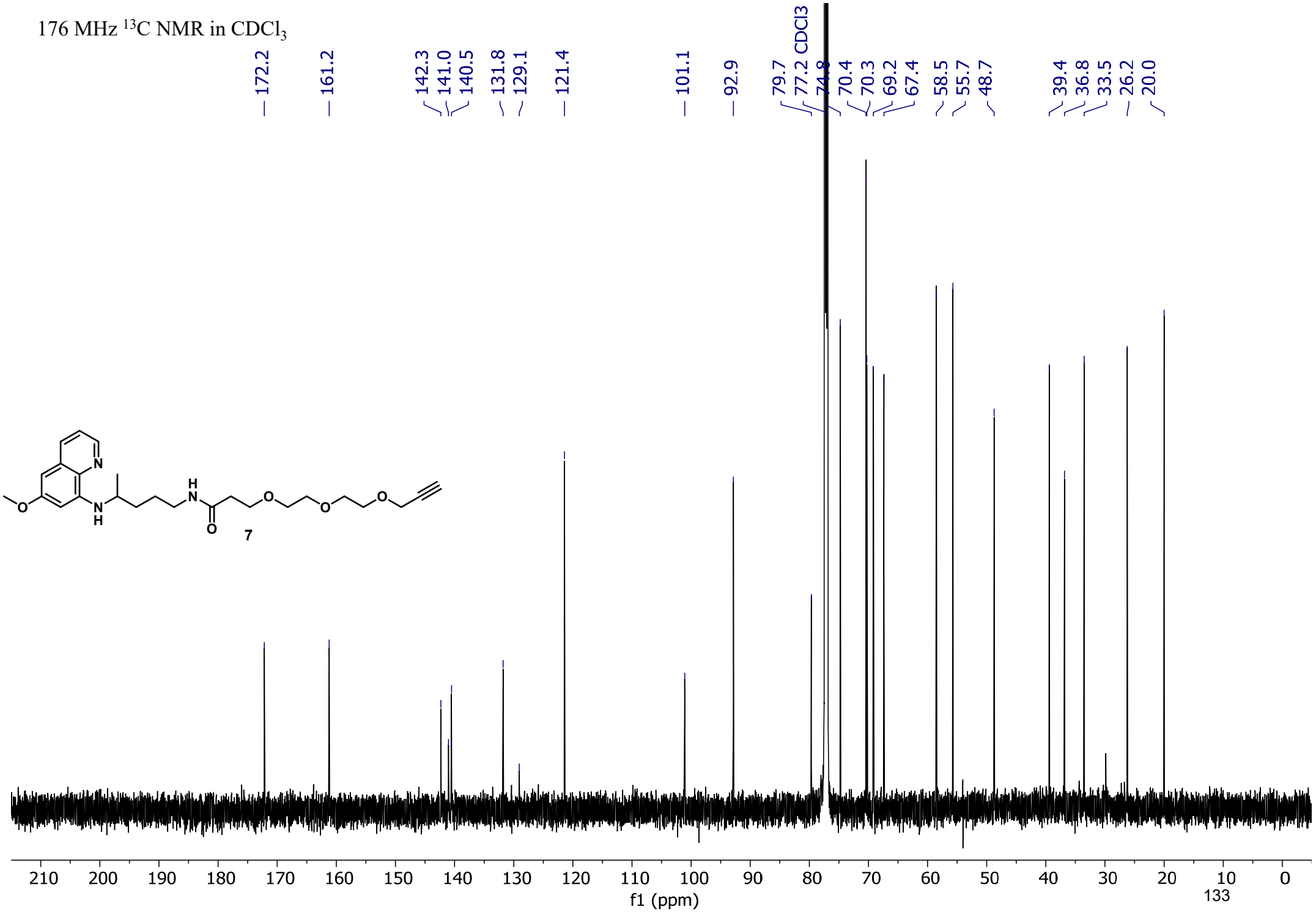

400 MHz ^{1}H NMR in $CDCl_3$

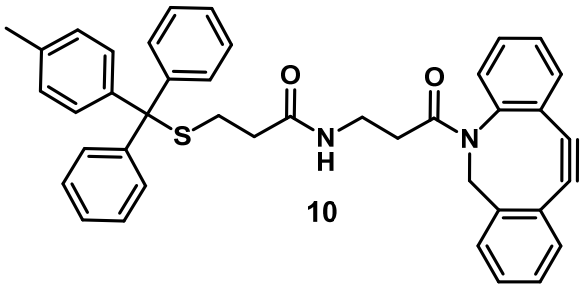

10

*H_2O

*grease

f1 (ppm)

101 MHz ^{13}C NMR in $CDCl_3$

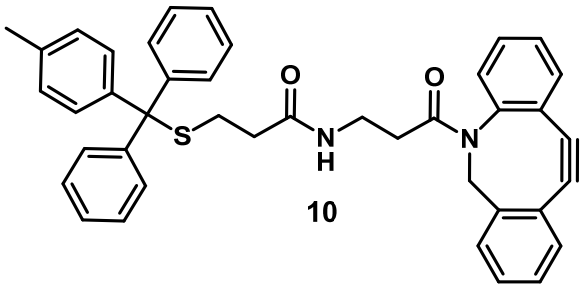

10

400 MHz ^{1}H NMR in $CDCl_3$

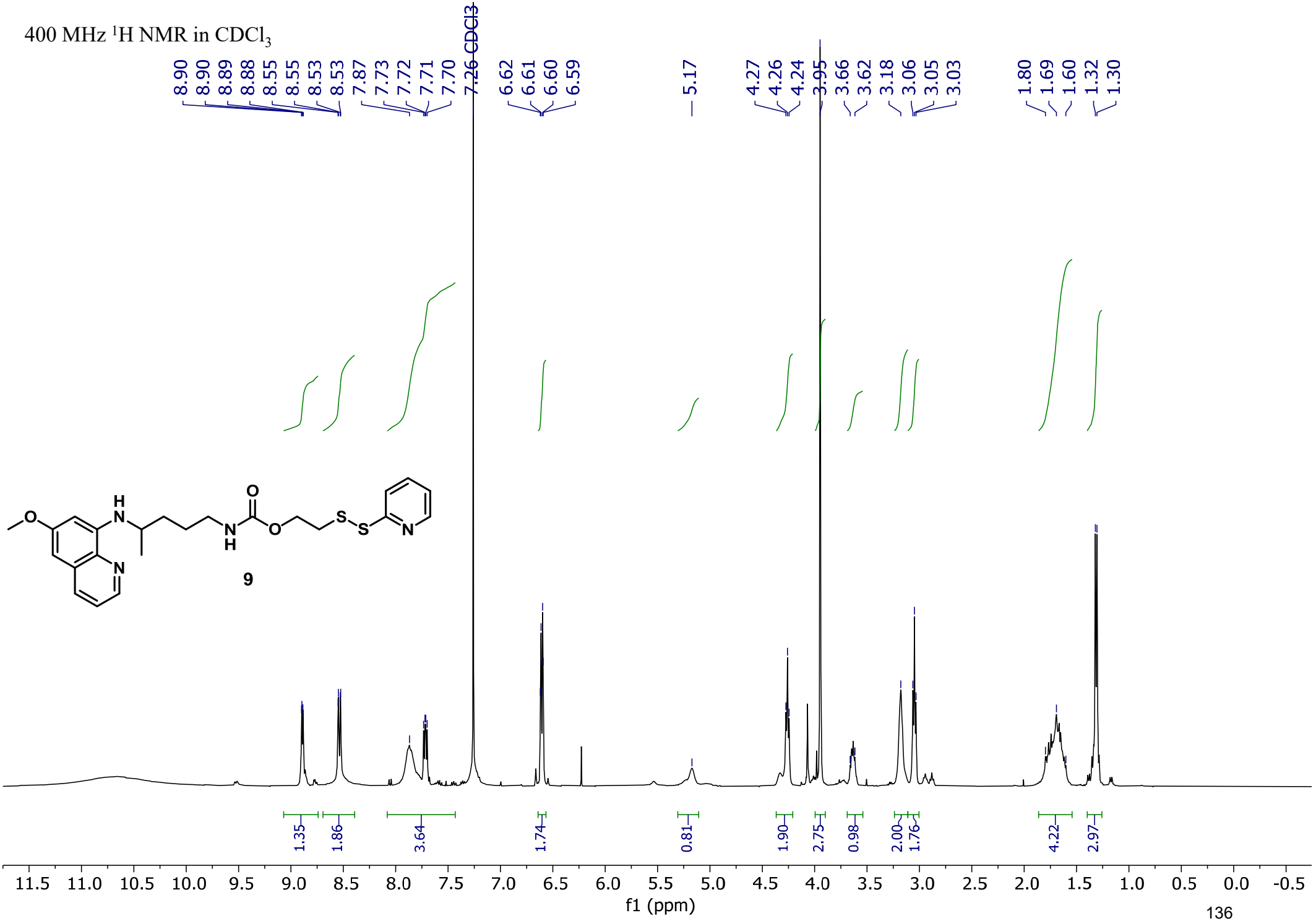

9

101 MHz ^{13}C NMR in $CDCl_3$

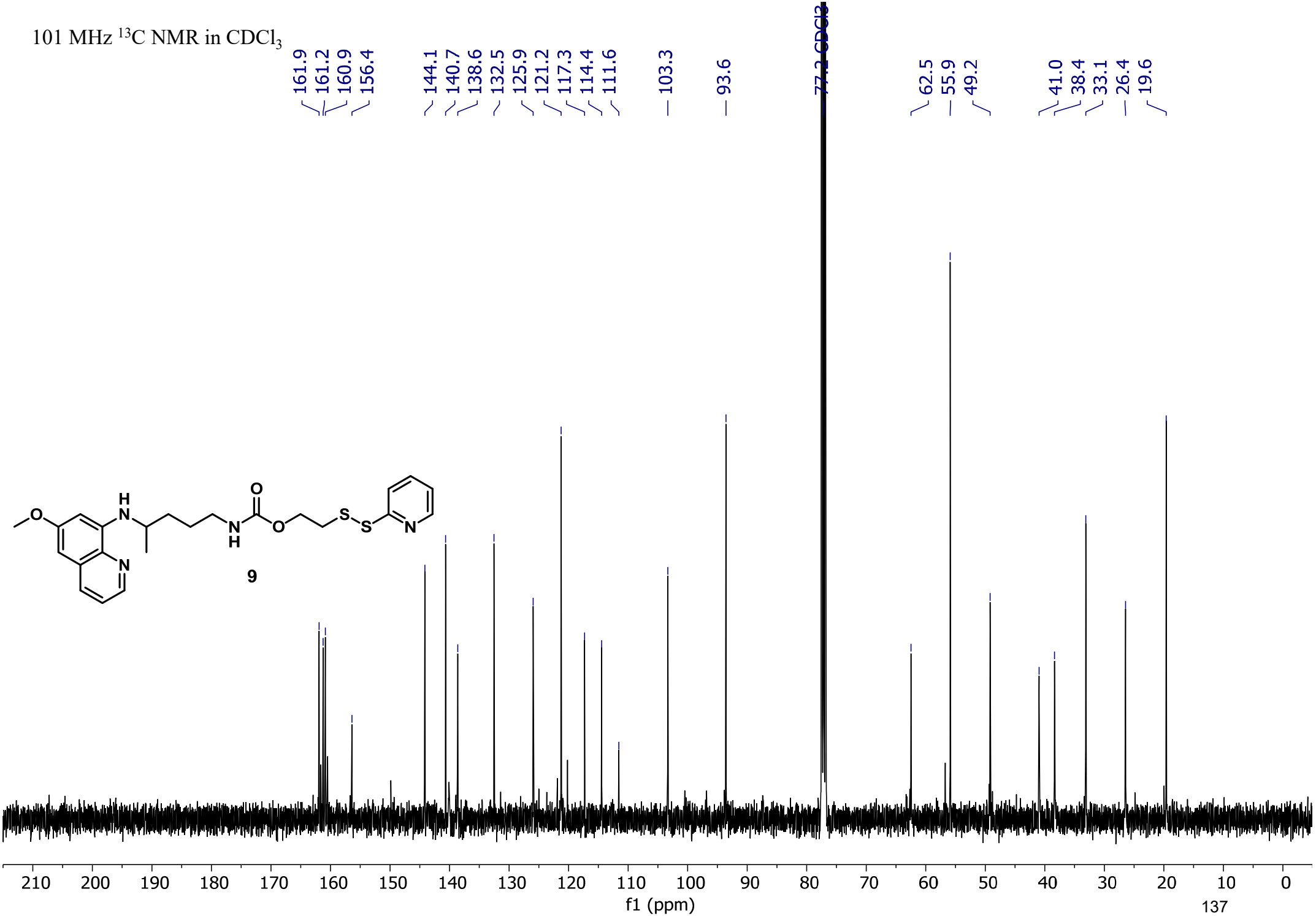

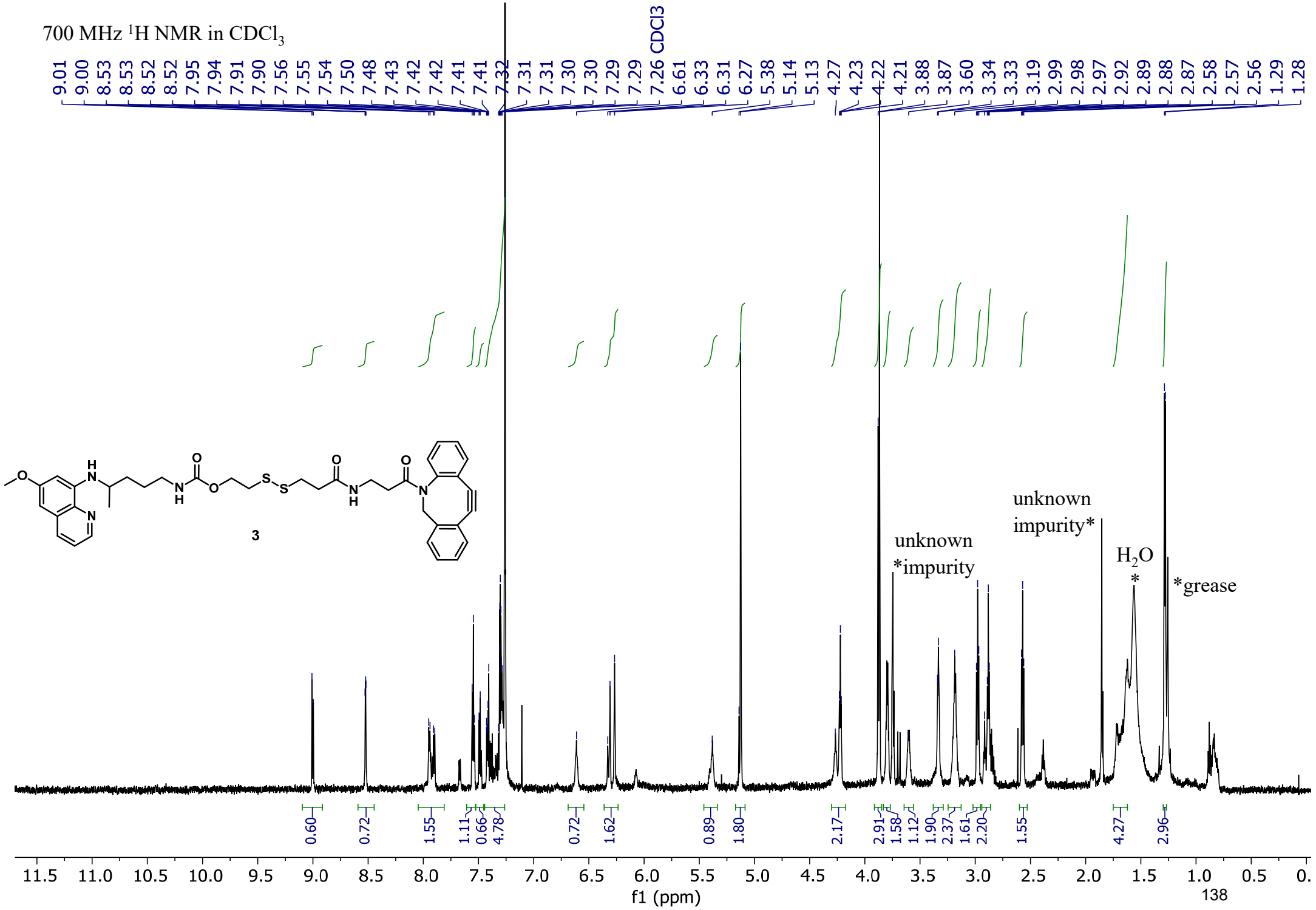
700 MHz ^{1}H NMR in $CDCl_3$
CDCl3
unknown
*impurity
unknown
impurity*
H_2O
*
*grease
3
f1 (ppm)

400 MHz ^{1}H NMR in $CDCl_3$

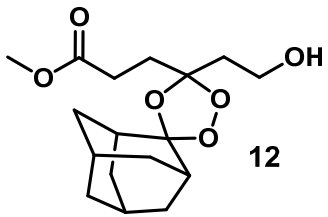

12

101 MHz ^{13}C NMR in $CDCl_3$

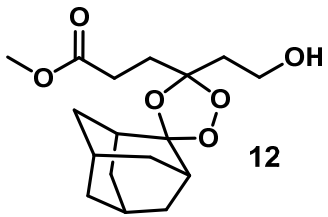

12

400 MHz ^{1}H NMR in $CDCl_3$

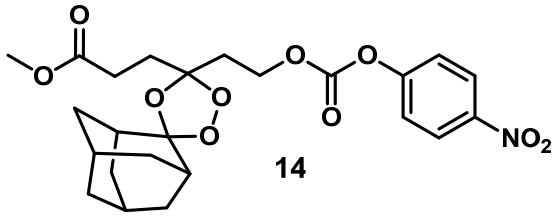

14

700 MHz ^{1}H NMR in $CDCl_3$

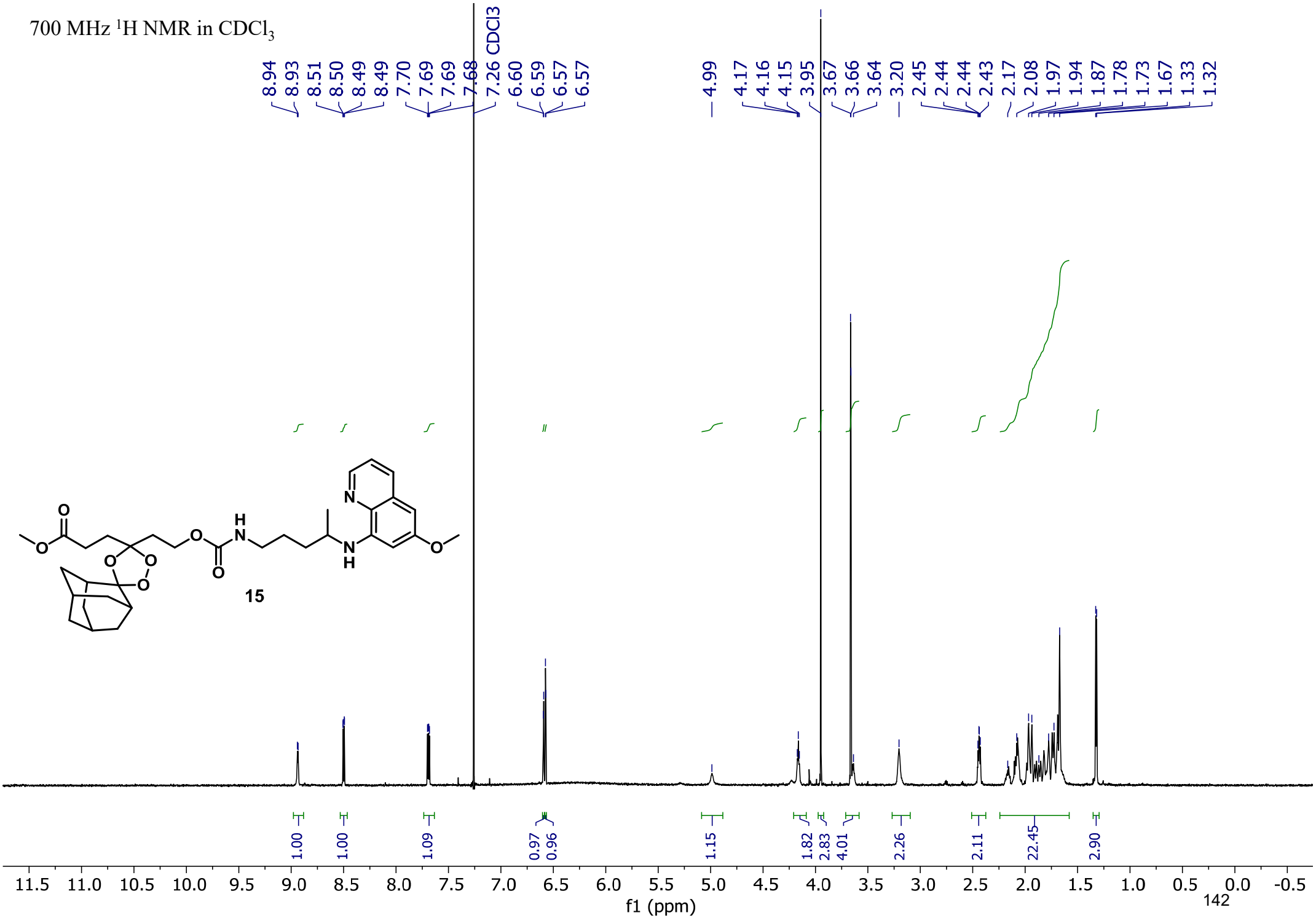

176 MHz ^{13}C NMR in $CDCl_3$

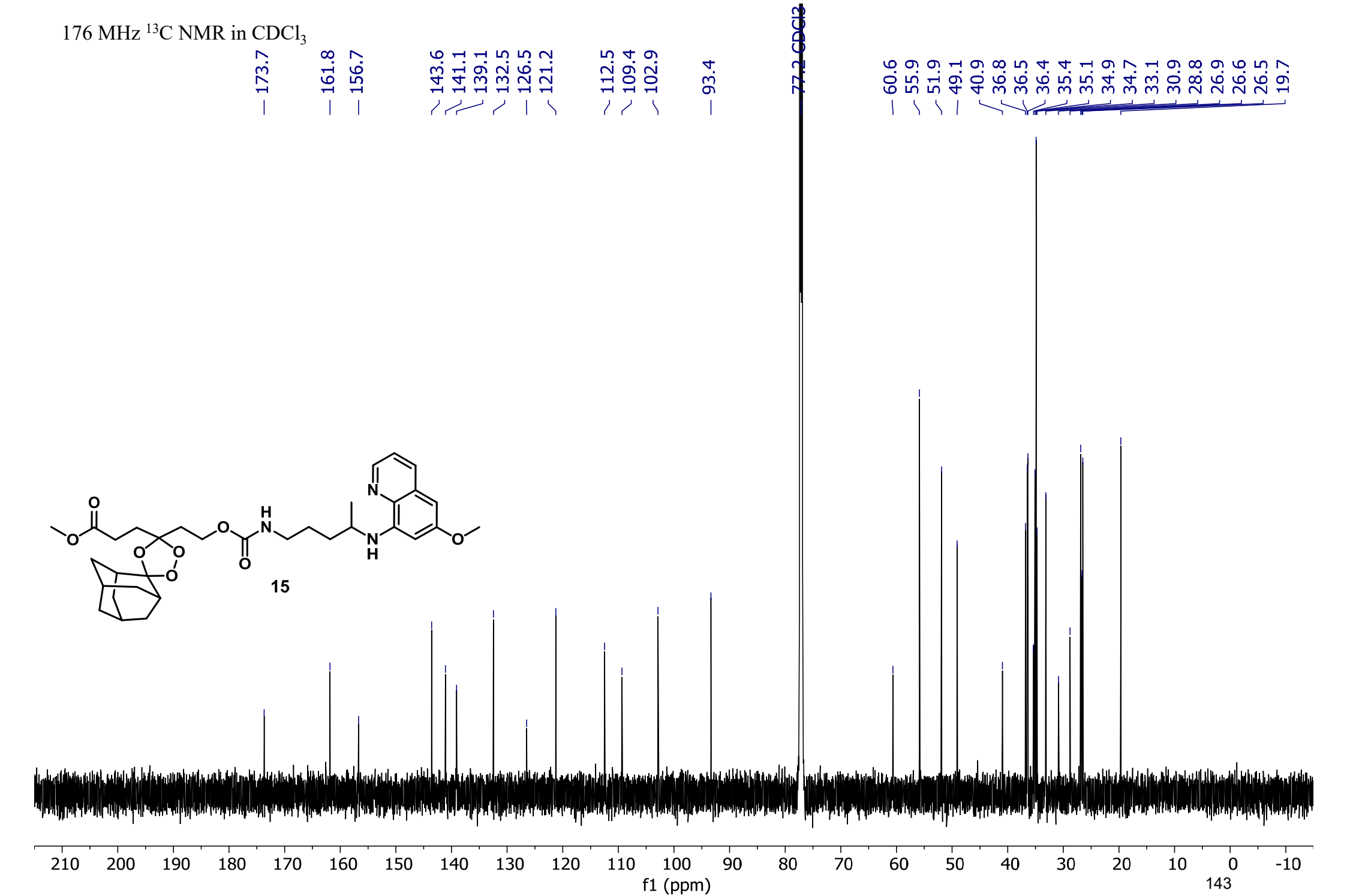

700 MHz ^{1}H NMR in $CDCl_3$

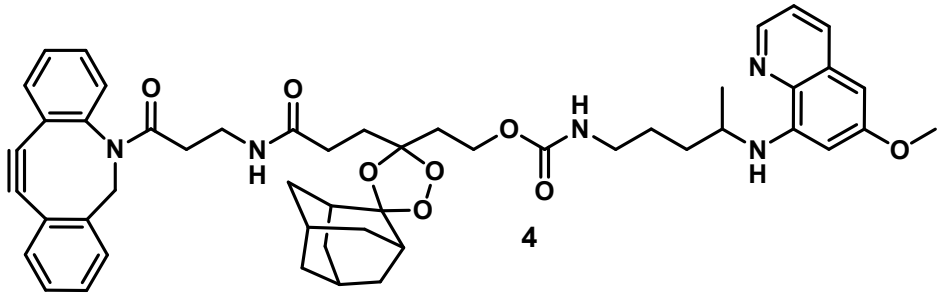

4

400 MHz ^{1}H NMR in CD_3OD

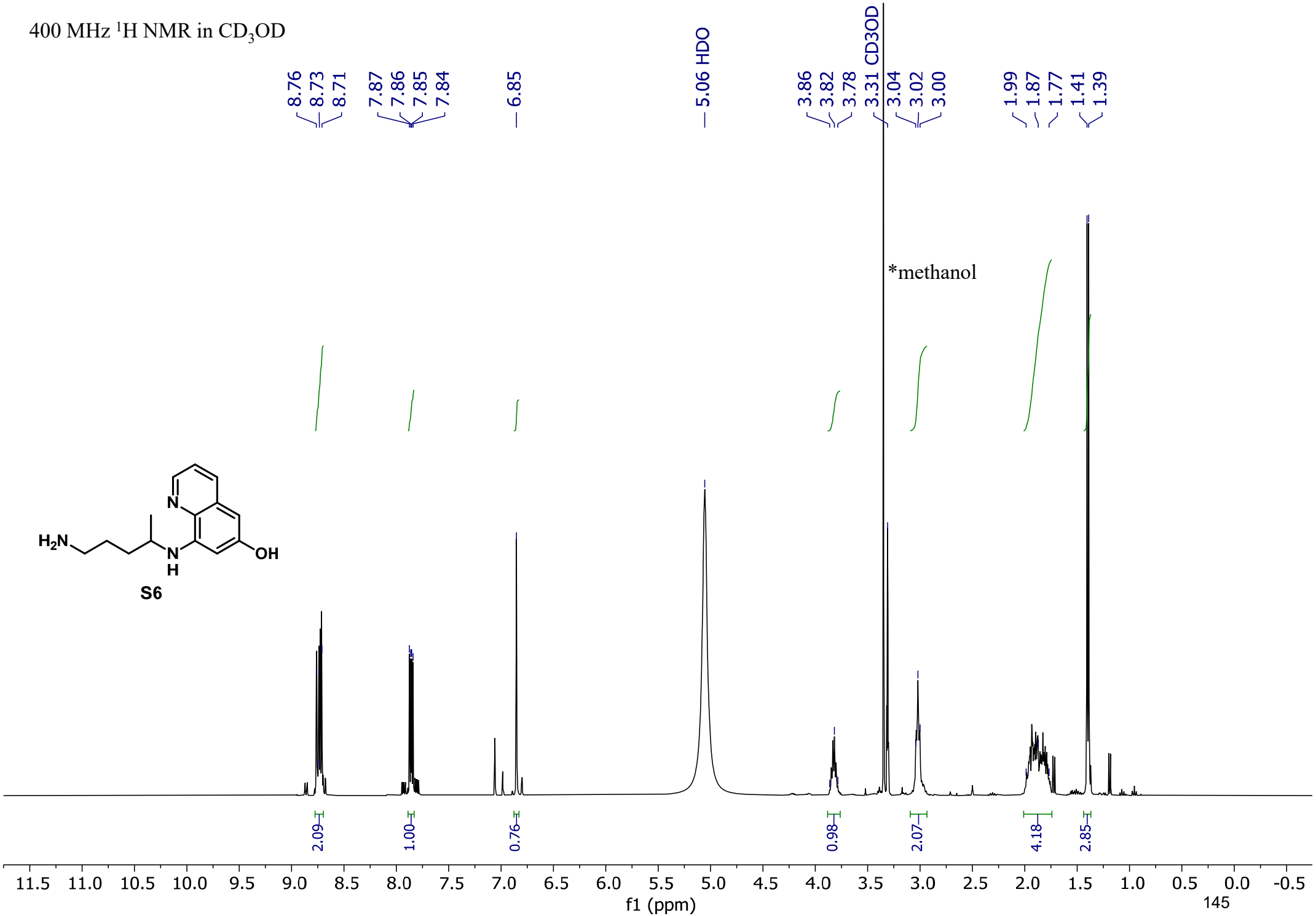

S6

101 MHz ^{13}C NMR in CD_3OD

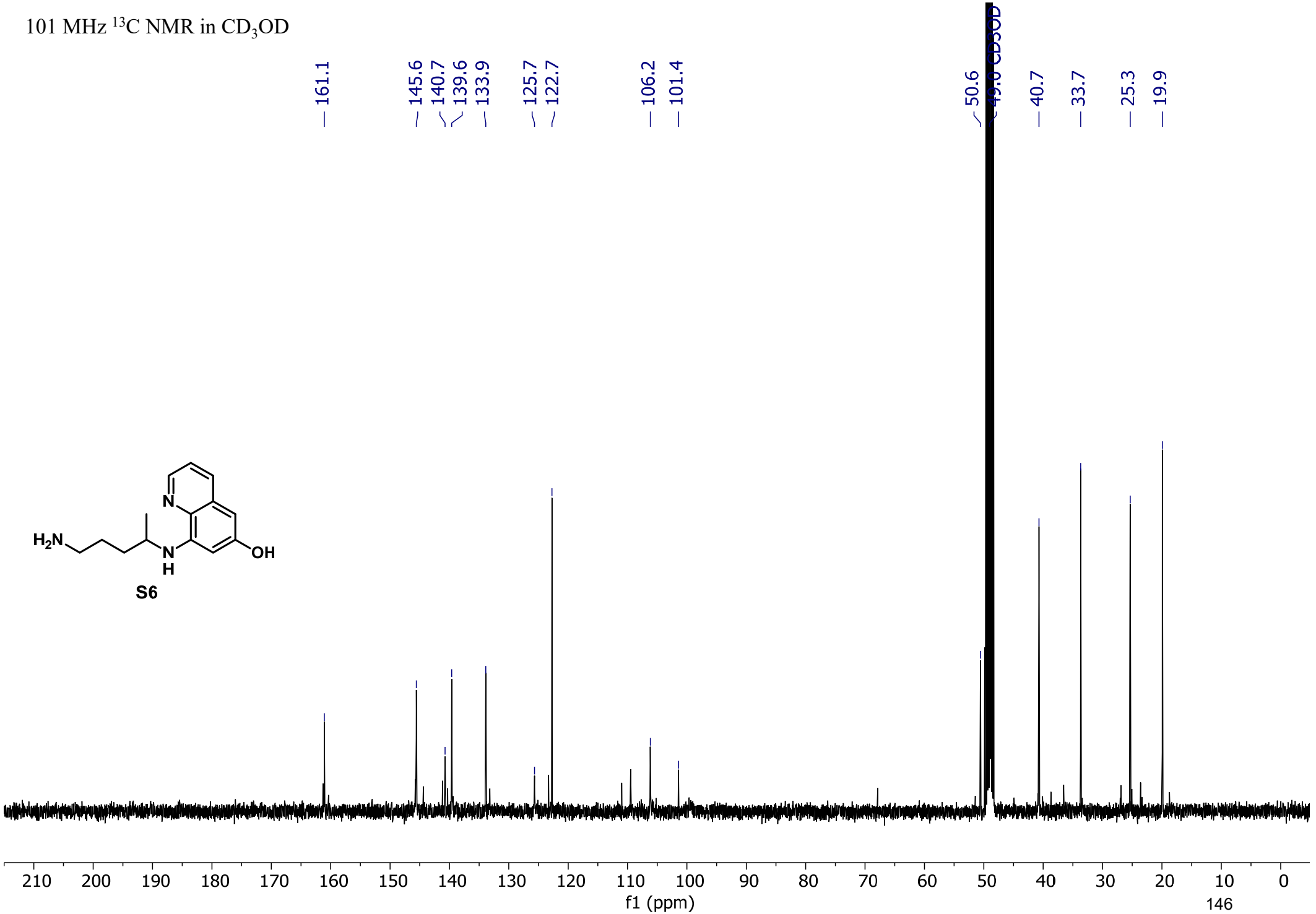

400 MHz ^{1}H NMR in CD_3OD

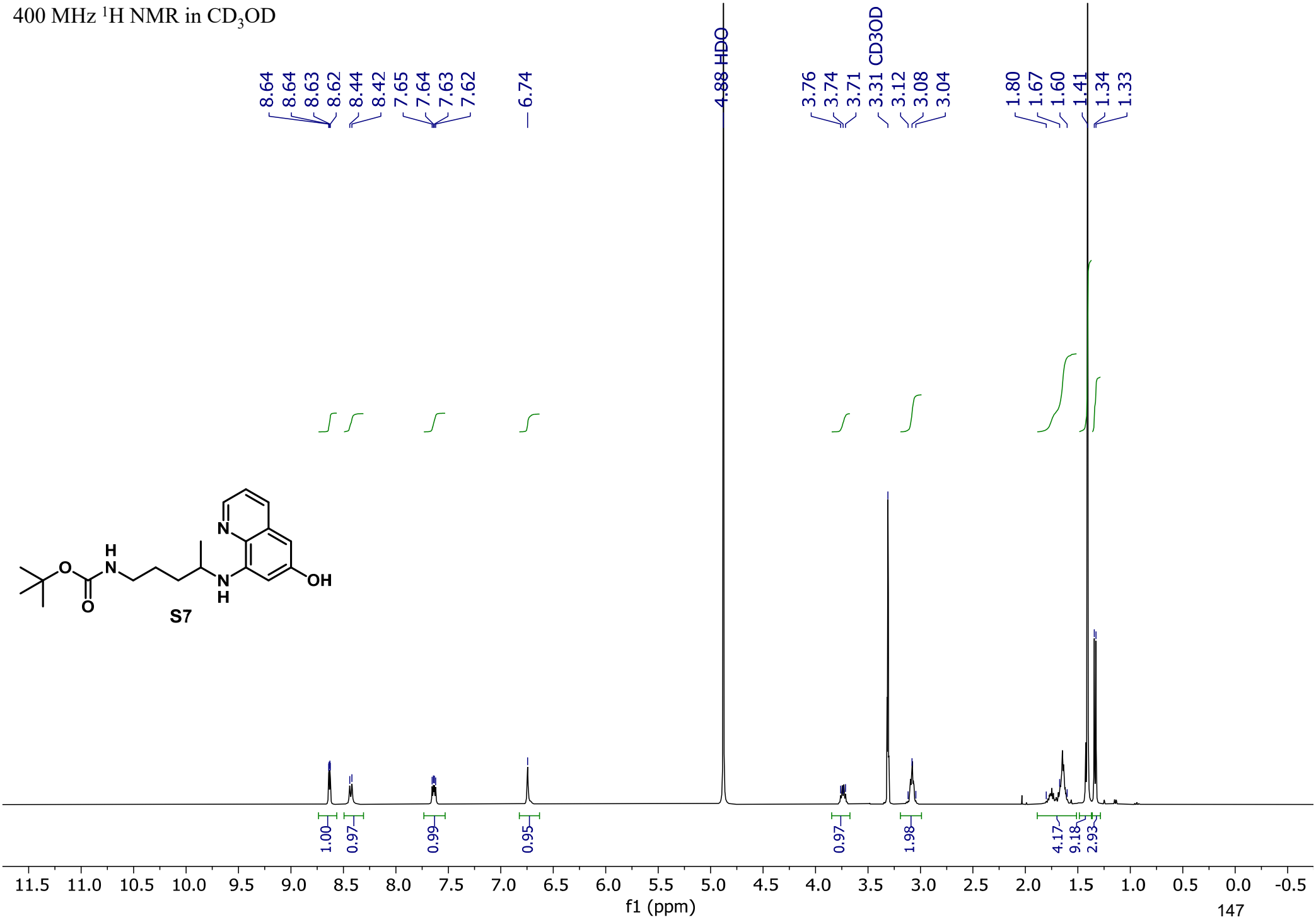

S7

101 MHz ^{13}C NMR in CD_3OD

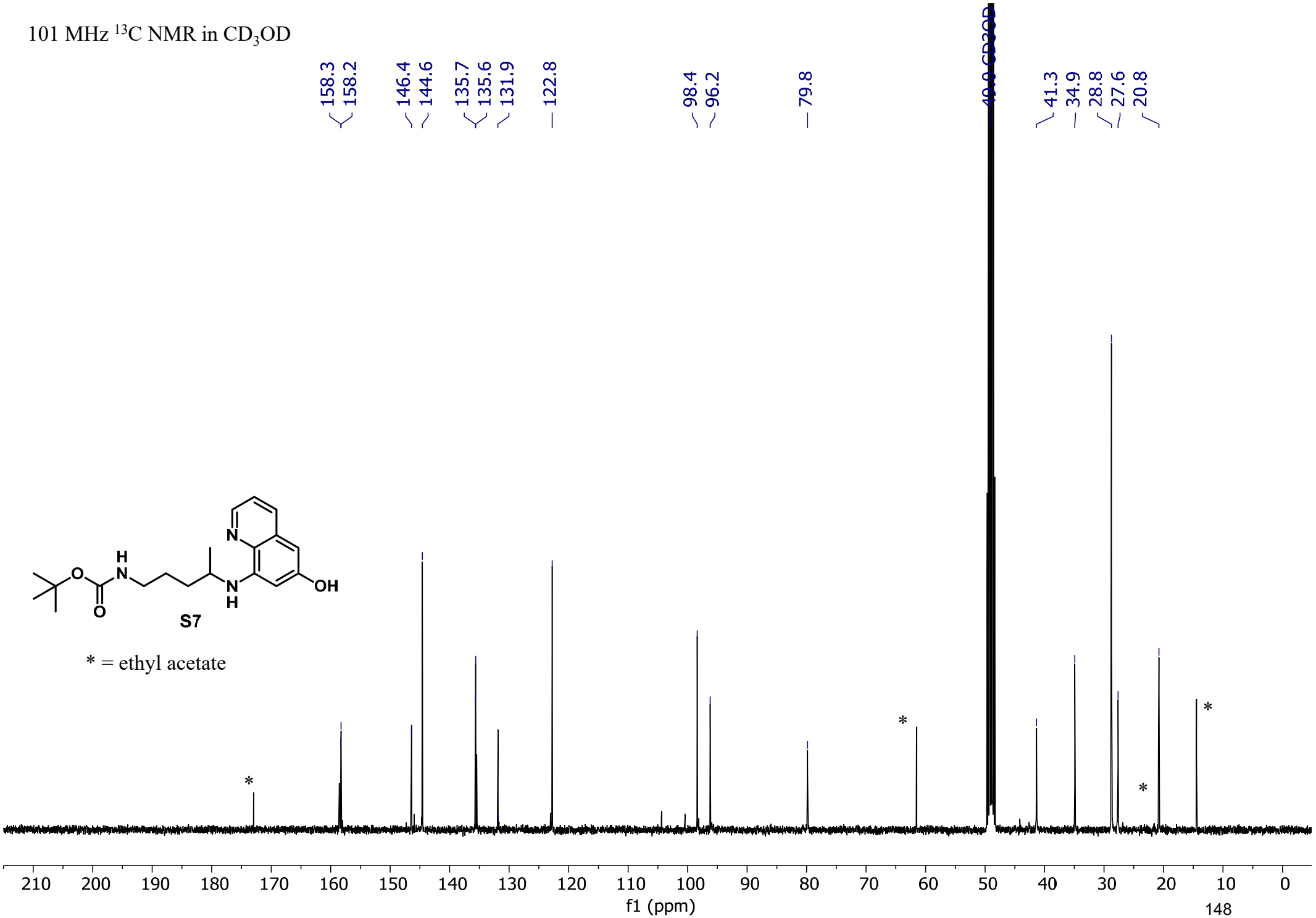

400 MHz, 101 MHz HSQC NMR
Spectrum of **S7** (recorded in CD_3OD)

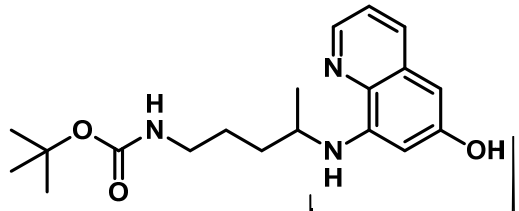

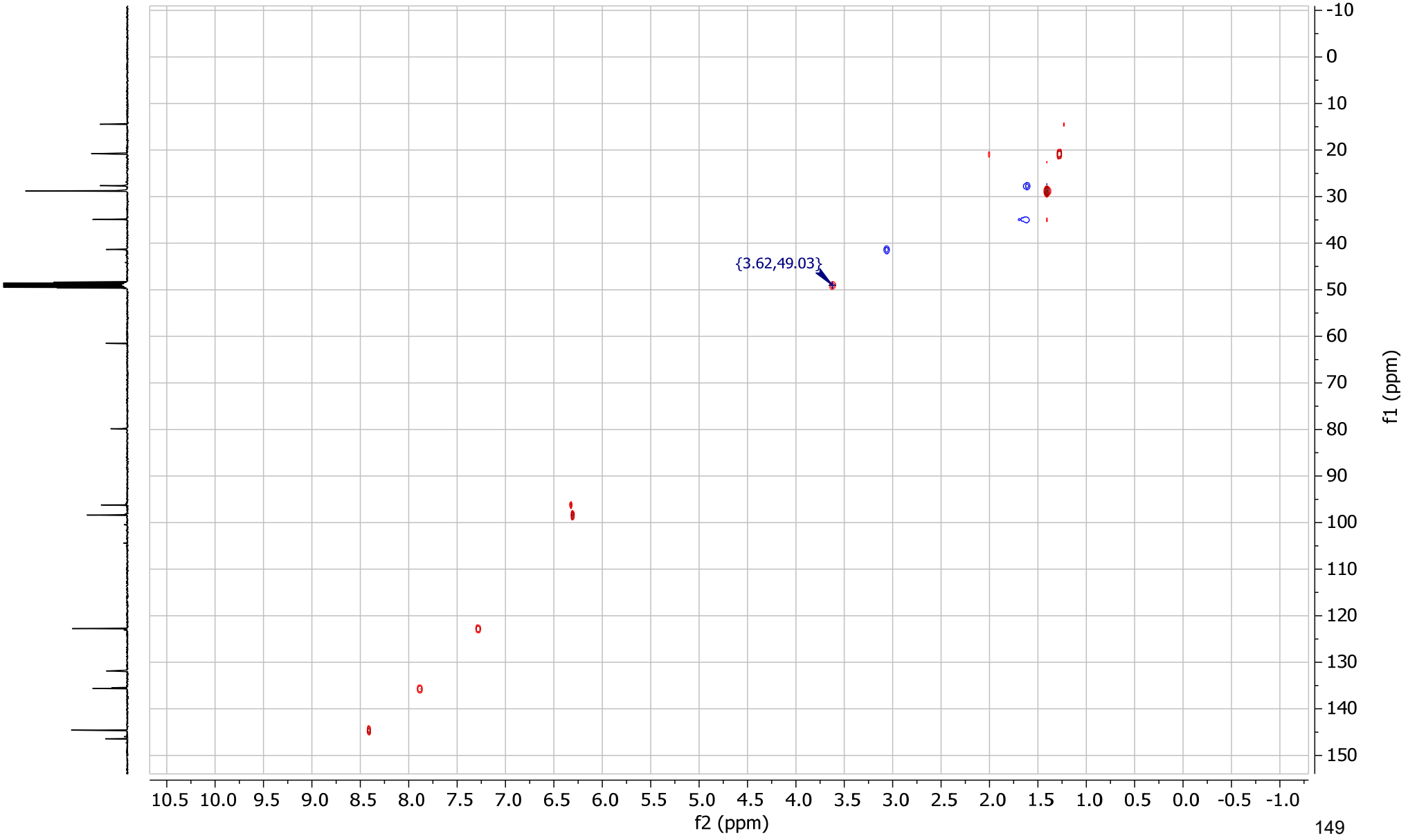

400 MHz ^{1}H NMR in $CDCl_3$

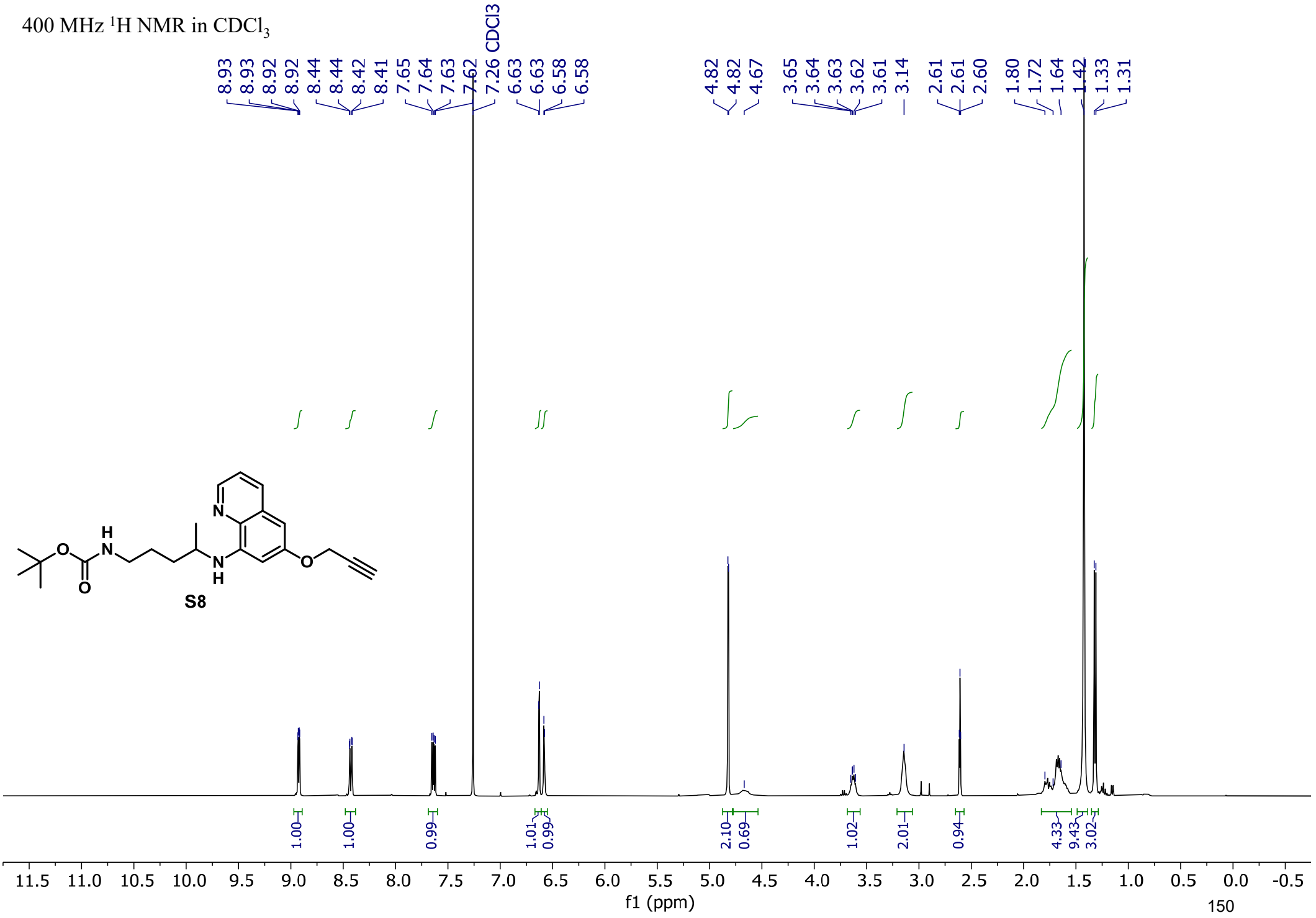

101 MHz ^{13}C NMR in $CDCl_3$

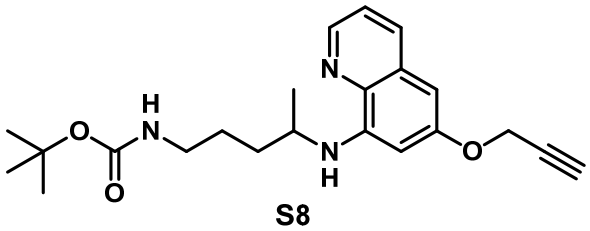

S8

400 MHz ^{1}H NMR in $CDCl_3$

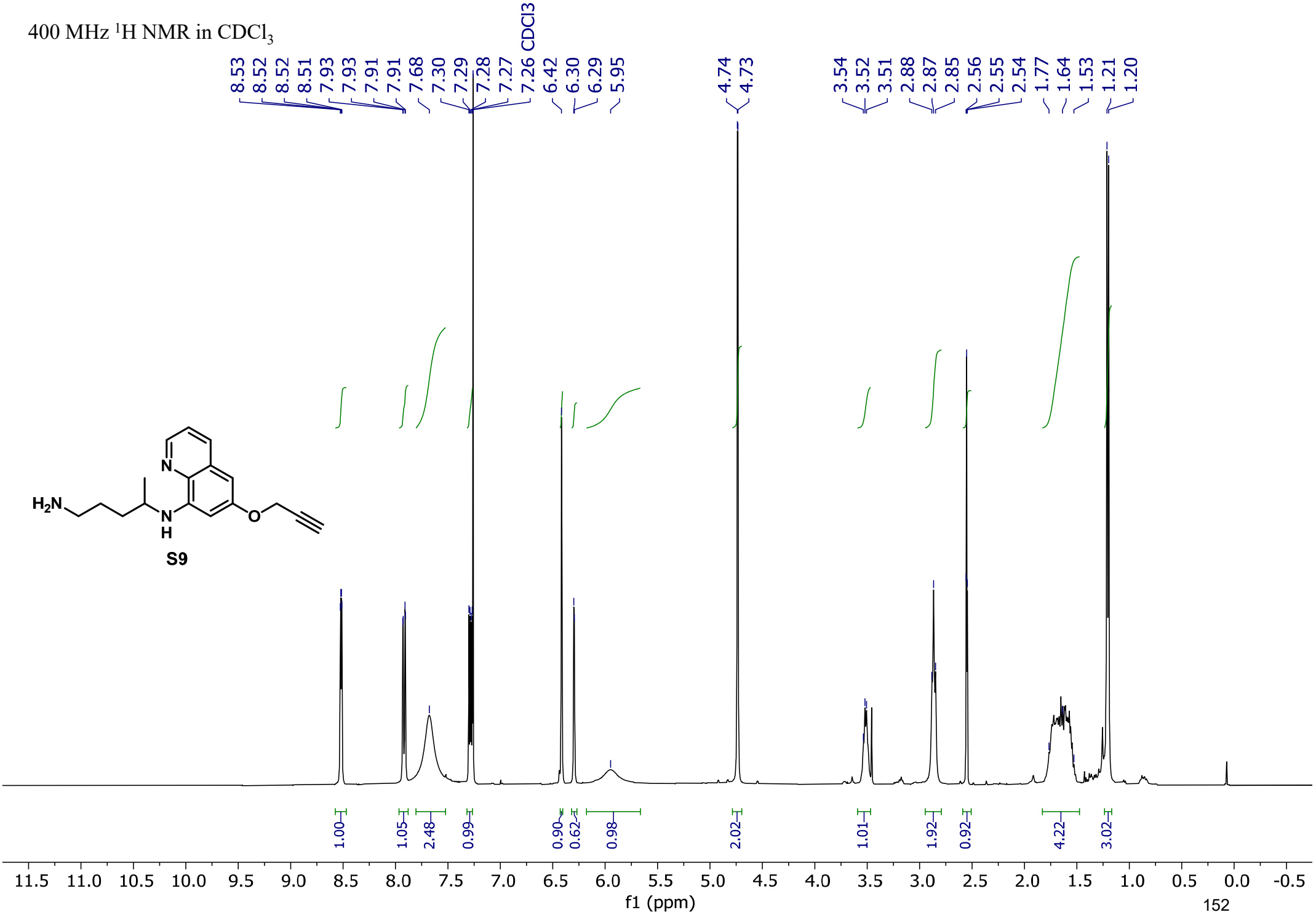

S9

101 MHz ^{13}C NMR in $CDCl_3$

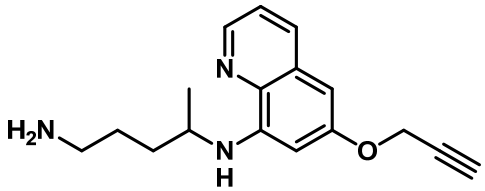

S9

References

(1) Lawrence, N., Dennis, A. S., Lehane, A. M., Ehmann, A., Harvey, P. J., Benfield, A. H., Cheneval, O., Henriques, S. T., Craik, D. J., and McMorran, B. J. (2018) Defense Peptides Engineered from Human Platelet Factor 4 Kill *Plasmodium* by Selective Membrane Disruption. *Cell Chem. Biol. 25*, 1140–1150.

(2) Lawrence, N., Philippe, G., Harvey, P. J., Condon, N. D., Benfield, A. H., Cheneval, O., Craik, D. J., and Henriques, S. T. (2020) Cyclic Peptide Scaffold with Ability to Stabilize and Deliver a Helical Cell-Impermeable Cargo across Membranes of Cultured Cancer Cells. *RSC Chem. Biol. 1*, 405–420.

(3) Mahajan, S. S., Deu, E., Lauterwasser, E. M., Leyva, M. J., Ellman, J. A., Bogyo, M., and Renslo, A. R. (2011) A Fragmenting Hybrid Approach for Targeted Delivery of Multiple Therapeutic Agents to the Malaria Parasite. *ChemMedChem 6*, 415–419.

(4) Spangler, B., Kline, T., Hanson, J., Li, X., Zhou, S., Wells, J. A., Sato, A. K., and Renslo, A. R. (2018) Toward a Ferrous Iron-Cleavable Linker for Antibody−Drug Conjugates. *Mol. Pharm. 15*, 2054–2059.

(5) Kularatne, S. A., Venkatesh, C., Santhapuram, H. K. R., Wang, K., Vaitilingam, B., Henne, W. A., and Low, P. S. (2010) Synthesis and Biological Analysis of Prostate-Specific Membrane Antigen-Targeted Anticancer Prodrugs. *J. Med. Chem. 53*, 7767–7777.

(6) Zhou, Y., Mowlazadeh Haghighi, S., Liu, Z., Wang, L., Hruby, V. J., and Cai, M. (2020) Development of Ligand-Drug Conjugates Targeting Melanoma through the Overexpressed Melanocortin 1 Receptor. *ACS Pharmacol. Transl. Sci. 3*, 921–930.

(7) Flood, D. T., Hintzen, J. C. J., Bird, M. J., Cistrone, P. A., Chen, J. S., and Dawson, P. E. (2018) Leveraging the Knorr Pyrazole Synthesis for the Facile Generation of Thioester Surrogates for Use in Native Chemical Ligation. *Angew. Chem. Int. Ed. 57*, 11634–11639.

(8) Hong, V., Presolski, S. I., Ma, C., and Finn, M. G. (2009) Analysis and Optimization of Copper-Catalyzed Azide-Alkyne Cycloaddition for Bioconjugation. *Angew. Chem. Int. Ed. 48*, 9879–9883.

(9) Lau, Y. H., Wu, Y., Rossmann, M., Tan, B. X., De Andrade, P., Tan, Y. S., Verma, C., McKenzie, G. J., Venkitaraman, A. R., Hyvönen, M., and Spring, D. R. (2015) Double Strain-Promoted Macrocyclization for the Rapid Selection of Cell-Active Stapled Peptides. *Angew. Chem. Int. Ed. 54*, 15410–15413.

(10) McChesney, J. D., and Sarangan, S. (1984) Rapid Aromatic Hydrogen Exchange in the Antimalarial Primaquine. *Pharm. Res. 1*, 184–186.

Supporting Information for Chapter 3:

Camptothecin PDCs

Supporting Information

Synthesis and Biological Evaluation of Peptide–Drug Conjugates Comprising a Human Protein-Derived Cell-Penetrating Peptide and the Anticancer Drug Camptothecin

Isabella R. Palombi,[a,b] Andrew M. White,[a,b] Yasuko Koda,[c,d] David J. Craik,[c,d] Nicole Lawrence,*[c,d] Lara R. Malins*[a,b]

[a] Research School of Chemistry, Australian National University, Canberra, ACT 2601, Australia

[b] Australian Research Council Centre of Excellence for Innovations in Peptide and Protein Science, Australian National University, Canberra, ACT 2601, Australia

[c] Institute for Molecular Bioscience, The University of Queensland, Brisbane, QLD 4072, Australia

[d] Australian Research Council Centre of Excellence for Innovations in Peptide and Protein Science, The University of Queensland, Brisbane, QLD 4072, Australia

*Email: lara.malins@anu.edu.au; n.lawrence@imb.uq.edu.au.

Contents

Supplementary Figures

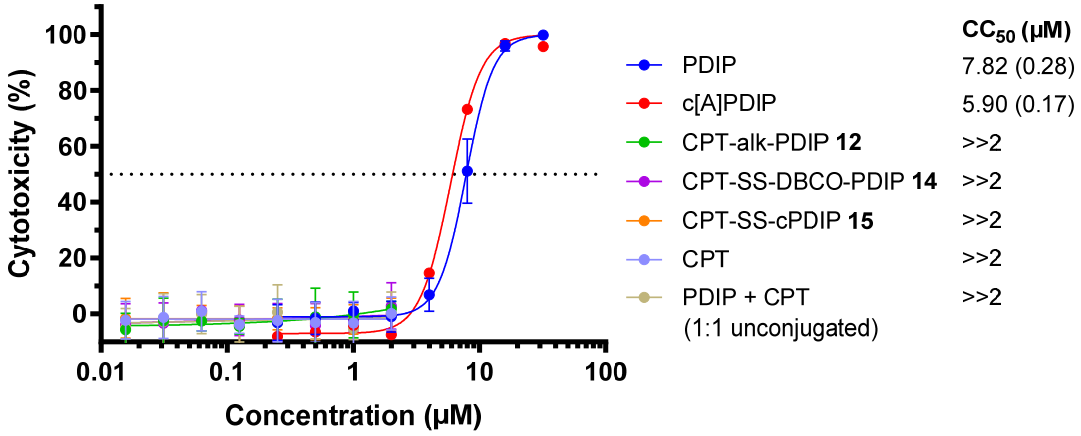

Figure S1. Cytotoxicity of PDCs, CPT, and peptides against HT144 cultured melanoma cells, following incubation for 24 h. Cell death was measured using resazurin, with 0.1% (v/v) Triton X-100 as a control for 100% cell death. Data points are expressed as mean ± SD for at least two biological replicates. CC_{50} values are expressed as mean (SEM). Note: CPT-dipeptide-PDIP was not included in this study. c[A]PDIP is a desulfurized variant of cPDIP **2** (see Table S1) to prevent the presence of free thiol during assays.

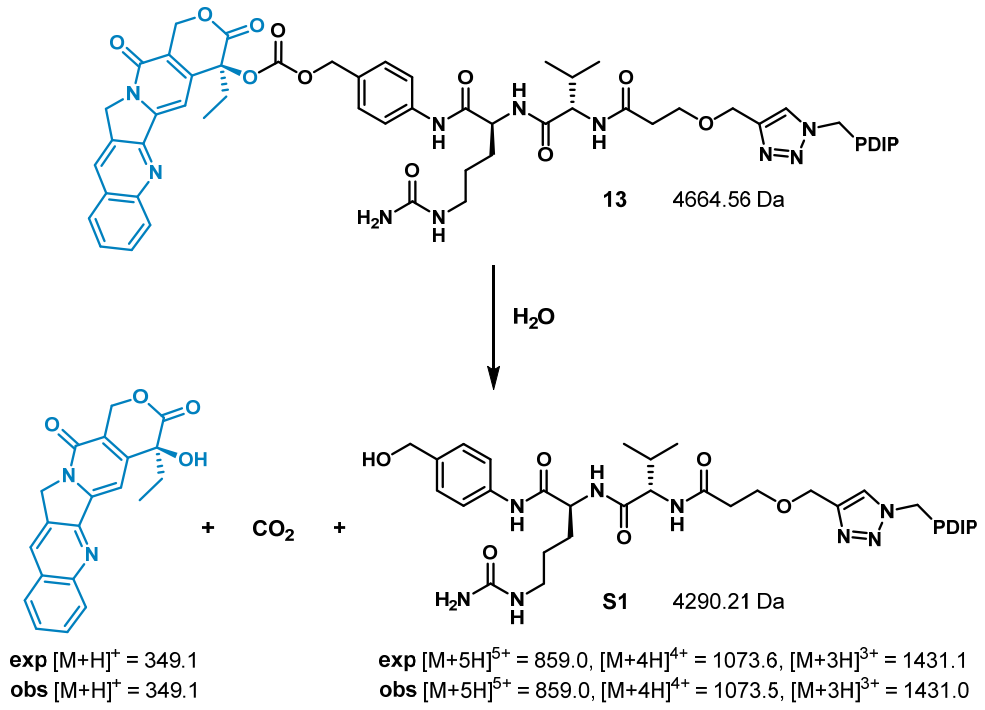

Scheme S1. Proposed degradation of PDC **13** observed in the cell-free environment for PAMPA. Hydrolysis of the carbonate functional group and subsequent decarboxylation releases CPT, CO_2, and alcohol containing **S1**. The *m/z* values obtained from LC–MS analysis in support of this breakdown pathway are shown underneath each product.

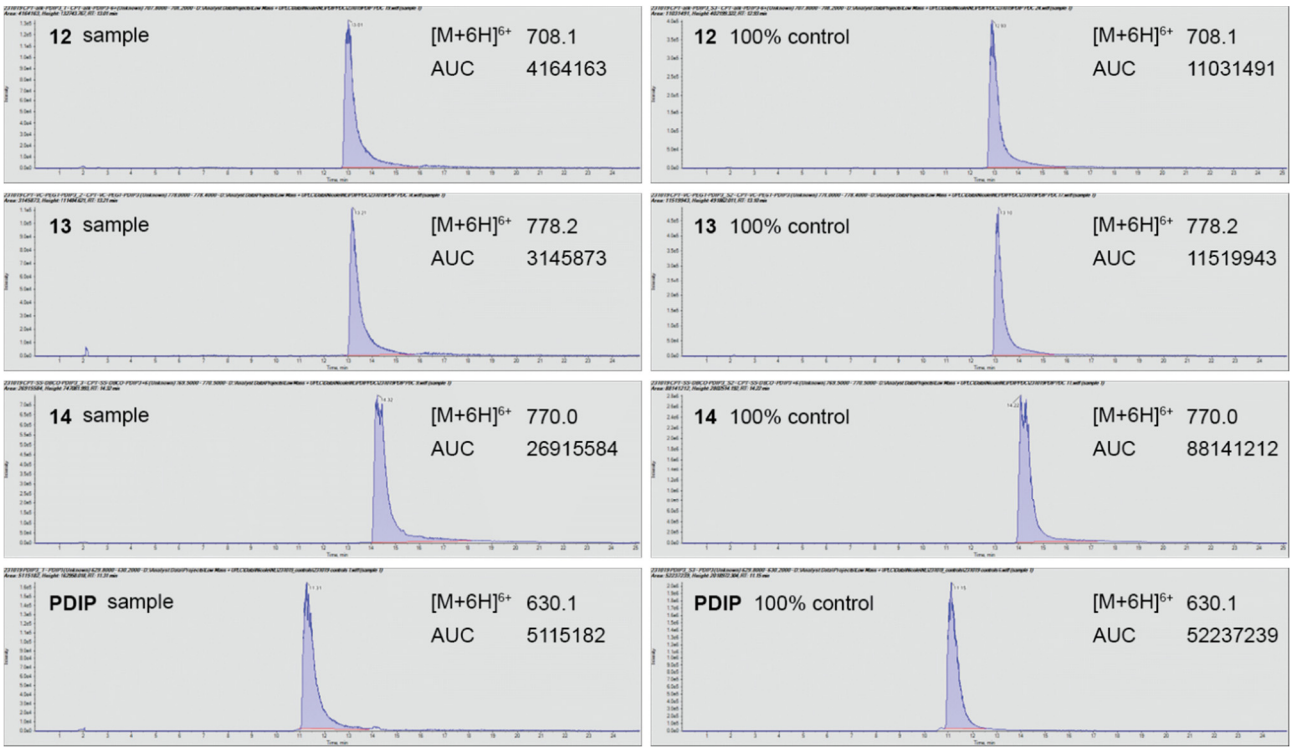

Figure S2. Representative MS extracted ion chromatograms for PDCs **12-14** and PDIP following extraction of treated and control HT144 cells. Samples and controls were analyzed using a Qstar elite TOF-MS with a 2% gradient containing 0.1% (v/v) formic acid in H_2O against 0.1% (v/v) formic acid in 90% (v/v) MeCN/H_2O. The area under the curve (AUC) for the $[M+6H]^{6+}$ *m/z* peak for each compound was determined using Sciex MultiQuant software.

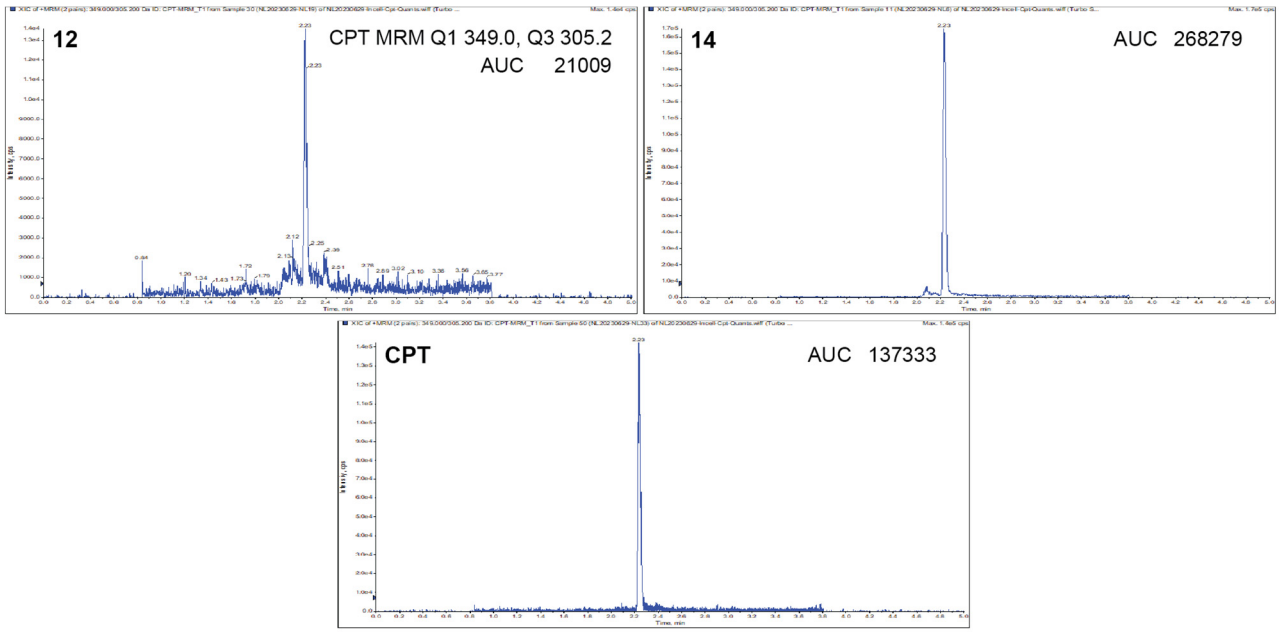

Figure S3. Representative extracted ion chromatograms for CPT using targeted multiple reaction monitoring (MRM), following treatment of HT144 cells with PDCs **12** and **14**, or CPT for 6 h. Samples were analyzed using a Sciex QTRAP® 6500+ MS coupled to an Exion UPLC system. Scans were performed with low resolution in quadrupole 1 (Q1) and unit resolution in quadrupole 3 (Q3), with the following MRM parameters: Q1 (*m/z*) 349.0, Q3 305.2, collision energy 40, and declustering potential 80. The area under the curve (AUC) for CPT was determined for each sample using Sciex MultiQuant software.

Table S1. Sequences/structures and properties of PDIP peptide analogues and PDCs.

Peptide or PDC	Sequence or structure	MW (Da)[a]	MW (Da) TFA salt[b]	Charge at pH 7.4[c]	RT (min)[d]
PDIP	GCGGPLYKKIIKKLLESGGSGGAPLYKKIIKKLCES*	3775.6	4801.8	9	14.8
PDIP-Az **1**	GCGGPLYKKIIKKLLESGGXGGAPLYKKIIKKLCES*	3800.6	4826.8	9	16.8
cPDIP **2**	c[GGCGGAPLYKKIIKKLLESGGSGGAPLYKKIIKKLLES]	3898.8	4810.9	8	18.1
c[A]PDIP[e]	c[GG**A**GGAPLYKKIIKKLLESGGSGGAPLYKKIIKKLLES]	3866.7	4778.9	8	18.0
CPT-alk-PDIP **12**	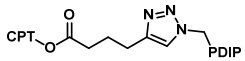	4243.1	5383.3	9	18.8
CPT-dipeptide-PDIP **13**	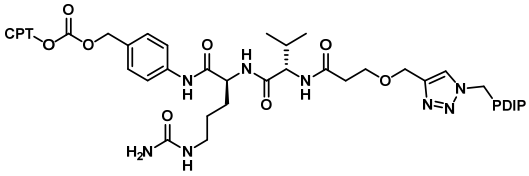	4664.6	5804.8	9	19.1
CPT-SS-DBCO-PDIP **14**	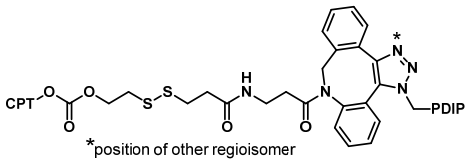 *position of other regioisomer	4615.6	5755.8	9	20.9, 21.2 (two regio-isomers)
CPT-SS-cPDIP **15**	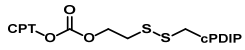	4349.2	5375.4	8	21.1

X = azidoalanine

* denotes an amidated C-terminus

c[ ] = backbone cyclized

[a] Molecular weight was calculated from the contributions of amino acids, linker, and drug components, using ChemDraw v23. For peptides and PDCs containing a cyclic disulfide, the oxidized molecular weight is provided.

[b] Calculated TFA salt molecular weight includes the mass of TFA counterions resulting from protonation of basic residues and the N-terminal amine (if present) within the peptides (for peptides and PDCs), and protonation of the quinoline moiety within CPT (for PDCs), after HPLC purification with acidic eluent (0.1% TFA). The molecular weight assumes no salt-bridge formation between amino acids.

[c] The calculated charge of each compound at pH 7.4 (physiological pH similar to assay conditions), assuming no salt-bridge formation between amino acids.

[d] Retention time (RT) was determined using analytical reverse-phase HPLC with a gradient of 5% to 65% MeCN (0.1% TFA) over 30 min. More hydrophobic compounds have a longer RT.

[e] A desulfurized variant of cPDIP was employed in cytotoxicity assays to prevent the presence of a free thiol during assays.

General Chemistry Procedures

^{1}H and $^{13}C\{^{1}H\}$ NMR spectra were recorded on a Bruker AVANCE spectrometer (400/800 MHz) at 298 K, in the solvents specified. $CDCl_3$ was treated with K_2CO_3(s) and 4 Å molecular sieves prior to use. For ^{1}H NMR and ^{13}C NMR spectra, signals arising from the residual protio-form and deutero-form of the solvent, respectively, were used as an internal reference. These correspond to δ_H 7.26 and δ_C 77.16 for $CDCl_3$, and δ_H 3.31 and δ_C 49.00 for CD_3OD. ^{1}H NMR data are recorded as follows: chemical shift (δ) [multiplicity, coupling constant(s) *J* (Hz), relative integral] where multiplicity is defined as: s = singlet; d = doublet; t = triplet; m = multiplet or combinations of the above. Coupling constants are quoted to the nearest 0.1 Hz.

High-resolution mass spectrometry (HRMS) was carried out using positive ESI on a Waters Synapt G2-Si mass spectrometer. Preparative high-performance liquid chromatography (HPLC) was performed on a Waters 600 Controller with a Waters 717 plus Autosampler and a Waters 2996 Photodiode Array Detector running Empower Pro Empower 3 software. Liquid chromatography–mass spectrometry (LC–MS) was performed a Shimadzu LCMS-2050 mass spectrometer with a Shimadzu LC40Dx3 UHPLC system. Analytical HPLC was performed on an Agilent 1100 Analytical HPLC with an Agilent Zorbax SB-C18 column or a Shimadzu LCMS-2020 instrument with a Phenomenex 5 µm C18 / 300 Å / 150 × 2 mm LC column. Linear gradients of water (solvent A) and MeCN (solvent B) were used for LC–MS, preparative and analytical HPLC with solvents containing 0.1% TFA for HPLC or 0.01% formic acid for LC–MS. Any deviations from the above are specified in the corresponding protocol. Dry solvents were obtained from a Glass Contour solvent purification system.

Peptide and PDC masses for yields were determined on a Mettler Toledo UMX2 microbalance to 0.001 mg accuracy. PDIP (formerly known as cPF4PD), cPDIP and c[A]PDIP were synthesized using published protocols;[1–3] PDIP-Az was manufactured by Wuxi AppTec or Mimotopes. Fmoc-azido-alanine and Boc-Val-Cit-PAB-PNP were manufactured by Combi-Blocks, other amino acids were purchased from GL Biochem or AK Scientific, PEG1-alkyne from BroadPharm and VA-044 from Fujifilm Wako Chemicals.

CPT-alkyne (3) synthesis

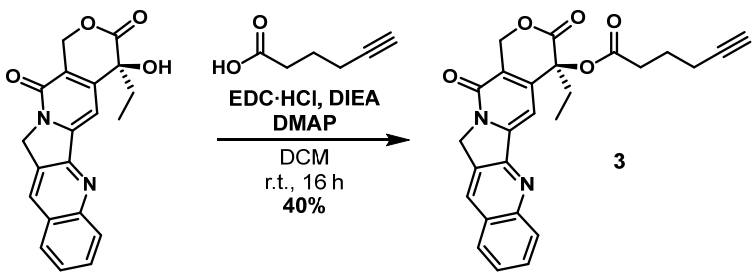

Following a procedure adapted from Li *et al.*:[4] A magnetically stirred mixture of camptothecin (CPT) (50 mg, 0.14 mmol, 1.0 equiv.), 5-hexynoic acid (40 µL, 0.36 mmol, 2.5 equiv.) and DIEA (125 µL, 0.724 mmol, 3.0 equiv.) in DCM (2 mL) maintained under an atmosphere of nitrogen was treated with EDC·HCl (69 mg, 0.36 mmol, 2.5 equiv.) and DMAP (8.5 mg, 70 µmol, 0.5 equiv.). The mixture was stirred at room temperature for 16 h. The mixture was diluted with chloroform (30 mL) and the organic phase was washed sequentially with saturated aqueous $NaHCO_3$ (10 mL) and brine (10 mL). The organic phase was dried (Na_2SO_4), filtered and concentrated under reduced pressure to give a crude product that was subjected to purification by reverse-phase semi-preparative HPLC (40 to 90% MeCN over 20 min) to afford **3** (31 mg, 40%) as a bright-yellow solid (TFA salt).

^{1}H NMR: (400 MHz, $CDCl_3$) δ 8.44 (s, 1H), 8.26 (d, J = 8.2 Hz, 1H), 7.96 (d, J = 8.2 Hz, 1H), 7.90 – 7.82 (m, 1H), 7.74 – 7.65 (m, 1H), 7.29 (s, 1H), 5.69 (d, J = 17.2 Hz, 1H), 5.41 (d, J = 17.2 Hz, 1H), 5.35 – 5.29 (m, 2H), 2.76 – 2.56 (m, 2H), 2.36 – 2.23 (m, 3H), 2.21 – 2.09 (m, 1H), 2.02 (t, J = 2.6 Hz, 1H), 1.93 – 1.83 (m, 2H), 0.99 (t, J = 7.5 Hz, 3H) ppm; **^{13}C NMR:** (101 MHz, $CDCl_3$) δ 172.3, 167.6, 157.5, 152.4, 148.9, 146.3, 146.3, 131.5, 131.0, 129.6, 128.6, 128.4, 128.4, 128.3, 120.4, 96.5, 83.2, 76.0, 69.6, 67.2, 50.1, 32.6, 32.0, 23.3, 17.8, 7.7 ppm; **HRMS:** (ESI+) *m/z* observed 465.1428, calculated for $C_{26}H_{22}N_2O_5Na$ $[M+Na]^+$ 465.1421.

Disulfide linkers (5 and 8) synthesis

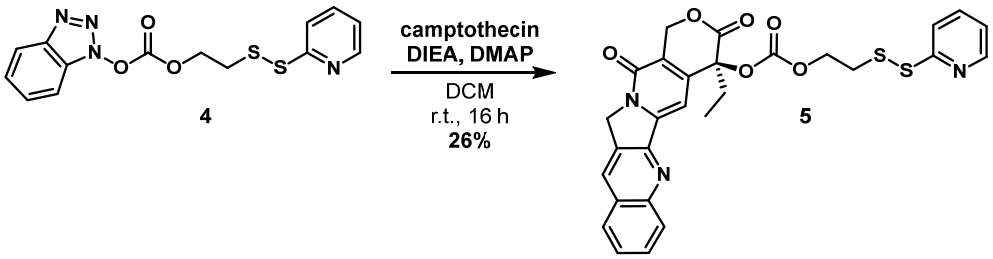

A magnetically stirred mixture of CPT (25 mg, 72 µmol, 1.0 equiv.) and carbonate **4**[5] (37 mg, 0.11 mmol, 1.5 equiv.) in DCM (5 mL) maintained under an atmosphere of nitrogen was treated with DIEA (35 µL, 0.20 mmol, 2.8 equiv.) and DMAP (2.2 mg, 18 µmol, 0.25 equiv.). The mixture was stirred at room temperature for 16 h, then concentrated under a stream of nitrogen and purified by reverse-phase semi-preparative HPLC (40 to 70% MeCN over 20 min) to afford **5** (15 mg, 26%) as a yellow solid (2 x TFA salt).

^{1}H NMR: (400 MHz, $CDCl_3$) δ 8.61 – 8.56 (m, 1H), 8.47 (s, 1H), 8.27 (d, J = 8.6 Hz, 1H), 8.00 – 7.91 (m, 3H), 7.90 – 7.84 (m, 1H), 7.75 – 7.68 (m, 1H), 7.42 (s, 1H), 7.33 – 7.27 (m, 1H), 5.70 (d, J = 17.3 Hz, 1H), 5.40 (d, J = 17.3 Hz, 1H), 5.37 – 5.32 (m, 2H), 4.40 – 4.27 (m, 2H), 3.11 (t, J = 6.3 Hz, 2H), 2.33 – 2.10 (m, 2H), 1.02 (t, J = 7.5 Hz, 3H) ppm; **^{13}C NMR:** (101 MHz, $CDCl_3$) δ 167.3, 158.9, 157.6, 153.5, 151.8, 148.4, 147.0, 146.5, 146.1, 140.7, 132.2, 131.5, 129.1, 128.7, 128.6, 128.5

(2C), 122.2, 122.1, 120.5, 97.5, 78.2, 67.0, 66.2, 50.5, 37.6, 32.0, 7.7 ppm; **HRMS:** (ESI+) *m/z* observed 562.1104, calculated for $C_{28}H_{24}N_3O_6S_2$ $[M+H]^+$ 562.1101.

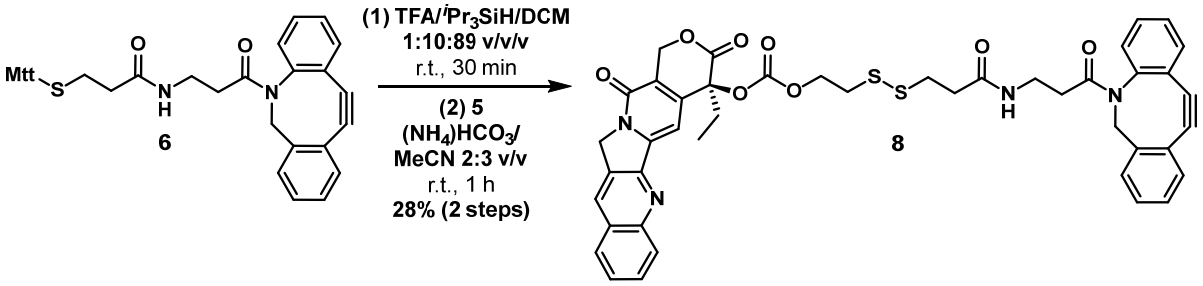

Compound **6**[6] (3.7 mg, 6.0 µmol, 1.5 equiv.) was suspended in a mixture of TFA/^{i}Pr$_3$SiH/DCM (1:10:89 v/v/v, 0.5 mL total) and magnetically stirred at room temperature for 30 min. The mixture was concentrated under a stream of nitrogen and the resulting residue was redissolved in argon purged MeCN (1.5 mL). This solution was transferred to a flask containing **5** (TFA salt, 3.0 mg, 3.8 µmol, 1.0 equiv.), followed by the addition of an argon purged aqueous ammonium bicarbonate solution (200 mM, pH 8, 1 mL). The mixture was magnetically stirred at room temperature for 1 h, then concentrated under a stream of nitrogen. Purification with reverse-phase semi-preparative HPLC (40 to 95% MeCN over 20 min) afforded **8** (1.0 mg, 28% over two steps) as a yellow solid (TFA salt).

^{1}H NMR: (400 MHz, $CDCl_3$) δ 8.45 – 8.41 (m, 1H), 8.27 – 8.22 (m, 1H), 7.98 – 7.93 (m, 1H), 7.87 – 7.82 (m, 1H), 7.72 – 7.61 (m, 2H), 7.44 – 7.27 (m, 8H), 6.47 – 6.39 (m, 1H), 5.70 (apparent dd, *J* = 17.3, 2.4 Hz, 1H), 5.39 (d, *J* = 17.3 Hz, 1H), 5.34 – 5.30 (m, 2H), 5.10 (d, *J* = 13.9 Hz, 1H), 4.44 – 4.29 (m, 2H), 3.66 (apparent dd, *J* = 13.9, 4.0 Hz, 1H), 3.39 – 3.26 (m, 2H), 2.91 (t, *J* = 6.7 Hz, 2H), 2.82 – 2.76 (m, 2H), 2.52 – 2.38 (m, 3H), 2.34 – 2.09 (m, 2H), 2.02 – 1.91 (m, 1H), 1.01 (t, *J* = 7.4 Hz, 3H) ppm; **HRMS:** (ESI+) *m/z* observed 815.2216, calculated for $C_{44}H_{39}N_4O_8S_2$ $[M+H]^+$ 815.2204.

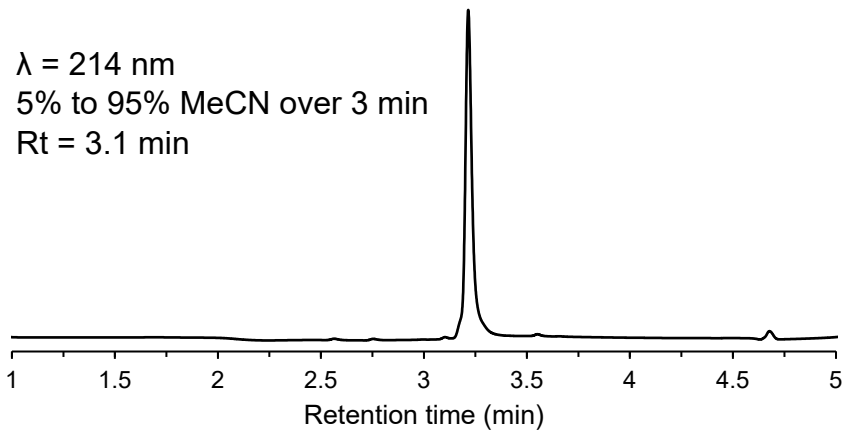

Dipeptide linker (11) synthesis

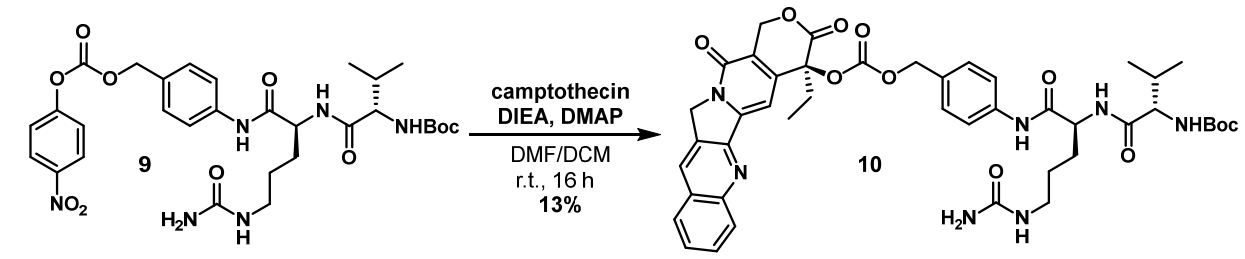

A magnetically stirred mixture of Boc-Val-Cit-PAB-PNP (**9**, 40 mg, 62 µmol, 1.0 equiv.) and CPT (30 mg, 86 µmol, 1.4 equiv.) in DMF (0.75 mL) and DCM (0.75 mL) maintained under an atmosphere of nitrogen was treated with DIEA (22 µL, 0.25 mmol, 4.0 equiv.) and DMAP (1.9 mg, 16 µmol, 0.25 equiv.). The mixture was stirred at room temperature for 16 h, then concentrated under a stream of nitrogen and purified by reverse-phase semi-preparative HPLC (40 to 90% MeCN over 20 min) to afford **10** (7.9 mg, 13%) as a light-yellow solid (TFA salt).

^{1}H NMR: (800 MHz, $CDCl_3$) *four N–Hs not observed* δ 8.98 (br s, 1H), 8.41 (s, 1H), 8.23 (d, *J* = 8.5 Hz, 1H), 7.94 (d, *J* = 8.5 Hz, 1H), 7.85 (apparent t, *J* = 7.4 Hz, 1H), 7.68 (apparent t, *J* = 7.4 Hz, 1H), 7.50 – 7.41 (m, 2H), 7.41 – 7.34 (m, 2H), 7.25 – 7.19 (m, 2H), 5.65 (d, *J* = 16.7 Hz, 1H), 5.36 (d, *J* = 16.7 Hz, 1H), 5.28 (s, 2H), 5.10 (d, *J* = 12.4 Hz, 1H), 4.95 (d, *J* = 12.4 Hz, 1H), 4.64 – 4.53 (m, 1H), 4.00 – 3.90 (m, 1H), 3.25 – 3.08 (m, 2H), 2.28 – 2.21 (m, 1H), 2.17 – 2.06 (m, 2H), 1.95 – 1.83 (m, 1H), 1.76 – 1.64 (m, 1H), 1.60 – 1.50 (m, 2H), 1.40 (s, 9H), 1.00 – 0.90 (m, 9H) ppm; **^{13}C NMR:** (201 MHz, $CDCl_3$) *one carbon signal not observed (or overlapping with another signal)* δ 173.3, 170.3, 167.9, 161.3, 157.5, 156.7, 153.7, 152.0, 148.7, 146.5, 146.2, 138.0, 131.8, 131.2, 130.8, 129.5, 129.3 (2C), 128.6, 128.4, 128.4, 120.4 (2C), 120.2, 96.8, 81.0, 78.1, 70.3, 67.2, 60.8, 53.6, 50.3, 39.8 (assigned from ^{1}H–^{13}C HSQC), 32.0, 30.6, 29.3, 28.4 (3C), 25.7, 19.4, 18.1, 7.7 ppm; **HRMS:** (ESI+) *m/z* observed 854.3729, calculated for $C_{44}H_{52}N_7O_{11}$ $[M+H]^+$ 854.3719.

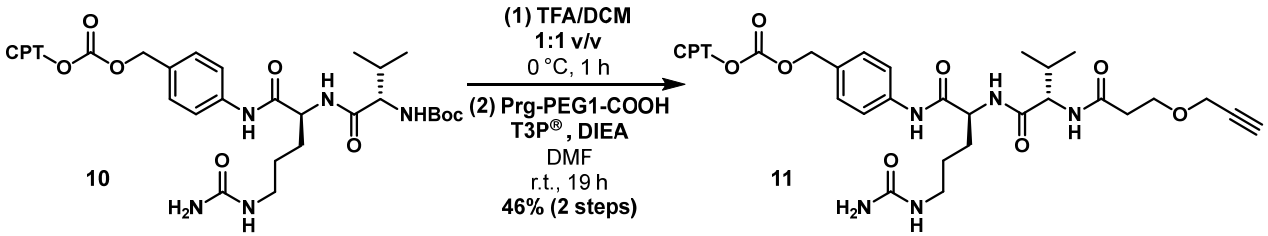

Compound **10** (TFA salt, 4.9 mg, 5.1 µmol, 1.0 equiv.) was suspended in a mixture of TFA/DCM (1:1 v/v, 0.2 mL total) and magnetically stirred at 0 °C (ice bath) for 1 h, after which the mixture was concentrated under a stream of nitrogen followed by vacuum. The resulting residue was redissolved in DMF (0.5 mL) and treated with propargyl-PEG1-acid (1.3 mg, 10 µmol, 2.0 equiv.), T3P® (50% in EtOAc, 9.7 µL, 15 µmol, 3.0 equiv.) and DIEA (6.0 µL, 31 µmol, 6.0 equiv.). The mixture was magnetically stirred at room temperature for 16 h, after which additional propargyl-PEG1-acid (1.3 mg), T3P® (9.7 µL) and DIEA (6.0 µL) were added to the reaction. The mixture was stirred at

room temperature for a further 3 h, then concentrated under a stream of nitrogen and subjected to purification by reverse-phase semi-preparative HPLC (35 to 75% MeCN over 20 min) to afford **11** (2.3 mg, 46% over two steps) as a light-yellow solid (TFA salt).

^{1}H NMR: (800 MHz, CD_3OD) *six N–Hs not observed* δ 8.59 (s, 1H), 8.15 (d, *J* = 8.3 Hz, 1H), 8.08 – 8.02 (m, 1H), 7.91 – 7.85 (m, 1H), 7.72 (apparent t, *J* = 7.1 Hz, 1H), 7.48 (d, *J* = 8.2 Hz, 2H), 7.35 (s, 1H), 7.27 (d, *J* = 8.2 Hz, 2H), 5.62 (d, *J* = 16.4 Hz, 1H), 5.47 (d, *J* = 16.4 Hz, 1H), 5.32 – 5.22 (m, 2H), 5.14 – 5.05 (m, 2H), 4.44 – 4.40 (m, 1H), 4.22 – 4.18 (m, 1H), 4.13 (t, *J* = 2.4 Hz, 2H), 3.81 – 3.75 (m, 2H), 3.23 – 3.16 (m, 1H), 3.12 – 3.07 (m, 1H), 2.82 (t, *J* = 2.4 Hz, 1H), 2.59 – 2.53 (m, 2H), 2.28 – 2.22 (m, 1H), 2.21 – 2.15 (m, 1H), 2.13 – 2.08 (m, 1H), 1.86 – 1.80 (m, 1H), 1.71 – 1.64 (m, 1H), 1.60 – 1.48 (m, 2H), 1.02 (t, *J* = 7.4 Hz, 3H), 0.97 (t, *J* = 7.2 Hz, 6H) ppm; **^{13}C NMR:** (201 MHz, CD_3OD) δ 174.2, 173.8, 172.1, 169.4, 162.4, 158.9, 154.9, 153.3, 149.6, 148.0, 147.8, 140.0, 133.3, 132.0, 131.9, 130.8, 130.2 (2C), 130.0, 129.9, 129.7, 129.2, 121.0 (2C), 120.9, 97.6, 80.4, 79.5, 76.1, 71.3, 67.8, 67.0, 60.6, 58.9, 54.8, 51.6, 40.4 (assigned from ^{1}H–^{13}C HSQC), 37.2, 32.2, 31.7, 30.4, 27.8, 19.8, 18.7, 8.0 ppm; **HRMS:** (ESI+) *m/z* observed 864.3568, calculated for $C_{45}H_{50}N_7O_{11}$ $[M+H]^+$ 864.3563.

Synthesis and purification of cPDIP (2) and c[A]PDIP

Assembly and backbone cyclization of cPDIP

Following a previously reported procedure from Lawrence *et al*.:[3] cPDIP was synthesized as a linear peptide hydrazide on Fmoc-NHNH-chlorotrityl resin[7,8] using standard automated Fmoc solid-phase chemistry (Symphony, Protein Technologies Inc). The peptide hydrazide was deprotected and cleaved from the resin using a mixture of TFA/H_2O/$^{i}Pr_3SiH$ (95:2.5:2.5 v/v/v) and collected by precipitating with ice-cold ether. The crude peptide was subsequently purified by reverse-phase preparative HPLC using a Shimadzu system and Phenomenex Gemini C18 column with a gradient of solvent B (90% MeCN/water, 0.05% TFA v/v) against solvent A (water, 0.05% TFA v/v).

The lyophilized linear peptide hydrazide—bearing an N-terminal cysteine residue—was backbone cyclized *via* intramolecular native chemical ligation.[9] To convert the C-terminal hydrazide to a thioester, the peptide (1.0 equiv.) was prepared as a 3 mM solution in Gn·HCl (6 M, pH <3), with 4-mercaptophenylacetic acid (200 mM) and acetyl acetone (9 mM, 3.0 equiv.),[10] and stirred at room temperature for 4 h. Head-to-tail cyclization was achieved by diluting the reaction to produce a 0.5 mM peptide solution in Gn·HCl (6 M), NaH_2PO_4 (100 mM) and TCEP (50 mM). The mixture was adjusted to pH 7 and stirred overnight at room temperature. The cyclized peptide was purified by reverse-phase preparative HPLC as above.

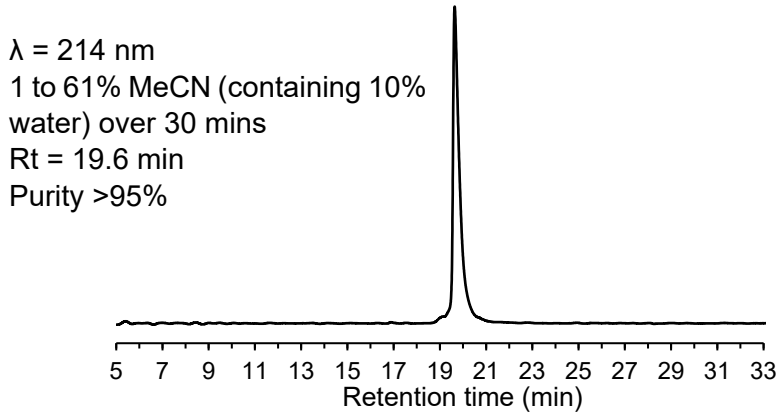

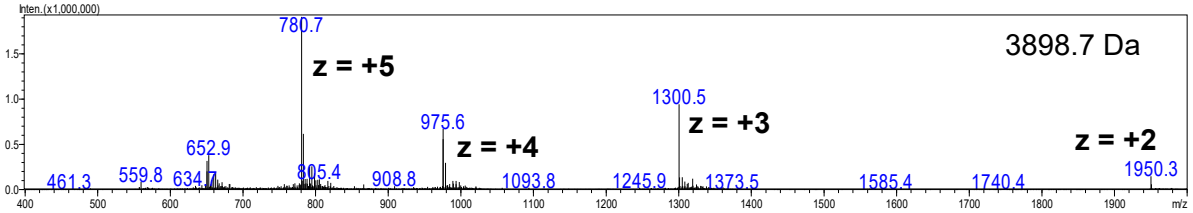

Desulfurization of cPDIP

cPDIP (**2**) was treated with TCEP (0.25 M), Gn·HCl (3 M), NaH_2PO_4 (50 mM), reduced glutathione (10 mM) and VA-044 (50 mM). The mixture was adjusted to pH 6.5, purged with argon, and incubated overnight at 65 °C.[11] The cyclized peptide was purified by reverse-phase preparative HPLC as above.

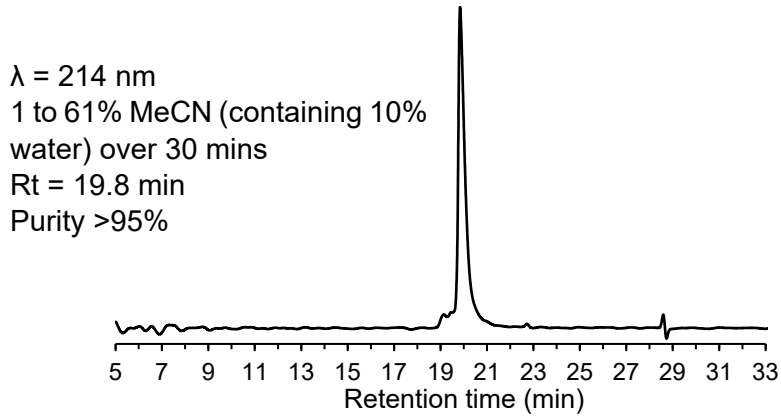

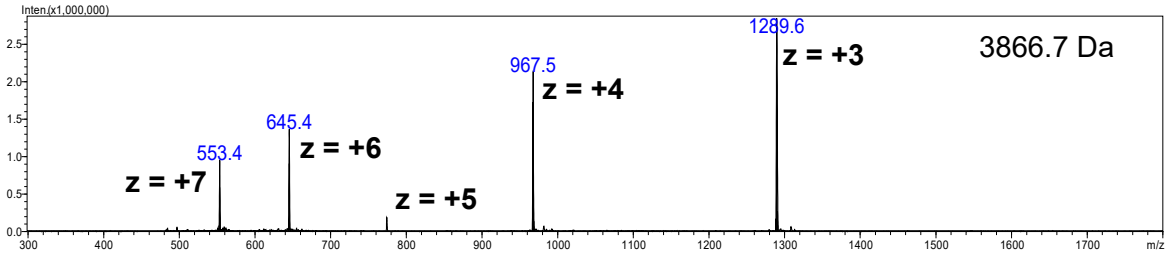

General procedure: CuAAC conjugation

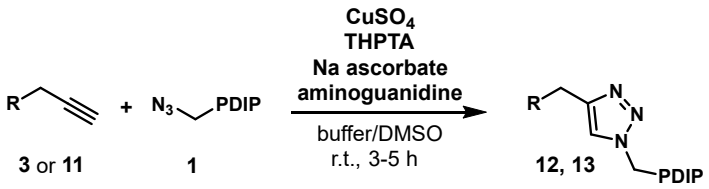

Following a procedure adapted from Hong *et al*.:[12] All reagent stock solutions were prepared in water, unless otherwise specified, to the following concentrations: aminoguanidine hydrochloride 100 mM, copper(II) sulfate 20 mM, tris(3-hydroxypropyltriazolylmethyl)amine (THPTA) 50 mM, sodium ascorbate 100 mM (freshly prepared), ethylenediaminetetraacetic acid (EDTA) 100 mM and drug-alkyne (**3** or **11**) 20 mM (in DMSO).

PDIP-Az (**1**, 1.0 equiv.) was dissolved in 100 mM sodium phosphate buffer (prepared by mixing 100 mM Na_2HPO_4 with 100 mM NaH_2PO_4 until pH = 7) to produce a final peptide concentration of 200 µM (based on total reaction volume including reagents to be added). An aliquot of DMSO was included to make the conjugation reaction mixture 20% organic/80% aqueous by volume. The following reagents were then added sequentially to the reaction vial and magnetically stirred after each new addition: aminoguanidine hydrochloride (5 mM[i], 25 equiv.), drug-alkyne (400 µM, 2.0 equiv.), copper(II) sulfate (100 µM, 0.5 equiv.) pre-mixed with THPTA (500 µM, 2.5 equiv.), and sodium ascorbate (5 mM, 25 equiv.). The conjugation mixture was magnetically stirred at room temperature for 3 – 5 h. The reaction was quenched with EDTA (5.0 equiv.) and purified by reverse-phase semi-preparative HPLC. Reported yields were determined by weight on a microbalance and were calculated using the mass of the TFA salt of the product (assuming all basic residues, the N-terminal amine and the quinoline moiety within CPT are protonated).

*CPT-alk-PDIP (**12**)*

Prepared with PDIP-Az **1** and CPT-alkyne **3** on a 0.44 µmol scale (2.1 mg peptide). Purification with semi-preparative HPLC (20 to 50% MeCN over 40 min) yielded **12** (0.60 mg, 26%) as a light-yellow solid.

[i] Concentration of each component refers to the final concentration in the reaction mixture

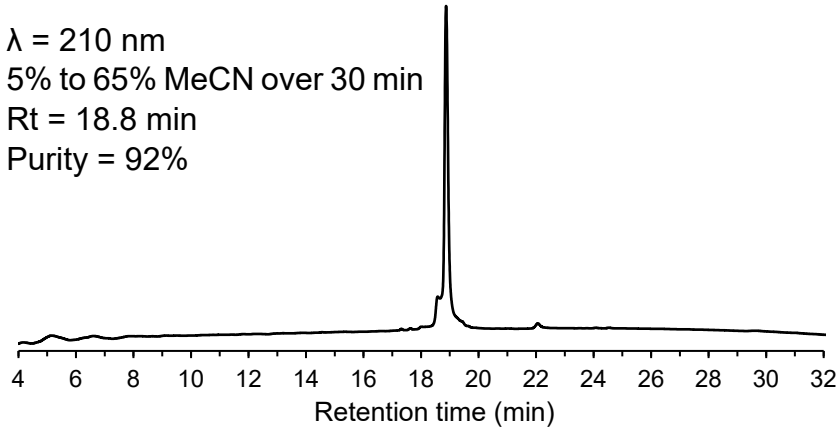

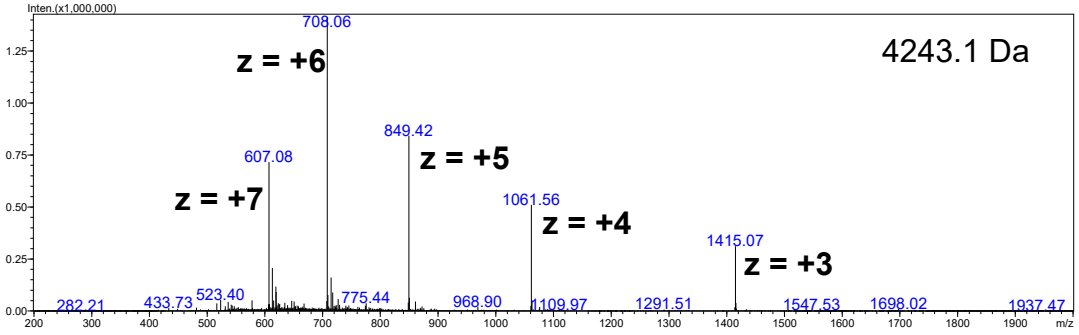

*CPT-dipeptide-PDIP (**13**)*

Prepared with PDIP-Az **1** and CPT-dipeptide-PEG1-alkyne **11** on a 0.31 µmol scale (1.5 mg peptide). Purification with semi-preparative HPLC (30 to 50% MeCN over 40 min) yielded **13** (0.73 mg, 40%) as a light-yellow solid.

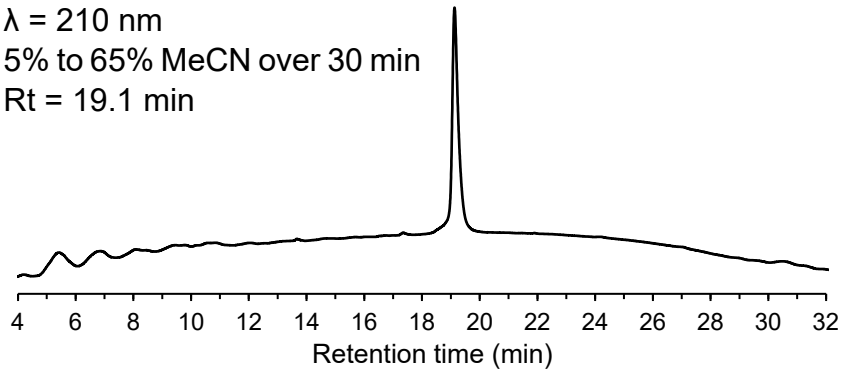

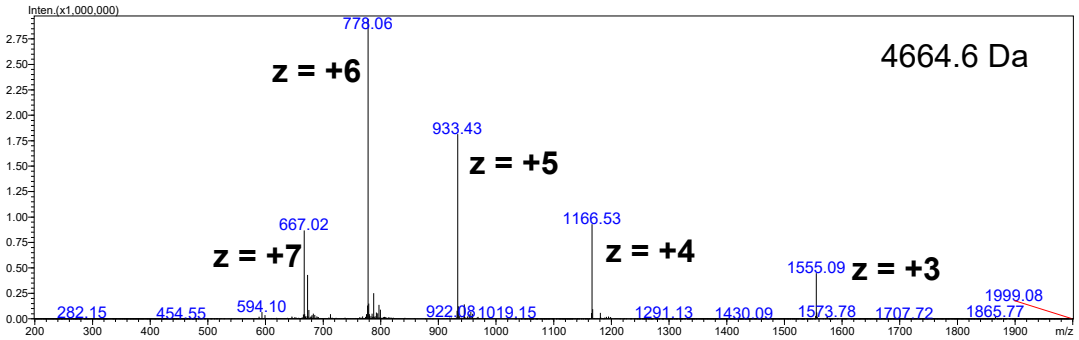

CPT-SS-DBCO-PDIP (14) synthesis

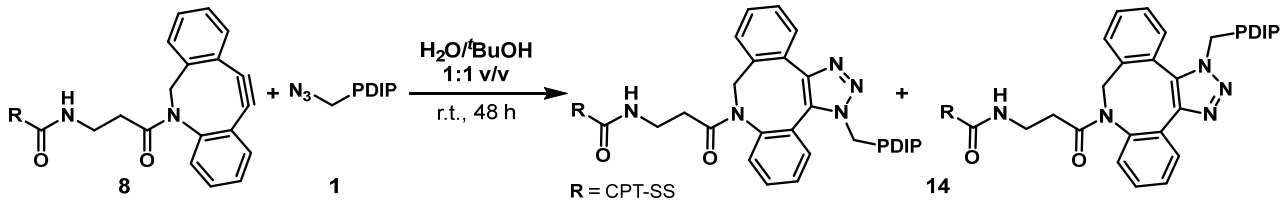

Following a procedure adapted from Lau *et al.*:[13] PDIP-Az **1** (3.8 mg, 0.79 µmol, 1.0 equiv.) and CPT-SS-DBCO **8** (1.0 mg, 1.2 µmol, 1.6 equiv.) were dissolved in water/*t*-butanol (1:1 v/v, 1 mL total). The mixture was stirred for 48 h to produce two regioisomers that were purified by reverse-phase semi-preparative HPLC (30 to 60% MeCN over 40 min) to afford **14** (2.48 mg, 55% for the combined regioisomers) as a light-yellow solid. Reported yield was determined by weight on a microbalance and was calculated using the mass of the TFA salt of the product (assuming all basic residues, the N-terminal amine and the quinoline moiety within CPT are protonated).

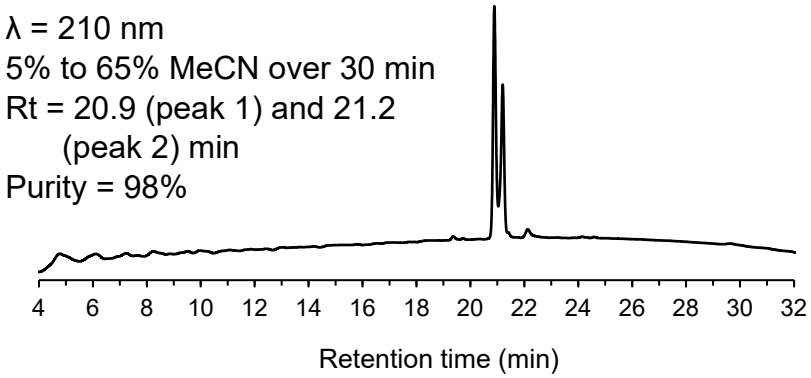

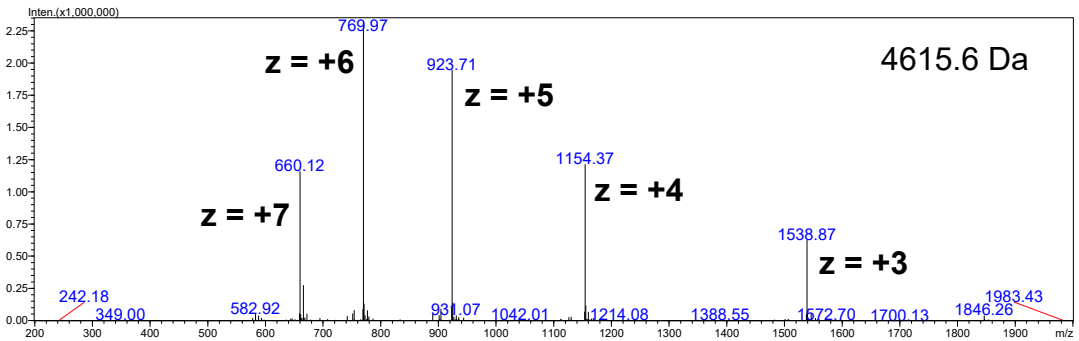

CPT-SS-cPDIP (15) synthesis

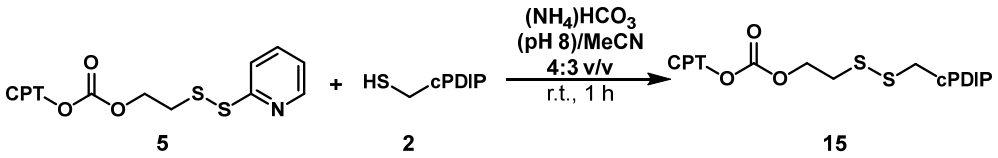

Following a procedure adapted from Zhou *et al.*:[14] cPDIP **2** (2.9 mg, 0.60 µmol, 1.0 equiv.) was dissolved in argon purged H_2O (1 mL). This solution was transferred to a flask containing **5** (0.8 mg, 1.2 µmol, 2.0 equiv.) in argon purged MeCN (1.5 mL), followed by the dropwise addition of an argon purged aqueous ammonium bicarbonate solution (200 mM, pH 8, 1 mL). The mixture was magnetically stirred at room temperature for 1 h, then purified by reverse-phase semi-preparative HPLC (25 to 50% MeCN over 40 min) to afford **15** (1.22 mg, 38%) as a light-yellow solid. Reported yield was determined by weight on a microbalance and was calculated using the mass of the TFA salt of the product (assuming all basic residues and the quinoline moiety within CPT are protonated).

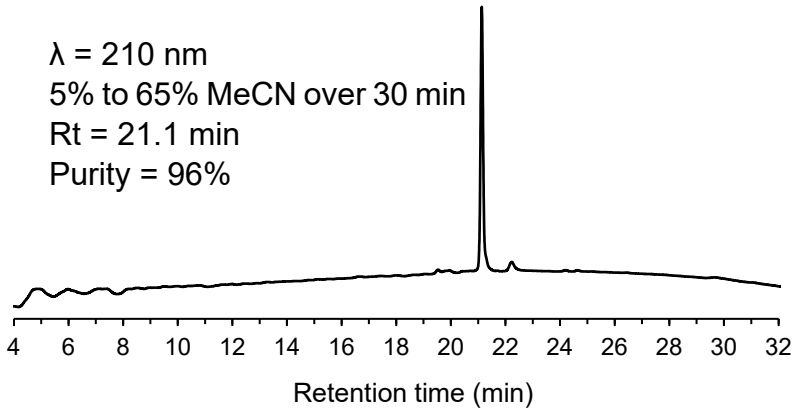

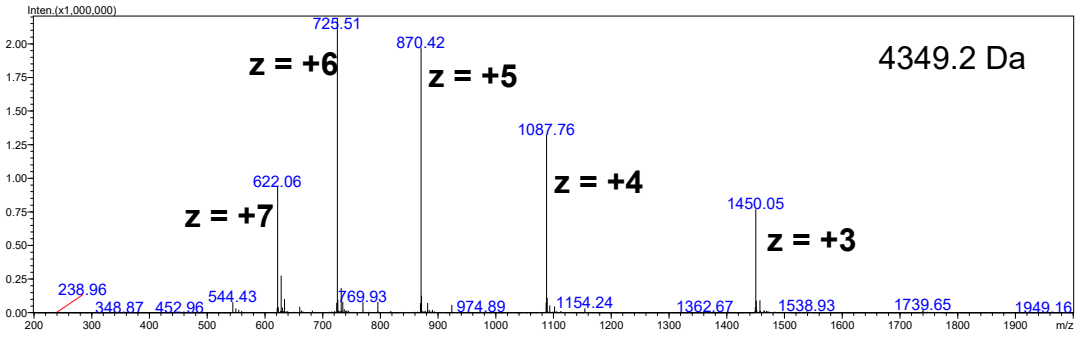

Cell culture

HaCaT cells were grown in DMEM medium and HT144 cells were grown in RPMI medium supplemented with 2 mM L-glutamine and 10 mM sodium pyruvate. Media were supplemented with 10% (v/v) fetal bovine serum, 100 units/mL of penicillin and 100 mg/mL of streptomycin. Flasks of cultured cells were maintained in a humidified incubator (37 °C, 5% CO_2) and passaged every 2–3 days to maintain cultures between 20–90% confluence. Cell line identity was verified by comparing

STR profiles of the cell lines against database entries from the DSMZ-German collection of microorganisms and cell cultures, GmBH https://celldive.dsmz.de/str/browse.

Marker	STR Alleles	
	HT144	HaCaT
D5S818	11,13	12
D13S317	11,12	10,12
D7S820	11	9,11
D16S539	12,13	9,12
vWA	16,18	16,17
TH01	9	9.3
Amel	X,Y	X
TPOX	8,11	11,12
CSF1PO	12	9,11

Cell toxicity

Toxicity to the HT144 and HaCaT cell lines was tested following peptide treatment by measuring the metabolism of resazurin into fluorescent resorufin. The assays were performed with 5000 cells/well (96-well plate) in serum free media. Cells were incubated with serially diluted peptides, PDCs or drugs for 72 h or 24 h (37 °C, 5% CO_2). PBS and 0.1% (v/v) Triton X-100 were included as controls for 0% and 100% toxicity. Resazurin was added at 0.02% (w/v) final concentration 2 h prior to the assay end point. Fluorescence (λ_{ex} = 560 nm, λ_{em} = 585 nm) was measured using a Tecan infinite M1000Pro multiplate reader. Percentage cytotoxicity was calculated relative to 0% and 100% controls. Dose-response curves were fitted and CC_{50} values were determined using [inhibitor] *vs* response with four parameters with the top constrained to 100% (GraphPad Prism version 10.0.2). Data was collected as three biological replicates, with experiments conducted on different days.

Red blood cell (RBC) lysis

Human RBCs and serum were obtained from healthy volunteers via the Red Cross Lifeblood, Brisbane, Australia. RBCs were washed three times with PBS and stored in culture medium (RPMI supplemented with 2 mM L-glutamine, 10 mM sodium pyruvate, 2 g/L D-glucose, 52 nM gentamicin, 2.5 g/L Albumax II and 5% human serum). For the lysis assay, RBCs were plated in 96-well plates at 0.25% (v/v) hematocrit in culture medium. Serially diluted compounds were added to the wells, alongside controls including PBS (0% lysis) and 0.1% (v/v) Triton X-100 (100% lysis). The membrane disruptive peptide melittin[15] was also included, starting at 8 μM. The plates were incubated for 72 h (37 ºC, 5% CO_2), then were centrifuged (800 x g, 5 min), before the supernatant was transferred to a new plate. RBC lysis was determined by measuring released hemoglobin at 405 nm using a Tecan infinite M1000Pro multiplate reader. Percentage of lysed RBC was calculated relative to 0% and 100% controls. Data was collected from two technical replicates.

Parallel artificial membrane permeability assay (PAMPA)

PAMPA was performed according to the manufacturer instructions for the BD Gentest pre-coated PAMPA plate system (BD Biosciences), as previously described.[16] Briefly, peptides and PDCs (4 μM in PBS) were added to the apical side of PAMPA wells and incubated for 4 h at 37 °C, 5% CO_2 with 95% humidity. Soluble fractions were recovered from the apical and basolateral sides, and compound concentration was quantified using a Shimadzu LCMS-2020 instrument with a Phenomenex 5 μm C18 / 300 Å / 150 x 2 mm LC column. Data was collected from three technical replicates for each compound. The % recovery was determined from (combined from apical and basolateral fractions) relative to the starting concentration:

$$Recovery\ rate{:}\ R\ (\%) = \frac{(C_A \times V_A + C_B \times V_B)}{C_0 \times V_A} \times 100$$

where C_A and C_B are the apical and basolateral concentrations (μM), V_A and V_B are the apical and basolateral volumes (mL), and C_0 is the initial concentration (μM).

The apparent permeability coefficient (Papp) was calculated using the following equations[17] and where A is the membrane surface area (cm^2):

$$Papp\ (cm/s) = \frac{-\ln\left(1 - \frac{C_B}{C_e}\right)}{A \times \left(\frac{1}{V_A} + \frac{1}{V_B}\right) \times time(s)} \qquad C_e = \frac{(C_A \times V_A + C_B \times V_B)}{V_A + V_B}$$

Compound internalization/association with HT144 cells

HT144 cells (5000 cells/well, 96-well plate) were incubated in serum free media with each treatment (final concentration 4 μM) for 1 h (37 °C, 5% CO_2). Media was removed from treated cells, which were washed with PBS, then lysed with ice cold 75% (v/v) MeCN in mQH_2O (containing 1.75% (v/v) TFA) before being transferred to tubes containing PBS (10 μL). Untreated cells were used as controls and were processed in the same way before being transferred to tubes containing an aliquot of each treatment (10 μL, final concentration 4 μM). Cells were incubated for 10 mins at 0 °C (ice), centrifuged (21,000 x g, 4 °C, 20 min) and the supernatant was analyzed using a Qstar elite TOF-MS with a 2% gradient containing 0.1% (v/v) formic acid in H_2O against 0.1% (v/v) formic acid in 90% (v/v) MeCN/ H_2O. The $[M+6H]^{6+}$ *m/z* peak for each compound was identified using Sciex Analyst software, and area under the curve (AUC) was determined for the exact mass using Sciex MultiQuant software. The percentage of internalized peptide was determined from: treated sample AUC / (average of (PBS controls + post-added compound) AUC) × 100% for each peptide analogue. Data was collected from three technical replicates for each treatment and control.

CPT detection inside HT144 cells

HT144 cells were plated and treated with 4 μM of CPT-alk-PDIP (**12**), CPT-SS-DBCO-PDIP (**14**), or CPT, then washed and extracted as above. The recovered supernatant was analyzed using a Sciex QTRAP® 6500+ MS coupled to an Exion UPLC system, with modifications to previously reported quantification methods.[18] Quantification experiments were performed using a Phenomenex Kinetex C18 UPLC column (100 × 2.1 mm, 1.7 μm) at constant temperature of 40 °C or 60 °C using a linear acetonitrile gradient at a flow rate of 0.4 mL min^{-1}. The source setting of electrospray voltage was set at 5500 V, temperature at 600 °C. Targeted multiple reaction monitoring (MRM) scans were performed with low resolution in quadrupole 1 (Q1) and unit resolution in quadrupole 3 (Q3), with the following MRM parameters: Q1 (*m/z*) 349.0, Q3 305.2, collision energy 40, and declustering potential 80. Sciex MultiQuant software was used to integrate the AUC for three technical replicates of each compound.

^{1}H and $^{13}C\{^{1}H\}$ NMR

400 MHz ^{1}H NMR in $CDCl_3$

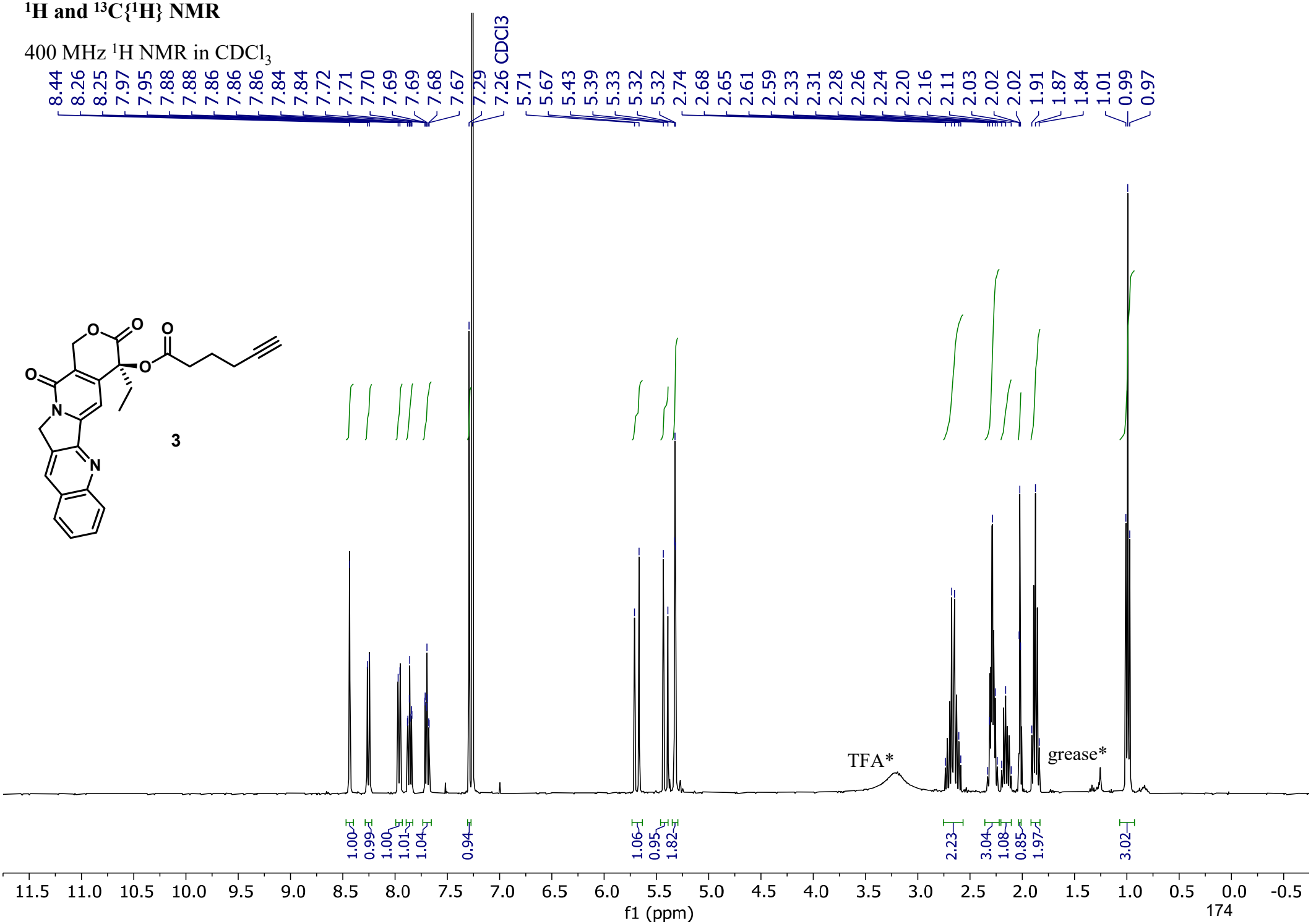

101 MHz ^{13}C NMR in $CDCl_3$

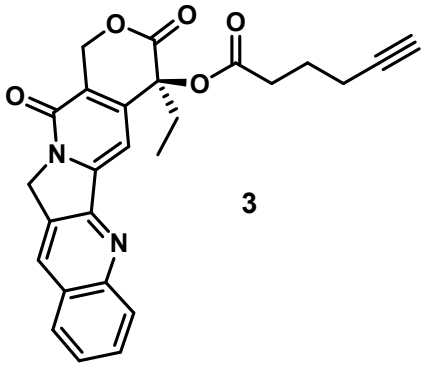

3

400 MHz ^{1}H NMR in $CDCl_3$

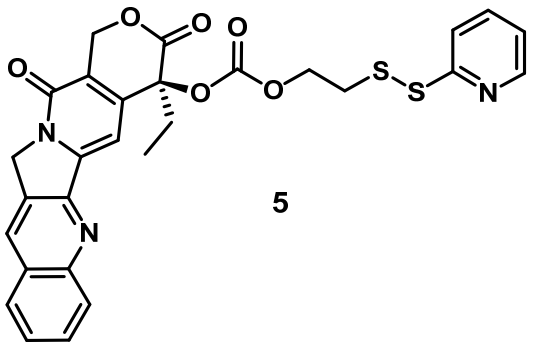

5

exchangeable
NH*

f1 (ppm)

101 MHz ^{13}C NMR in $CDCl_3$

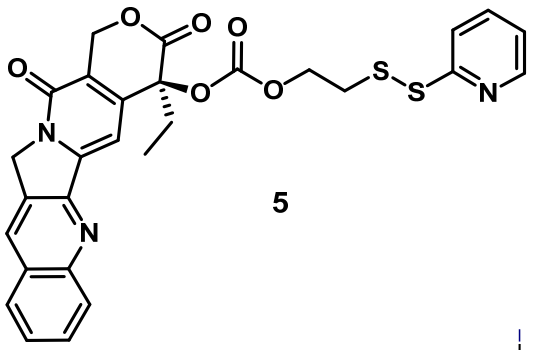

5

400 MHz ^{1}H NMR in $CDCl_3$

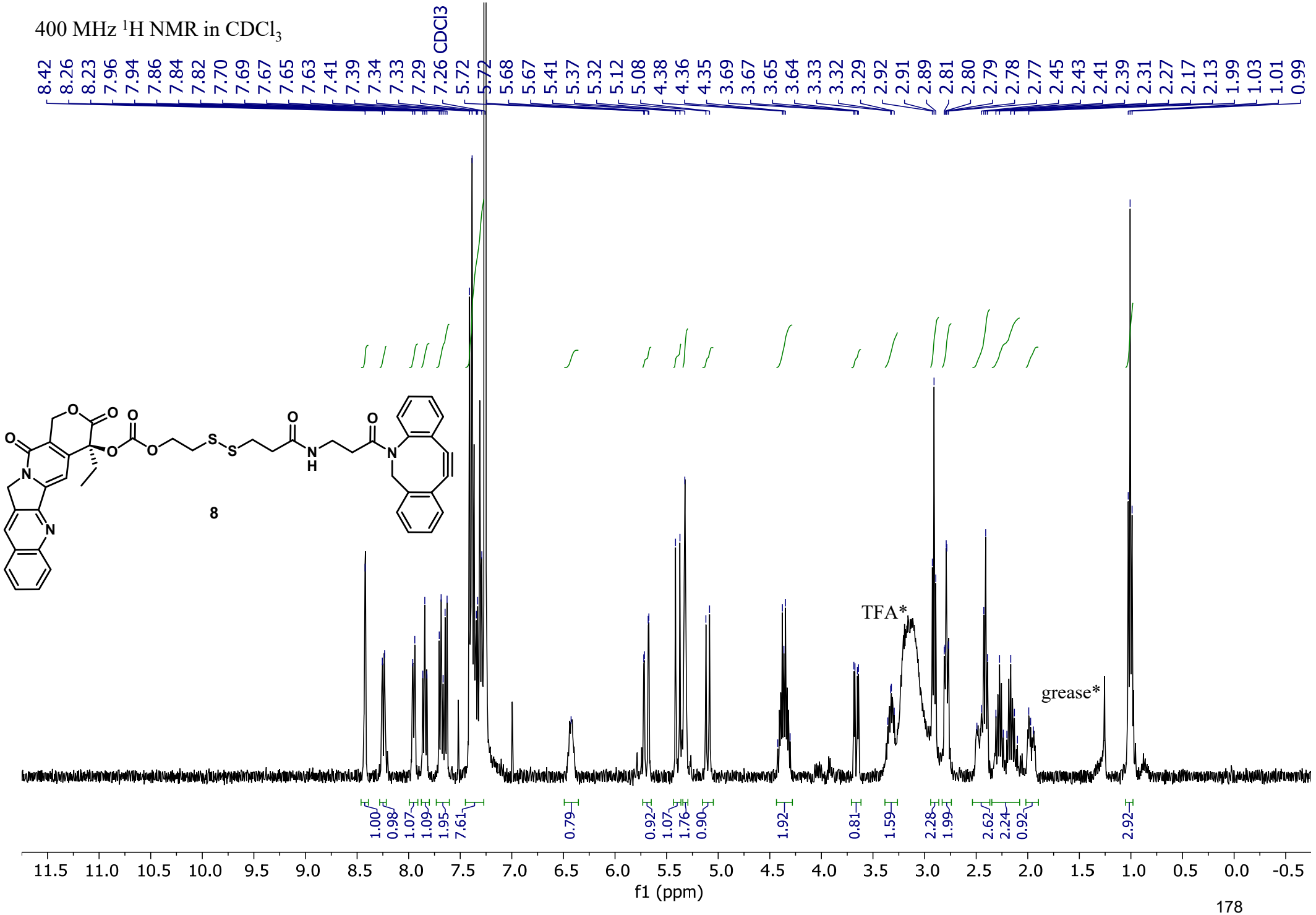

8

800 MHz ^{1}H NMR in $CDCl_3$

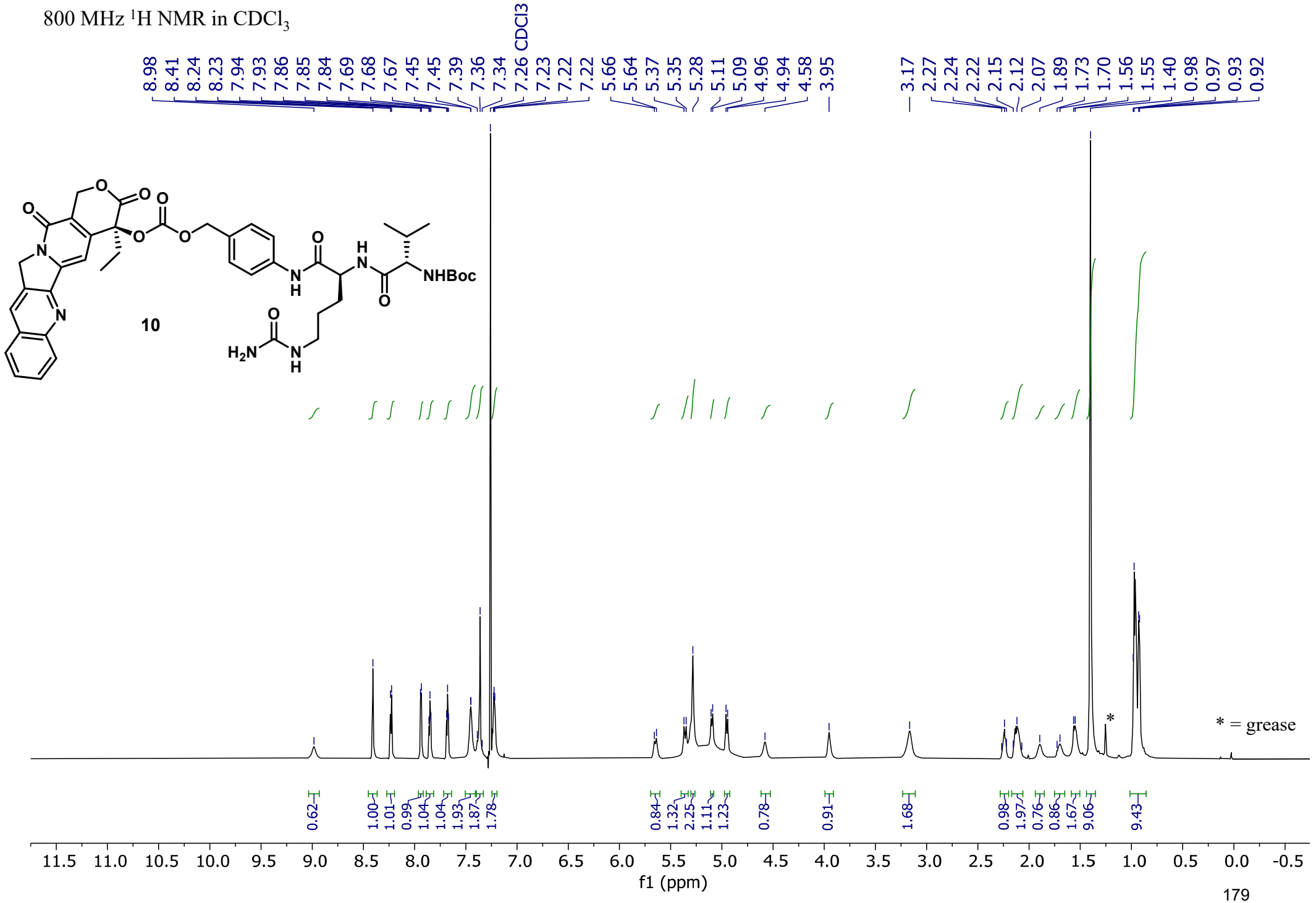

201 MHz ^{13}C NMR in $CDCl_3$

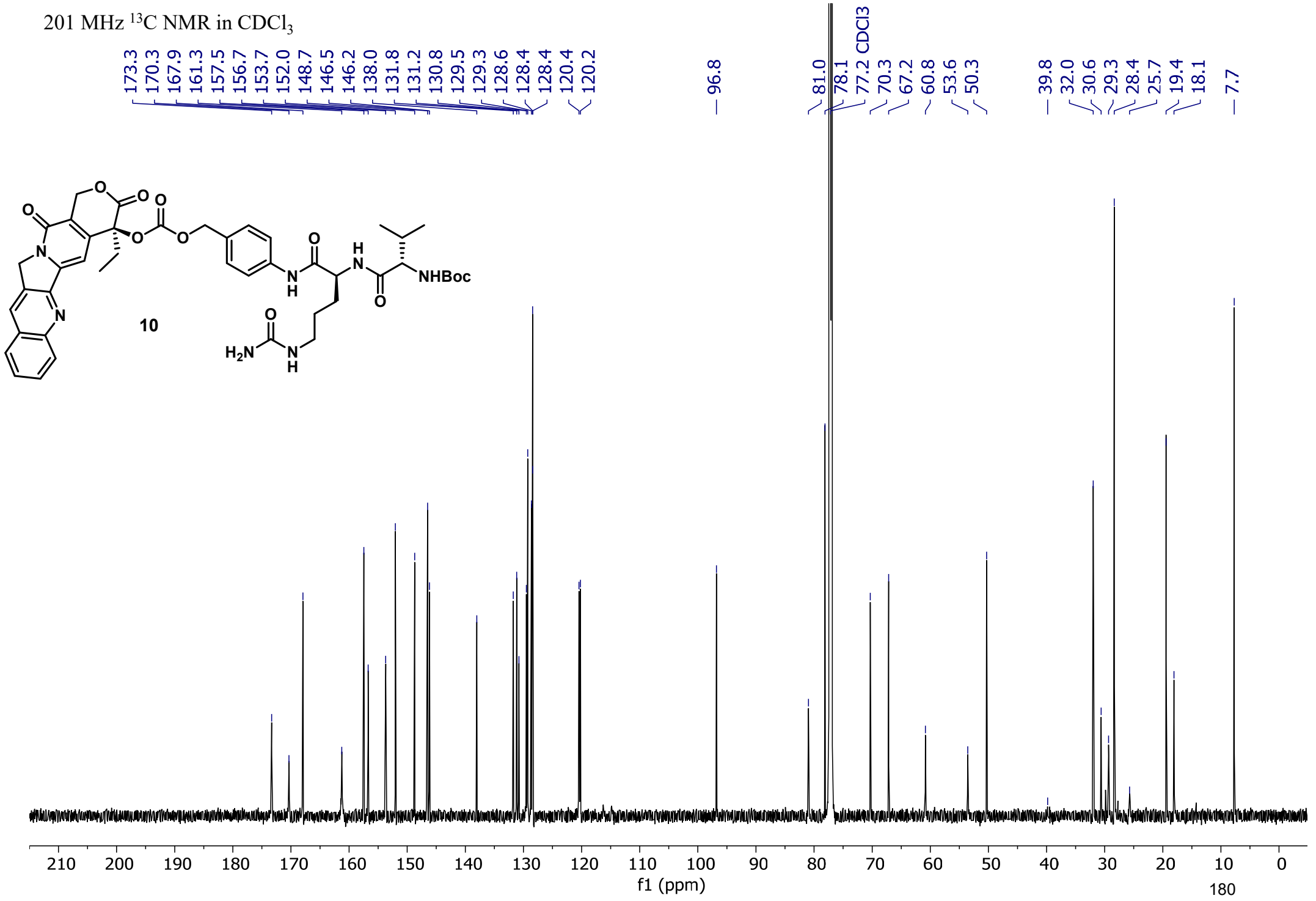

800 MHz, 201 MHz ^{1}H–^{13}C
HSQC in $CDCl_3$

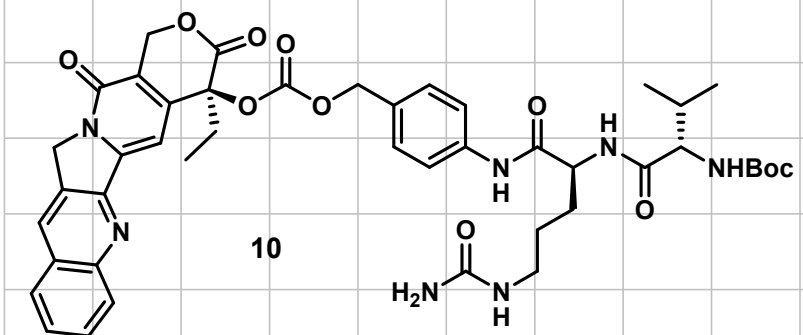

10

{3.16,39.81}

f2 (ppm)

f1 (ppm)

800 MHz ^{1}H NMR in CD_3OD

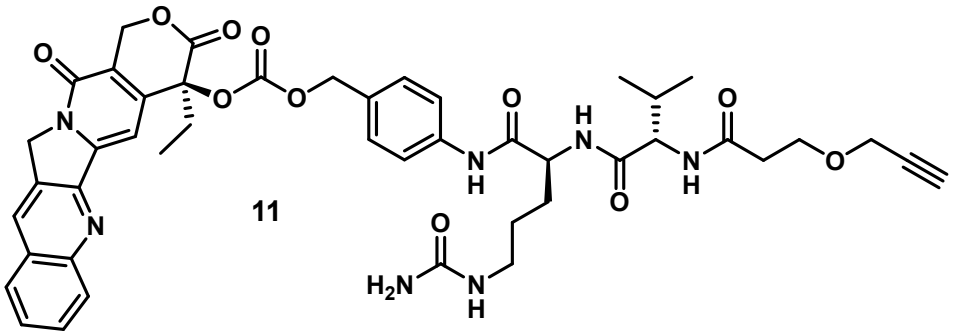

* = grease

f1 (ppm)

201 MHz ^{13}C NMR in CD_3OD

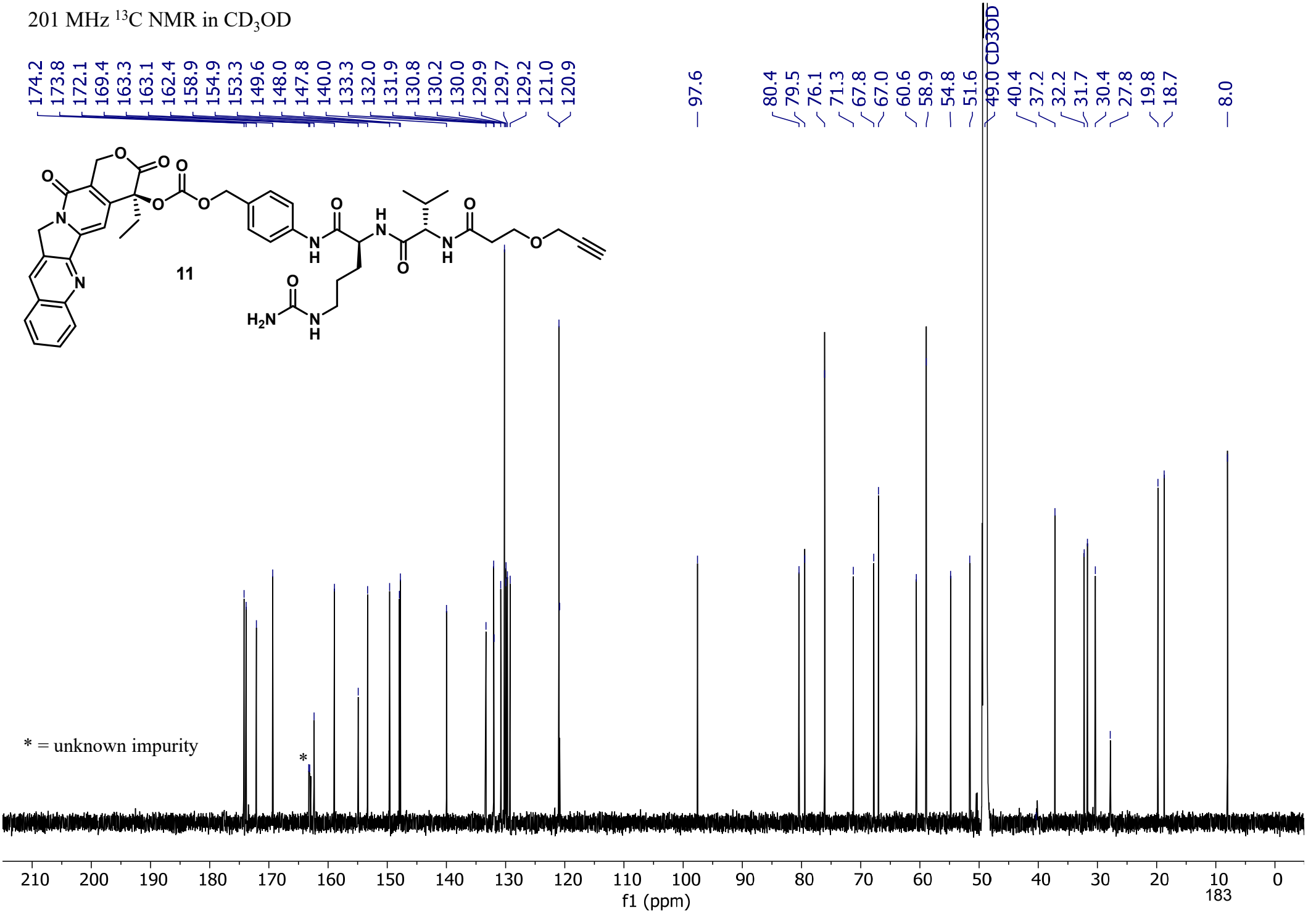

800 MHz, 201 MHz ^{1}H–^{13}C
HSQC in $CDCl_3$

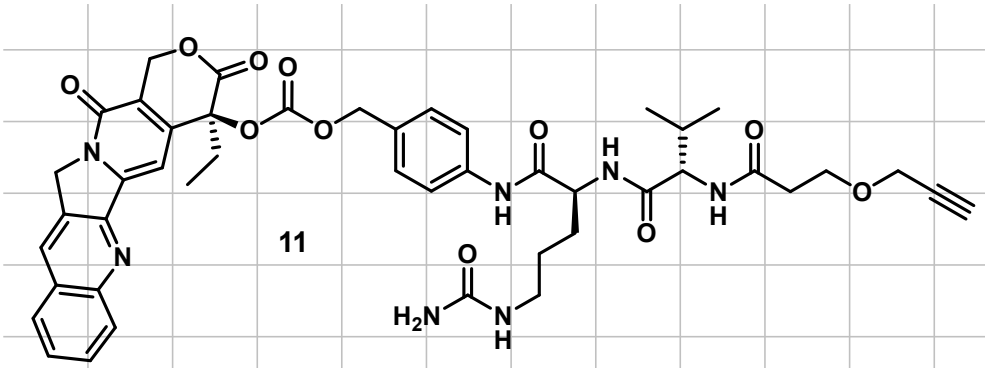

{3.19,40.44}
{3.10,40.44}

f2 (ppm)
f1 (ppm)

References

(1) Lawrence, N.; Dennis, A. S.; Lehane, A. M.; Ehmann, A.; Harvey, P. J.; Benfield, A. H.; Cheneval, O.; Henriques, S. T.; Craik, D. J.; McMorran, B. J. *Cell Chem. Biol.* **2018**, *25*, 1140–1150.

(2) Lawrence, N.; Philippe, G.; Harvey, P. J.; Condon, N. D.; Benfield, A. H.; Cheneval, O.; Craik, D. J.; Henriques, S. T. *RSC Chem. Biol.* **2020**, *1*, 405–420.

(3) Lawrence, N.; Handley, T. N. G.; de Veer, S. J.; Harding, M. D.; Andraszek, A.; Hall, L.; Raven, K. D.; Duffy, S.; Avery, V. M.; Craik, D. J.; Malins, L. R.; McMorran, B. J. *ACS Infect. Dis.* **2024**, *10*, 2899–2912.

(4) Li, Q.; Lv, H.; Zu, Y.; Qu, Z.; Yao, L.; Su, L.; Liu, C.; Wang, L. *Bioorg. Med. Chem. Lett.* **2009**, *19*, 513–515.

(5) Kularatne, S. A.; Venkatesh, C.; Santhapuram, H. K. R.; Wang, K.; Vaitilingam, B.; Henne, W. A.; Low, P. S. *J. Med. Chem.* **2010**, *53*, 7767–7777.

(6) Palombi, I. R.; Lawrence, N.; White, A. M.; Gare, C. L.; Craik, D. J.; McMorran, B. J.; Malins, L. R. *Bioconjug. Chem.* **2023**, *34*, 1105–1113.

(7) Huang, Y. C.; Chen, C. C.; Li, S. J.; Gao, S.; Shi, J.; Li, Y. M. *Tetrahedron* **2014**, *70*, 2951–2955.

(8) Bird, M. J.; Dawson, P. E. *Pept. Sci.* **2022**, *114*, e24268.

(9) Cistrone, P. A.; Bird, M. J.; Flood, D. T.; Silvestri, A. P.; Hintzen, J. C. J.; Thompson, D. A.; Dawson, P. E. *Curr. Protoc. Chem. Biol.* **2019**, *11*, e61.

(10) Flood, D. T.; Hintzen, J. C. J.; Bird, M. J.; Cistrone, P. A.; Chen, J. S.; Dawson, P. E. *Angew. Chem. Int. Ed.* **2018**, *57*, 11634–11639.

(11) Cergol, K. M.; Thompson, R. E.; Malins, L. R.; Turner, P.; Payne, R. J. *Org. Lett.* **2014**, *16*, 290–293.

(12) Hong, V.; Presolski, S. I.; Ma, C.; Finn, M. G. *Angew. Chem. Int. Ed.* **2009**, *48*, 9879–9883.

(13) Lau, Y. H.; Wu, Y.; Rossmann, M.; Tan, B. X.; De Andrade, P.; Tan, Y. S.; Verma, C.; McKenzie, G. J.; Venkitaraman, A. R.; Hyvönen, M.; Spring, D. R. *Angew. Chem. Int. Ed.* **2015**, *54*, 15410–15413.

(14) Zhou, Y.; Mowlazadeh Haghighi, S.; Liu, Z.; Wang, L.; Hruby, V. J.; Cai, M. *ACS Pharmacol. Transl. Sci.* **2020**, *3*, 921–930.

(15) Asthana, N.; Yadav, S. P.; Ghosh, J. K. *J. Biol. Chem.* **2004**, *279*, 55042–55050.

(16) Bergeron, C.; Bérubé, C.; Lamb, H.; Koda, Y.; Craik, D. J.; Henriques, S. T.; Voyer, N.; Lawrence, N. *Pept. Sci.* **2024**, 10.1002/PEP2.24380.

(17) Sevin, E.; Dehouck, L.; Fabulas-da Costa, A.; Cecchelli, R.; Dehouck, M. P.; Lundquist, S.; Culot, M. *J. Pharmacol. Toxicol. Methods* **2013**, *68*, 334–339.

(18) Yap, K.; Du, J.; Looi, F. Y.; Tang, S. R.; de Veer, S. J.; Bony, A. R.; Rehm, F. B. H.; Xie, J.; Chan, L. Y.; Wang, C. K.; Adams, D. J.; Lua, L. H. L.; Durek, T.; Craik, D. J. *Green Chem.* **2020**, *22*, 5002–5016.

Supporting Information for Chapter 4:

Vemurafenib PDCs

Supporting Information

Combining Bioactive Cell-Penetrating Peptides and Vemurafenib to Produce Peptide–Drug Conjugates with Activity Against Drug-Resistant Melanoma Cells

Isabella R. Palombi,[a,b] Andrew M. White,[a,b] Yasuko Koda,[c,d] David J. Craik,[c,d] Sónia Troeira Henriques,[d,e] Nicole Lawrence,*[c,d] Lara R. Malins*[a,b]

[a] Research School of Chemistry, Australian National University, Canberra, ACT 2601, Australia

[b] Australian Research Council Centre of Excellence for Innovations in Peptide and Protein Science, Australian National University, Canberra, ACT 2601, Australia

[c] Institute for Molecular Bioscience, The University of Queensland, Brisbane, QLD 4072, Australia

[d] Australian Research Council Centre of Excellence for Innovations in Peptide and Protein Science, The University of Queensland, Brisbane, QLD 4072, Australia

[e] Translational Research Institute, Faculty of Health, School of Biomedical Sciences, Queensland University of Technology, Brisbane 4102 QLD, Australia

*Email: lara.malins@anu.edu.au; n.lawrence@imb.uq.edu.au.

Contents

General Chemistry Procedures

^{1}H and $^{13}C\{^{1}H\}$ NMR spectra were recorded on a Bruker AVANCE spectrometer (400/800 MHz) at 298 K, in the solvents specified. $CDCl_3$ was treated with K_2CO_3(s) and 4 Å molecular sieves prior to use. For ^{1}H NMR and ^{13}C NMR spectra, signals arising from the residual protio-form and deutero-form of the solvent, respectively, were used as an internal reference. These correspond to δ_H 7.26 and δ_C 77.16 for $CDCl_3$, and δ_H 2.50 and δ_C 39.52 for *d*$_6$-DMSO. ^{1}H NMR data are recorded as follows: chemical shift (δ) [multiplicity, coupling constant(s) *J* (Hz), relative integral] where multiplicity is defined as: s = singlet; d = doublet; t = triplet; m = multiplet or combinations of the above. Coupling constants are quoted to the nearest 0.1 Hz.

High-resolution mass spectrometry (HRMS) was conducted using positive ESI on a Waters Synapt G2-Si mass spectrometer. Preparative high-performance liquid chromatography (HPLC) was performed on a Waters 600 Controller with a Waters 717 plus Autosampler and a Waters 2996 Photodiode Array Detector running Empower Pro Empower 3 software. Liquid chromatography–mass spectrometry (LC–MS) was performed a Shimadzu LCMS-2050 mass spectrometer with a Shimadzu LC40Dx3 UHPLC system. Analytical HPLC was performed on an Agilent 1100 Analytical HPLC with an Agilent Zorbax SB-C18 column or a Shimadzu LCMS-2020 instrument with a Phenomenex 5 μm C18 / 300 Å / 150 × 2 mm LC column. Linear gradients of water (solvent A) and MeCN (solvent B) were used for LC–MS, preparative and analytical HPLC with solvents containing 0.1% TFA for HPLC or 0.01% formic acid for LC–MS. Any deviations from the above are specified in the corresponding protocols. Dry solvents were obtained from a Glass Contour solvent purification system.

Peptide and PDC masses for yields were determined on a Mettler Toledo UMX2 microbalance to 0.001 mg accuracy. PDIP (formerly known as cPF4PD) was synthesized using published protocols[1] and PDIP-Az was manufactured by Wuxi AppTec or Mimotopes. Fmoc-azido-alanine and DBCO-COOH were manufactured by Combi-Blocks and other amino acids were purchased from GL Biochem or AK Scientific.

Vem-NH_2 (7) synthesis

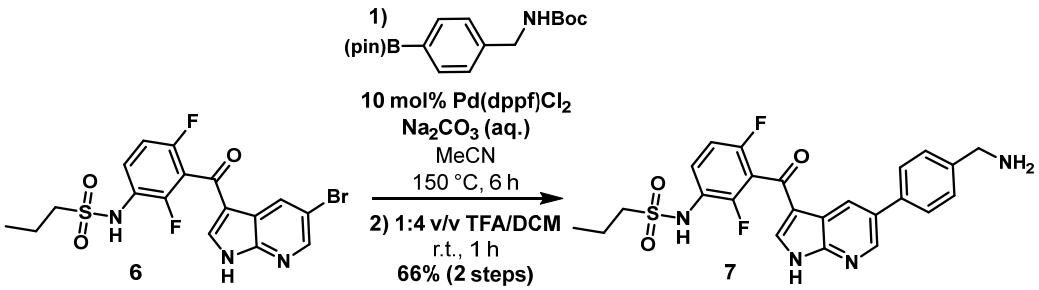

Following a procedure adapted from Mikula *et al*.:[2] Compound **6** (60 mg, 0.13 mmol, 1.0 equiv.) and 4-(*N*-Boc-amino)phenylboronic acid pinacol ester (65 mg, 0.20 mmol, 1.5 equiv.) were placed in a sealed tube and suspended in acetonitrile (1 mL) and an aqueous Na_2CO_3 solution (2 M, 0.3 mL, 4.5 equiv.). The mixture was degassed with argon for 5 min, followed by the addition of $Pd(dppf)Cl_2$ (9.6 mg, 13 μmol, 0.1 equiv.). The tube was sealed and heated at 150 °C for 6 h, then the resulting dark-red mixture was poured into water (20 mL) and extracted with ethyl acetate (3 × 10 mL). The organic phase was washed with brine (10 mL), dried (Na_2SO_4) and concentrated under reduced pressure. The crude residue was dissolved in DCM (2 mL) and TFA (0.5 mL) was added slowly before the mixture was magnetically stirred at room temperature for 1 h. The mixture was then concentrated under a stream of nitrogen and subjected to purification by flash column chromatography (10% v/v ammonia saturated methanol/DCM) to afford **7** (41 mg, 66% over two steps) as a beige solid.

A small portion of the product (13 mg) was further purified by reverse-phase semi-preparative HPLC (20 to 50% MeCN over 20 min) to afford a white solid used for biological testing (9.9 mg recovered, TFA salt, see purity trace below).

^{1}H NMR: (800 MHz, *d*$_6$-DMSO) *three N–H not observed* δ 8.74 (d, *J* = 2.2 Hz, 1H), 8.67 (br s, 1H), 8.26 (s, 1H), 7.84 (d, *J* = 7.8 Hz, 2H), 7.64 – 7.56 (m, 3H), 7.28 (apparent t, *J* = 8.7 Hz, 1H), 6.55 (s, 1H), 4.12 (s, 2H), 3.16 – 3.09 (m, 2H), 1.79 – 1.69 (m, 2H), 0.96 (t, *J* = 7.4 Hz, 3H) ppm; **^{13}C NMR:** (201 MHz, *d*$_6$-DMSO) δ 180.8, 156.0 (dd, J_{CF} = 247.6, 6.7 Hz), 152.4 (dd, J_{CF} = 250.1, 8.7 Hz), 149.0, 144.1, 139.1, 138.3, 133.6, 130.9, 129.7 (2C), 128.8 (d, J_{CF} = 9.4 Hz), 127.3 (2C), 127.1, 122.1 (d, J_{CF} = 13.9 Hz), 118.1 (t, J_{CF} = 23.8 Hz), 117.5, 115.7, 112.4 (d, J_{CF} = 22.9 Hz), 53.4, 42.1, 16.9, 12.6 ppm; **HRMS:** (ESI+) *m/z* observed 507.1273, calculated for $C_{24}H_{22}F_2N_4O_3SNa$ $[M+Na]^+$ 507.1280.

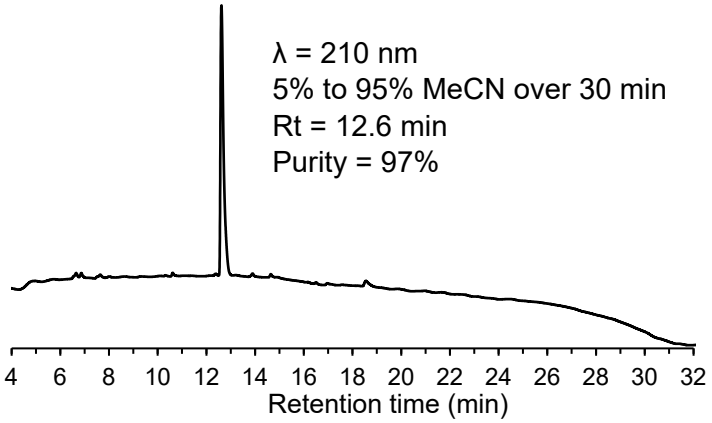

Vem-DBCO (8) synthesis

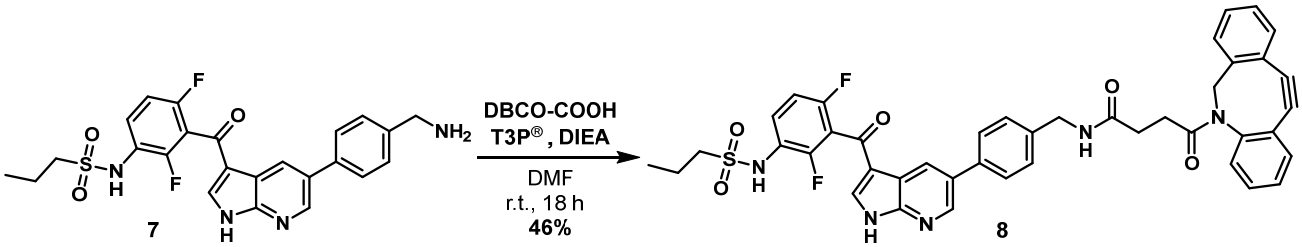

A magnetically stirred mixture of compound **7** (30 mg, 62 µmol, 1.0 equiv.) and DBCO-COOH (28 mg, 93 µmol, 1.5 equiv.) in DMF (0.7 mL) was treated with T3P® (50% in EtOAc, 79 µL, 0.12 mmol, 2.0 equiv.) and DIEA (43 µL, 0.25 mmol, 4.0 equiv.). The mixture was magnetically stirred at room temperature for 18 h, then concentrated under a stream of nitrogen and subjected to purification by flash column chromatography (0-2.5% v/v methanol/DCM) to afford **8** (22 mg, 46%) as a light-yellow solid.

^{1}H NMR: (800 MHz, $CDCl_3$) *one N–H not observed* δ 11.67 (br s, 1H), 8.73 (br s, 1H), 8.05 (br s, 1H), 7.95 (s, 1H), 7.79 (apparent td, J = 8.4, 5.3 Hz, 1H), 7.70 (d, J = 7.9 Hz, 1H), 7.56 (d, J = 7.3 Hz, 1H), 7.49 – 7.44 (m, 1H), 7.43 – 7.40 (m, 2H), 7.39 – 7.33 (m, 3H), 7.23 (d, J = 7.7 Hz, 2H), 7.18 (d, J = 7.3 Hz, 1H), 7.12 (apparent t, J = 8.4 Hz, 1H), 7.08 – 7.01 (m, 2H), 5.14 (d, J = 14.1 Hz, 1H), 4.45 – 4.34 (m, 2H), 3.71 (d, J = 14.1 Hz, 1H), 3.14 – 3.10 (m, 3H), 2.68 – 2.63 (m, 1H), 2.31 (dt, J = 15.2, 5.1 Hz, 1H), 1.97 – 1.88 (m, 3H), 1.05 (t, J = 7.4 Hz, 3H) ppm; **^{13}C NMR:** (201 MHz, $CDCl_3$) *peaks for major conformer reported* δ 180.8, 173.5, 172.3, 156.7 (dd, J_{CF} = 249.0, 6.8 Hz), 150.3 (dd, J_{CF} = 248.4, 8.1 Hz), 151.1, 148.3, 148.2, 143.8, 137.9, 137.6, 136.7, 132.6, 132.1, 129.7, 129.5, 129.2 (2C), 129.1, 128.7, 127.8, 127.7, 127.6 (2C), 127.3, 125.9 (2 overlapping Cs, see ^{1}H–^{13}C HSQC[a]), 123.6, 122.6, 122.0 (dd, J_{CF} = 13.8, 3.7 Hz), 118.8 (t, J_{CF} = 23.5 Hz), 118.6, 117.0, 114.4,

[a] One of the overlapping signals corresponds to a carbon in the difluorobenzene ring. Fluorine splitting could therefore not be determined for this carbon signal.

112.8 (dd, J_{CF} = 22.8, 3.6 Hz), 108.1, 56.1, 54.5, 43.7, 31.2, 29.9, 17.4, 13.0 ppm; **HRMS:** (ESI+) *m/z* observed 794.2213, calculated for $C_{43}H_{35}F_2N_5O_5SNa$ $[M+Na]^+$ 794.2219.

DBCO-amide (9) synthesis

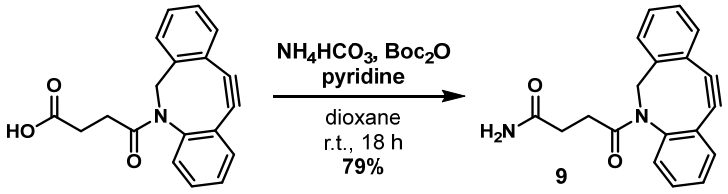

Following a procedure adapted from Sayers *et al.*:[3] A magnetically stirred mixture of DBCO-COOH (31 mg, 0.10 mmol, 1.0 equiv.) in dioxane (0.5 mL) was treated with NH_4HCO_3 (12 mg, 0.15 mmol, 1.5 equiv.), pyridine (18 μL, 0.22 mmol, 2.2 equiv.) and Boc_2O (26 mg, 0.12 mmol, 1.2 equiv.). The mixture was magnetically stirred at room temperature for 18 h, then concentrated under a stream of nitrogen. The resulting residue was redissolved in ethyl acetate (10 mL) and washed sequentially with saturated aqueous NH_4Cl (2 × 10 mL), saturated aqueous $NaHCO_3$ (10 mL) and brine (10 mL). The organic phase was dried (Na_2SO_4) and concentrated under reduced pressure to afford **9** (24 mg, 79%) as an off-white solid, that was used without further purification.

^{1}H NMR: (400 MHz, *d*$_6$-DMSO) δ 7.71 – 7.66 (m, 1H), 7.62 (apparent dd, *J* = 7.3, 1.6 Hz, 1H), 7.54 – 7.42 (m, 3H), 7.41 – 7.26 (m, 3H), 7.16 (br s, 1H), 6.62 (br s, 1H), 5.03 (d, *J* = 14.0 Hz, 1H), 3.61 (d, *J* = 14.0 Hz, 1H), 2.61 – 2.51 (m, 1H), 2.27 – 2.15 (m, 1H), 2.03 – 1.92 (m, 1H), 1.81 – 1.70 (m, 1H) ppm; **^{13}C NMR:** (101 MHz, *d*$_6$-DMSO) δ 173.2, 171.2, 151.6, 148.5, 132.4, 129.7, 128.9, 128.1, 128.0, 127.7, 126.8, 125.2, 122.6, 121.4, 114.2, 108.2, 54.9, 30.1, 29.6 ppm; **HRMS:** (ESI+) *m/z* observed 327.1111, calculated for $C_{19}H_{16}N_2O_2Na$ $[M+Na]^+$ 327.1104.

cGm6 and [R/r]cGm6 synthesis

cGm6 and [R/r]cGm6 (see Figure 1A for cyclic sequences) were first synthesized as the linear peptide, followed by backbone cyclization with native chemical ligation[4] and orthogonal folding of the disulfide pairs. The two cysteine residues at position 5 and 10 (see sequences below) were protected with an Acm group to allow for orthogonal oxidation of the disulfide bonds. The sequences of the linear peptides were as follows:

```
                 1    5        10       15
Linear cGm6:     CRRLXYRQRXVTYCRGRK-NHNH2
Linear [R/r]cGm6: CRrLXYRQrXVTYCRGrK-NHNH2
```

Where X = Cys(Acm), $–NHNH_2$ = C-terminal hydrazide and r = D-Arg

General iterative peptide assembly

The linear peptides were assembled using automated Fmoc solid phase synthesis (Symphony, Protein Technologies Inc), according to the following protocols:

Preparation of 2-Cl-Trt-NHNH$_2$ resin: 2-chlorotrityl chloride resin was swollen in DCM then washed with DCM (5 × 5 mL) and DMF (5 × 5 mL). The resin was manually treated twice with Fmoc-hydrazide (Chem Impex) as a solution in DMF (5% in DMF, 2 mL) for 45 min each time, then washed with DMF (5 × 5 mL). Following deprotection of the hydrazide (see below protocol) to produce the hydrazine resin, peptide synthesis commenced with lysine (position 18), to generate a precursor with an N-terminal cysteine (position 1).

Deprotection: The resin was treated with 20% piperidine/DMF (3 mL, 2 × 5 min) then washed with DMF (5 × 5 mL).

General amino acid coupling: A solution of Fmoc-amino acid (4.0 equiv.), Oxyma® (4.0 equiv.) and *N,N'*-diisopropylcarbodiimide (DIC, 4.0 equiv.) in DMF (final concentration 0.15 M) was added to the resin. The resin was heated under microwave conditions (50 °C) for 30 min before washing with DMF (5 × 5 mL).

Capping: A solution of acetic anhydride/DMF (1:4 v/v) and DIEA (8 equiv.) was added to the resin and agitated for 10 min. The resin was then washed with DMF (5 × 5 mL).

Cleavage: A mixture of TFA/^{i}Pr$_3$SiH/H$_2$O (95:2.5:2.5 v/v/v) was added to the resin and shaken at room temperature. After 2.5 hours, the resin was washed with TFA (3 × 2 mL) and DCM (3 × 2 mL). The combined cleavage solution and TFA and DCM washes were filtered and concentrated under reduced pressure. The residue was treated with cold Et$_2$O (15 mL) to precipitate the peptide. The precipitate was centrifuged to form a pellet, the Et$_2$O was removed, and the pellet redissolved in MeCN/H$_2$O (containing 0.05% TFA), filtered and purified by reverse-phase preparative HPLC (10 to 50% solvent B over 40 minutes, where B is 90% v/v MeCN in water with 0.05% v/v TFA).

Backbone cyclization

The semi-purified linear peptide bearing an N-terminal cysteine (C2) residue and a C-terminal acyl hydrazide (K1) was subjected to backbone cyclization using intramolecular native chemical ligation.[5] The linear peptide hydrazide was prepared as a 1 mM solution in ligation buffer A (6.0 M Gn·HCl, pH 3.0) with a suspension of MPAA (200 equiv.). Acetyl acetone (3.0 equiv., 10% in H$_2$O) was added, and the resulting mixture was stirred for 4 h at room temperature, followed by a 6-fold dilution with ligation buffer B (6.0 M Gn·HCl, 0.2 M NaH$_2$PO$_4$, pH 8.8) containing TCEP (50 equiv.). The pH was adjusted to 7.0 with 5 M NaOH and the reaction was stirred for 18 h. The sample was diluted with MeCN/H$_2$O (containing 0.05% TFA), acidified with 1 M HCl (until pH < 5), filtered and purified by

reverse-phase semi-preparative HPLC (10 to 50% solvent B over 40 minutes, where B is 90% v/v MeCN in water with 0.05% v/v TFA).

Orthogonal disulfide formation

The backbone cyclized peptide was dissolved in MeCN/H_2O (1 mL) and added slowly to an aqueous solution of NH_4HCO_3 (0.1 M) until the peptide was diluted to a concentration of 0.5 mg/mL. The resulting mixture was stirred for 18 h at room temperature, then acidified with 1 M HCl (until pH < 5), filtered and purified by reverse-phase semi-preparative HPLC, as above.

The purified peptide was redissolved in MeCN/H_2O (0.5 mg/mL) and the solution was degassed with N_2 (5 min). Excess iodine was added to glacial acetic acid (brown color) and the resulting mixture added dropwise to the peptide solution until a yellow color was observed. The N_2 line was removed from the vessel, which was capped and wrapped in foil to protect the solution from light. The mixture was stirred for 2 h at room temperature, then diluted in H_2O (containing 0.05% TFA), filtered and purified by reverse-phase semi-preparative HPLC, as above. Purity and correct mass of cGm6 and [R/r]cGm6 were confirmed using a Shimadzu LC–MS 2020 instrument with a Phenomenex 5 µm C18 / 300 Å / 150 x 2 mm LC column (1 to 60% solvent B over 30 minutes, where B is 90% v/v MeCN in water with 0.05% v/v formic acid).

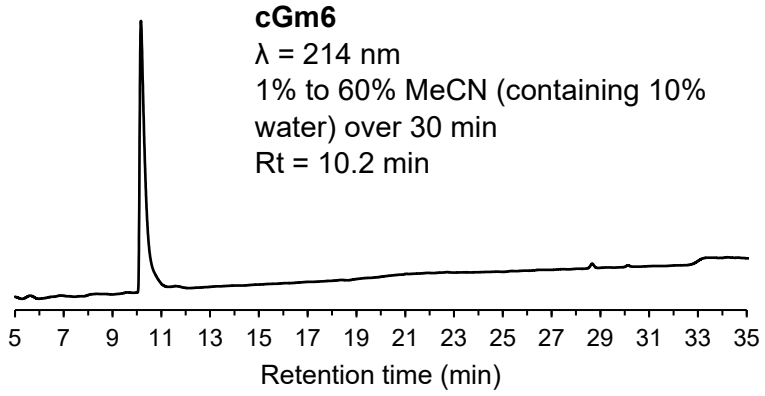

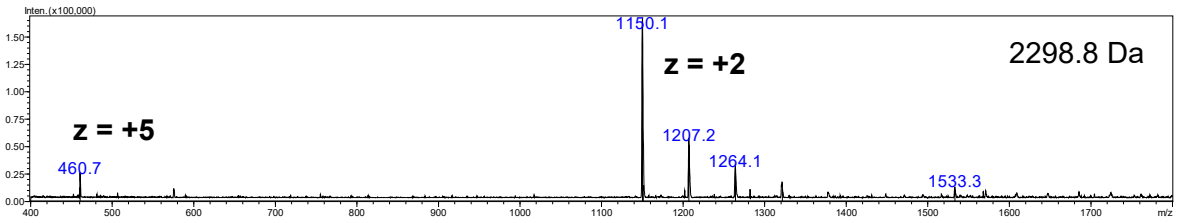

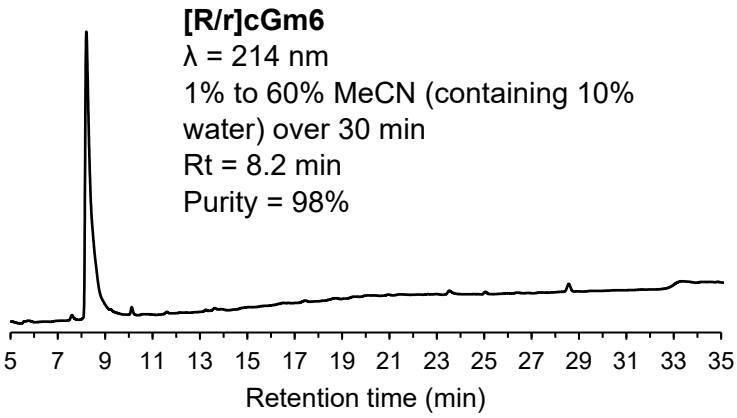

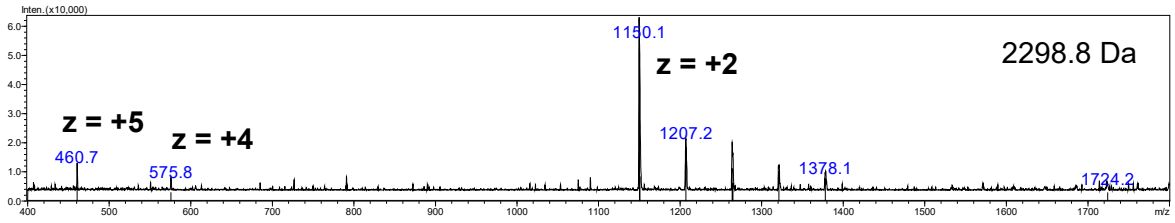

Azide modification of cGm peptides

cGm6 and [R/r]cGm6 were modified *via* amide bond formation to install an azide conjugation handle at the single lysine residue. cGm6 or [R/r]cGm6 (1 mM, 1 equiv.) was dissolved in aqueous sodium bicarbonate (0.1 M, pH 8.2) and treated with azidoacetic acid NHS ester or azido-peg4-NHS ester (2 equiv.) and DIEA (5 equiv.). The mixture was sonicated to dissolve any insoluble material then incubated for 18 h at room temperature, followed by purification with reverse-phase semi-preparative HPLC (15 to 40% solvent B over 50 minutes, where B is 90% v/v MeCN in water with 0.05% v/v TFA). The azide-modified peptides (**2**-**4**) were used semi-pure (~90-95% purity) in subsequent conjugation reactions as they were not being tested on cells. Product formation was confirmed by mass spectrometry (ESI+, see Table S1).

Table S1. Mass spectrometry data for the azide modified cGm peptides.

Peptide	**LRMS (ESI+)**	
	Observed (*m/z*)	Calculated (*m/z*)
cGm6-Az **2**	1191.8 $[M+2H]^{2+}$, 794.8 $[M+3H]^{3+}$	1191.9 $[M+2H]^{2+}$, 795.0 $[M+3H]^{3+}$
[R/r]cGm6-Az **3**	1191.7 $[M+2H]^{2+}$, 794.9 $[M+3H]^{3+}$	1191.9 $[M+2H]^{2+}$, 795.0 $[M+3H]^{3+}$
cGm6-peg4-Az **4**	1287.2 $[M+2H]^{2+}$, 858.6 $[M+3H]^{3+}$, 643.9 $[M+4H]^{4+}$	1287.0 $[M+2H]^{2+}$, 858.4 $[M+3H]^{3+}$, 644.0 $[M+4H]^{4+}$
[R/r]cGm6-peg4-Az **5**	1286.8 $[M+2H]^{2+}$, 858.3 $[M+3H]^{3+}$, 644.0 $[M+4H]^{4+}$	1287.0 $[M+2H]^{2+}$, 858.4 $[M+3H]^{3+}$, 644.0 $[M+4H]^{4+}$

General procedure: SPAAC conjugation

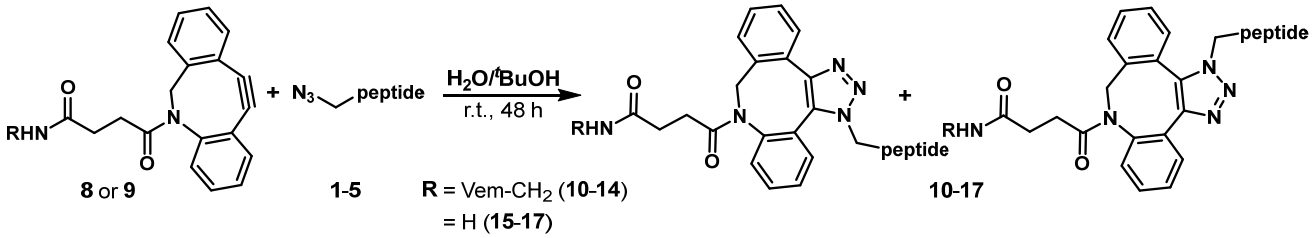

Following a procedure adapted from Lau *et al.*:[6] Peptide-azide (**1-5**, 1.0 equiv.) and drug-alkyne (**8** or **9**, 2.0 equiv.) were dissolved in water/*t*-butanol (0.7-0.8 mM with respect to the peptide). The mixture was stirred for 48 h to produce two regioisomers that were purified by reverse-phase semi-preparative HPLC. Reported yields were determined by weight on a microbalance and were calculated using the mass of the TFA salt of the product (assuming all basic residues, the N-terminal amine and the 7-azaindole moiety within Vem are protonated).

*PDIP-DBCO-Vem (**10**)*

Prepared with PDIP-Az (**1**) and Vem-DBCO (**8**) on a 0.31 µmol scale (1.5 mg peptide) in 4:5 v/v water/*t*-butanol. Purification with semi-preparative HPLC (20 to 50% MeCN over 40 minutes) yielded **10** (1.44 mg, 81%) as a white solid. The two regioisomers were collected together.

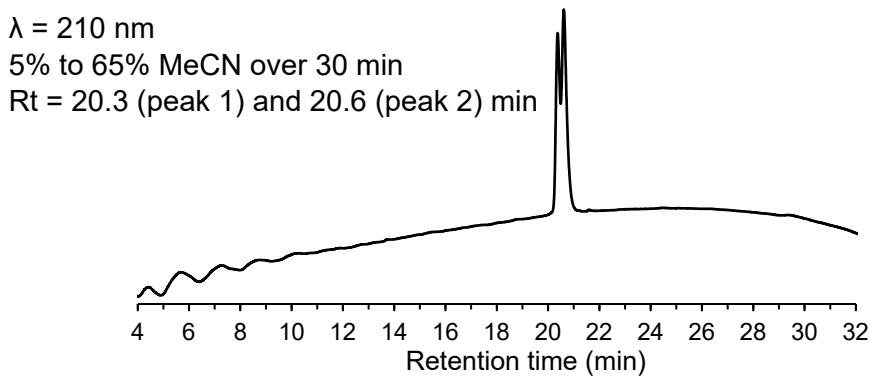

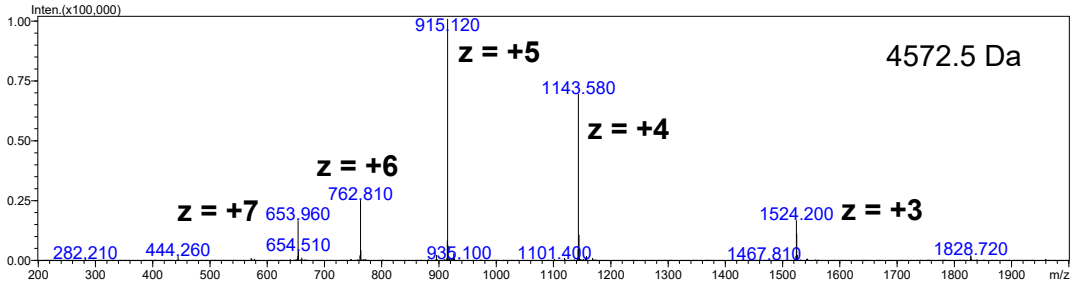

*PDIP-DBCO-amide (**15**)*

Prepared with PDIP-Az (**1**) and DBCO-amide (**9**) on a 0.31 µmol scale (1.5 mg peptide) in 4:5 v/v water/t-butanol. Purification with semi-preparative HPLC (20 to 50% MeCN over 40 minutes) yielded **15** (1.12 mg, 70%) as a white solid. The two regioisomers were collected together.

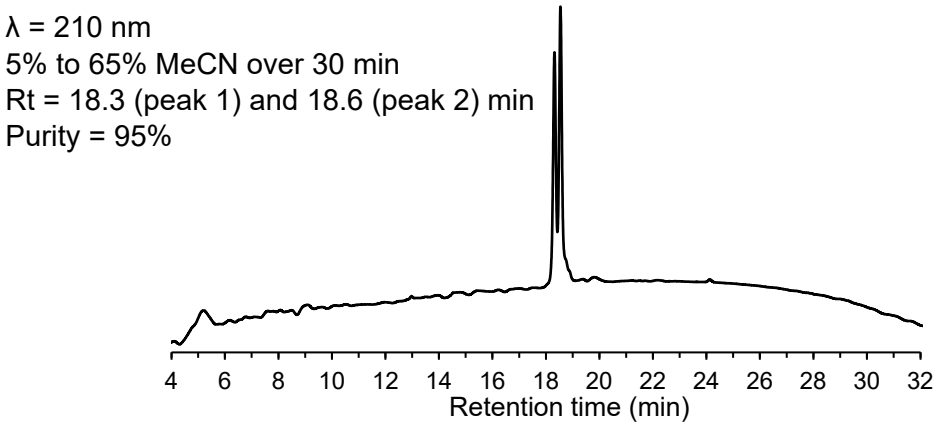

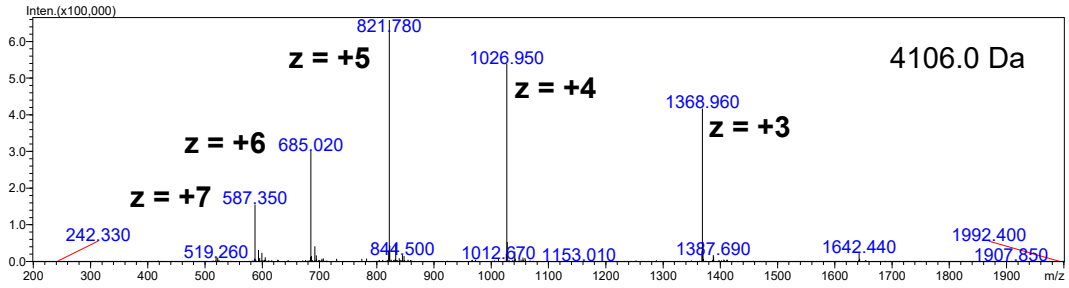

*cGm6-DBCO-Vem (**11**)*

Prepared with cGm6-Az (**2**) and Vem-DBCO (**8**) on a 0.16 µmol scale (0.5 mg peptide) in 1:2 v/v water/t-butanol. Purification with semi-preparative HPLC (10 to 50% MeCN over 40 minutes) yielded **11** (0.56 mg, 87%) as a white solid. The two overlapping regioisomers were collected together.

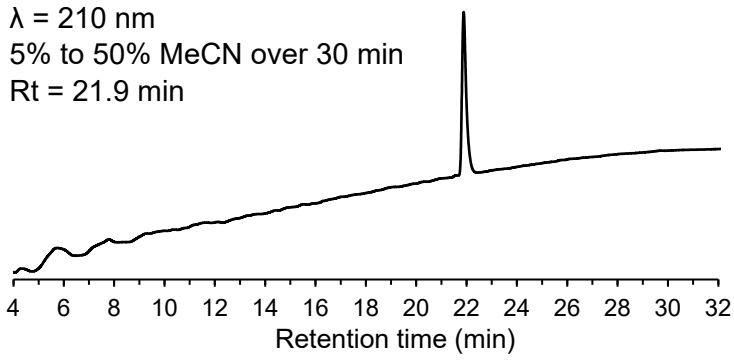

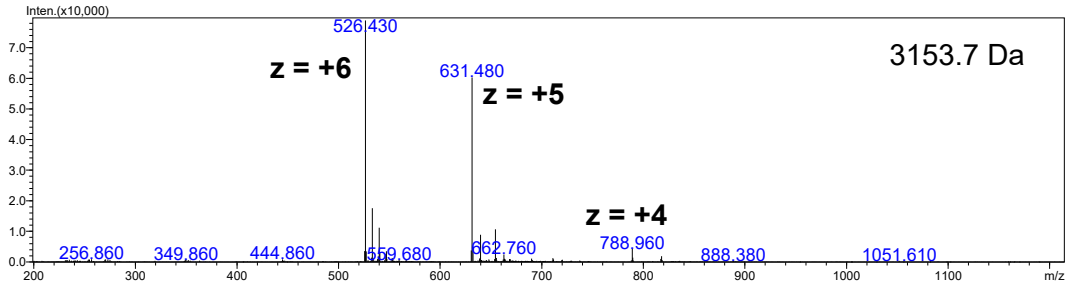

*[R/r]cGm6-DBCO-Vem (**12**)*

Prepared with [R/r]cGm6-Az (**3**) and Vem-DBCO (**8**) on a 0.16 µmol scale (0.5 mg peptide) in 1:2 v/v water/t-butanol. Purification with semi-preparative HPLC (10 to 50% MeCN over 40 minutes) yielded **12** (0.57 mg, 88%) as a white solid. The two overlapping regioisomers were collected together.

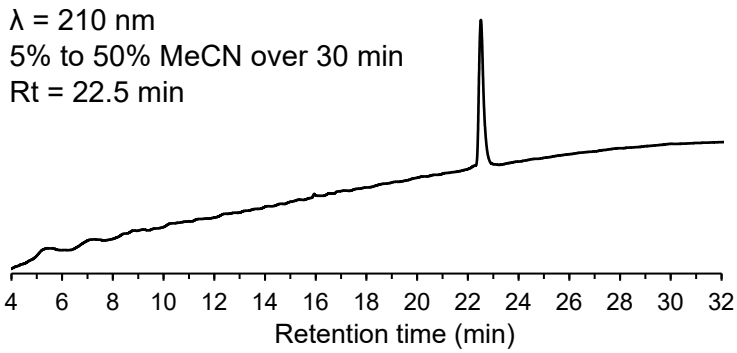

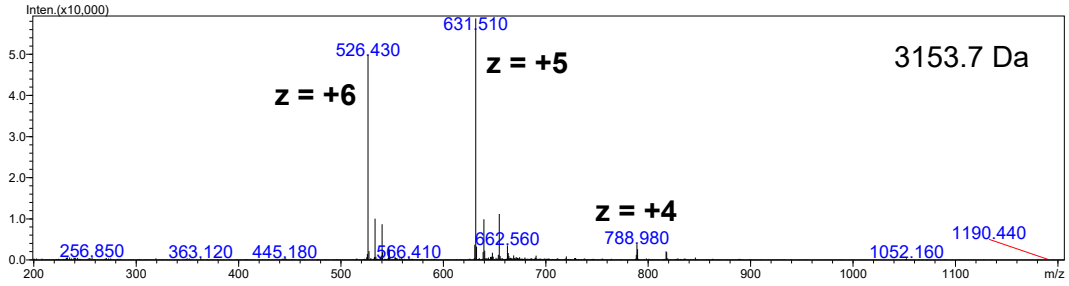

*cGm6-peg4-DBCO-Vem (**13**)*

Prepared with cGm6-peg4-Az (**4**) and Vem-DBCO (**8**) on a 0.15 µmol scale (0.5 mg peptide) in 1:1 v/v water/t-butanol. Purification with semi-preparative HPLC (10 to 50% MeCN over 40 minutes) yielded **13** (0.40 mg, 63%) as a white solid. The two regioisomers were collected together.

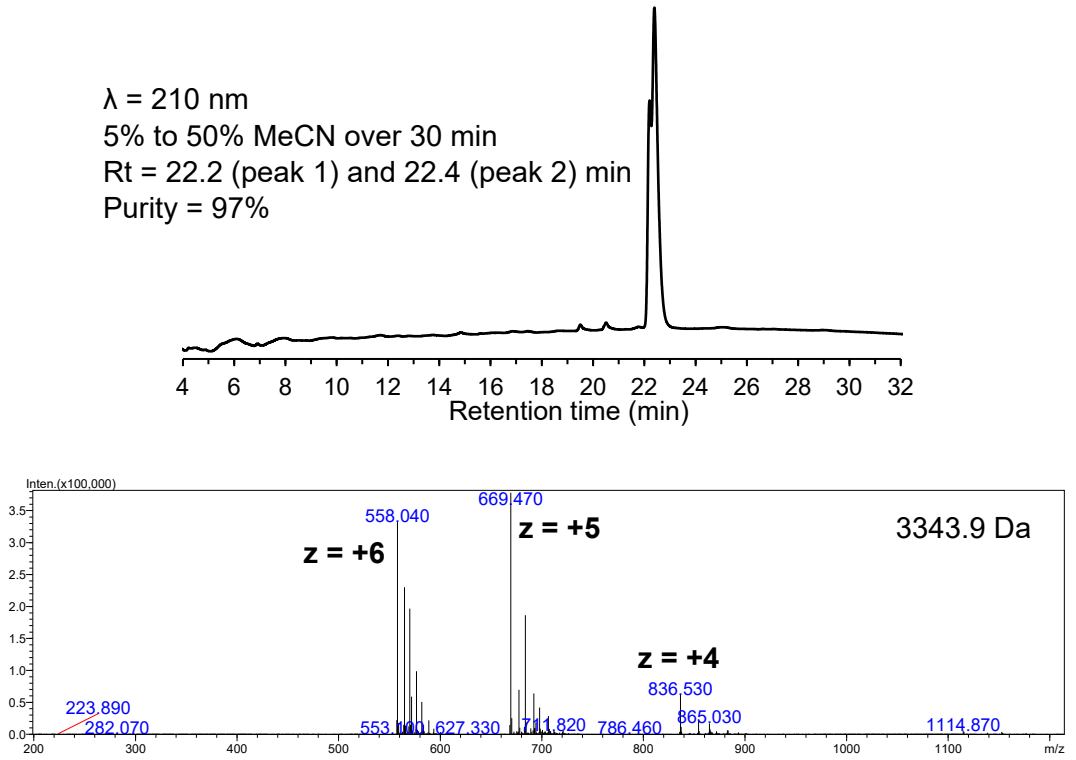

*[R/r]cGm6-peg4-DBCO-Vem (**14**)*

Prepared with [R/r]cGm6-peg4-Az (**5**) and Vem-DBCO (**8**) on a 0.15 µmol scale (0.5 mg peptide) in 1:1 v/v water/t-butanol. Purification with semi-preparative HPLC (10 to 50% MeCN over 40 minutes) yielded **14** (0.41 mg, 64%) as a white solid. The two regioisomers were collected together.

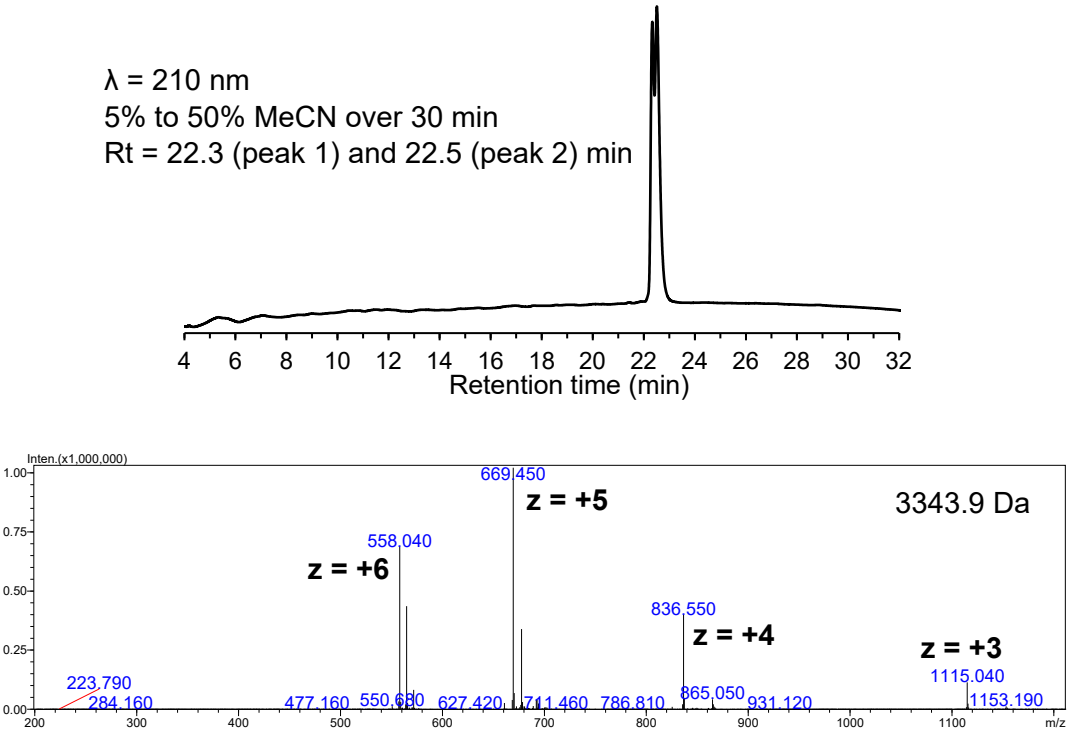

*cGm6-DBCO-amide (**16**)*

Prepared with cGm6-Az (**2**) and DBCO-amide (**9**) on a 0.23 µmol scale (0.7 mg peptide) in 3:4 v/v water/t-butanol. Purification with semi-preparative HPLC (10 to 50% MeCN over 40 minutes) yielded **16** (0.72 mg, 94%) as a white solid. The two regioisomers were collected together.

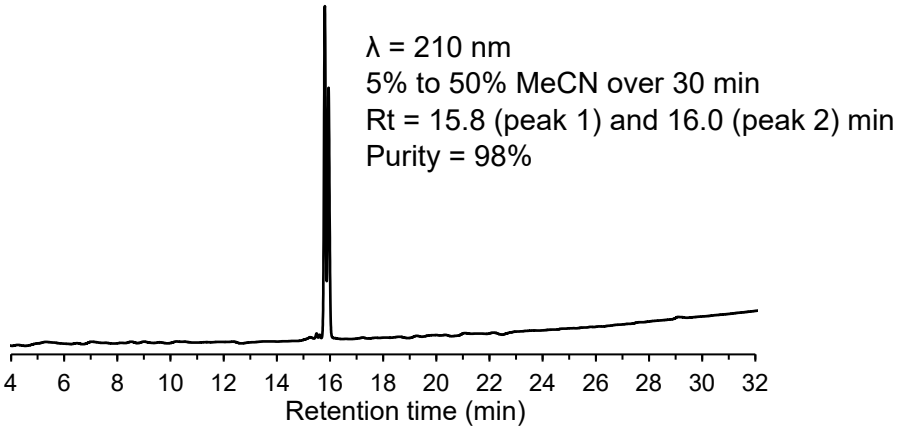

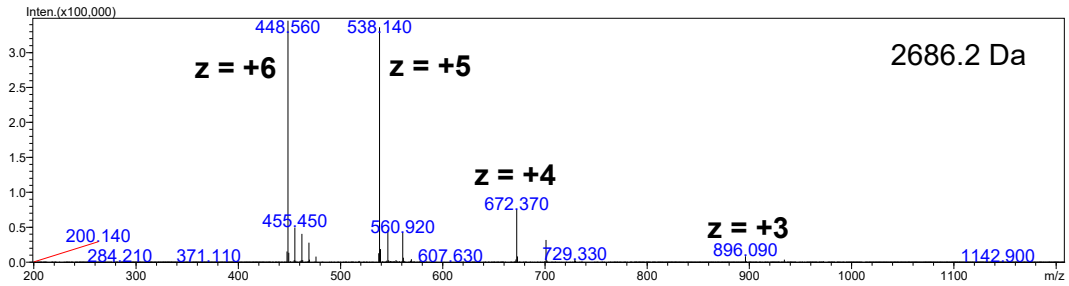

*[R/r]cGm6-DBCO-amide (**17**)*

Prepared with [R/r]cGm6-Az (**3**) and DBCO-amide (**9**) on a 0.26 µmol scale (0.8 mg peptide) in 3:4 v/v water/t-butanol. Purification with semi-preparative HPLC (10 to 50% MeCN over 40 minutes) yielded **17** (0.84 mg, 95%) as a white solid. The two regioisomers were collected together.

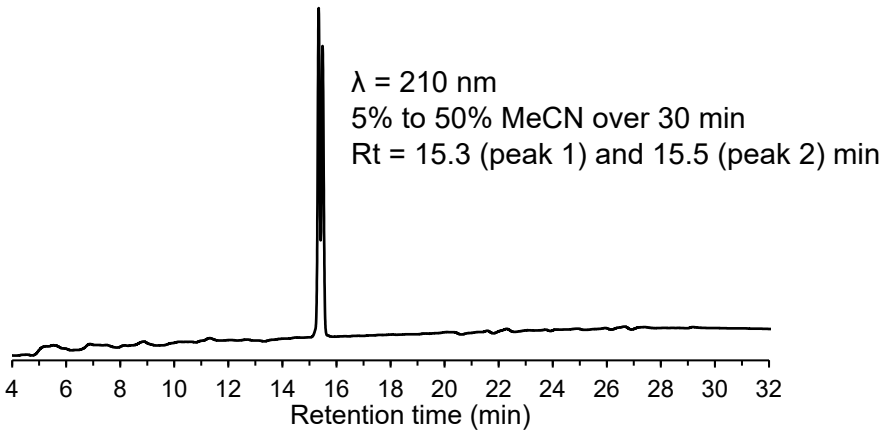

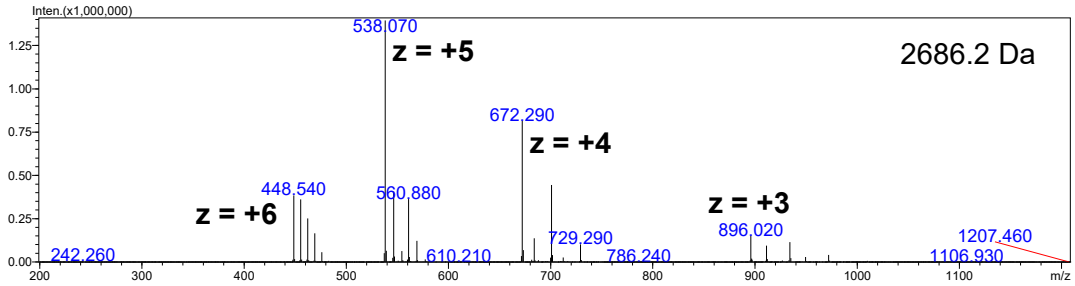

Cell lines and cultures

HT144 is a melanoma cell line that has mutated BRAF (V600E variant) and is sensitive to Vem and dabrafenib (Dab) treatment (both BRAF-V600E inhibitors). Dab-PDRC is a HT144 cell line with permanent drug resistance to Dab, that was previously generated in the Henriques lab by continuously culturing the cells in the presence of sublethal concentrations of Dab.[7] HaCaT is a noncancerous epidermal cell line with wildtype BRAF, so was used as a control.

HaCaT cells were grown in DMEM medium and HT144 and Dab-PDRC cells were grown in RPMI medium supplemented with 2 mM L-glutamine and 10 mM sodium pyruvate. For all cells, the culture media was supplemented with 10% (v/v) fetal bovine serum, 100 units/mL of penicillin and 100 mg/mL of streptomycin. Dab (100 nM) was included in the culture media for Dab-PDRC cells to maintain drug resistance. Flasks of cultured cells were maintained in a humidified incubator (37 °C, 5% CO_2) and passaged every 2–3 days to maintain cultures between 20–90% confluence. Cell line identity was verified by comparing STR profiles of the cell lines against database entries from the DSMZ-German collection of microorganisms and cell cultures, GmBH https://celldive.dsmz.de/str/browse.

Marker	STR Alleles	
	HT144	HaCaT
D5S818	11,13	12
D13S317	11,12	10,12
D7S820	11	9,11
D16S539	12,13	9,12
vWA	16,18	16,17
TH01	9	9.3
Amel	X,Y	X
TPOX	8,11	11,12
CSF1PO	12	9,11

Cell toxicity

Toxicity to the HT144, Dab-PDRC and HaCaT cell lines was tested following peptide treatment by measuring the metabolism of resazurin into fluorescent resorufin. The assays were performed with 5000 cells/well (96-well plate) in serum free media. Cells were incubated with serially diluted peptides, PDCs or drugs for 72 h (37 °C, 5% CO_2). Dab was not added to the culture media for

Dab-PDRC cells during cell toxicity assays. PBS and 0.1% (v/v) Triton X-100 were included as controls for 0% and 100% toxicity. Resazurin was added at 0.02% (w/v) final concentration 2 h prior to the assay end point. Fluorescence (λ_{ex} = 560 nm, λ_{em} = 585 nm) was measured using a Tecan infinite M1000Pro multiplate reader. Percentage cytotoxicity was calculated relative to 0% and 100% controls. Dose-response curves were fitted and CC_{50} values were determined using [inhibitor] *vs* response with four parameters with the top constrained to 100% (GraphPad Prism version 10.0.2). Data was collected as three biological replicates, with experiments conducted on different days.

Unless otherwise indicated, dose response curves were obtained for treatments between 0.25 – 32 μM for both HT144 and Dab-PDRC cell lines and 0.5 – 64 μM for HaCaT. Deviations include cGm6 (0.13 – 16 μM HT144/Dab-PDRC cell lines), Vem (0.5 – 64 μM HT144/Dab-PDRC cell lines), Dab (0.008 – 1 μM HT144, 0.016 – 2 μM HaCaT), PDIP, cGm6, Vem-NH_2 and peptide-DBCO controls **15-17** (0.25 – 32 μM HaCaT).

Parallel artificial membrane permeability assay (PAMPA)

PAMPA was performed according to the manufacturer instructions for the BD Gentest pre-coated PAMPA plate system (BD Biosciences), as previously described.[8] Briefly, peptides and PDCs (4 μM in PBS) were added to the apical side of PAMPA wells and incubated for 4 h at 37 °C, 5% CO_2 with 95% humidity. Soluble fractions were recovered from the apical and basolateral sides, and compound concentration was quantified using a Shimadzu LCMS-2020 instrument with a Phenomenex 5 μm C18 / 300 Å / 150 x 2 mm LC column. Data was collected from three technical replicates for each compound. The % recovery was determined from the combined apical and basolateral fractions relative to the starting concentration:

$$Recovery\ rate\text{: } R\ (\%) = \frac{(C_A \times V_A + C_B \times V_B)}{C_0 \times V_A} \times 100$$

where C_A and C_B are the apical and basolateral concentrations (μM), V_A and V_B are the apical and basolateral volumes (mL), and C_0 is the initial concentration (μM).

The apparent permeability coefficient (Papp) was calculated using the following equations[9] and where A is the membrane surface area (cm^2):

$$Papp\ (cm/s) = \frac{-\ln\left(1 - \frac{C_B}{C_e}\right)}{A \times \left(\frac{1}{V_A} + \frac{1}{V_B}\right) \times time(s)} \qquad C_e = \frac{(C_A \times V_A + C_B \times V_B)}{V_A + V_B}$$

Compound internalization/association with HT144 cells

HT144 cells (5000 cells/well, 96-well plate) were incubated in serum free media with each treatment (final concentration 4 μM) for 1 h (37 °C, 5% CO_2). Media was removed from treated cells, which were washed with PBS, then lysed with ice cold 75% (v/v) MeCN in mQH_2O (containing 1.75% (v/v) TFA) before being transferred to tubes containing PBS (10 μL). Untreated cells were used as controls and were processed in the same way before being transferred to tubes containing an aliquot of each treatment (10 μL, final concentration 4 μM). Cells were incubated for 10 mins at 0 °C (ice), centrifuged (21,000 x g, 4 °C, 20 min) and the supernatant was analyzed using a Qstar elite TOF-MS with a 2% gradient containing 0.1% (v/v) formic acid in H_2O against 0.1% (v/v) formic acid in 90% (v/v) MeCN/ H_2O. The $[M+6H]^{6+}$ *m/z* peak for each compound was identified using Sciex Analyst software, and area under the curve (AUC) was determined for the exact mass using Sciex MultiQuant software. The percentage of internalized peptide/PDC was determined from: treated sample AUC / (average of (PBS controls + post-added compound) AUC) × 100% for each peptide/PDC. Data was collected from three technical replicates for each treatment and control.

^{1}H and ^{13}C{^{1}H} NMR

800 MHz ^{1}H NMR in d_6-DMSO

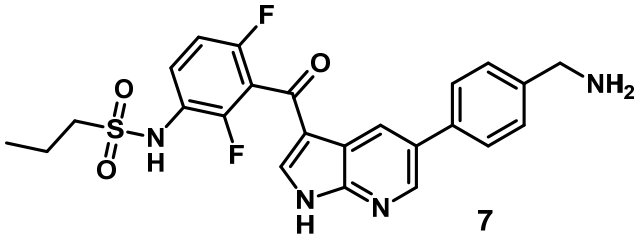

7

201 MHz ^{13}C NMR in d_6-DMSO

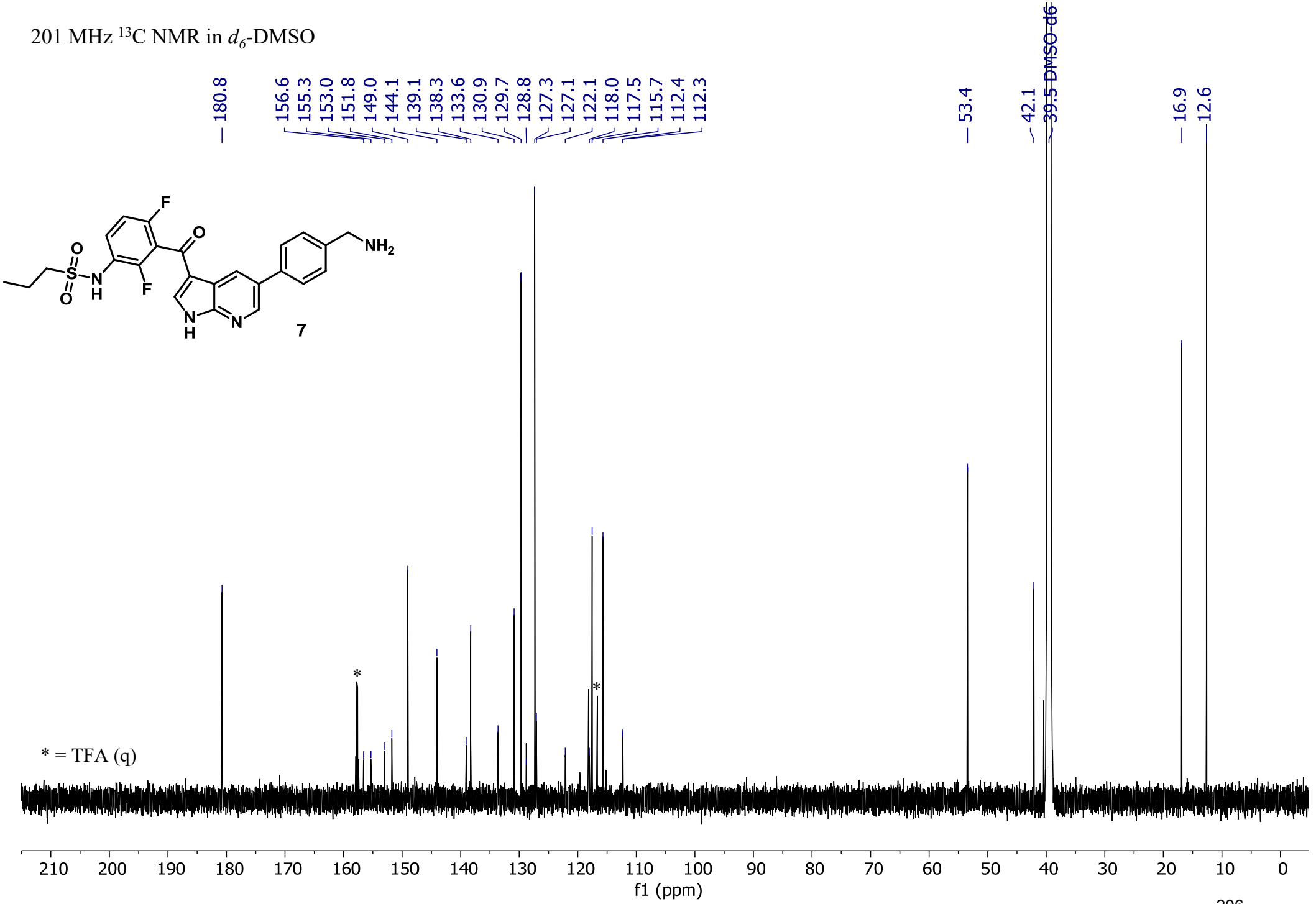

800 MHz ^{1}H NMR in $CDCl_3$

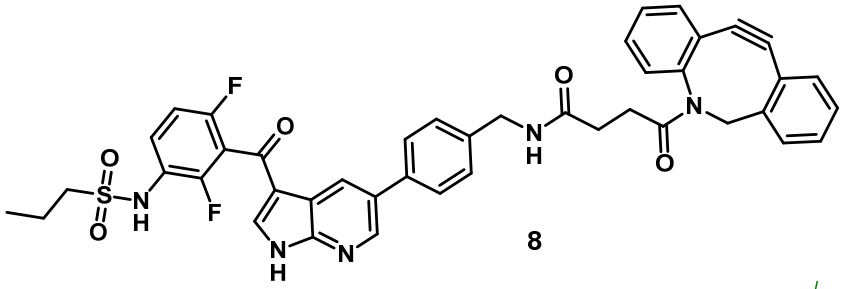

8

grease*

*H_2O

f1 (ppm)

201 MHz ^{13}C NMR in $CDCl_3$

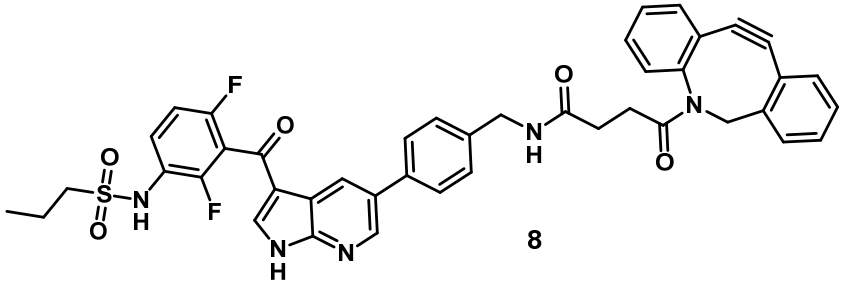

8

800 MHz, 201 MHz $^{1}H–^{13}C$
HSQC in $CDCl_3$

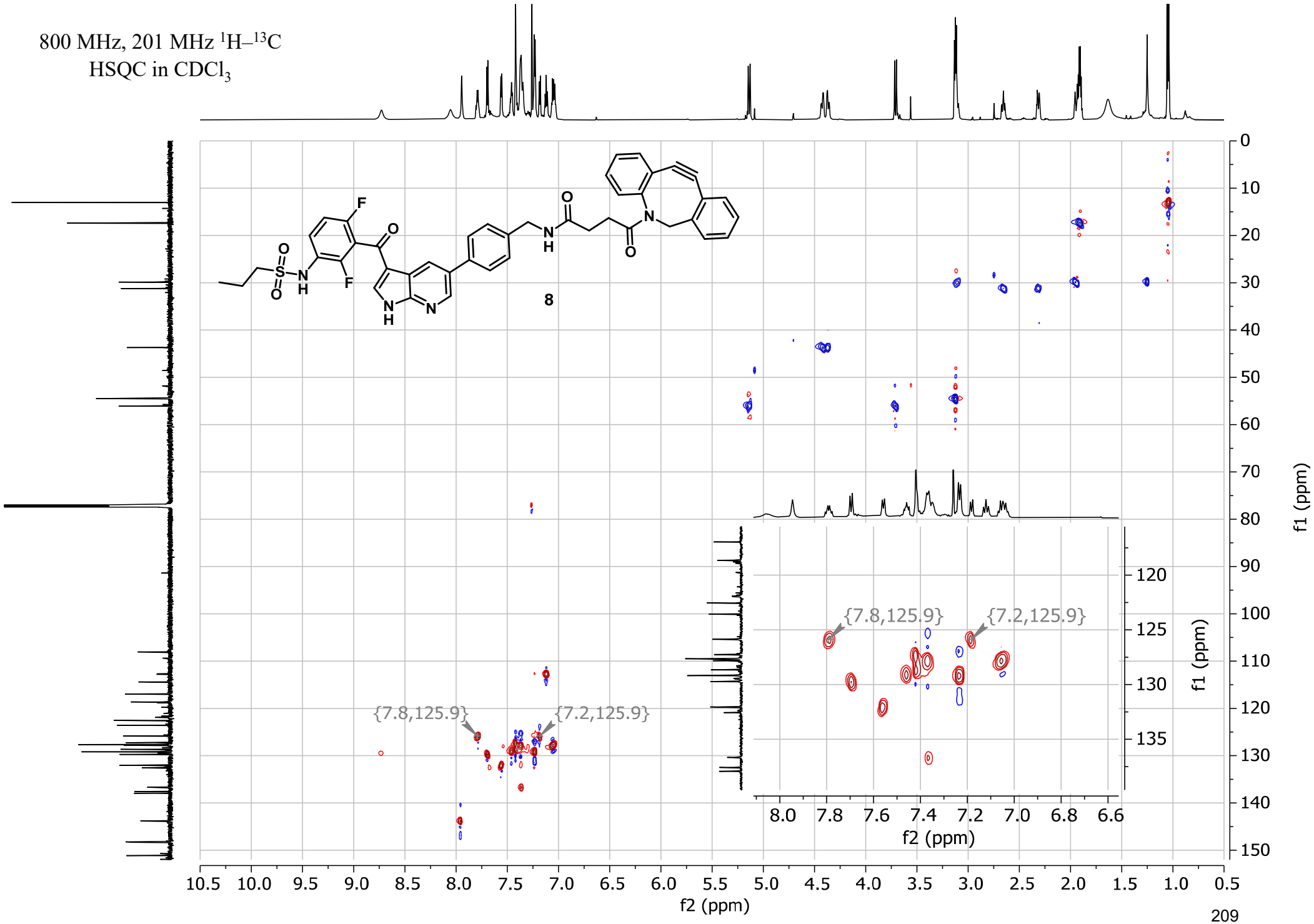

400 MHz ^{1}H NMR in d_6-DMSO

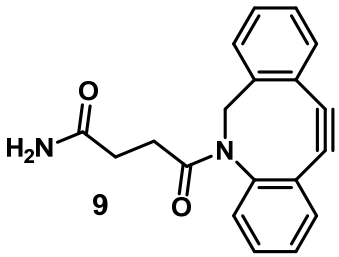

9

*grease

f1 (ppm)

101 MHz ^{13}C NMR in d_6-DMSO

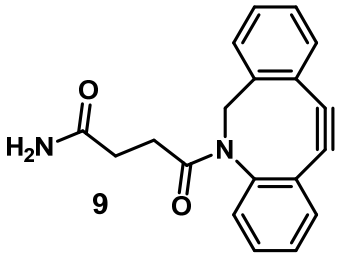

9

References

(1) Lawrence, N.; Dennis, A. S.; Lehane, A. M.; Ehmann, A.; Harvey, P. J.; Benfield, A. H.; Cheneval, O.; Henriques, S. T.; Craik, D. J.; McMorran, B. J. *Cell Chem. Biol.* **2018**, *25*, 1140–1150.

(2) Mikula, H.; Stapleton, S.; Kohler, R. H.; Vinegoni, C.; Weissleder, R. *Theranostics* **2017**, *7*, 1257–1265.

(3) Sayers, J.; Thompson, R. E.; Perry, K. J.; Malins, L. R.; Payne, R. J. *Org. Lett.* **2015**, *17*, 4902–4905.

(4) Cistrone, P. A.; Bird, M. J.; Flood, D. T.; Silvestri, A. P.; Hintzen, J. C. J.; Thompson, D. A.; Dawson, P. E. *Curr. Protoc. Chem. Biol.* **2019**, *11*, e61.

(5) Flood, D. T.; Hintzen, J. C. J.; Bird, M. J.; Cistrone, P. A.; Chen, J. S.; Dawson, P. E. *Angew. Chem. Int. Ed.* **2018**, *57*, 11634–11639.

(6) Lau, Y. H.; Wu, Y.; Rossmann, M.; Tan, B. X.; De Andrade, P.; Tan, Y. S.; Verma, C.; McKenzie, G. J.; Venkitaraman, A. R.; Hyvönen, M.; Spring, D. R. *Angew. Chem. Int. Ed.* **2015**, *54*, 15410–15413.

(7) Benfield, A. H.; Vernen, F.; Young, R. S. E.; Nadal-Bufí, F.; Lamb, H.; Hammerlindl, H.; Craik, D. J.; Schaider, H.; Lawrence, N.; Blanksby, S. J.; Henriques, S. T. *Pharmacol. Res.* **2024**, *207*, 107298.

(8) Bergeron, C.; Bérubé, C.; Lamb, H.; Koda, Y.; Craik, D. J.; Henriques, S. T.; Voyer, N.; Lawrence, N. *Pept. Sci.* **2024**, 10.1002/PEP2.24380.

(9) Sevin, E.; Dehouck, L.; Fabulas-da Costa, A.; Cecchelli, R.; Dehouck, M. P.; Lundquist, S.; Culot, M. *J. Pharmacol. Toxicol. Methods* **2013**, *68*, 334–339.